

April 2018

Investigation of Alcohol-Induced Changes in Hepatic Histone Modifications Using Mass Spectrometry Based Proteomics

Crystina Leah Kriss

University of South Florida, ckriss@mail.usf.edu

Follow this and additional works at: <https://digitalcommons.usf.edu/etd>

 Part of the [Biology Commons](#), [Cell Biology Commons](#), and the [Molecular Biology Commons](#)

Scholar Commons Citation

Kriss, Crystina Leah, "Investigation of Alcohol-Induced Changes in Hepatic Histone Modifications Using Mass Spectrometry Based Proteomics" (2018). *USF Tampa Graduate Theses and Dissertations*.
<https://digitalcommons.usf.edu/etd/7185>

This Dissertation is brought to you for free and open access by the USF Graduate Theses and Dissertations at Digital Commons @ University of South Florida. It has been accepted for inclusion in USF Tampa Graduate Theses and Dissertations by an authorized administrator of Digital Commons @ University of South Florida. For more information, please contact digitalcommons@usf.edu.

Investigation of Alcohol-Induced Changes in Hepatic Histone Modifications Using Mass Spectrometry
Based Proteomics

by

Crystina L. Kriss

A dissertation submitted in partial fulfillment
of the requirements for the degree of
Doctor of Philosophy
Department of Cellular Biology, Microbiology, and Molecular Biology
College of Arts and Sciences
University of South Florida

Co-Major Professor: Stanley M. Stevens, Jr, Ph.D.
Co-Major Professor: Brant Burkhardt, Ph.D.
Committee Member: Meera Nanjundan, Ph.D.
Committee Member: James Garey, Ph.D.

Date of Approval:
March 22th, 2018

Keywords: Mass-Spectrometry, Alcohol Liver Disease, Metabolic Tracing, Tyrosine Nitration, Epigenetics,
Histone, Acetylation

Copyright © 2018, Crystina L. Kriss

Dedication

First of all, I want to thank God, without him I would not be here today. Next, to my amazing parents, Al and Laura Kriss, Thank you so much for your endless support and encouragement throughout this process (Thank God for your amazing genetic material!). Without your years of guidance, patience, and bail money; none of this would have been possible. I love you more than I can ever express. Thank you from the bottom of my heart and I dedicate this research to you! I would also like to dedicate this dissertation to my Grandparents; Grandma & Grandpa Lew, Grandpa Johnson, and Grandma & Grandpa Kriss. I couldn't have done it without you either! To my brother, Michael Kriss, you will always be my little brother (and best friend), I love you. To my dogs, aka my emotional support animals: Mika Bella, Sassy Maxi, and Mr. Beauregard. Thank you for all of the kisses and snuggles when mommy cried while pursuing my Ph.D., I love you to the moon and back. I would also like to thank my extended family for all of your love and support over the years. I love you. Last but certainly not least: To my sister's from different misters: Kriss, Michelle, Poynter, Dluge, and Rachel: I can't thank you enough for always being there for me and supporting me over the years. You taught me what it's like to have the best sisters in the world. I love you all so much and wouldn't be here today without your endless love and support— Ride or Die Forever— Love you, ladies!

Acknowledgments

First and foremost, I would like to acknowledge and thank my mentor, Dr. Stanley Stevens, for all of the support, guidance, and giving me the opportunity to take this research to the next level. Thank you for entertaining most of my crazy ideas and pushing me when times were tough.

I would also like to acknowledge and thank my committee, Dr. Brant Burkhardt, Dr. Meera Nanjundan, and Dr. James Garey, for all of your suggestions, feedback, and guidance in helping my project to evolve over the years.

I would like to acknowledge and thank Dr. Sameer Varma and Nalvi Duro for your help in the molecular dynamic simulations.

I would also like to acknowledge my previous mentors for their endless support and guidance in helping push me towards beginning my Ph.D. Dr. Andrew Hu, your insatiable passion for science and patience for teaching, continue to inspire me. I would not be writing this today if you didn't believe in me and push me to evolve into the best scientist that I can become. Dr. Wayne Price, you opened the first door for me to join the scientific community and paved the way for me. Thank you both for seeing something in me that I couldn't, and believing in me so much that I began to believe in myself.

I would like to acknowledge and thank the Moffitt Cancer Center Histology Core and thank Mr. Noel Clark for their work on the histology shown throughout.

Thank you to Nicole Johnson at Zymo Research Corp. for your work on the ChIP-sequencing and validation.

Jenny Guergues thank you for your endless patience in teaching me proper English and verb tenses.

To my undergrads, Gabby, Emily and Omar thank you very much for the help over the years, I wish many years of success to you all.

Lastly, a huge thank you to all my labmates: Brandi Cook, Joao Costa Pinho, Daniel Martin, Jennifer Guergues, Dale Chaput, Ashley Culver-Cochran, & Harris Bell-Temin. Thank you for all of the help and discussions over the years, I couldn't have asked for better colleagues.

Table of Contents

List of Tables	iv
List of Figures	v
List of Acronyms	viii
Abstract	xiii
Chapter 1: Introduction	1
Pathology of Alcohol Liver Disease	1
Ethanol Metabolism.....	4
Oxidative Ethanol Metabolism.....	4
Ethanol Metabolism and Mitochondrial Dysfunction.....	8
Ethanol Metabolism and Oxidative Stress.....	11
Alcohol and Epigenetics	14
Ethanol-Induced Histone Tyrosine Nitration	15
Ethanol-Induced Histone Lysine Acetylation	17
Epigenetics & Proteomics	19
Overview of Mass Spectrometry	19
Labeling Techniques in Mass Spectrometry	22
Project Aims and Rational	23
Aim 1: Identify and characterize site-specific targets of tyrosine nitration on histone proteins regulated by ethanol exposure	23
Aim 2: Identify ethanol-induced sites of acetylation on histone proteins and assess their effects on gene regulation during oxidative stress.....	25
Chapter 2: Global Proteomic Analysis of Sex-Differences using a Chronic-Binge Mouse Model of Alcohol Liver Disease.....	28
Abstract.....	28
Introduction	29
Materials and Methods.....	32
Chemicals and Reagents	32
Chronic-Binge Mouse Model of Alcohol Liver Disease	33
Histological Analysis and Liver Injury Assays	34
Histology Analysis.....	34
Serum Blood Alcohol Content, ALT & AST Liver Injury Assays	34
Sample Processing	34
Sample Processing for Proteomic Analysis	34
Nuclear Fractionation.....	35
LC-MS/MS and Statistical Analysis	36

Western Blots.....	37
IPA Analysis.....	37
Scaffold Protein Analysis.....	38
Results.....	38
Characterization of 10-Day Chronic-Binge and Liver Injury in Male and Female Mice	38
Sex-Specific Differences in Hepatic Protein Expression Profiles After Chronic-Binge Ethanol Feeding	41
Alcohol, Oxidative Stress, and Mitochondria Dysfunction Leads to Alterations in Post-Translational Modifications on Histone Proteins	45
Discussion	49
Chapter 3: Chronic Ethanol Exposure Induces Hepatic Histone Protein Nitration in Male Mice	53
Abstract.....	53
Introduction	55
Materials and Methods.....	57
Chemicals and Reagents	57
Experimental Design and Statistical Rational	58
Animals and 28-Day Leiber-DiCarli Ethanol Feeding	58
Liver Histology, IHC and Densitometry Analysis of Nitrotyrosine Staining	59
Sample Preparation, Mass Spectrometry and Data Analysis.....	60
Nuclear Fractionation.....	60
LC-MS/MS	61
Extracted Chromatogram Analysis	62
Western Blots.....	62
Dot Blots	63
Nitro-Peptide Synthesis Mass Spectrometric Analysis and Validation of Histone Nitrotyrosine Identification.....	63
Molecular Dynamics Simulations	64
H3nY41 Antibody Synthesis & Chromatin Immunoprecipitation	66
Results.....	67
28-Day Chronic Ethanol Diet in 8-Week Male Mice Promotes Liver Injury & Nitrotyrosine Formation	67
Functional Analysis of Nuclear Enrichment and Protein Tyrosine Nitration.....	69
Identification of Nitrotyrosine Modifications on Histone Proteins	70
Implications of Histone Tyrosine Nitration and Gene Regulation	77
Protein Tyrosine Nitration Targets Proteins Involved in Gene Regulation.....	77
Molecular Dynamics Predict H3nY41 induces a conformational change in the DNA	79
H3(nitro)Y41 and Antibody Validation by CHIP-Seq and qPCR	82
Discussion	85
Chapter 4: Metabolic Tracing of ¹³ C ₂ -Labeled Ethanol to Histone Acetylation Demonstrates the Contribution of Acetyl-CoA derived from Ethanol Metabolism.....	90
Abstract.....	90
Introduction	91
Materials and Methods.....	95

Acute-Binge Mouse Model using $^{13}\text{C}_2$ -Labeled Alcohol or Maltose-Dextrin	95
Blood Alcohol Test	96
Sample Processing and LC-MS.....	97
Tissue Lysis, Histone Extraction, and Derivatization.....	97
LC-MS, Data Analysis	98
Isotopic Precursor Intensity Extraction Using R.....	99
Results.....	99
Blood Alcohol Levels after an Acute Alcohol Binge Correlate with $^{13}\text{C}_2$ Incorporation over 24 hours	99
Characterization of $^{13}\text{C}_2$ -label incorporation on Histone Proteins after an Acute Ethanol Gavage.....	102
Isotope Simulation Suggests a Mixture of $^{13}\text{C}_2$ Incorporation on the Double Acetylated Peptide after 4-hours Ethanol Exposure.....	105
H3K9-R17 Analysis of $^{13}\text{C}_2$ Incorporation on the Doubly Acetylated Peptide After 4-hours Ethanol Gavage.....	105
H3K18-R26 Analysis of $^{13}\text{C}_2$ Incorporation on the Doubly Acetylated Peptide 4-hours After Ethanol Gavage.....	107
Incorporation of $^{13}\text{C}_2$ on Multiple N-Terminal Acetylation Sites on H4 K5-R17	109
Discussion	110
Chapter 5: Conclusions and Future Directions.....	115
Alcoholism and Alcohol Liver Disease a Review	115
Overview of Major Findings	116
Future Directions	122
Conclusions.....	125
Literature Cited.....	127
Appendix A: IACUC Approval-Impact of Ethanol-Induced Protein Nitration on the Histone Modification Code	142
Appendix B: IACUC Approval-Role of Methylation in Ethanol-Induced Microglia Activation	143
Appendix C: AALAS Certification of USF Animal Research Orientation	144

List of Tables

Table 2.1:	Gender Specific Fold-Change in Male and Female Mice	44
Table 2.2:	Differentially Expressed Acetylated Proteins Identified by Sex and Cellular Compartment Following 10-day Chronic-Binge, Corresponding to Figure 2.7	47
Table 3.1:	MaxQuant Nitrotyrosine Identification in Mouse Liver Following the 28-days Chronic Alcohol Diet.....	71
Table 3.2:	XIC Analysis of Nitrotyrosine on Histone Proteins following the 28-day Chronic Ethanol Diet in Mice	72
Table 3.3:	Novel Targets of H3nY41 Nitration	83
Table 3.4:	qPCR of Ano2 and Dpp9 Following CHIP-Seq.....	85

List of Figures

Figure 1.1:	Hematoxylin-Eosin Stain of Mouse Liver Post 28-Day Chronic Ethanol Exposure	2
Figure 1.2:	Overview of Ethanol Metabolism.....	6
Figure 1.3:	Overview of NADH: NAD ⁺ Regulation during Ethanol Metabolism.....	10
Figure 1.4:	Ethanol Metabolism Induces Oxidative Stress in the Mitochondria.....	11
Figure 1.5:	Reactive Oxygen Species, Superoxide (O ₂ ⁻) and Nitric Oxide (NO) Lead to the Formation of Nitrotyrosine (nY)	12
Figure 1.6:	General Overview of LC-MS Analysis.....	20
Figure 2.1:	H&E Staining of Mouse Liver following the 10-day Chronic-Binge Ethanol Diet	39
Figure 2.2:	Average Serum BAC Levels Following the 10-Day Chronic-Binge Ethanol Diet in 8-Week Old Mice.....	40
Figure 2.3:	ALT and AST Liver Injury Marker Assay Following the 10-day Chronic-Binge Alcohol Diet.....	40
Figure 2.4:	Ingenuity Pathway Analysis of Male and Female Mice Predicts Liver Damage in Females and Liver Injury in Males	41
Figure 2.5:	Predicted Upstream Activation Initiated by Ethanol Suggests that Cytochrome P450 Proteins amongst Others Play a Role in Liver Injury.....	42
Figure 2.6:	Fold-Change in Cytochrome P450 Family of Proteins Post 10-day Chronic- Binge Ethanol Diet.....	43
Figure 2.7:	Venn-Diagram Depicting Differences in Gender-Specific Acetylated Proteins following the 10-day Chronic-Binge	46

Figure 2.8:	Western Blots Obtaining from Whole Cell Liver Lysate following the 10-Day Chronic-Binge Ethanol Diet	48
Figure 3.1:	Histological Analysis of Mouse Liver following the 28-Day Leiber-DeCarli Chronic Ethanol Diet	68
Figure 3.2:	Quantitative Analysis of Mass Spectrometrically Derived Nuclear Fractionation and Changes in Protein Upregulation	70
Figure 3.3:	Identification and Validation of Histone Tyrosine Nitration that Passed Validation	73
Figure 3.4:	Annotation of Synthetic Peptides H3nY41, H4nY51, H4nY72, and H1nY70	74
Figure 3.5:	Potential Sites of Histone Tyrosine Nitration That Did Not Pass Validation	75
Figure 3.6:	Annotation of Synthetic Peptides Pertaining to H1nY27, H ₂ BnY50, & H4nY98	76
Figure 3.7:	Site-Specific Identification of Nitrotyrosine on Heterogeneous Nuclear Ribonucleoproteins & Eef1a1.....	78
Figure 3.8:	Tracking the Time Evolution of Histones and DNA RMSDs.....	79
Figure 3.9:	Molecular Dynamic Simulations Predict the DNA Prefers a Different Conformation upon Histone Tyrosine Nitration.....	80
Figure 3.10:	Distance from H3Y41 to a Set of the DNA Phosphorus (P) Atoms.....	80
Figure 3.11:	RDF Analysis was performed on DNA P, K ⁺ , Cl ⁻ , and Water with Respect to the Carbon at Position ε2 of H3Y41.....	81
Figure 3.12:	Potassium Ion Presence is in the Cavity Formed by DNA and the H3 Tail Bearing H3nY41, thereby Displacing the DNA Further Away.....	82
Figure 3.13:	Dot Blots Used to Test the Specificity of the H3nY41 Antibody	83
Figure 3.14:	ChIP-Seq Peak Identification in the H3nY41 Pull-Down Shows 5 Peaks Found within the Intron Region of Genes Important in Metabolism and Liver Disease.....	84
Figure 3.15:	qPCR Validation of Ano2 and Dpp9	85

Figure 4.1:	Site-Specific Incorporation of Heavy-Labeled Ethanol Peaks Around 4-Hours following the Same Trend as Serum BAC Levels.....	101
Figure 4.2:	Label Incorporation for each H3 Peptide were Quantified by Extracted Ion Chromatogram Analysis.	103
Figure 4.3:	Overall Changes in Total Acetylation on H3 were quantified by Extracted Ion Chromatogram Analysis	104
Figure 4.4:	Mass Spectra of the H3 Doubly Acetylated Peptide Representative of H3K9/K14 Suggests Site-Specific and Time-Dependent Incorporation of the Heavy-Label Ethanol	106
Figure 4.5:	Four-Hour Comparison of Simulated Mass Spectra to the Experimental MS of the H3 Doubly Acetylated Peptide H3K18/K23 Suggests Site-Specific and Time-Dependent Incorporation of the Heavy-Label Ethanol.....	108
Figure 4.6:	R Facilitates Quantitation of $^{13}\text{C}_2$ Incorporation for the Multiple Acetylation Sites on Histone 4 (G4-R17).....	109
Figure 4.7:	Tandem Mass Spectrometry in Conjunction with De Novo Sequencing Offers Potential Insight in Quantifying $^{13}\text{C}_2$ -Label Incorporation on Peptides with Multiple Acetylation Sites such as Histone 4 G4-R17	111

List of Acronyms

ABL1	Abelson murine leukemia viral oncogene homolog 1
ACL	ATP-citrate lyase
ALD	alcohol dehydrogenase
ALD	Alcohol liver disease
ADH	Alcohol dehydrogenase
ALDH2	Acetaldehyde dehydrogenase
ALI	Alcohol liver injury
ALT	Alanine aminotransferase
AST	Aspartate aminotransferase
ATP	Adenosine triphosphate
BAX	BCL-2-associated X protein
BSA	Bovine Serum Albumin
CEBPA	CCAAT/Enhancer Binding Protein Alpha
CID	Collision-induced dissociation
Cl ⁻	Chloride Ion
CO ₂	Carbon Dioxide
CYP(xxx)	Cytochrome P450 (family-isoform)
CYP2E1	Cytochrome IIE1
DIA	Data-independent acquisition
DBU	1, 8-diazobicyclo[5, 4, 0]undec-7-ene

DCM	Dichloromethane
DMF	N-methylmorpholine in dimethylformamide
Eef1a1	Elongation factor 1-alpha 1
EGFR	Epidermal growth factor receptor
ESI	Electrospray ionization
ETNPPL	Ethanolamine-phosphate phospho-lyase
EtOH	Ethanol
FDR	False discovery rate
H&E	Hematoxylin and Eosin stain
GPx	Glutathione peroxidase
GSH	Glutathione
H ₂ O ₂	Hydrogen peroxide
H&E	Hematoxylin and eosin staining
HAT	Histone deacetylase proteins
H3	Histone H3
H3K9	Histone H3 lysine 9
H3K9Ac	Histone H3 lysine 9 acetylation
H3K14	Histone H3 lysine 14
H3K14Ac	Histone H3 lysine 14 acetylation
H3K18	Histone H3 lysine 18
H3K18Ac	Histone H3 lysine 18 acetylation
H3K23	Histone H3 lysine 23
H3K23Ac	Histone H3 lysine 23 acetylation
H4	Histone H4

HCTU	5-chloro-1-[bis(dimethylamino)methylene]-1H-benzotriazolium 3-oxide
HDAC	Histone deacetylase
HnRNPA3	Heterogeneous nuclear ribonucleoprotein A3
HTN	Histone tyrosine nitration
IPA	Ingenuity Pathway Analysis
IHC	Immunohistochemistry
iNOS	Inducible nitric oxide synthase
iTRAQ	Isobaric tags for relative and absolute quantification
JAK2	Janus kinase 2
K ⁺	Potassium Ion
kD	Kilodalton
LC	Liquid chromatography
LFQ	Label-free quantitation
MALDI	Matrix-assisted laser desorption/ionization
MEOS	Microsomal ethanol-oxidizing system
Mg	Magnesium
MN	Manganese
MS	Mass spectrometer
MS ¹	Full scan mass spectrometry
MS ²	Tandem mass spectrometry
NAD ⁺ /NADH	Nicotinamide adenine dinucleotide
NASH	Non-alcoholic steatohepatitis
NCE	Normalized collision energy
NIAAA	National Institute on Alcohol Abuse and Alcoholism

NMP	N-methylpyrrolidone
NO ⁻	Nitric oxide
NQO1	NAD(P)H Quinone Dehydrogenase 1
NRF2	Nuclear factor (erythroid-derived 2)-like 2
nY	Nitrotyrosine
O ₂ ⁻	Superoxide
ONOO ⁻	Peroxynitrite
PBS	Phosphate-buffered saline
PDB	Protein data bank
PPAR α	Peroxisome proliferator-activated receptor α
PTM	Post-translational modification
PTN	Protein tyrosine nitration
QE	Q-Exactive Plus mass spectrometer
qPCR	Quantitative polymerase chain reaction
ROS	Reactive oxygen species
RNA	Ribonucleic acid
RNS	Reactive nitrogen species
RRM	RNA recognition motif domain
SEM	Standard error of the mean
SER	Smooth endoplasmic reticulum
SILAC	Stable isotope labeling by amino acids
SOD	Superoxide dismutase
TMT	Tandem mass tags
TOF	Time-of-flight mass spectrometer

TNF α	Tumor necrosis factor alpha
tRNA	Transfer RNA
UHPLC	Ultra-high performance liquid chromatography
XIC	Extracted ion chromatogram

Abstract

Alcohol liver disease (ALD) is a major health concern throughout the world. Currently, in the United States, 17 million people suffer from alcoholism, of which 1.4 million people are receiving treatment [1, 2]. The link between ethanol metabolism, reactive oxygen species (ROS) and liver injury in ALD has been well characterized over the last couple decades [3-10]. Ethanol metabolism relies on the availability of the cofactor NAD⁺ for the oxidation of ethanol into acetate, consequently causing alterations in redox potential. Redox dysfunction within the mitochondria can affect multiple pathways important in maintaining cellular homeostasis. Chapter 1 provides an introduction to the role of ethanol metabolism in oxidative stress and alcohol liver injury (ALI). During ethanol metabolism, both the cytochrome bc₁ and NADH dehydrogenase complexes within the mitochondria have been demonstrated to be major contributors to ROS formation and “leak” free radicals [11-13]. As a result, the free radicals superoxide (O₂⁻) and hydrogen peroxide (H₂O₂) is diffused into the cytoplasm where they can react with other molecules, proteins and DNA and cause tissue injury [4, 14]. Chapter 1 aims to introduce the link between ethanol metabolism and histone post-translational modifications (PTM) such as tyrosine nitration and lysine acetylation using proteomics techniques.

Chapter 2 uses a global proteomic study to identify links between gender and ALI. A 10-day chronic-binge mouse model was employed in order to identify gender-specific proteins that may influence the development of ALD. It has previously been established that females are more susceptible to developing ALD, however, the cause is still unknown. This study identifies gender differences in the family of cytochrome P450 proteins using a mouse model for chronic-binge alcohol exposure. The cytochrome P450 family of proteins are important in the metabolism of toxic compounds, such as acetaldehyde, a

byproduct of ethanol metabolism. Interestingly, I also identified that female mice expressed naturally higher levels of histone acetylation prior to alcohol exposure when compared to males. Following alcohol exposure, the female mice did not show much change in acetylation, whereas male acetylation levels were raised to similar levels of the female mice. These acetylation changes raised the question, how does alcohol influence epigenetic marks on histone proteins? Recently, new evidence has emerged that supports the role of epigenetics in the pathophysiology of ALD [4, 14-27].

Ethanol metabolism will promote shifts in redox potential and mitochondrial dysfunction, the result is the formation of reactive oxygen and/or nitrogen species (ROS/RNS) [4, 5, 7, 10, 14, 28]. As ethanol is metabolized, the accumulation of ROS/RNS species such as NO^\cdot and O_2^\cdot can induce the post-translational modification nitrotyrosine. Shifts in redox potential will cause the electron transport chain to “leak” the free radical O_2^\cdot . Another free radical known as nitric oxide (NO^\cdot) has been shown to be elevated during times of ethanol consumption [29, 30]. Traditionally, NO has a protective role within the cell at low concentrations, however, in surplus can lead to tissue damage. Ethanol-induced increases in NO^\cdot and O_2^\cdot can instigate to peroxynitrite (ONOO^\cdot) formation; a potent oxidant and nitrating agent of tyrosine residues [29, 31-34]. Chapter 3 examines the indirect effect of alcohol metabolism and ROS/RNS formation on histone tyrosine nitration. This project used mass-spectrometry to identify novel targets of histone tyrosine nitration using a mouse-model of chronic-binge alcohol exposure. Interestingly, histone H3 was found to be nitrated on the hinge-region of the N-terminal tail at tyrosine 41. Molecular dynamics of the nitrated and unmodified proteoforms revealed that the DNA prefers a change in conformation upon H3Y41 nitration. Further studies using an antibody synthesized against the nitrated H3y41 region of the protein revealed potential targets within the genome important in fatty acid synthesis and metabolism.

Chapter 4 looks at the direct influence of alcohol metabolism and its contribution to histone acetylation via acetate production and acetyl-CoA. Alcohol metabolism has traditionally been thought influence acetylation through the sirtuin family of deacetylase proteins. Sirtuin deacetylases are NAD^+ -

dependent and have been shown to regulate protein acetylation within the mitochondria, cytoplasm, and nucleus during times of ethanol exposure [35-37]. Shifts in redox potential attributed to ethanol metabolism can inhibit sirtuin deacetylase activity by out-competing the enzymes for available NAD⁺, ultimately leading to mitochondrial and nuclear hyperacetylation [17, 28, 38-42]. Currently, there is evidence that ethanol increases acetylation of histone 3 lysine 9, which then targets activation of the alcohol dehydrogenase gene (ADH) [17, 18, 43]. Moreover, Shukla *et.al.* (2008) support the idea that ethanol can alter epigenetic transcriptional activation based on which modification is selected for a site during times of stress when it can be occupied by more than one modification [22]. Chapter 4 demonstrates the use of mass-spectrometry to metabolically trace ¹³C₂-labeled ethanol *in vivo*. These new data show clear evidence of ¹³C₂ heavy-labeled ethanol being incorporated into known sites of acetylation on the N-terminal tails of histone H3 and H4. Incorporation of heavy-label was calculated using extracted ion chromatograms (XIC) for the double and singly acetylated and unmodified peptides belonging to H3K9-R17 and H3K18-R23. Total change in acetylation was also assessed for each peptide using the ratio of ratios of total acetylation to unmodified peptide over the fold change in ethanol- to control-fed groups. An interesting observation was observed in that the incorporation of heavy-label suggests site-selectivity of lysine residues over time. Histone 4 contains multiple sites of acetylation on the peptide H4K5-R17, making it hard to quantify manually. MaxQuant evidence files in conjunction with R were used to calculate the ¹³C₂ incorporation on the multiple H4 acetyl-sites over 24-hours. Ethanol-heavy label incorporation at multiple acetyl-sites occurred as a mixture suggesting a role in transcriptional regulation.

These new data establish a link between alcohol metabolism and known epigenetic marks on histone proteins. These studies have now established that alcohol metabolism is indirectly linked to histone tyrosine nitration through increased ROS/RNS and directly through acetate production. Understanding how these epigenetic marks fluctuate as ALD progresses will provide potential targets for the development of new drug therapies. The epigenetic marks identified in these studies have previously

been established to be important activators in transcription. These data provide novel techniques using proteomics-based metabolic tracing *in vivo*. Future studies will assess how these marks change after chronic ethanol exposure and whether the changes in epigenetics are heritable. Understanding hereditary of alcoholism will provide insight to those predisposed to the disease.

Chapter 1

Introduction

Pathology of Alcohol Liver Disease

Alcoholic liver disease (ALD) is the broad term given to encapsulate the multiple stages of liver damage ensued by the overconsumption of alcohol. Although preventable, ALD is currently the major contributor to liver disease in Westernized civilizations. Recently, the World Health Organization (WHO) reported that alcohol abuse contributed to over 3.3 million deaths globally, and was the 5th leading risk for premature death and disability [1, 44-46]. Alcohol consumption can be linked to over 200 diseases and injury-related ailments, which in turn results in the expenditure of hundreds of billions of dollars in healthcare-related cost annually [1]. Alone, the United States currently spends more than \$249 billion USD annually on the misuse of alcohol; of which $\frac{3}{4}$ of the cost originates from binge-drinking [1, 2]. The National Institute on Alcohol Abuse and Alcoholism (NIAAA) defines binge drinking as any pattern of drinking that raises the blood alcohol level to greater than 0.08 g/dL in a sitting, which translates into approximately 4-5 drinks in 2 hours depending on physique [2, 44, 45]. On the other hand, heavy or chronic alcohol consumption has been defined as drinking greater than 5 alcoholic beverages within the same sitting on more than 5 occasions per month (30 days) [2, 44, 45]. Alcohol dependency, whether chronic or binge, will eventually lead to alcoholic liver injury and if not corrected, and ultimately lead to steatosis, hepatitis, cirrhosis and/or cancer [2, 47-49].

The term “alcohol liver disease” is a broad term that encompasses a range of pathological conditions ranging from reversible steatosis (fatty liver) to irreversible liver scarring and tumorigenesis, termed cirrhosis. The first stage of ALD is called steatosis, also known as fatty liver, and is typically

characterized by the development of either micro- or macrovesicles of lipids within the hepatocytes (**Figure 1.1 A & B respectively**). Although micro- and macrovesicle lipid accumulation can be observed in many other liver diseases by histology, it can be differentiated in ALD by the displacement of the nucleus to the cell membrane, which is otherwise not observed in nonalcoholic steatohepatitis (NASH) [47]. Microvesicle accumulation observed during steatosis becomes more prominently expressed during periods of binge drinking with acute decomposition (**Figure 1.1A**) [47]. Following steatosis, a more severe form of injury called alcohol steatohepatitis (hepatitis) can develop, and severity can be characterized

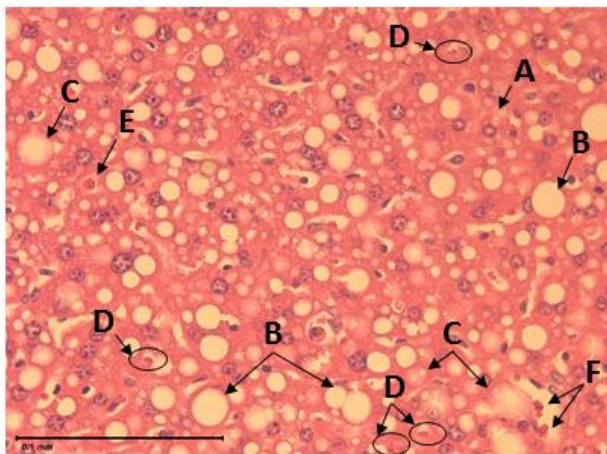


Figure 1.1: Hematoxylin-Eosin Stain of Mouse Liver Post 28-Day Chronic Ethanol Exposure. The image was taken at 40X magnification and demonstrates mild alcoholic steatohepatitis. The liver exhibits micro- (A) and macrovesicle formation (B), which can be seen in a variety of liver diseases. Degrees of alcoholic steatohepatitis are characterized by a degree of factors including the nucleus placement to the cell membrane (B), the formation of Mallory-Denk bodies (C), neutrophilic invasion (D) and acidophil formation and necrosis (E). As the disease progresses, neutrophilic invasion can be observed at sites of injury (F).

according to the number of histological features present within the liver tissue. Although there is not a clear line of distinction between steatosis and steatohepatitis (or hepatitis) when there is evidence of hepatic injury in addition to the fat vesicle deposition, typically the grading system for nonalcoholic steatohepatitis (NASH) consisting of mild, moderate, and severe can be used [47]. Because there is no clear line between steatosis and hepatitis, the general term alcoholic steatohepatitis is commonly used to describe the development of ALD. There are prominent features of liver injury seen in ALD that are not observed in NASH, which can be used to help classify the severity of alcohol steatohepatitis beyond micro- and macrovesicle formation.

Mild hepatitis consists of both micro- and macrovesicle initial formation as well as increased hepatocyte ballooning and degeneration (**Figure 1.1C**). Hepatocyte ballooning, which can resemble

macrovesicle formation, is distinguishable by the central placement of the nuclei as well as possible Mallory-Denk body formation [47]. Mild hepatitis will also include one or more of the following features at low to moderate levels. Swollen hepatocytes will begin to exhibit the presence of Mallory-Denk bodies (**Figure 1.1D**). Mallory-Denk bodies are visualized as a spindle-like formation, caused by the condensation of denatured cytokeratin filaments within the hepatocyte cytoplasm [47]. These filaments are often ubiquitinated and mark the cell for apoptosis and degradation. The liver will also begin to show signs of cell death and necrosis, marked by individual acidophil formation (**Figure 1.1E**) [47]. As the severity of liver damage increases, the neutrophil invasion will become elevated surrounding injured hepatocytes; and becomes much more prominent and concentrated in moderate to severe hepatitis than what is shown above (**Figure 1.1F**). More moderate to severe cases of hepatitis are denoted by the drastic accumulation of foamy hepatocyte degenerates, which is a foam-like appearance that is formed by the lipid, bile and pigment accumulation in the cytoplasm [50]. Hepatocytes also accumulate glycogenated nuclei and begin to show signs of sclerosing hyaline cartilage development in the centrilobular dropout region[47].

Moderate hepatitis also includes all of the aforementioned in addition to an increase in the number of apoptotic hepatocytes, also known as acidophils (or Councilman) bodies (**Figure 1.1E**) [47]. Apoptotic hepatocytes can be recognized by their shrunken size, a dense eosinophilic cytoplasm, and pyknotic nucleus [47]. The last grade and most severe stage of hepatitis include all of the above in high densities in addition to the large deposits hyaline cartilage in the centrilobular region. This marks the beginning stages of fibrosis/cirrhosis

Fibrosis is scar tissue accumulation due to the imbalance of connective tissue formation and hepatocyte degradation [47]. Fibrosis results only from alcohol abuse and is not observed in the non-alcoholic form of liver disease, making it a clear diagnostic marker. Fibrosis is irreversible and often detrimental to disease outcome because of diminished liver function due to the surplus of connective tissue, which can restrict the blood flow into lobes causing tissue death from lack of oxygen and nutrients

[47]. Fibrosis typically begins near the central vein and spiderwebs down into the lobules as the disease progresses[47].

The beginning stages of cirrhosis are recognizable by fibroid tissue banding, nodule formation and severe bridging between the central and portal veins ensued by the decrease in blood flow [47]. Cirrhosis begins with the classical accumulation of micronodules and structural deformities of the liver [47]. Once cirrhosis progresses, the fibro-connective tissue matrix is maximized and pseudo-lobule formation occurs. Although micronodules are most commonly observed, during periods of prolonged alcohol abstinence, changes in patterns between micro- and macronodules has been observed [47]. Alcoholic patients that are diagnosed with cirrhosis also increase their risk of developing hepatocellular carcinoma 5-15% [47]. Abstinence from alcohol is currently the only way to prevent cirrhosis of the liver.

Ethanol Metabolism

Oxidative Ethanol Metabolism

The pathogenesis of alcoholic liver disease (ALD) depends on an array of factors, with only a minority of heavy drinkers actually developing fibrosis/cirrhosis of the liver [47-49, 51]. Once ethanol is ingested, the body begins the first-pass metabolism in the stomach. First, pass metabolism encompasses gastric emptying and hepatic metabolism, and 20% of ethanol metabolism is estimated to occur in this phase [52-59]. Although there is much debate about the relative contribution of gastric over hepatic metabolism, both pathways depend on the rate of gastric emptying and the availability of their resident alcohol metabolite [52-60]. Gastric metabolism is said to only account for a small percentage (<20%) of ethanol metabolism due to the fact most of the ethanol is absorbed by the jejunum within the small intestine and delivered to the liver through the portal vein where hepatic metabolism is initiated [51, 57, 58]. Hepatic metabolism is understood to be the primary mode of ethanol metabolism, largely because of the availability of the metabolite alcohol dehydrogenase (ADH) that is found in the liver. The liver is a

profound organ consisting of many metabolites, which are able to metabolize many compounds and drugs efficiently, such as xenobiotics and steroids, as well as regulate the oxidization of alcohol and fatty acids [57]. Hepatic metabolism of ethanol is an oxidative process that is catalyzed by one [or more] of the 3 pathways within the liver. The three separate pathways consist of the catalase pathway, alcohol dehydrogenase (ADH), and microsomal ethanol oxidizing system (MEOS) (**Figure 1.2**) [61]. The pathway utilized to metabolize ethanol is largely dependent on the availability of the metabolite as well as the quantity and duration of ethanol exposure. Once the ethanol is absorbed and metabolized by the liver it enters circulation as the metabolite acetate, where it can be delivered to other organs in the body as energy or excreted as waste [57, 58].

The ADH pathway is currently the most extensively characterized pathway in hepatic metabolism, and it primarily takes place in the cytosol of the cell [9, 10, 51, 54-56, 59, 60, 62-66]. Two alcohol dehydrogenase isozymes combine in order to form a dimer with an average molecular weight of 80 kD. There are 5 total classes of ADH isozymes, each class results in a unique hybridization of isozymes that will allow for ADH optimization [58, 59]. Upon dimerization, the different combinations of subunits allow for activation of ADH and kinetic optimization [58, 59]. Only 4 of the 5 classes are found in the liver, they are class I-III and V. Class IV or ADH7 consists of μ & σ subunits and is found in the stomach, esophagus, and mucosal linings [58, 59]. All Class I isozymes are all present in the liver and each possesses their own unique subunit; ADH1 (α), ADH2 (β_{1-3}) (liver and lung), and ADH3 (γ_{1-2}) (liver and stomach). During ethanol metabolism ADH1 is thought to be the key factor in protecting a cell from acetaldehyde toxicity [57-59]. The ADH class II of proteins consists of ADH4 (π) and is found both in the liver and the cornea. ADH4 found within the liver is primarily located within mitochondria of the hepatocyte, ADH4 is the primary barrier to the intracellular toxic build-up of acetaldehyde [57, 58]. Class III consists of ADH5 (χ); ADH5 is found in most tissues types including the brain, however, it does not take part in the oxidation of ethanol due to its low affinity for the substrate [57, 58]. The last class of ADH isozymes is class V and consists only

of the ADH6 isoform. ADH6 is found in the liver and stomach, and currently little is known regarding its role in ethanol metabolism. Ethanol metabolism of mild to moderate consumption (1-7 drinks/week) occurs mostly through class I ADH proteins, however, class II & IV play a significant role during times of greater alcohol consumption [57, 58].

Ethanol metabolism by ADH begins by catalyzing the oxidation of ethanol to acetaldehyde while at the same time reducing NAD^+ to NADH (**Figure 1.2, center**). This reaction is initiated by the binding of ADH to the coenzyme NAD^+ [66]. Next, the ADH and NAD^+ complex binds the alcohol substrate with of zinc [66]. Upon forming a complex with zinc a series of deprotonation reactions occur on ADH, NAD^+ , and ethanol [66]. Finally, a hydride transfer from the alkoxide ion to NAD^+ takes place, this leads to the formation acetaldehyde, which is released as a byproduct [66]. Acetaldehyde is toxic when it accumulates and therefore is almost immediately oxidized into acetate where it can be used in cellular respiration. As

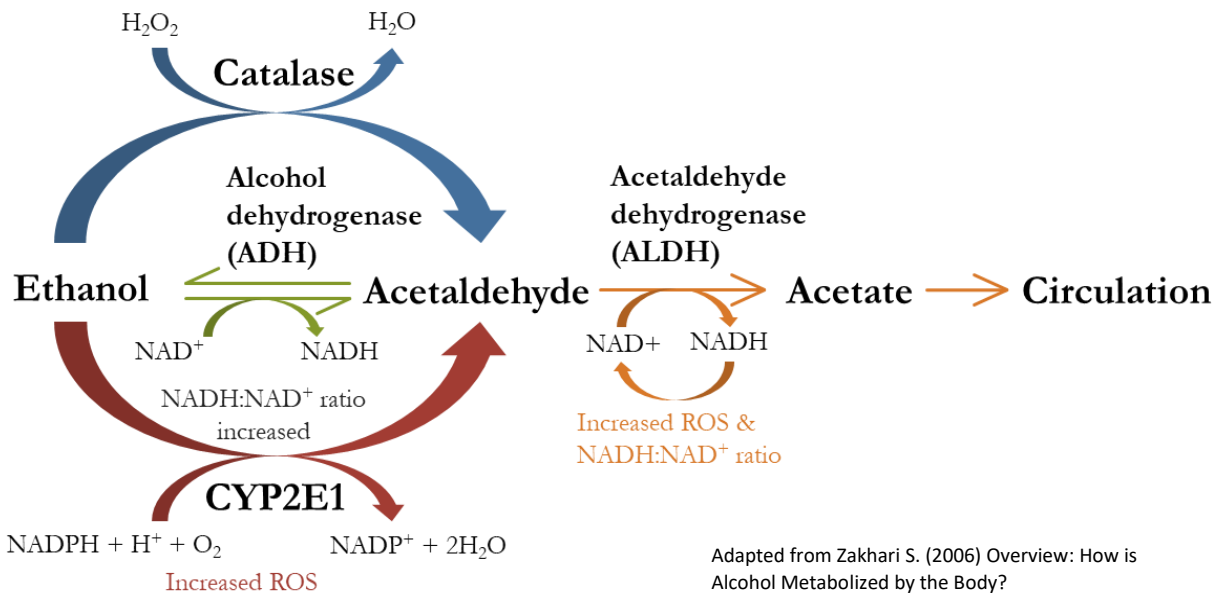


Figure 1.2: Overview of Ethanol Metabolism. Ethanol is metabolized by 1 more of the three pathways: (Center) Alcohol dehydrogenase (ADH) in the cytosol, (Bottom) Cytochrome P450 2E1 (CYP2E1) in microsomes, (Top) Catalase in peroxisomes. ADH results in increased $\text{NADH}:\text{NAD}^+$ ratios, both CYP2E1 and ADH produce increased reactive oxygen species. Catalase is shown to have no contribution to ethanol metabolism *in vivo*.

a result of the ADH pathway, there is a shortage of NAD^+ , which in turn induces mitochondrial dysfunction. In turn, the mitochondrial dysfunction leads to an increase in intracellular ROS/RNS.

The second pathway in ethanol metabolism is the microsomal ethanol oxidizing system (MEOS) [9, 52, 57, 63, 65, 67]. The MEOS pathway occurs within the smooth endoplasmic reticulum (SER) and has been the subject of extensive research in recent years [63-65, 68, 69]. When initially discovered, MEOS was thought to stem from either ADH or catalase contamination, however, it is now known to work with the Cytochrome P450 family of isozymes [64, 65, 69, 70]. The cytochrome P450's metabolize numerous types of reactions in the liver including toxic compounds, drugs, alcohol and liver byproducts [71]. Cytochrome 2E1 (CYP2E1) is the key enzyme responsible for the metabolism of ethanol in the MEOS pathway [57, 58]. CYP2E1 has a higher affinity for alcohol than most of the ADH enzymes but is only upregulated during periods of long-term exposure to large quantities of alcohol exposure [57, 58, 63, 69]. Although CYP2E1 levels can increase 4-10-fold during times of alcohol consumption, the increase in expression is transient and abstaining from alcohol greater than one-week returns CYP2E1 levels back to basal levels [57, 58]. It has been speculated that because only protein [not mRNA] levels of CYP2E1 are increased during ethanol metabolism, that degradation of CYP2E1 may somehow be inhibited [65, 72]. *CYP2E1* gene activation and mRNA stabilization have been ruled out as causes for protein upregulation during times of ethanol consumption [71, 73-76]. It is now being proposed that CYP2E1 accumulation can be attributed to protein stabilization possibly caused by changes in post-translational modifications on the protein itself, although no scientific evidence has been proposed to date [64].

Because the MEOS/CYP2E1 pathway is also important in the metabolism of xenobiotics and other drugs, alcohol metabolism may be subjected to competition for the cofactor NADPH oxidase. The main function of P450 cytochromes is to modify metabolites in order to make them easier to be excreted [71]. Other types of compounds and metabolites such as acetaminophen [77], CCL4 [78], acetone [79, 80], and N-nitrosodimethylamine (NDMA) [81] may need to be cleared from the liver at the same time that alcohol

is being metabolized [64]. Competition in metabolism may offer insight to the stalled CYP2E1 degradation observed during times of prolonged alcohol consumption.

Ethanol metabolism by CYP2E1 occurs inside a microsome. The reaction occurs when NADPH is reduced to NADP⁺, and ethanol is reduced to acetaldehyde (**Figure 1.2, bottom**). Acetaldehyde is then released as an intermediate and oxidized further into acetate. As ethanol is metabolized, available NADPH becomes depleted, and as a result, ROS/RNS are produced. The production of superoxide (O₂⁻) and hydrogen peroxide (H₂O₂) are prevalent and these free radicals are then free to move about the cell causing harm.

The last and third oxidative pathway in alcohol metabolism is the catalase pathway (**Figure 2, top**). The catalase pathway has not been shown *in vivo* to significantly contribute to ethanol metabolism under physiological conditions and therefore will not be addressed in these studies [64].

No matter which pathway is used to metabolize ethanol, the first step is to convert ethanol into acetaldehyde, which then enters the mitochondria where it is converted into the metabolite acetate. Acetaldehyde is the intermediate step in both pathways and is quickly converted into acetate and NADH to avoid toxicity. NADH can accumulate within the mitochondria and in turn, can cause dysfunction in the electron transport chain as copious amounts of acetaldehyde become oxidized. The more mitochondrial dysfunction, the more ROS/RNS is generated. Acetate derived from acetaldehyde is typically transported through the bloodstream where it is used for energy and then converted by other organs into CO₂ [82]. Acetate may also be converted into acetyl-CoA where it can be used in lipid metabolism or as an acetyl donor by acetyltransferases [82].

Ethanol Metabolism and Mitochondrial Dysfunction

Acetaldehyde production, during ethanol metabolism, is pathway independent and as a result, NADH accumulates and reactive oxygen species are generated. Ethanol is first metabolized into

acetaldehyde by ADH within the cytoplasm (**Figure 1.3**). Acetaldehyde is toxic to the cell because of its ability to modify other enzymes and proteins as well as it being a carcinogenic [57, 59, 83]. Because of the toxicity, acetaldehyde is rapidly metabolized within the mitochondria, into acetate by acetaldehyde dehydrogenase (ALDH2) using the cofactor NAD⁺. Decreased levels of the antioxidant glutathione (GSH) signify acetaldehyde adduct formation, which can lead to protein retention within the liver, hepatomegaly and many other many toxic manifestations [57]. GSH is a scavenger of toxic free radicals, and its depletion allows for acetaldehyde-induced free radical formation toxicity and lipid peroxidation [57, 64]. As a result, excess NADH found within the mitochondria and cytosol of the cell that is caused by the conversion of ethanol to acetate has been linked to hyperlactacidemia, can lead to acidosis [64]. If not rectified acidosis will then lead to secondary hyperuricemia, enhanced purine degradation and even more increases in reactive oxygen species (ROS) [64]. Increases in NADH can also inhibit fatty acid oxidation and raise the concentration of α -glycerophosphate to encourage triglyceride formation in the liver (**Figure 1.3**). Moreover, increased levels of NADH may inhibit glycolysis by blocking pyruvate formation through lactic acid accumulation [84]. As a chain reaction, the citric acid cycle is also distressed due to the unavailability of NAD. The electron transport chain is forced to use hydrogen equivalents obtained from ethanol, rather than from the oxidation of fatty acids, as the main energy source of the liver [64]. The disruption in the citric acid cycle can also promote triglyceride formation in the liver due and ultimately will promote hepatic lipogenesis [64, 84].

Acetaldehyde is next converted into acetate within the mitochondria (**Figure 1.3**). Ethanol metabolism can be assessed by quantifying the acetate levels found in the bloodstream. Acetate is very important for cell metabolism, it can travel safely throughout the bloodstream to other organs and used in the Krebs cycle to make adenosine triphosphate (ATP). Acetate is further metabolized into acetyl-CoA, where it can then enter the TCA cycle to produce energy. Acetyl-CoA is then able to donate its acetyl group to other proteins and histones with the help of acetyltransferase. In tandem, the altered redox

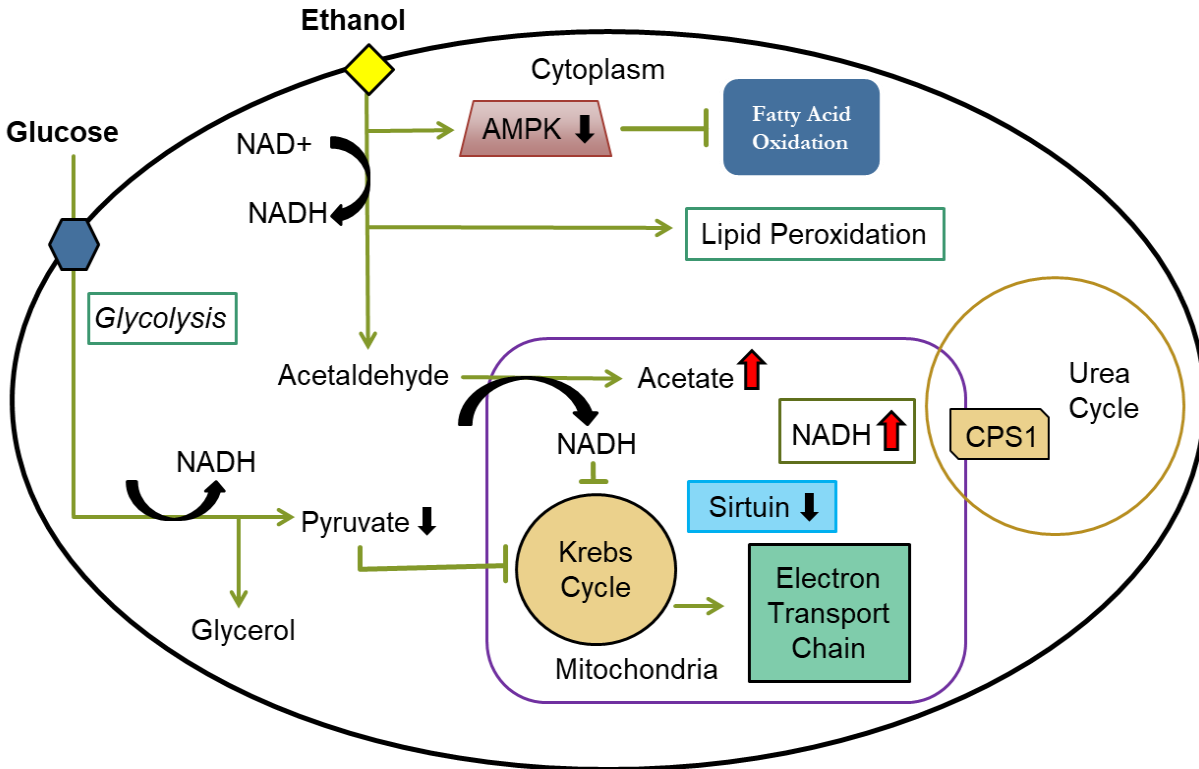


Figure 1.3: Overview of NADH: NAD⁺ Regulation during Ethanol Metabolism. Ethanol metabolism affects numerous pathways within the cell. The metabolism of ethanol relies on a large amount of NADH, which it uses from the available stocks required to maintain cellular homeostasis. Ethanol causes dysfunction in glycolysis, as well as the Krebs cycle and electron transport chain. Disruption in mitochondria homeostasis can cause dysfunction in protein regulation such as a decrease in sirtuin deacetylase. Down regulation in deacetylase activity can further disrupt protein expression via hyperacetylation (i.e. CPS1 and histone proteins).

state promotes hyperacetylation throughout the cell by inhibiting deacetylase activity [85-88]. Protein acetylation is a reversible modification and has recently become recognized as a significant contributor to not only cell metabolism but also gene regulation through epigenetics [89-91]. The increased acetylation observed during ethanol metabolism may be due to inactivation of the sirtuin family of deacetylases or increased acetylation due to rising levels of acetyl-CoA (**Figure 1.3**). The sirtuin proteins are NAD-dependent deacetylase proteins that control protein expression within the cell by facilitating the removal of acetyl groups on proteins, their function is imperative in maintaining hepatic homeostasis [35-37]. It is possible that ethanol metabolism can inhibit sirtuin activity by out-competing the sirtuin enzymes for

available NAD^+ , thus resulting in increased protein acetylation and mitochondrial dysfunction following long periods of alcohol consumption (**Figure 1.3**) [38].

Ethanol Metabolism and Oxidative Stress

Ethanol consumption induces substantial amounts of ROS/RNS in the liver during its metabolism, which primarily originates from mitochondria dysfunction induced by oxidative stress. Ethanol can increase redox pressure along the electron transport chain via NADH, resulting in an even larger increase of available ROS (**Figure 1.4**) [14]. Both the cytochrome bc_1 and NADH dehydrogenase complexes within the electron transport chain have been found to be major contributors to ROS formation and “leak” free radicals during ethanol metabolism [11-13]. As a result, the free radicals, superoxide (O_2^-) and hydrogen peroxide (H_2O_2) are diffused into the cytoplasm where they can react with other molecules, proteins and

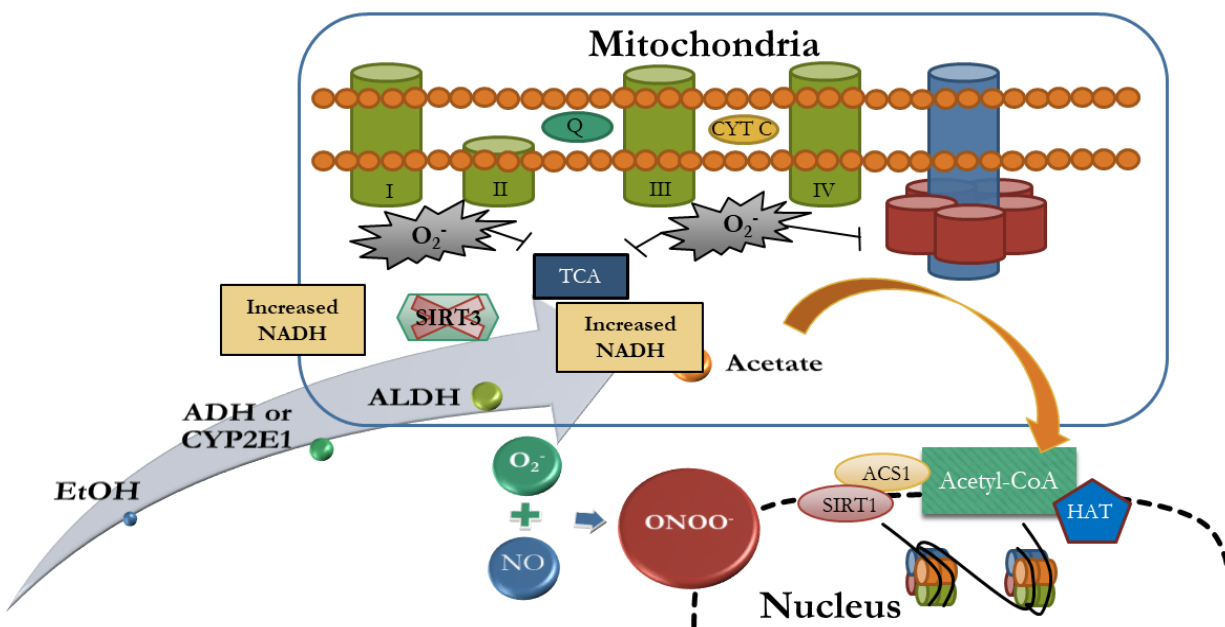


Figure 1.4: Ethanol Metabolism Induces Oxidative Stress in the Mitochondria. As ethanol (EtOH) is metabolized increased levels of acetaldehyde and NADH are produced. Acetaldehyde enters the mitochondria where it is converted into acetate. Acetate is further used in cellular respiration for acetyl-CoA production. As EtOH is broken down, levels of NADH also increases causing mitochondria dysfunction and ROS production. Increases in ROS/RNS promote the formation of peroxynitrite that can then nitrate tyrosine residues throughout the cell.

even DNA [4, 14]. Oxidative stress can have detrimental effects on homeostasis if not tightly regulated [4, 14, 92]. Recently it has been demonstrated that at high levels of ethanol (600 mM) exposure (in conjunction with the resulting increased levels of ROS), initiate high levels of BCL-2-associated X protein (BAX) recruitment to the mitochondria, ultimately leading to cell death [93]. Traditionally, during times of mitochondria dysfunction, mitochondrial fission and autophagy are activated in an ethanol concentration-dependent manner [93]. Inhibition of the autophagy pathway during ethanol-induced ROS resulted in increased mitochondrial fission and cell death [93]. However, upon autophagy pathway stimulation, the mitochondria showed signs of autophagy having a protective role in the removal of damaged mitochondria [93]. Furthermore, when high levels of BAX recruitment to the mitochondria was blocked cells treated with ethanol responded in mitochondrial fission and autophagy and not cytotoxicity [93]. Upon ROS/RNS formation the liver can activate an inflammatory response via tumor necrosis factor alpha

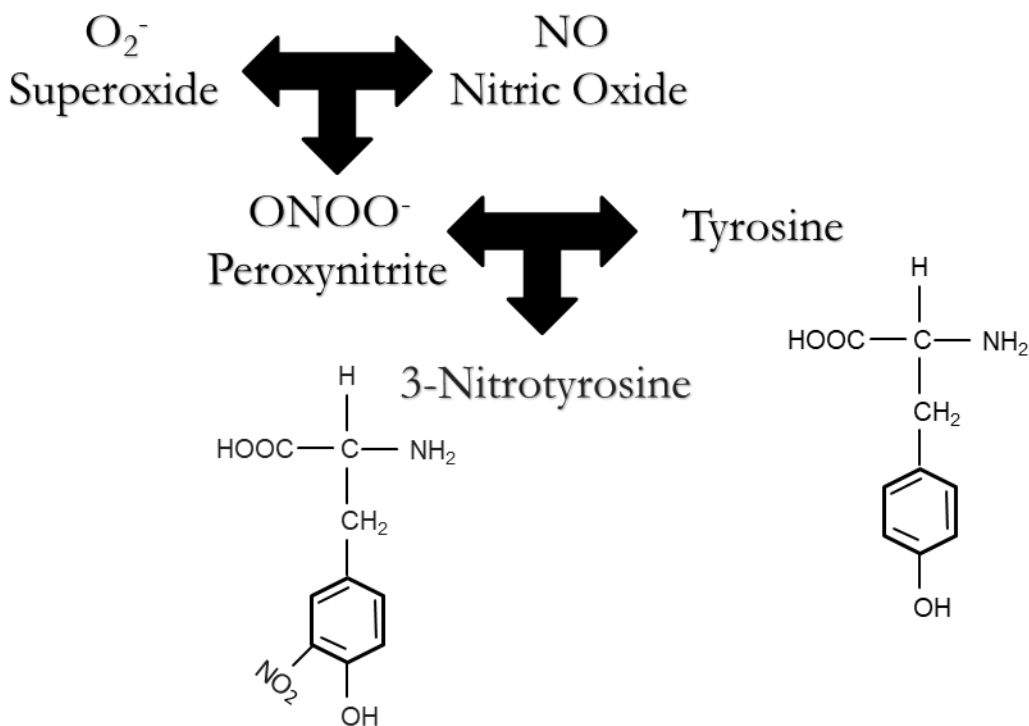


Figure 1.5: Reactive Oxygen Species, Superoxide (O_2^-) and Nitric Oxide (NO) Lead to the Formation of Nitrotyrosine (nY). When excess superoxide and nitric oxide are formed, they can react to form the highly reactive peroxynitrite. Peroxynitrite can add the post-translational modification of a nitro group to cysteine, tyrosine and threonine residues.

(TNF α). Kupffer cells, the resident immune cells of the liver, are responsible for producing an inflammatory signaling molecule, and also a free radical, nitric oxide (NO $^{\cdot}$), [94]. Generally, NO $^{\cdot}$ has a protective role at low concentrations, however, in surplus can lead to tissue damage. Nitric oxide synthase (NOS) is the protein responsible for NO $^{\cdot}$ formation. Three isoforms of NOS exist, inducible (iNOS), neuronal (nNOS), and epithelial (eNOS) and when combined with L-arginine; NO $^{\cdot}$ and L-citrulline are formed as a byproduct [30, 95]. NO $^{\cdot}$ levels have been shown to be elevated during times of ethanol consumption, which has been suggested to play a role in the onset of liver injury [29, 30]. Previous research has demonstrated that both TNF α and endotoxin receptors are involved in the development of ALI through increased levels of NO, which can combine with O $_2^{\cdot-}$ to form the powerful nitrating agent peroxynitrite (ONOO $^{\cdot}$)[94]. Recently a study showed that when iNOS was knocked out liver damage due to alcohol abuse was blunted, whereas eNOS did not have any effect on liver injury [94]. The current working hypothesis states that endotoxins are released or “leaked” from the gut as a result of alcohol consumption, activating the inflammatory response, which in turn releases ROS/RNS that can induce liver injury [94]. The reasoning for this is due in part by ethanol-induced increases in NO $^{\cdot}$ and O $_2^{\cdot-}$ that can lead to peroxynitrite (ONOO $^{\cdot}$) formation, a potent oxidant and nitrating agent of tyrosine residues (**Figure 1.5**) [29, 31-34].

Together all of these mechanisms provide a conducive environment for framing epigenetic marks on histone proteins. Altogether ethanol metabolism causes, shifts in redox potential, increased ROS/RNS, increased acetate, increased inflammatory response and when combined with decreased sirtuin activity it provides all of the components conducive to implementing changes to epigenetics [96]. It is important to understand how the molecular mechanisms of ethanol-induced changes can lead to the variation of epigenetic regulation of gene expression.

Alcohol and Epigenetics

Genetics are very important in the progression of ALD and how individual genes are controlled during ethanol metabolism need to be tightly regulated [58]. Alcohol-induced epigenetic changes prompted by liver injury have become of great interest to researchers recently. Genetics and race have previously been recognized to link the predisposition of alcoholism from epigenetic marks inherited at birth [16, 25-27]. Surprisingly, little is currently known about the mechanisms relating to alcohol-induced epigenetic changes. The term epigenetics refers to phenotypic changes within the cell, without altering the deoxyribose nucleic acid (DNA). Typically, these are transient marks or post-translational modifications (PTM) that act as activators or silencers within the genome. When a post-translational modification is added to a protein it can act as a substrate, catalyst, inhibitor as well as aid in protein folding [97]. Alcohol consumption has been shown to induce PTM changes in protein acetylation, methylation, phosphorylation, DNA hypomethylation as well as induce alterations in miRNA generation and function [15-18, 24-26, 39, 40, 96, 98]. These modifications are thought to be influenced by the increase in reactive oxygen species (ROS) and reactive nitrogen species (RNS) generated as a result of ethanol metabolism [96]. ROS and RNS are able to move throughout the cell and alter any proteins they may come into contact with, both cytoplasmic and nuclear. When ROS and RNS enter the nucleus, they are able to target histone protein tails, which are known to be important modulators of transcriptional regulation through epigenetic marks. Histone tails can be acetylated, methylated, phosphorylated and ubiquitinated just like other proteins, however, the histone tails can interplay with the DNA causing changes in gene regulation and transcriptional machinery recruitment. The study of epigenetics investigates how the various PTM combinations added to the histone proteins or DNA effect transcription [99]. Histones tails are responsible for regulating many epigenetic mechanisms; altering their post-translational modifications may result in differential gene expression and impaired recruitment of the necessary proteins needed for transcription [89-91]. Understanding the underlying mechanisms of how

alcohol metabolism influences epigenetic alterations and how those changes affect the progression of alcoholic liver disease has become an increasingly large interest in the Stevens lab as well as in other labs over the past few years. These data presented throughout show a link between alcohol consumption and epigenetics, whether by an indirect mechanism of histone tyrosine nitration via increased ROS and ONOO⁻ or directly to histone acetylation through acetyl-CoA.

Ethanol-Induced Histone Tyrosine Nitration

Protein tyrosine nitration (PTN) is a type of post-translational modification specifically induced by oxidative/nitrative stress. The role of PTN in epigenetics and alcohol liver disease is currently largely unexplored. PTN occurs when O₂⁻ generated from ethanol metabolism reacts with upregulated NO and results in the formation of peroxynitrite (ONOO⁻) (**Figure 1.5**). Peroxynitrite is a potent oxidant and nitrating agent, which is able to nitrate tyrosine, cysteine and threonine residues that it comes in contact with. PTN poses an interesting target in ethanol metabolism and epigenetics as there is now an emerging role for tyrosine phosphorylation as an epigenetic modification [100]. Specifically, tyrosine nitration may have a direct role in altering histone-mediated gene transcription processes, or indirectly by affecting histone phosphotyrosine levels that have an impact on these processes [101]. Previous work has demonstrated that protein tyrosine nitration can affect the phosphorylation status of tyrosine residues by competition (inhibition), as well as by stimulating phosphorylation events [34, 102-105]. Furthermore, it is interesting to note that selective nitration of histone proteins has been reported previously in another pathophysiological condition where Mutatect tumors showed a marked increase in tyrosine nitration on the low MW histone isoforms [106]. Bartesaghi *et. al.* (2007) describe PTN as very selective; only 1-2% out of all of the available tyrosine residues within the cell can be nitrated, and it largely depends on both the environment and the structure of the protein to be nitrated [107]. Due to the minimum amount of tyrosine residues available for nitration, the positively charged lysine, and arginine residues of the histone

N-terminal tails within the nucleosome offer promising targets for histone tyrosine nitration (HTN) during times of ethanol-induced oxidative stress [108]. This observation prompted us to ask whether tyrosine nitration on histone proteins can be an established epigenetic mark induced by ethanol, and if so, what is its biological relevance. Preliminary data from our laboratory suggest that during times of increased oxidative stress, such as binge or chronic drinking, PTN also increases. *In vivo* data presented in chapter 3 shows an increase in pan-nitrotyrosine that was localized to the nucleus after 4-weeks chronic ethanol exposure.

Definitive identification of novel nY sites *in vivo* has proven to be a difficult task for researchers to study because of the many different obstacles encountered at both the cellular and technical level. Currently, most of the available research on nY has been completed *in vitro* using synthetic peptides and peroxyntirite to initiate nitration [103, 104, 107, 109-112]. This method works well to give insight to specific tyrosine residues that can be targeted for nitration, however, there has been little to no data reproducibility due to the inability of peroxyntirite to mimic the physiological synthesis of nitric oxide by endogenous cells [31, 33, 101]. Tyrosine nitration research is also limited by the gap in knowledge pertaining to the mechanism underlining tyrosine nitration as well as the possibility for dinitrase activity. Currently, there are several reports of dinitrase activity *in vitro* but the underlying mechanism or the type of cellular environment needed for promoting dinitrase activity has yet to be elucidated [109, 113-117]. These data presented in chapter 3 focus on how ethanol metabolism and an increase in ROS indirectly affects tyrosine nitration on histone proteins. This study will identify novel sites of tyrosine nitration on histones and examine whether these sites are important regulators of transcription. Moreover, the mechanistic detail regarding the impact of oxidative stress on other histone modifications is essentially unknown. Chapter 3 investigates how ethanol-induced ROS formation influences tyrosine nitration and its possible role in the development of alcohol liver disease.

Ethanol-Induced Histone Lysine Acetylation

Lysine acetylation is a post-translational modification that has caught the attention of many scientists over the last 50 years [91]. Lysine acetylation is a reversible modification that has been implicated in many biological processes that link metabolism and cell signaling. More specifically, lysine acetylation has been shown to have roles in regulating protein interactions, as well as affecting protein activity and localization [89]. Lysine acetylation of histone proteins is a known activating mark of transcriptional regulation because of its ability to loosen the negatively charged DNA [89]. Recent studies show ethanol metabolism can affect the acetylation status of proteins, usually resulting in a hyperacetylation status of proteins. Currently, much of the research on ethanol-induced protein acetylation has occurred on mitochondrial proteins [85, 88, 118, 119]. Although the mechanism surrounding ethanol-induced hyperacetylation is poorly understood, it is thought that the hyperacetylation of mitochondrial proteins is due in part to the competition of NAD⁺ by both ethanol and the deacetylase proteins, sirtuins [38]. The sirtuin proteins are NAD⁺-dependent deacetylase proteins that regulate protein expression through deacetylating target lysine residues [35-37]. Fritz *et al.* (2013) now show that hyperacetylation of mitochondrial proteins can be induced by ethanol metabolism directly rather than a sirtuin deficiency [118].

More recently the research has shifted to understanding how ethanol-induced changes in lysine acetylation affect epigenetics through histone modifications. Park *et al.* (2003) discovered that acetylation of histone H3 lysine 9 was upregulated in hepatocytes over the course of 24 hours when treated with 50 and 100 mM ethanol [80]. Additionally, Kendrick *et al.* (2010), showed that metabolically available acetyl-CoA from acetate is vital to the increased acetylation of histones that target proinflammatory genes and consequently the proinflammatory response in ethanol-treated macrophages [120]. Most recent, Shukla *et al.* (2015) confirmed that ethanol and acetate exhibit different experimental outcomes when used to assess the metabolic effects of metabolism on hepatic gene expression [23]. The

study presented in chapter 4 identifies differences in histone acetylation following binge drinking. Also, the study aims to understand how ethanol metabolism contributes to lysine acetylation on hepatic histone N-terminal tails and what effect it has on gene regulation.

A recent link is now being established between, ethanol metabolism, oxidative stress and subsequent epigenetic modifications, such as acetylation within the liver (as well as other tissue types) triggered by ethanol exposure [20]. For example, ROS production in rat hepatocyte primary culture after ethanol exposure was shown to contribute to the known liver epigenetic marker, acetylation of histone H3 at Lys9 (H3K9Ac) [18, 43]. Histone acetylation, in particular, is regulated by the activities of various histone acetyltransferases (HATs) and histone deacetylases (HDACs) where the activities of these enzymes are altered in hepatocytes following ethanol exposure [17, 18, 23, 39, 43, 121]. Furthermore, ethanol-induced changes in histone acetylation patterns have been shown to selectively alter gene expression in rat livers while not affecting global protein expression [43]. However, the molecular mechanisms underlying ethanol-induced oxidative stress and its relationship to histone acetylation in hepatocytes are still unclear. Acetylation of the tail region of histones H3 and H4 are currently known to be transcriptional activators in numerous scenarios ranging from normal cellular homeostasis to disease progression. Chapter 4 investigates how ethanol affects histone acetylation with the help of acetyl-CoA and histone acetyltransferases.

Currently, the details regarding the impact of alcohol-induced oxidative stress on histone modifications are essentially unknown. The conclusion of these studies will identify how ethanol metabolism contributes to epigenetic modifications on histone tails. The focus of the following chapters is to identify the role of ethanol metabolism and its ability to influence changes in PTM's, more specifically the epigenetics of histone proteins. Increases in ROS indirectly affects tyrosine nitration on histone proteins most likely by the formation of ONOO⁻. The following studies will identify and validate novel sites of tyrosine nitration on histones and further examine whether these sites are important regulators of

transcription. They will also investigate how ethanol-induced acetate formation influences histone acetylation through the formation of acetyl-CoA and use of histone acetyltransferase.

Epigenetics and Proteomics

Overview of Mass Spectrometry

Over the past decade, liquid chromatography and mass spectrometry-based technology have greatly advanced. Liquid chromatography (LC), has transitioned over the years through high-pressure liquid chromatography (HPLC) into ultra-high performance (UHPLC) technology by using smaller particles in conjunction with higher pressure [122]. This allows for better binding, separation, and elution of peptides as they flow through the column. Peptide separation techniques and sensitivity levels have reached new levels of speed and resolution to complement the increasing sensitivity and selectivity of mass spectrometers. There are numerous methods of data collection that can be used in order to obtain good separation of complex samples and optimize results [123]. The methodology primarily used in the following studies applied reversed-phased UHPLC-MS in conjunction with a top-10 data-dependent acquisition (DDA) method. UHPLC has two primary functions, reduce sample complexity and enhance the peptide concentration before entering the mass analyzer [124]. In reversed-phase liquid chromatography, samples are bound by hydrophobic forces and released during a mobile phase of increasing organic solvent. Eluted peptides are ionized as they come off the column and enter the mass analyzer. Mass spectrometers consist of 3 major parts, the ion source, the mass analyzer, and the detector (**Figure 1.6**) [124]. The ion source creates the ions, either by electrospray ionization (ESI) or matrix-assisted laser desorption/ionization (MALDI). Currently, the most commonly employed mass analyzers are the time-of-flight (TOF), quadrupole, ion trap, Orbitrap, and Fourier transform (FT) ion cyclotron resonance [125]. The detector, electron multipliers as an example, detect signals and then converts them into a spectrum and then the intensity of each peak is recorded as relative abundance.



Figure 1.6: General Overview of LC-MS Analysis. Sample is resuspended in HPLC-H₂O and loaded onto the LC where it will bind the separation column. As organic solvent is increased, the peptides eluting off the column will be ionized into the gas phase. The mass analyzer will next separate the precursor ions on mass to charge. In tandem MS, the precursor ions can then be further fragmented by CID into daughter ions. The detectors calculates the number of ions for each peptides and the computer records the data as relative abundance and/or intensities.

The following experiments utilized UHPLC and Q-Exactive Plus mass spectrometer (Thermo Fisher Scientific). The Q-Exactive Plus (QE) is a hybrid high-resolution mass spectrometer (MS) designed using ESI technology and 2 mass analyzers, the quadrupole, and the Orbitrap, which provides more enhanced peptide selectivity and tandem MS sensitivity. The first mass analyzer in the QE Plus is the quadrupole, and it functions to isolate the most abundant precursor ions, as designated by the method, to send into the 2nd mass analyzer, an Orbitrap where the ions cycle the Orbitrap at different frequencies while oscillating across the horizontal axis where the current is recorded and converted into mass spectrum using the Fourier transform function of the recorded signal. These studies predominantly used a top -10 DDA methodology, which selects the 10 most abundant precursor ions within each mass spectrum to be selected for further fragmentation by tandem MS [or MS²]. Tandem MS is a coupled with MS¹, where peptides with matching precursor ions are selected, isolated and further fragmented using collision-induced dissociation (CID) [123, 124]. CID works by the collision of a neutral gas against the peptide, resulting in either a b-ion or y-ion series. The ion series is represented as specific fragment ions generated by cleavage of the amide bonds where charge retention occurs on N- or C-terminal side of the fragment ion. When fragmented, each peptide will create a unique set of fragment ions, just like a fingerprint.

Tandem MS, is run in parallel to MS¹ and the precursor ion is selected for further fragmentation that produces daughter ions. The daughter ions can be used for *de novo* sequencing or validation of peptides by taking the difference in mass to charge (m/z) of sequential residues. Adequate sequence coverage must be obtained in order to ensure complete sequencing by *de novo* methods. For example, the N-terminal region of a peptide produces b-ions, which typically fragment into low m/z values giving them an easier likelihood of being deflected while traveling through the mass analyzer. B-ion deflection may result in minimal coverage of peptides in low m/z regions making validating and sequencing in that region difficult. Methods of validation are important to prevent misidentification of proteins. Stevens *et al* (2008) describe proper validation measures using *de novo* sequencing in order to ensure correct identification of peptides and PTM while lessening the chances of false-positives [126]. True peaks should have greater than 20% relative abundance in the given spectra, have a run in consecutive ions within a series greater than 4 ions, and exhibit conventional fragmentation patterns [126]. The validation of spectra by tandem MS has been used recently in the identification of novel sites of post-translational modifications on histone proteins (epigenetics) and was used in chapter 3 in order to validate novel targets of histone nitration. Histone PTM marks have a regulatory role in chromatin structure and functions [124]. The same DDA analysis described above can be used for histone PTM identification. Every PTM has a unique elemental composition and m/z, thus it can be considered a new amino acid. Two factors depend on efficient detection of a PTM, which are the stability and the abundance of the modification. The mass shift observed for the newly modified residue can be compared to their unmodified counterpart, however, all mass shifts come with an increased error and/or false discovery rate (FDR) [127, 128]. Computer-based algorithms, such as MaxQuant (Andromeda), MASCOT, and SEQUEST are now becoming widely used to identify and quantify PTM. These applications make it easier to identify novel PTM on previously unidentified sites, however, there are still concerns about false positives and search errors [127, 128].

Labeling Techniques in Mass Spectrometry

Numerous labeling strategies are currently being used in order to achieve better quantification of histone PTM identified by MS. N-terminal histone tails typically contain an abundance of lysine and arginine residues, which are cleaved C-terminally by trypsin prior to MS. Often this cleavage can lead to short hydrophilic peptides that cannot be retained on a column [124]. In turn, using a protein or peptide labeling system to identify relative changes in histone PTM allows for better coverage and quantitation by mass spectrometry. Stable isotope labeling by amino acids in cell culture (SILAC) has become widely used in MS and is a useful tool for *in vitro* experimentation because of the ease in quantifying changes in protein expression [129]. SILAC is typically used in cell lines that can be cultured and passaged several times to ensure complete label incorporation into the proteins. After six passages, complete label incorporation is accepted to occur. The separate treatment groups of cells are then mixed as a 1:1 ratio of heavy to light labeled peptides so they can be analyzed as an equal mixture. Recently this technique is now being applied *in vivo* using stable isotope labeled feeding chow. Chapter 4 uses a method similar in order to metabolically trace $^{13}\text{C}_2$ heavy-labeled ethanol to histone acetylation.

Although SILAC is optimal for proliferating cells, when cells are terminally differentiated such as primary hepatocytes, other chemical labeling techniques can be used instead. Chemical labeling can be completed at the peptide level using tandem mass tags (TMT), or isobaric tags for relative and absolute quantification (iTRAQ) [130]. These tags are chemically attached to lysine residues and can be used for quantitation after proteolysis. More recently, Andromeda has implemented a label-free quantitation (LFQ) option in the MaxQuant algorithm, which has both pros and cons to chemically derive labeling systems [131, 132]. Chapter 4 uses a labeling method called propionylation in order to detect and increase the hydrophobicity of N-terminal histone tails [133]. Lysine derivatization adds a propionyl group to unmodified lysine residues. Upon derivatization, smaller histone peptide fragments will become more hydrophobic and therefore will stay on the column and provide better separation. The following

experiments utilize both label-free quantitation and propionylation approaches in order to better understand how alcohol consumption alters the epigenetics of histone proteins.

Project Aims and Rational

Aim 1: Identify and characterize site-specific targets of tyrosine nitration on histone proteins regulated by ethanol exposure.

Increasing evidence suggests that epigenetic regulation through DNA methylation and histone modifications plays a major role in numerous human diseases, including alcohol liver disease (ALD) [96]. Alcohol through metabolism is a major contributor to the production and release of reactive oxygen species (ROS) and reactive nitrogen species (RNS) [4, 134-137]. Consequently, free radicals are then able to move freely throughout a cell and interact with an array of molecules and proteins causing destruction in their path [4, 5, 135-139]. Accumulation of free radicals such as nitric oxide (NO), peroxynitrite (ONOO⁻) and superoxide (O₂⁻), have the ability to oxidize the proteins they come into contact with, therefore modifying their function and altering signaling events [5, 92, 101, 135, 136, 139-142]. During normal metabolism, the antioxidant glutathione (GSH), found in the liver, acts as a reductant to keep oxidative stress within the cell minimal and close to physiological conditions [107]. Glutathione (GSH) levels drop during ethanol metabolism as a result of ROS formation, allowing ROS to accumulate even more [143-145]. When GSH levels drop, ONOO⁻ can form when the superoxide anion (O₂⁻) reacts with free nitric oxide (NO) within the cell [29, 30, 33]. Inducible nitric oxide synthase (iNOS), a signaling protein that becomes upregulated during times of inflammation, is responsible for the excess production NO [94]. When iNOS expression is knocked out in mice or blunted by the inhibitor 1400W, tyrosine nitration is minimized and liver injury is blunted [94]. Mice that were void of iNOS also exhibited no clear evidence of alcohol liver disease formation following 4-weeks of intragastric ethanol feeding [94]. These data show a suggested link between ROS, NO, and pathogenesis of ALD, this aim strives to further investigate the role of ethanol-induced tyrosine nitration on histone proteins and the role of histone nitration in the development of ALD.

Nitric oxide (NO) has a dual role in the body. NO has been demonstrated to have protective properties when expressed at endogenous levels, and harmful effects when found at higher levels [4]. Ethanol has been demonstrated to cause an increase in available NO within the cell upon activation of inflammatory modulators such as TNF α [29, 30]. Nitric oxide is found within every organ system in the body, and functions as a key signaling molecule and regulator of immune response, vasculature homeostasis and inflammation [4, 141, 146]. Furthermore, recent studies now show NO is able to contribute to the regulation of epigenetics by modifying methylation and acetylation sites on histone proteins [147-149]. However, the link between oxidative stress and subsequent epigenetic modifications in the liver (as well as other tissue types) triggered by ethanol exposure is only recently being investigated. For example, histone acetylation has become increasingly popular amongst the alcohol research community. One study determined that ROS production in rat hepatocyte primary culture following ethanol exposure was shown to contribute to the known epigenetic marker, acetylation of histone H3 at Lys9 (H3K9Ac), which has also been shown to be induced by ethanol, [18, 43]. Histone acetylation is largely regulated by the activities of various histone acetyltransferases (HATs) and histone deacetylases (HDACs) where the activities of these enzymes are altered in hepatocytes after ethanol exposure due to shifts in redox potential and increased oxidative stress [17, 18, 23, 39, 43, 121]. Furthermore, ethanol-induced changes in histone acetylation patterns have been shown to selectively alter gene expression in rat livers while not affecting global protein expression [43]. However, the molecular mechanisms underlying ethanol-induced oxidative stress and histone tyrosine nitration in hepatocytes are still unclear. Moreover, the mechanistic detail regarding the impact of histone nitration modifications is essentially unknown.

Histone tyrosine residues pose as an interesting target of nitration seeing as there is now an emerging role for tyrosine phosphorylation as an epigenetic modification [100]. Specifically, tyrosine nitration may act as a transcriptional regulator, or possibly as a negative regulator of tyrosine

phosphorylation, in turn, impacting on phosphorylation signaling processes [101]. Previous work has demonstrated that protein tyrosine nitration can affect the phosphorylation status of tyrosine residues by competitive inhibition as well as stimulating phosphorylation events, however, the effect of alcohol on tyrosine nitration and phosphorylation are unknown [34, 102-105]. Recent reports found a marked increase in tyrosine nitration on the low MW histone in Mutatect tumors, suggesting a role for histone tyrosine nitration in oncogenesis [106]. Moreover, histones pose as an interesting target of tyrosine nitration even though PTN as very selective, and only 1-5 tyrosine residues in 10,000 can be nitrated [107, 108]. The nitration of tyrosine is largely dependent on the environment and structure of the protein and histone proteins fit the criteria [107, 108]. Seeley *et al.* (2012) have previously demonstrated that tyrosine nitration was preferential when the tyrosine is bordered by basic residues or an adjacent uncharged polar residue when compared to hydrophobic and acidic residues [108]. Histones provide a positively charged environment that is lysine and arginine-rich suggesting the nucleosome would be promising for histone tyrosine nitration (HTN) during times of ethanol-induced oxidative stress [108]. This observation prompted the investigation to determine whether tyrosine nitration could occur as a post-translational modification on histone proteins and if so, whether histone tyrosine nitration is important in gene regulation. It was hypothesized that ethanol metabolism encourages selective tyrosine nitration on histone tails, which is able to influence protein recruitment necessary for transcriptional regulation and gene expression.

Aim 2: Identify ethanol-induced sites of acetylation on histone proteins and assess their effects on gene regulation during oxidative stress

Protein acetylation has very important roles throughout the cell, such as metabolic regulation, cellular signaling, transcriptional programming and more recently, epigenetics [89-91, 150]. During times of ethanol exposure, lysine acetylation has been shown to be altered in a variety of cell types and

organelles [85, 86, 88, 119, 151, 152]. Hyperacetylation is the most prominent change observed in the cell after ethanol exposure, and most frequently detected within the mitochondria [85, 86, 88, 119]. The metabolism of ethanol within the liver is largely dependent on the ratio of NADH/NAD⁺, which is essential to metabolism and can be obtained from the mitochondria and cytoplasm within the cell [9, 82, 153]. The oxidation of NADH to NAD⁺ induces oxidative stress, which in turn causes dysfunction in numerous metabolic pathways [14, 154]. Ethanol-induced oxidative stress has been demonstrated to increase lysine acetylation and alter protein regulation within the mitochondria and throughout the cell [14, 155, 156]. The increase in lysine acetylation has been attributed to the reduced availability of the cofactor NAD⁺ and, in turn, inhibiting sirtuin activity caused by the overproduction of NADH from ethanol metabolism [118]. Although ethanol exposure can lead to decreases in the activity of sirtuin 1 and 3 proteins, previous research has shown no overall changes in sirtuin protein abundance [38, 118, 157].

Post-translational modifications (PTMs), such as lysine acetylation, play important roles in protein regulation and signaling throughout the cell [158, 159]. Site-specific identification and characterization of PTMs are necessary for the understanding of their biological functions within the cell [158]. Lysine acetylation has been implicated to be one of the most important regulators of cellular processes and protein regulation [159-162]. Moreover, lysine acetylation has been shown to crosstalk with other PTMs under different environmental conditions in order to control many aspects of cellular signaling and maintain cellular homeostasis [162]. Recent studies have shifted their focus to understanding how histone lysine acetylation and their targets are affected following ethanol exposure [24, 151]. Changes in patterns of lysine acetylation of histone proteins have been attributed to a combination of the metabolism of ethanol [39], oxidative stress [163], and mitogen-activated protein kinase (MAPK) signaling pathways. Gene regulation can be altered by changes to acetylation patterns located on histone tails, including those influenced by ethanol. The mechanism underlying how ethanol contributes to alterations in acetylation patterns on histone tails has yet to be established.

One hypothesis is that during the metabolism of ethanol, free acetate levels rise, where it can then be incorporated into the acetyl-CoA pool. Acetate levels have been recorded as high as 1.4 $\mu\text{Mol}/\text{min}$ per 10^8 cells or as high as 10mM in the perfusate of rat liver [23]. Once acetate levels rise it can be converted into acetyl-CoA. Acetyl-CoA is then used by histone acetyltransferase to acetylate histone proteins [23, 120]. A recent rise in the interest of how ethanol affects epigenetics has researchers focusing on histone tails and transcriptional regulation. Acetylation of histone 3 lysine 9 (H3AcK9) induced by ethanol has been shown to be both dose and time-dependent, with notable increases occurring between 5 and 100 mM and highest acetylation occurring at 24 hours [23, 151]. Although 100 mM dose of ethanol seems high for human consumption, it is a concentration commonly observed in the serum of binge drinkers and chronic alcoholics [23]. In humans, a blood alcohol level (BAC) of approximately 0.20 g/dL would equal an approximate dose of 50mM ethanol and 100mM would be equivalent to a BAC of 0.400 g/dL. When acetate is used to mimic ethanol toxicity, doses of 1-10 mM showed a marked increase in H3K9Ac over the course of 4 hours and then plateauing until 24 hours when it begins to decrease [23]. These data were also verified in rat hepatocytes that were treated with ethanol, showing a necessity for H3K9Ac in ethanol metabolism and a possible role in liver injury [151]. Chapter 4 aims to further investigate how lysine acetylation is altered on histone proteins during times of binge alcohol consumption. It also aims to further the understanding of how alcohol metabolism regulates histone acetylation patterns over time on the N-terminal tails. It is hypothesized in Chapter 4 that ethanol influences epigenetics marks of histone acetylation on the N-terminal tails directly through ethanol metabolism via acetyl-CoA and histone acetyltransferases.

Chapter 2

Global Proteomic Analysis of Sex-Differences using a Chronic-Binge Mouse Model of Alcohol Liver Disease

Abstract

Sex differences in alcohol-induced liver injury (ALI) have previously been described in both humans and animal models of chronic ethanol exposure. Females often present with ALI to a greater extent than males; however, the exact molecular mechanisms underlying this process are still unclear. The purpose of this study utilized the 10-day chronic-binge mouse model in order to evaluate gender-specific hepatic proteome profiles in order to gain novel insight regarding protein markers and their related molecular pathways, which could account for the more severe liver injury observed in females. ALI was induced in age-matched male and female mice by administering the Lieber-DeCarli ethanol- or control-liquid diet for 10 days followed by a single bolus gavage of ethanol (5 g/kg body weight). After the conclusion of the ethanol feeding, the female mice indeed displayed a more pronounced phenotype in terms of liver injury histology, although the serum levels of alanine aminotransferase and aspartate aminotransferase, indicators of liver injury, were comparable with their ethanol-fed male mice counterparts. Liver samples were processed for mass spectrometry, and the respective analysis was completed using the MaxQuant application. Over 3,000 proteins were identified at a false discovery rate of 1% for both the protein and peptide level. Relative quantitation of protein expression showed gender differences in protein expression for ALI originating with the oxidative metabolism of ethanol. Among the proteins identified in both genders was the ethanol metabolizing enzyme CYP2E1. Interestingly, in addition to CYP2E1, the proteomic analysis identified 25 other cytochrome P450 enzymes, several of which were drastically different in fold-change expression upon a comparison between the male and

female experimental groups. Moreover, functional analysis using Ingenuity Pathway Analysis revealed sex-specific pathway alterations which included those associated with lipid metabolism, acute phase response signaling, and cellular stress response pathways. Results from this analysis have provided new information at the protein level for future mechanistic studies aimed towards the role of CYP P450 enzymes in gender-specific development of ALI. This study also suggests a role of oxidative metabolism and epigenetics as a potential target for the identification of therapeutic targets with consideration of possible sex-specific strategies for prevention or treatment of alcoholic liver disease.

Introduction

Alcoholism is a disease that affects a vast majority of the population worldwide. Alcoholism was linked to 3.3 million deaths globally in 2012, of which were 7.6% male and 4.0% female [1]. Currently, in the United States, 17 million people suffer from alcoholism, of which 1.4 million people are currently receiving direct or indirect treatment for alcohol abuse [1]. Not only is alcohol abuse a social and economic burden, it can also be linked to the progression of numerous diseases, injuries, and other related health conditions [1]. Alcohol dependency and long-term abuse will eventually lead to alcohol liver injury (ALI), steatosis, cirrhosis, and possibly cancer, all which are stages in the progression of alcoholic liver disease (ALD) [47, 51, 83, 164]. Variables such as age, race, gender and socio-economic status have all been shown to play a role in a person's susceptibility to alcohol-related health conditions and outcomes [165-167]. Although men drink twice as much as women on average and are two times more likely to die from liver disease, women are more susceptible to cancer, gastrointestinal or cardiovascular diseases, when exposed to equal or lesser amounts of alcohol [166]. Currently, the suggested mechanism for the development of ALD begins with changes in transcriptional regulation via transcription factors that are mediated by cytokine secretion and inflammatory response [47, 51, 83, 164, 165, 168-170]. Other factors that have been determined to aid in the pathogenesis of ALD include mitochondria dysfunction and decreased ATP production, altered levels of CYP2E1 and NADPH, and

increases in ROS/RNS with simultaneous decreases in antioxidants glutathione peroxidase (GPx) and superoxide dismutase (SOD) [47, 51, 83, 164, 165, 168-170]. Although the proposed mechanism is widely accepted within the scientific community, there are still major gaps in knowledge preventing a complete understanding of how ALD progresses and why some people and genders are more susceptible to liver damage than others. It is important to understand why some persons, especially females, are more prone to ALI in order to develop appropriate gender-specific therapeutic approaches.

Currently, multiple hypotheses are being pursued in the understanding of gender-specific liver injury markers and the pathogenesis of ALD. Although all three proposed mechanisms are closely related there are gaps in knowledge between them, which are all currently under investigation. The first main gap in knowledge consists of trying to find the link between sex hormones, oxidative stress, and metabolic pathways that are important in the development of ALD [171-177]. Another mechanism thought to contribute to ALD that is currently being explored examines gender differences in immune regulation [178, 179]. The inflammatory response is known to have a very active role in the pathogenesis of ALD and perhaps one gender has the advantage at regulating or suppressing the inflammatory response pathway [7, 170-172, 180, 181]. Lastly, the third gap in knowledge focuses on understanding how transcriptional regulation changes in response to alcohol metabolism and liver injury between genders [182-184]. Previous studies suggest that the answer may lie in differences between the male and female sex-hormone expression, moreover estrogen production may hold the answer to why females are subjected to a greater risk of ALI [165, 166, 180, 185-188]. These data presented here aim to contribute answers pertaining to the above gaps in knowledge. This study uses 8-week male and female mice to assess differences between male and female mice receiving the Lieber-DeCarli 10-day chronic binge alcohol liquid diet [189].

The Lieber-DeCarli ethanol diet is currently the most widely used method to study alcoholic fatty liver development [165, 190]. Although there are multiple options for the delivery of alcohol for *in vivo*

mouse experimentation that can be used effectively in order to achieve a specific phenotype of ALD, the Lieber-DeCarli liquid diet is the favorite amongst researchers. The Lieber-DeCarli liquid diet is the preferred method because of its affordability, ease of administration and reproducibility of inducing fatty liver in mice similar to what is observed in humans [165]. There are different mouse models using the Lieber-DeCarli ethanol feeding that have been well characterized to achieve different ALI phenotypes [189]. The following study used the chronic-binge ethanol diet in order to assess gender differences in the development of ALI. The chronic-binge diet is a 10-day pair feeding study done administered in 8-week mice followed with a single gavage prior to euthanasia [189]. Following the 10-day alcohol feeding, data should present to have marked increases in alanine aminotransferase (ALT) and steatosis [189]. *In vivo* experimentation is the preferred method over *in vitro* studies of ALD liver research due to the unavailability of current cell lines in possessing acceptable levels of protein expression in regards to the ALD and CYP2E1 pathways of alcohol metabolism.

More times than not, sex differences play a role in alcohol-induced liver injury (ALI) where the greater liver injury is commonly observed in female animal models of chronic ethanol exposure, which is similar to the trends observed in humans [171, 176, 186, 191, 192]. Previous work investigating these differences have shown several contributing factors including direct effects of ethanol on sex hormone levels [165, 188, 193, 194] as well as the potential pathogenic role of estrogen in terms of gut permeability, endotoxin levels and inflammatory response in the liver [15, 24, 96, 169, 170, 176, 180, 195]. Further evidence has been provided through gene expression profiling studies that showed sex differences in gene networks associated with hepatoprotection, oxidative stress and inflammation after ethanol exposure [169, 176, 180, 181, 192, 196]. These data warrant further evaluation as the efficacy of therapeutic intervention using hormone gender-based specific therapies seems plausible in the emerging era of personalized medicine. The purpose of this study was to evaluate hepatic proteome profiles in both male and female mice after a chronic-binge ethanol diet in order to gain novel insight

into protein markers and related molecular pathways that could account for sex differences observed in ALI using a mouse model of ALD.

In order to comprehensively characterize molecular pathways that are involved in ALI sex differences and furthermore, to gain novel mechanistic insight, mass spectrometry-based proteomics was used. Mass spectrometry allowed for a global protein analysis of the livers of male and female mice and data was used for the identification of numerous sex-specific differentially expressed proteins and pathways. One group of enzymes identified were the cytochrome P450 family or CYP enzyme class of proteins. Data analysis revealed that several classes and proteins included in the CYP P450 family were differentially expressed following the chronic-binge and some striking differences in fold-change were identified after the comparison between male and female pair-fed groups. In addition to differential CYP expression, differences in pathway prediction showed gender differences in lipid metabolism and oxidative stress pathways. Although the role of CYP2E1 has been studied extensively in the context of ALI [173, 174, 177, 182, 197-199], the results from this study are intriguing as the contribution of other CYP enzymes in ALI is largely unexplored. Interestingly, female mice also possessed higher levels of basal histone acetylation observed on both Histone H3 and H4 that increased at the conclusion of the study to similar levels of the pair-fed male mice. The increased acetylation of known epigenetic marks may offer insight into gender-based transcriptional regulation and ALI. These data also aim to bridge the gap between gender, oxidative stress, inflammatory response and gene regulation.

Materials and Methods

Chemicals and Reagents

All chemicals were purchased from Fisher Scientific unless otherwise specified.

Chronic-Binge Mouse Model of Alcohol Liver Disease

A mouse model of chronic plus single binge ethanol consumption (referred as a chronic-binge model) was used as previously described [189, 190]. The Leiber-DeCarli liquid diet was used for both ethanol and control-fed mice (Bio-Serv, control F1259SP, and ethanol F1258SP). Eight-week-old male and female C57BL/6 mice (Jackson Laboratories) were each divided into two dietary groups with similar weights: Control chow (n=4 males; n=4 females) and ethanol chow (n=6 males; n=6 females). All mice were first acclimated, stepwise, to the liquid control diet for 5 days prior to ethanol diet containing 5% w/v ethanol [189]. Ethanol and control pair-fed groups were fed isocaloric equivalents for 10 days, and control-fed mice received limited chow when to match ethanol-fed consumption over 10 days. For mice on an ethanol-containing diet, animal cages were placed on heating pads to maintain body temperature and prevent ethanol-induced hypothermia. Food intake was recorded daily over the course of 10-days to limit over-eating of control chow. Throughout the course of the feeding period, control mice and their ethanol-fed counterparts were observed to consume similar volumes of their diets daily. On day 11, mice in ethanol groups were gavaged a single dose of ethanol (5g/kg body weight, 20% ethanol), while mice in control groups were gavaged an isocaloric dose of dextrin maltose [189]. The gavage was performed in the early morning, and mice had access to their respective diets after the alcohol gavage. On the afternoon of day 11, the mice were euthanized 9-hour post-gavage and blood and tissue samples were collected for analysis.

The studies were approved by the Institutional Animal Care and Use Committee of University of South Florida (Appendix A).

Histological Analysis and Liver Injury Assays.

Histology.

Dissected livers were allowed to fix in 10% formalin for 24 hours. They were submitted to the Tissue Core Facility at the H. Lee Moffitt Cancer Center and Research Institute (an NCI-designated Comprehensive Cancer Center (P30-CA076292), where they were processed for histological examination by light microscopy. After formalin fixation, tissues were processed in a Leica ASP 300 processor and embedded into paraffin blocks using a Leica EG1150C embedding station. Once embedded, 4 μ m paraffin sections were cut with a Leica RM2245 rotary microtome, mounted on glass slides, and stained with hematoxylin and eosin (Hematoxylin 2, Richard-Allan Scientific #7231 and Eosin Y Richard-Allan Scientific #7111) in a Leica AutoStainer XL automatic strainer. Upon completion, the slides were mounted with a coverslip.

Serum Blood Alcohol Content, ALT & AST Liver Injury Assays.

Whole blood was separated using serum separating microtainers (BD, 365967) according to the manufacturer's instructions. Serum was then aliquoted into microplates for blood alcohol level (BAC) (Pointe Scientific, A7504-01-873), ALT and AST (Pointe Scientific, A7526, and A7561 respectively) analysis. All assays were conducted using the protocols designated by the manufacturer, read using the Powerwave II microplate spectrophotometer (Biotek) and quantified using Excel (Microsoft Office, 2013).

Sample Processing

Sample Processing for Proteomic Analysis.

Eight-week-old C57BL6 mouse liver was homogenized in lysis buffer consisting of 4% SDS, 100 mM Tris-HCl, pH 7.6, 100 mM dithiothreitol. Homogenization was followed by lysis at 95 °C for 5 minutes prior

to sonication at 20% amplitude for six 3 second bursts. Samples were spun at 17,000 x g for 5 minutes at room temperature and pellets discarded. Protein concentrations were determined using a 660 nm Protein Assay with Ionic Detergent Compatibility Reagent (Pierce). An aliquot of, 50 µg of the sample was added to a spin column containing 200 µl of 8 M Urea and buffer exchanged to 8 M Urea over subsequent spins prior to Iodoacetamide alkylation as previously described [1-3]. Post alkylation, the samples were exchanged to 50 mM ammonium bicarbonate for trypsin digestion at a ratio of 50:1 with Mass Spec Grade Trypsin/Lys-C mix (Promega, V5073). Digestion was carried out overnight in a humidified incubator at 37° C. The following day, samples were desalted using solid phase enrichment C18 columns (Waters, WAT023590). Columns were activated using 100% ACN and washed in 0.1% formic acid in H₂O before adding the peptides. Peptides were then washed 3 times with 0.1% formic acid in H₂O and eluted using 90% acetonitrile/10% H₂O/0.1% Formic Acid. Samples were concentrated in a vacuum concentrator (Thermo Fisher Scientific) and resuspended in 0.1% formic acid and HPLC-water prior to LC-MS/MS analysis on the Q-Exactive Plus mass spectrometer.

Nuclear Fractionation

Livers were thawed on ice and 50 mg of tissue was cut and placed into 2 ml PBS (Alfa Aesar, Cat. #A1107922, Fisher Scientific, Hampton, New Hampshire) and protease inhibitor cocktail (Roche, Cat. # 1183617001, Sigma Aldrich, St. Louis, Missouri). Tissues were broken down into a single cell suspension using a Dounce homogenizer with pestle A only. The whole cell lysate suspensions were placed into 50 ml conical tubes (Corning, Cat. # 430291, Fisher Scientific, Hampton, New Hampshire) and spun at 1500 rpm for 10 minutes to form a pellet. The homogenization buffer was discarded and the pellets were washed again in homogenization buffer, the spin was repeated and wash was discarded. Nuclei were isolated using a nuclear extraction buffer (homogenization buffer with the addition of 0.1% NP-40 (Thermo Scientific, Cat. # 28324, Fisher Scientific, Hampton, New Hampshire). Pellets were triturated 5-times using a wide-bore pipet tip and placed into microcentrifuge tube on ice. Nuclei were pop-spun 10 sec in a

benchtop microcentrifuge and supernatant containing the cytoplasmic fractions were discarded. Nuclei were again washed in nuclear isolation buffer and pop-spun two times. Nuclei were then washed twice with PBS to remove excess detergent. Nuclei were resuspended and lysed by sonication (30% amp, 5s on/off for 1 min) while on ice and supernatant was checked for complete DNA shearing by pipetting up and down. If DNA was present then sonication was repeated until complete lysis. Nuclear lysate was spun at 14,000 rpm for 10 minutes and the supernatant was placed into a clean microcentrifuge tube. Nuclear lysate was quantified using the BCA kit (Pierce, Cat. # 23225, Thermo Scientific, Hampton, New Hampshire).

LC-MS/MS and Statistical Analysis.

Fractions were separated on a 10 cm x 75 μ m I.D. reversed phase column packed with 5 μ m C18 material with 300 Å pore size (Thermo Fisher Scientific) using 120-minute gradients of 2-28% ACN in 0.1% formic acid. The inline mass spectrometric analysis was performed on a Q-Exactive Plus (Thermo Fisher Scientific). MS¹ scans were performed at a resolving power of 72,000, and the top 10 most abundant peaks were selected for subsequent MS/MS analysis. Raw files were processed in MaxQuant 1.4.3 employing the Andromeda search algorithm and Perseus version 1.2.0.13 against the UniProt KB reference database for *Mus musculus*. The second database of known contaminants provided with the MaxQuant suite was also employed. Constant modification of carbamidomethylation of cysteine and variable modifications of oxidized methionine and acetylated protein N-termini were used. A false discovery rate of 1% was used for peptides and proteins. A minimum peptide length of 7 amino acids was used. Razor and unique peptides were used for identification and quantification. Ethanol-treated vs. control treated protein ratios were built by dividing the median normalized expression levels for all peptides across all biological samples for a given protein in the ethanol set by the median normalized expression levels for all peptides across all biological samples for a given protein in the control set separately for males and females.

Statistical significance of quantitation values was determined using a Welch's t-test and a significance value of $p < 0.05$.

Western Blots

Samples were lysed and quantified as stated above. Each replicate was suspended in 4X Laemmli buffer and loaded onto SDS-PAGE gels in accordance with sample size and molecular weight. Precast TGX gels and protein standard were purchased from Bio-Rad for use with their semi-dry turbo transfer system. Blots were transferred to either PVDF or nitrocellulose membranes depending on the protein of interest. Blots were blocked in a 5% (wt/vol) powdered milk in PBS solution for 1 hour at room temp. Next, the blots were washed in PBS for 1 hour prior to primary antibody incubation overnight at 4°C, shaking. Primary antibodies are resuspended in a 5% BSA/PBS stock solution containing 0.5% sodium azide as a preservative. The next day blots are washed 1 hour in PBS at room temperature prior to the addition of HRP-conjugated secondary antibody. The secondary antibody is prepared in 5% milk (wt/vol) and PBS at a 1:5000 dilution. Blots were incubated in secondary antibody (cell signaling) raised against the respective primary for 1 hour at room temperature and then washed for 2 hours in PBS prior to developing. Blots were incubated for 1 minute in Western Lighting-Plus Chemiluminescent Substrate (PerkinElmer, NEL104001EA) and developed using the AI06 Imager (Amersham). Primary antibodies are as follows: all dilutions are 1:1000 and purchased from Cell Signaling Technologies unless otherwise stated; ADH1 (#5295), H3AcK9 (#9649), H3AcK14 (#7627), H3 (#4499), H4AcK12 (#13944), H4AcK16 (#13534), H4 (#2935), ACL (#13390), β -Actin (#3700), GAPDH (#5174), ACL, β -Actin, GAPDH, pan-acetyl-lysine (#9814), and CYP2E1 (#ab28146, Abcam).

IPA Analysis

Proteins found to be significant using statistical analysis in Excel were uploaded into Perseus statistical software (v.1.5.5.3, <http://www.perseus-framework.org>) for further analysis. Data was first transformed into their log 2 values for normalization. Next, the male and female replicates were grouped

together for more stringent statistical analysis. Once the replicates were grouped, data were filtered based on 70% valid values in at least one group and rows not meeting the criteria were discarded. In order to correct for missing values, imputed values were added based on the normal distribution using default settings. Data was then exported back into Excel where it was transformed back into intensities to be uploaded into IPA for network prediction analysis. Calculated fold change for each group, males, and females, were next uploaded into Ingenuity Pathway Analysis (IPA) (Redwood City, CA) for further pathway analysis.

Scaffold Protein Analysis

Raw data files were analyzed using MaxQuant proteomic software (Max-Planck Institute, <http://www.biochem.mpg.de/5111795/maxquant>) and then uploaded into scaffold proteomic software (<http://www.proteomesoftware.com>). Proteins were filtered with a 1% false discovery at both the protein and peptide level.

Results

Characterization of 10-Day Chronic-Binge and Liver Injury in Male and Female Mice

Eight-week-old male and female mice were fed the 10-day Lieber-DeCarli liquid diet according to the 10-day chronic-binge parameters previously described [189]. Following the completion of the 10-day chronic-binge feeding model, livers were extracted and visually examined for phenotypic differences associated with ALI in both male and female mice. Upon extraction, livers of ethanol-fed mice had displayed visual signs of steatosis; livers were soft, swollen, discolored and possessed white blotches when compared to their control-fed counterparts. Hematoxylin and Eosin (H&E) stain revealed more pronounced morphological changes in the ethanol-fed mice, indicative of features associated with mild to moderate hepatic steatosis in both female and males when compared to their male control-fed counterparts (**Figure 2.1**). Visually, female mice that received the ethanol diet seemed to display a greater

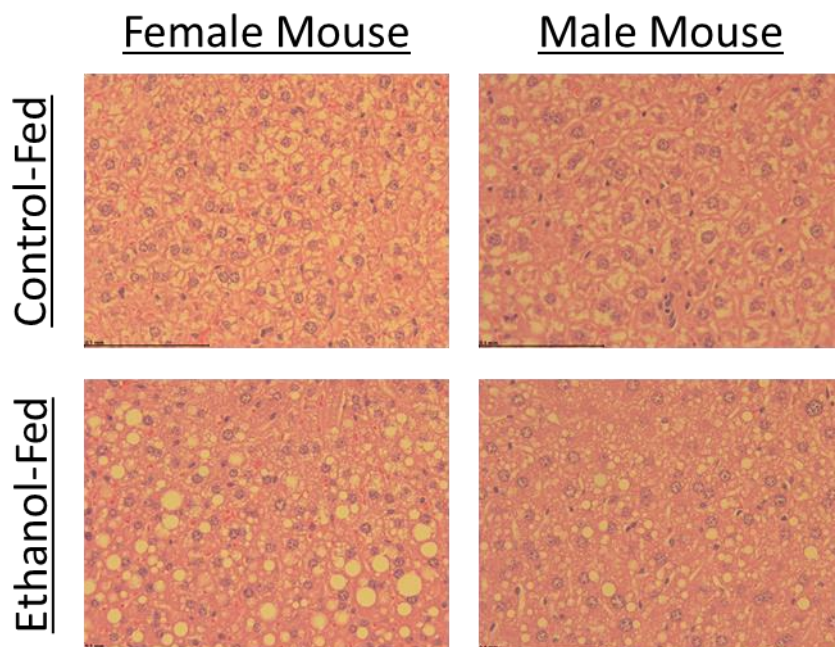


Figure 2.1: H&E Staining of Mouse Liver following the 10-day Chronic-Binge Ethanol Diet. Following the conclusion of the Leiber-DeCarli 10-day chronic-binge ethanol diet, female mice displayed a more pronounced indication of ALD after pair-feeding. These data suggest that female mice are more susceptible to pathogenesis of ALD as a result of lipid accumulation when compared to their male counterparts.

accumulation of lipids when compared to their ethanol-fed male counterparts (**Figure 2.1**). Next, serum blood alcohol levels were measured to quantify the amount of alcohol remaining in the bloodstream after the 9-hour recovery window post gavage (**Figure 2.2**). Average BAC levels were slightly higher in male mice, averaging 260 mg\dl, when compared to their female pair-fed counterparts, averaging 160 mg\dl (**Figure 2.2**). These data suggest that females exhibited faster clearance of ethanol than their male counterparts. Serum blood measurement of the liver injury markers, alanine aminotransferase (ALT) and aspartate aminotransferase (AST) were also measured and showed elevated levels in both male and female mice when compared to the control mice (**Figure 2.3**). Furthermore, although male mice exhibited higher BAC levels female mice displayed higher levels of alanine transaminase (ALT) and aspartate transaminase (AST) when compared to male mice (**Figure 2.3**). Liver enzymes, ALT, and AST are traditionally used in a clinical setting to establish hepatic injury in patients. A 2:1 ratio of AST to ALT denotes that ALI has occurred. These data show that both ALT and AST increase after the 10-day ethanol

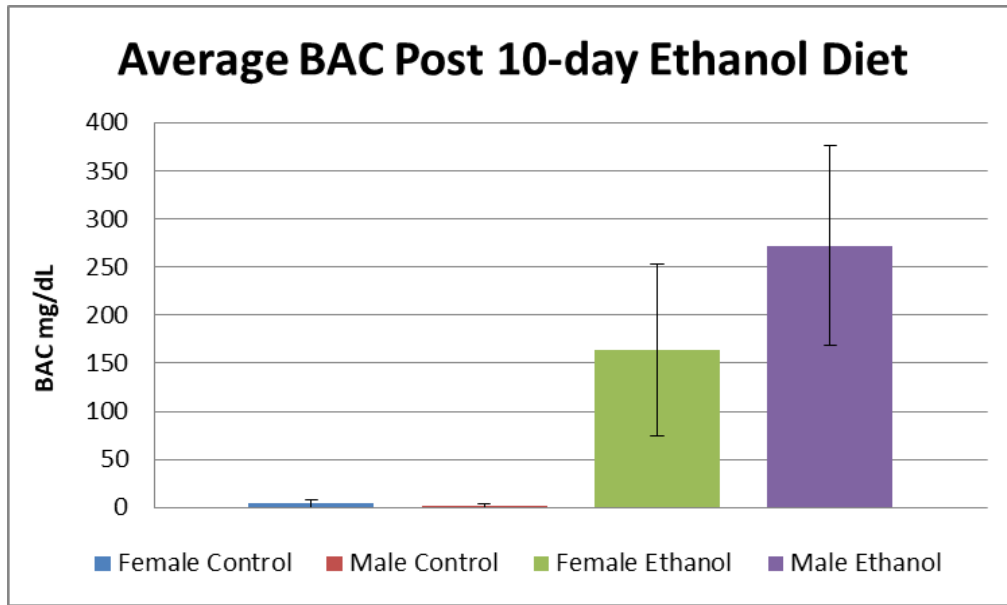


Figure 2.2: Average Serum BAC Levels Following the 10-Day Chronic-Binge Ethanol Diet in 8-Week Old Mice. Eight-week old, male and female C57bl/6 mice were administered either the control or ethanol feed over the course of 10-days followed by an isocaloric bolus gavage of either dextrin or ethanol 9-hours before euthanasia. Male mice portrayed higher serum BAC levels than their female counterparts.

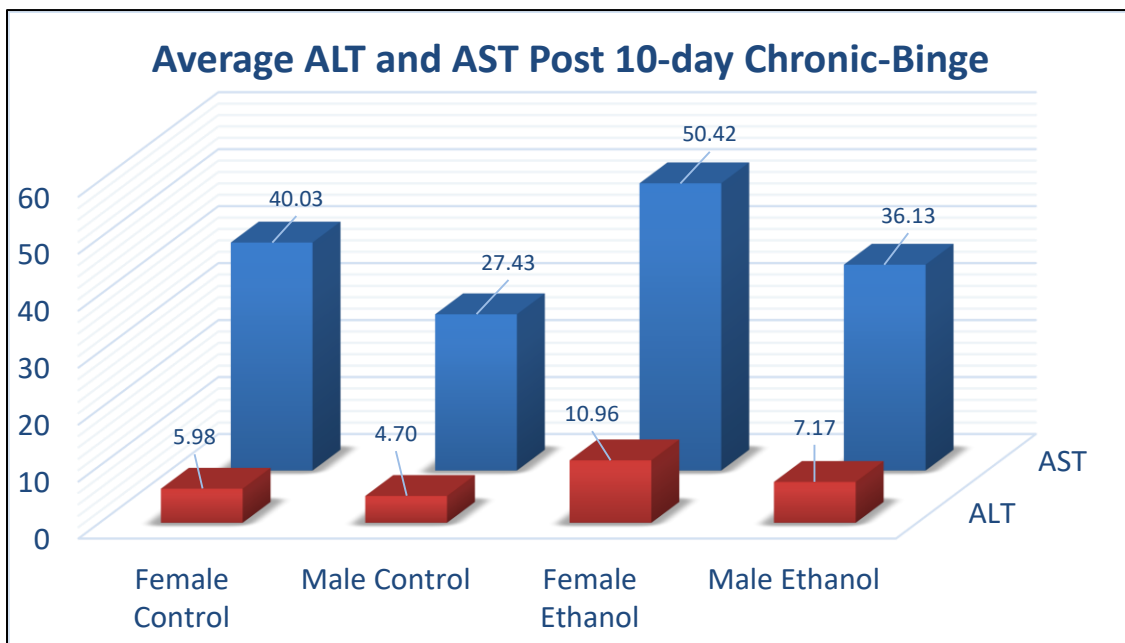


Figure 2.3: ALT and AST Liver Injury Marker Assay Following the 10-day Chronic-Binge Alcohol Diet. Serum was collected from male and female mice following the conclusion of the 10-day chronic binge ethanol diet. ALT and AST are commonly found to be upregulated during times of liver injury. Serum levels show an increase in ALT and AST in both males and females when compared to the control-fed mice. ALT values almost doubled whereas there was only a slight elevation in AST.

diet when compared to the control-fed mice. Nevertheless, the ratio of the two enzymes does not offer conclusive affirmation that ALI had occurred following the finish of the 10-day chronic binge ethanol study in mice. However, the histology data in conjunction with the BAC levels suggest that the chronic-binge ethanol diet is a good model to study gender differences in alcohol-induced liver injury (ALI).

Sex-Specific Differences in Hepatic Protein Expression Profiles After Chronic-Binge Ethanol Feeding

To further evaluate the ALI phenotype in male and female mouse liver through identification of novel pathways associated with sex differences in ALI, an innovative approach was performed using label-free quantitation and mass spectrometry-based proteomics. After mass spectrometry, analysis and database searching using MaxQuant, over 3,000 proteins were identified at a false discovery rate of 1% at both the protein and peptide level. Of these, 1,835 proteins, from both genders and treatment types, were quantified and found to be significant. Proteins from both male and female that were found to be significantly up or down regulated after ethanol exposure were uploaded into Ingenuity Pathway Analysis (IPA) in order to assess any network differences between genders. Further analysis of the ALI proteomic

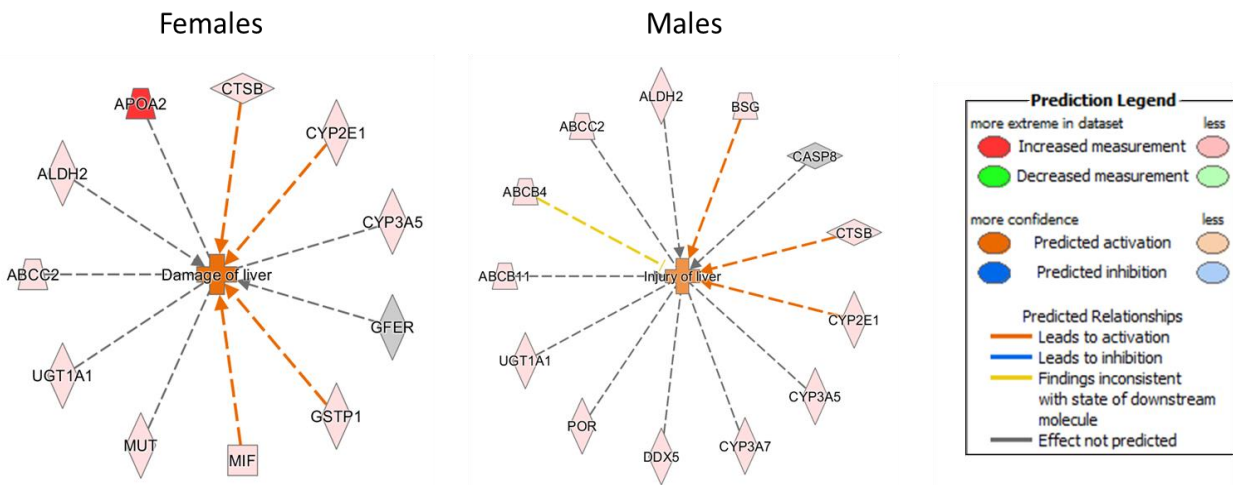


Figure 2.4: Ingenuity Pathway Analysis of Male and Female Mice Predicts Liver Damage in Females and Liver Injury in Males. Significant proteins identified in the male and female data sets from the primary analysis were uploaded into IPA for protein network interactions. IPA predicted that following the 10-day chronic binge diet in mice females were more susceptible to liver damage, whereas the male mice had more proteins upregulated commonly found in liver injury. The darker red the protein is pictured, the more it is predicted to be upregulated in the network. IPA identified proteins important in ethanol metabolism and metabolite transport and excretion.

dataset was performed and then filtered to focus on alcohol, aldehyde and CYP metabolic enzyme expression level in male and female livers after chronic-binge ethanol feeding. Interestingly, IPA pathway analysis predicted upregulation of proteins involved in liver damage in female mice, whereas male mice were only predicted to endure liver injury (**Figure 2.4**). Furthermore, male mice displayed upregulated measurements and more proteoforms in ATP-binding proteins (ABC) when compared to female mice (**Figure 2.4**). ATP-binding proteins are important in membrane transport and the uptake or exportation of molecules. Surprisingly, Apolipoprotein A2 (APOA2) was only observed in female mice and predicted to be drastically upregulated (**Figure 2.4**). These small differences in protein expression may offer potential targets to furthering the understanding in regards to why females exhibit greater liver injury over men during times of ethanol consumption.

In order to take a closer look at gender differences in liver injury, IPA was used to assess what proteins were predicted to be affected by ethanol metabolism (**Figure 2.5**). Both genders expressed similar upstream regulator predictions, however, a few genes and proteins stood out. For instance, the

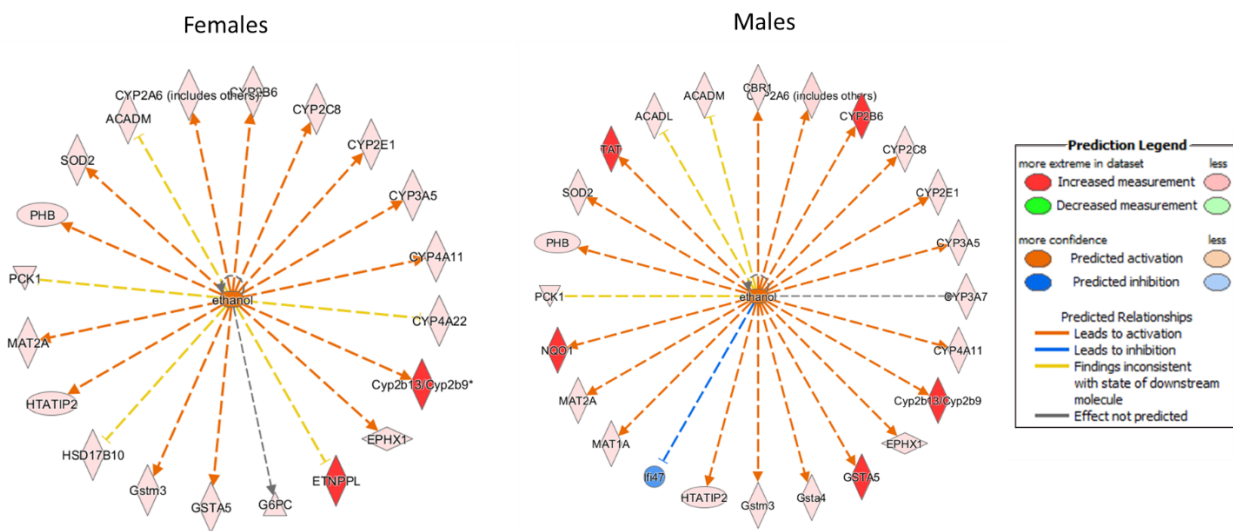


Figure 2.5: Predicted Upstream Activation Initiated by Ethanol Suggests that Cytochrome P450 Proteins amongst Others Play a Role in Liver Injury. Upstream predicted activation was found to be similar between male and female mice, however a few genes stood out. Lfi47 was predicted to be inhibited in male mice. Male mice also were predicted to have more activation of genes important in the oxidative stress pathways such as GST and NQO1. Female mice had similar predicted expression to males with the exception of ETNPPL, a protein important in the breakdown and clearance on ethanol.

gene *lfi47* predicted to be downregulated in male mice, is an interferon-inducible/regulatory gene, important in innate immunity and inflammation (**Figure 2.5, right**). The inflammatory response is an important pathway in the development of ALD and activated during times of heavy alcohol consumption and can be observed in both genders by the predicted increase in superoxide dismutase (SOD). Another interesting gene predicted to be upregulated in male mice after ethanol exposure is NAD(P)H Quinone Dehydrogenase 1 (NQO1) (**Figure 2.5, right**). NQO1 is a gene targeted by nuclear factor (erythroid-derived 2)-like 2 (NRF2) during oxidative stress. Glutathione S-transferase alpha-5 (GSTA5) is a gene important in

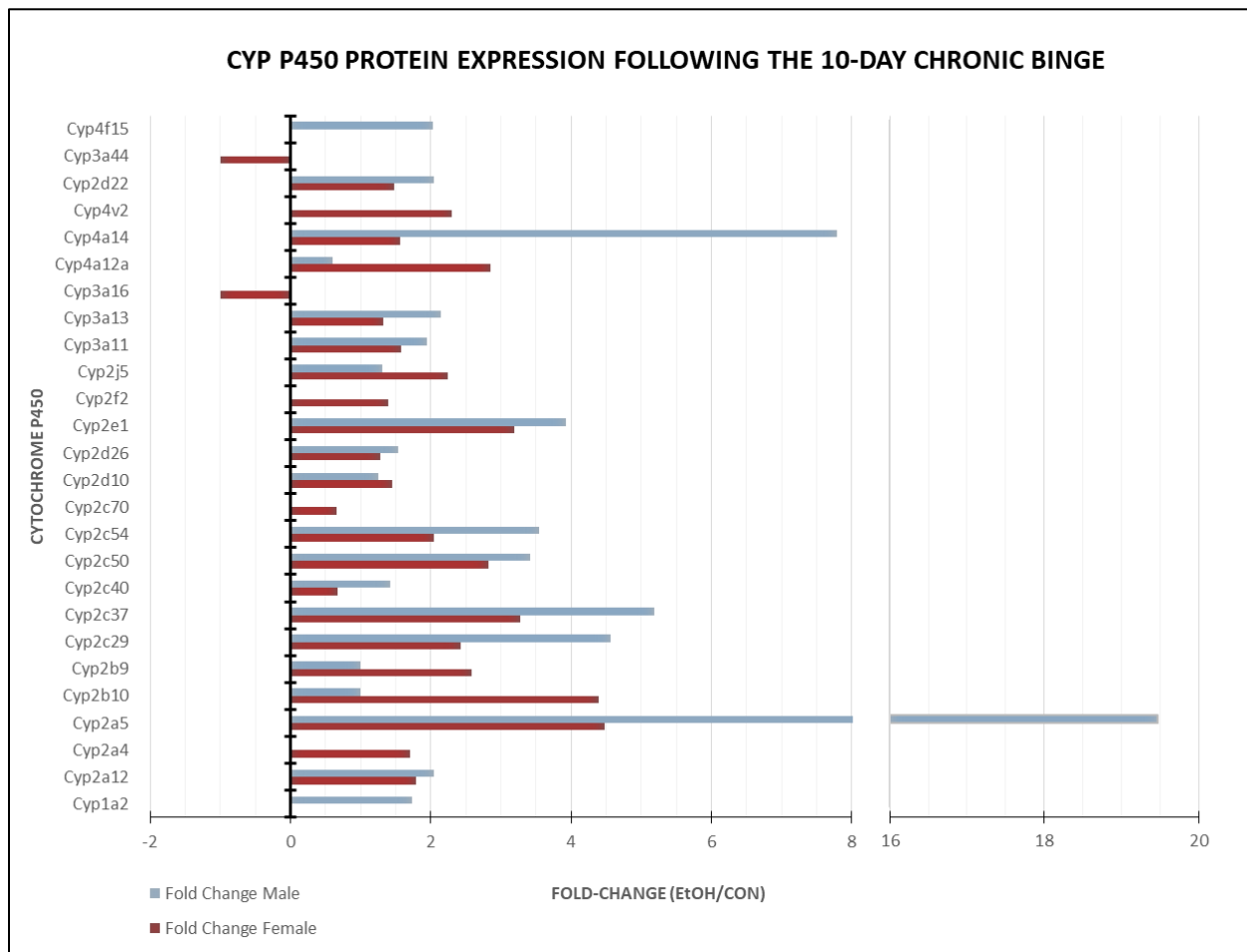


Figure 2.6: Fold-Change in Cytochrome P450 Family of Proteins Post 10-day Chronic-Binge Ethanol Diet. Cytochrome P450 proteins were quantified by taking the average intensities for control and ethanol-fed male and female mice. Next the ratio was taken for ethanol-to control-fed intensity and plotted. A fold-change of -1 represents only observed in control-fed mice and a +1 fold-change was only observed in ethanol-fed mice. If no fold-change is present for the cytochrome P450 isoform then no expression was observed for that gender and/or protein.

Table 2.1: Gender-Specific Fold-Change in Male and Female Mice

Gene Name	Fold Change Female	Fold Change Male
Cyp1a2	N/A	1.73
Cyp2a12	1.80	2.05
Cyp2a4	1.70	N/A
Cyp2a5	4.48	19.47
Cyp2b10	4.39	EtOH ONLY
Cyp2b9	2.58	EtOH ONLY
Cyp2c29	2.43	4.57
Cyp2c37	3.27	5.18
Cyp2c40	0.68	1.42
Cyp2c50	2.83	3.43
Cyp2c54	2.04	3.55
Cyp2c70	0.66	N/A
Cyp2d10	1.45	1.26
Cyp2d26	1.28	1.54
Cyp2e1	3.19	3.93
Cyp2f2	1.39	N/A
Cyp2j5	2.24	1.31
Cyp3a11	1.57	1.95
Cyp3a13	1.33	2.14
Cyp3a16	CON ONLY	N/A
Cyp4a12a	2.86	0.60
Cyp4a14	1.57	7.80
Cyp4v2	2.31	N/A
Cyp2d22	1.48	2.04
Cyp3a44	CON ONLY	N/A
Cyp4f15	N/A	2.03

the metabolism of alcohol and lipid peroxidation, it is often depleted during times of heavy drinking. These data predict upregulation in both genders, however, male mice are predicted to have increased upregulation of the GSTA5 gene over their female counterparts after the 10-day chronic binge diet (**Figure 2.5**). Furthermore, female mice were observed to have upregulation on the gene Ethanolamine-Phosphate Phospho-Lyase (ETNPPL), this gene is responsible for catalyzing the breakdown of acetaldehyde and converting phosphoethanolamine into ammonia (**Figure 2.5, left**). Another striking observation was the number of cytochrome P450 proteins that were predicted to be activated by following ethanol consumption in both genders (**Figure 2.6**). These data presented offer interesting targets of transcriptional regulation in regards to the relationship between CYP P450 proteins, metabolism, oxidative stress and gender-specific liver injury. Further evaluation of the entire ALI proteome dataset (includes proteins which are not

differentially expressed), identified 26 different CYP enzymes all having a wide range of relative protein expression as shown in **Table 2.1 & Figure 2.6**.

Cytochrome P450 proteins are found in almost every tissue within the body. Cytochrome P450 proteins function in many metabolic processes throughout the body such as hormone and cholesterol synthesis, as well as the metabolism of drugs and toxic compounds found in the liver. Further investigation

into the gene regulation of these proteins may offer insight into the understanding of gender differences in the development of ALD. As expected, CYP2E1 was found to be upregulated in both genders following the 10-day chronic binge. Interestingly, CYP2E1 was observed to have almost a fold-change difference in males when compared to females (**Table 2.1 & Figure 2.5**). In addition to the increased CYP2E1 expression in males, several other members of the Cyp P450 family were greatly increased over their female counterparts. CYP2A5 and CYP4A14 were drastically increased in the male mice exhibiting approximately a 19.5 and 8 fold increase respectively (**Table 2.1 & Figure 2.5**). Other cytochrome proteins with over a fold change difference between males and females included CYP2C29, CYP2C37, CYP2C50, CYP2C54, CYP3A13, and CYP4F15. Male mice also only exhibited expression of CYP2B10 and CYP2B9 after ethanol exposure and not in the control mice. The Cyp P450 enzymes are known to be involved in lipid metabolism (CYP4 family), and drug metabolism (CYP2 & CYP3 families). On the other hand, female mice lost CYP3A16 and CYP3A44 expression after ethanol exposure and were completely absent from male mice (**Table 2.1 & Figure 2.5**). Additionally, CYP2A4, CYP2C70, CYP2F2, and CYP4V2 were only expressed in female mice, whereas CYP1A2 and CYP4F15 were only expressed in male mice (**Table 2.1 & Figure 2.5**). CYP2J5 and CYP4A12 were the only proteins to be identified that were upregulated in female mice when compared to the male mice (**Table 2.1 & Figure 2.5**). It has been previously reported that CYP2J5 expression in the kidney is important for sex hormone regulation [194]. CYP2J5 upregulation in females was interesting because of its known role in oxidative stress, cardiac processes, lipid accumulation and estrogen regulation [200-202].

Alcohol, Oxidative Stress, and Mitochondria Dysfunction Leads to Alterations in Post-Translational Modifications on Histone Proteins

The upregulation of CYP P450, along with SOD and GST proteins observed in both genders (**Figure 2.5**) prompted further investigation into alcohol, oxidative stress, and post-translational modifications. Both SOD and GST proteins are key players in alcohol-induced oxidative/nitrosative stress and

inflammation. In addition to the gender differences in cytochrome proteins, it has been previously established that CYP2E1 sensitizes the liver to inflammation through elevated oxidative and nitrosative stress [182, 199]. Furthermore, alcohol-induced oxidative stress leads to mitochondrial dysfunction [95, 203, 204]. As a result, mitochondrial dysfunction has been demonstrated to induce changes in post-translational modifications, such as acetylation, following prolonged alcohol exposure [38, 85, 87, 118, 163, 204, 205]. In order to assess potential gender differences following ethanol exposure acetylation differences in males and females were observed using Scaffold for both whole cell lysate and nuclear fractions. Results show 30 acetylated proteins that were identified in both genders from the whole cell lysate and 13 mutually expressed proteins were observed in the nuclear fractions (**Figure 2.7**). Female mice exhibited 10 uniquely expressed proteins from their male counterparts, whereas males presented 14 unique proteins after 10-days of ethanol exposure (**Figure 2.7**). Examination of the nuclear fractions showed 8 differentially expressed proteins in females and only 3 in males (**Figure 2.7**). Table 2.2 list the differentially expressed proteins respective of gender and lysate complexity. Female mice expressed acetylation of proteins involved in metabolism and cellular stress, such as acetyl-CoA, ATP synthase,

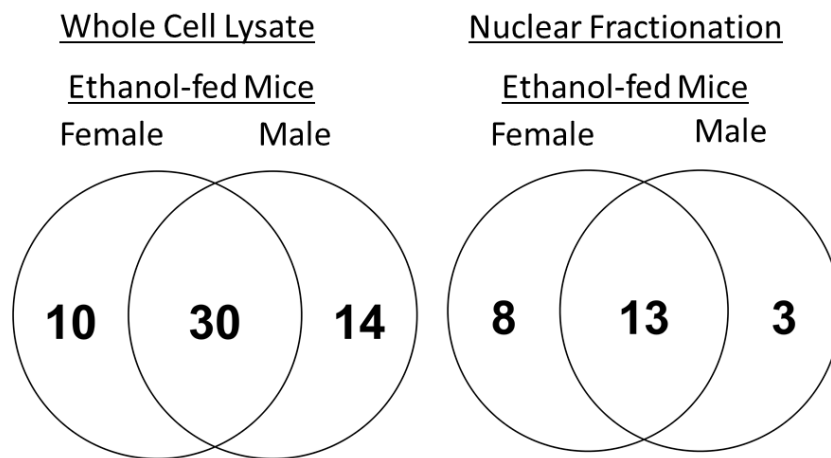


Figure 2.7: Venn-Diagram Depicting Differences in Gender-Specific Acetylated Proteins following the 10-day Chronic-Binge. Male and female mouse liver was lysed as either whole cell or nuclear fraction. Samples were analyzed using UHPLC-MS and data was processed using MaxQuant proteomic software. Analyzed data was uploaded into Scaffold and acetylation sites were assessed between male and female ethanol-fed mice.

Table 2.2: Differentially Expressed Acetylated Proteins Identified by Sex and Cellular Compartment following 10-Day Chronic-Binge, Corresponding to Figure 2.7

Female Ethanol Whole Cell Lysate	Male Ethanol Whole Cell Lysate	Female Ethanol Nuclear	Male Ethanol Nuclear
ATP synthase subunit beta, mitochondrial	Myosin-9	Heat shock cognate 71 kDa protein	Heterogeneous nuclear ribonucleoprotein U
ATP-dependent RNA helicase DDX54	Glutathione S-transferase Mu1	Microtubule-associated protein 4	HIV Tat-specific factor 1 homolog
Acetyl-CoA acetyltransferase, mitochondrial	Acetyl-coenzyme A synthetase, cytoplasmic	PC4 and SFRS1-interacting protein	Small ubiquitin-related modifier 1
GON-4-like protein	Glutathione S-transferase Mu4	Heterogeneous nuclear ribonucleoprotein A3	
Histone H4	Peptidyl-prolyl cis-trans isomerase CWC27 homolog	PC4 and SFRS1-interacting protein	
Isocitrate dehydrogenase [NADP], mitochondrial	Cholesterol 7-alpha-monooxygenase	Protein S100-A9	
Probable E3 ubiquitin-protein ligase HERC4	ADP/ATP translocase	Protein LOC102641013	
Protein NDRG2	Prostaglandin reductase 1	UPF0536 protein C12orf66 homolog	
Protein Zfp811	Transcription initiation factor TFIID subunit 13		
	Vacuolar protein sorting-associated protein		
	Glutathione S-transferase		
	Glutathione S-transferase A1		
	Glutathione S-transferase A2		

isocitrate dehydrogenase, NDRG2, and Heat shock cognate 71 (Table 2.2). On the other hand, male mice expressed changes in the acetylation of the oxidative stress regulator protein GST (Table 2.2). Other acetylated important in transcription, such as heterogeneous nuclear ribonucleoproteins were also found to have differentially expressed subunits in the nuclear fractions of both genders. Interestingly, both acetyl-CoA transferase and Histone 4 (H4) were identified to be uniquely expressed in female mice (Table 2.2). The identification of histone H4 and Acetyl-CoA prompted

further investigation into the effects of the chronic binge ethanol diet and histone acetylation.

Following the 10-day chronic-binge ethanol diet, Western blot analysis was used to evaluate gender-specific differences in proteins that are important for ethanol metabolism, as well as histones H3 and H4 acetylation. Results show, no comparable differences in alcohol dehydrogenase 1 (ADH1) in the control and ethanol-fed male and female mice (Figure 2.8A). On the other hand, CYP2E1 became

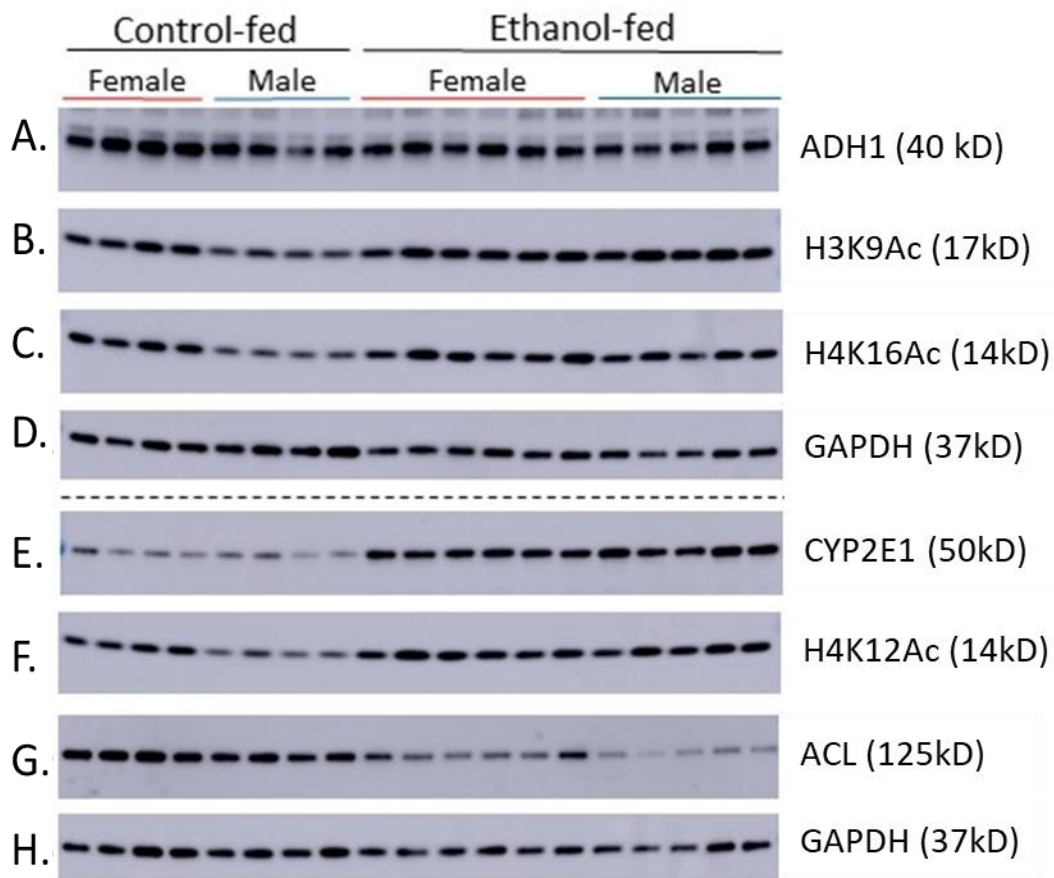


Figure 2.8: (A-H): Western Blots Obtaining from Whole Cell Liver Lysate following the 10-Day Chronic-Binge Ethanol Diet. Control-fed females (lanes 1-4) and males (lanes 5-8) are compared to their ethanol-fed counterparts (female: lanes 9-14 & males: lanes 15-20). Data is representative of 2 separate blots (dotted line) so that H3 lysine 9 and 14 & H4 lysine 12 and 16 acetylation sites would not interfere with each other's signal.

upregulated in the ethanol-fed mice in both genders following the 10-day chronic binge (**Figure 2.8E**). Both genders also displayed a decrease in ATP-citrate lyase (ACL), a protein that helps to produce acetyl-CoA, after ethanol exposure (**Figure 2.8G**). Next, acetylation on H3K9Ac, H4K12Ac and H4K16Ac was assessed and interestingly, male mice appear to have less acetylation at basal levels than their female counterparts before alcohol consumption (**Figure 2.8B, 2.8C & 2.8F**). Following alcohol exposure, the acetylation levels in the male mice rose to comparable levels of acetylation in female mice. Acetylation of H3K14Ac (data not shown) was not observed by Western blots in either control or ethanol-fed male

and female mice. These data suggest that the decrease in ACL and increase of histone acetylation in males may offer insight into a possible mechanism regarding the gender-specific alcohol-induced liver injury.

Discussion

Understanding how gender affects the development of alcohol liver disease is pivotal in finding novel mechanisms in the prevention and reversal of liver injury. Current gaps in knowledge may hold the key to further understanding which underlying mechanisms are responsible for the onset of ALI as well as the heightened liver injury observed in females. These data presented here aim to further close these gaps and broaden the understanding of novel mechanisms in the onset of ALD. Following the 10-day chronic binge ethanol diet, female mice were observed to have increased lipid accumulation over their male counterparts (**Figure 2.1**). This was interesting since the female mice also presented with higher ALT & AST levels (**Figure 2.3**) and lower serum BAC levels (**Figure 2.2**) when compared to male mice. ALT and AST are liver enzymes responsible for hepatocyte integrity, they break down amino acids and allow them to be used in the citric acid cycle [206]. The ratio of the two are typically used to predict liver injury, the higher the ratio translates into the more severe the liver injury [206-208]. Elevated levels of ALT and AST have also been linked to increased oxidative stress during times of alcohol consumption [209, 210]. Oxidative and Nitrosative stress has been linked either directly or indirectly to many pathways conducive to ALI, such as inflammation, transcriptional dysregulation, mitochondrial dysfunction and cellular respiration [3, 5, 7, 41]. These data presented gender-specific targets in ALI at both the protein and gene level that can be linked to increased oxidative/nitrosative stress.

Following the conclusion of the 10-day alcohol binge, CYP2E1 was found to be upregulated in both male and female mice (**Figures 2.4, 2.5 and 2.6**). CYP2E1 is known for its alcohol metabolizing capabilities and tend to be upregulated over ALD during longer times of alcohol exposure [71]. Interestingly, researchers are unclear to how CYP2E1 becomes upregulated because no increase in

mRNA transcript has been observed [71]. It is hypothesized that CYP2E1 accumulation stems from a PTM that blocks degradation, allowing the protein to accumulate and be available for alcohol oxidation during periods of chronic drinking. As CYP2E1 metabolizes alcohol it generates reactive oxygen species, which can accumulate and cause mitochondrial dysfunction and protein modifications, in turn altering transcriptional regulation. Identification of gender-specific novel transcriptional regulators will lead to potential targets and mechanisms responsible for gender differences in the development of ALI.

Subsequent analysis of gender differences induced directly from ethanol metabolism revealed striking differences between male and female upstream activation (**Figure 2.5**). Male mice exhibited gene activation in regards to inflammatory response and oxidative stress. Female mice, on the other hand, seemed to upregulated proteins such as ETNPPL and cytochrome P450, which are responsible for ethanol clearance and glucose metabolism instead of injury protection (**Figure 2.5**). Perhaps these upstream regulator predictions explain that females tend to exhibit liver damage, faster than males. In addition to CYP2E1, both genders portrayed numerous CYP proteins to be upregulated after ethanol exposure (**Figure 2.6**). Both genders showed similar expression for many of the identified cytochromes, however, a few were deemed to be gender selective. Both genders also displayed a marked fold-change in CYP2A5 following the 10-day chronic-binge. Females averaged a 4.5-fold change in CYP2A5 and male mice were almost five times more, averaging 19.5-fold increase. In chronic alcohol studies using CYP2A5 knock-out mice, liver injury was exuberated in the CYP2A5 null mice when compared to the wild-type pair-fed mice [211]. Males also possessed a large increase in CYP4A14, averaging 7.8-fold, whereas females only possessed a 1.5-fold change. CYP4A14 is an important regulator of fatty acid metabolism via activation by peroxisome proliferator-activated receptor alpha (PPAR α) [212-214]. CYP4A14 has been proposed as a therapeutic target in the attenuation of liver injury after overexpression of CYP4A14 promotes liver injury [212, 213]. These data suggest a possible interplay between CYP2A5 and CYP4A14 in liver injury, where the ratio of CYP2A5 expression will protect the hepatocyte from CYP4A14 damage. Many of the

cytochrome isoforms identified have been identified to participate in oxidative stress and lipid metabolism. Cytochrome P450 proteins utilize redox reactions in order to catalyze the breakdown and export of toxins and drugs within the liver, as a result, the byproducts cause a build-up of free radical formation and oxidative stress within the cell.

Increased oxidative stress within a cell after alcohol exposure has been linked to mitochondrial dysfunction, hyperacetylation, inflammation and the formation of free radicals such as superoxide (O_2^-), peroxide (H_2O_2) and nitric oxide (NO^-) [5, 7, 8, 38, 85, 87, 88]. As oxidative stress accumulates, free radicals are able to move throughout the cell and causing damage by lipid peroxidation, protein modifications, and DNA damage [4, 5, 7, 215, 216]. Following the 10-day ethanol diet, these data identified multiple isoforms of the antioxidant GST and the inflammatory regulator SOD to be upregulated (**Figure 2.5**). These data suggest an increase in the formation of free radicals such as O_2^- , H_2O_2 , and NO^- . NO^- and O_2^- can combine further and form peroxynitrite ($ONOO^-$) [31-34, 139, 217-220]. Peroxynitrite is highly reactive and has the capability of disrupting signaling pathways by adding a nitro-PTM to tyrosine residues. Furthermore, alcohol-induced oxidative stress has been shown to induce changes in protein acetylation (**Figure 2.7 & Figure 2.8**), methylation, phosphorylation, DNA hypomethylation as well as induce alterations in miRNA generation and function [15, 18, 24, 39, 40, 98].

Surprisingly, little is currently known about direct and indirect mechanisms relating to alcohol-induced oxidative stress and epigenetic changes. Epigenetic modifications are one or more PTM added to the N-terminal region of the histone tails. These modifications can act as activators and repressors controlling differential gene expression and recruitment of transcriptional proteins [89-91]. Alcohol-induced changes in epigenetic modifications can be the result of ROS/RNS generated by ethanol metabolism or another pathway responding to liver injury. For instance, $ONOO^-$ is formed as a result of alcohol metabolism and can travel throughout the cell. Peroxynitrite can alter a wide range of proteins that it may encounter by adding a NO. One such target of $ONOO^-$ is tyrosine, which forms nitrotyrosine.

Although having a short half-life, when ONOO^- enter the nucleus, it may be able to directly target histone protein tails, forming nitrotyrosine, where it could act as a negative regulator of tyrosine phosphorylation [103]. Additionally, there are numerous reports of alcohol-induced acetylation on histone H3 lysine 9 (H3K9Ac). Nevertheless, it is still unclear whether the acetylation is caused directly by ethanol metabolism or indirectly as a response to alcohol consumption [17, 18, 43].

Chapter 3

Chronic Ethanol Exposure Induces Hepatic Histone Protein Nitration in Male Mice

Abstract

Protein tyrosine nitration (PTN) is a post-translational modification that occurs as a result of oxidative and nitrative stress within the cell. These data show for the first time that changes in site-specific histone tyrosine nitration occurs in the liver of wild-type male C57bl/6 mice after being fed the Lieber-DeCarli chronic ethanol diet for 28 days. The results from this study suggest that in addition to the other currently accepted post-translational modifications of histone proteins (ie. acetylation, methylation, ubiquitination, and phosphorylation); tyrosine nitration may also be an important regulator in gene transcription and have an active role in alcohol-induced liver injury. Histology was completed using mouse livers, sectioned from both control and ethanol-fed groups. Histology demonstrated morphological changes indicative of steatosis development in both the control and ethanol-fed groups following 28-days. The control and ethanol-fed mice were both administered with an equivalent high-fat caloric daily intake, however, more severe lipid accumulation occurred in the ethanol-fed mice when compared with the pair-fed control mice. In addition, immunohistochemical analysis was performed to assess potential changes in global protein tyrosine nitration (PTN) levels between the control and ethanol-fed mice. Immunohistochemistry revealed significant and selective nitration, localized to nuclei structures within the liver of the ethanol-fed mice. Additionally, densitometry of the nitrotyrosine stained livers revealed nitrotyrosine immunoreactivity was significantly increased ($p < 0.0001$) in the chronic ethanol-fed treatment group. In order to confirm the immunohistochemistry results, site-specific nitration identification and validation were performed using mass spectrometry-based proteomic analysis. Nuclei,

obtained from control and ethanol-fed mouse livers, were enriched using subcellular fractionation using ultra-centrifugation. Several sites of nitration were identified within the nuclear fraction, with most nitration sites occurring on the histone isoforms, as well as heterogeneous nuclear ribonucleoproteins. Positively identified nitrotyrosine sites on histones were validated using a direct infusion of a respective synthetic nitro-peptide equivalent to the histone nitrotyrosine sites identified *in vivo*. These are the first data to definitively show ethanol-induced protein nitration through site-specific identification using mass spectrometry. One nitration site identified on histone 3 tyrosine 41 (H3nY41) was interesting because of its location in the hinge region of the histone H3 tail, which is located near the DNA interface. Next, an investigation of the structural and functional consequences was conducted using molecular dynamic simulations of the nucleosome structure, in order to visualize the predicted DNA-H3 interface for both the nitrated and unmodified proteoforms of H3. The results from the simulations suggest that the nitration of H3Y41 causes the DNA to open, which may advocate a potential role of histone tyrosine nitration in chromatin remodeling and a possible role in gene regulation that are instigated in the liver after chronic ethanol exposure. In order to investigate these DNA conformational changes further, ChIP-sequencing was performed on livers obtained from ethanol-fed mice following the 28-day ethanol study. Further investigation of the H3nY41 modification using ChIP-sequencing revealed 18 novel potential targets for H3nY41 within the genome spanning 11 chromosomes. Among some of the identified targets were proteins involved with the transport of metabolites, type-2 diabetes, and cancer, making them respectable targets for further validation by qPCR. Surprisingly, 13 identified peaks were located in unannotated parts of the genome and, once these regions become known, they may provide insight into novel proteins and pathways important in the development of ALD. The results of this study are the first to identify that chronic ethanol exposure induces histone tyrosine nitration within the nucleus of the hepatocyte. Tyrosine nitration is able to modify histone tails, including H3Y41, which may influence chromatin structural changes, as well as alter transcriptional targets within genome following chronic

ethanol consumption. Further analysis of histone tyrosine nitration may provide new pathways to target for treatment approaches in the development of alcohol liver disease.

Introduction

Increasing evidence suggests that epigenetic regulation through DNA methylation and histone modifications play a major role in numerous human diseases, including alcoholic liver disease (ALD) [96]. Alcohol is known to be a major contributor to the production of reactive oxygen species (ROS) and reactive nitrogen species (RNS) during ethanol metabolism [4, 134-137]. Consequently, free radicals are then able to move freely throughout a cell and interact with an array of molecules and proteins causing destruction in their path [4, 5, 135-139]. Accumulation of free radicals such as nitric oxide (NO), and superoxide (O_2^-), are free to react with each other to form the highly reactive molecule peroxynitrite ($ONOO^-$). $ONOO^-$ is more reactive than NO and O_2^- , but all ROS have the ability to oxidize the proteins they come into contact with, therefore modifying their function and altering signaling events [5, 92, 101, 135, 136, 139-142].

During normal metabolism, glutathione (GSH) within the cell acts as a reductant to keep oxidative stress within the cell minimal under stressful conditions [107]. Glutathione (GSH) levels drop within the liver during ethanol metabolism, allowing ROS to accumulate [143-145]. When GSH levels drop, $ONOO^-$ can form when the superoxide anion (O_2^-) combines with free nitric oxide within the cell [29, 30, 33]. Inducible nitric oxide synthase (iNOS) is the protein responsible for the synthesis of NO and found to be upregulated during times of inflammation [94]. When iNOS activity is decreased in mice by the inhibitor 1400W, tyrosine nitration and liver injury are blunted following chronic ethanol exposure [94]. These data show a direct link between ROS, NO, and pathogenesis of ALD, however, this study aims to further investigate the role of ethanol-induced tyrosine nitration on histone proteins and gene regulation.

Whereas $ONOO^-$ formation is the result of the combination of NO and O_2^- , NO is naturally synthesized within in the body. Nitric oxide is often thought of as an injury marker that has a dual role within the cell and functions as a key signaling molecule and regulator of inflammation, as well as immune

and cardiovascular systems [4, 141, 146]. NO has been demonstrated to have protective properties when expressed at endogenous levels, and deleterious effects at higher levels [4]. Ethanol has previously been shown to increase free NO within the cell during times of prolonged drinking [29, 30]. Nitric oxide is found within every organ system in the body, and although its function as a key signaling molecule and regulator of immune response, vasculature homeostasis, and inflammation has been well established, its role in ethanol-induced oxidative stress and epigenetic modulation in the development of ALD is still unclear [4, 141, 146].

Currently, an interesting link is now being established between oxidative stress and subsequent epigenetic modifications in the liver (as well as other tissue types) triggered by ethanol exposure [20]. Notably, NO signaling has previously been demonstrated to modulate histone hyperacetylation during cranial development as well as aid in the development of oral cancer [147, 148]. Furthermore, recent studies now show NO is able to contribute to the regulation of epigenetics by modifying methylation and acetylation sites on histone proteins [147-149]. For example, ROS production in rat hepatocyte primary culture after ethanol exposure was shown to contribute to the known epigenetic marker, acetylation of histone H3 at Lys9 (H3K9_{ac}), which is also induced by ethanol consumption [18, 43]. Histone acetylation, in particular, is regulated by the activities of various histone acetyltransferases (HATs) and histone deacetylases (HDACs) where the activities of these enzymes are altered in hepatocytes after ethanol exposure [17, 18, 23, 39, 43, 121]. Furthermore, ethanol-induced changes in histone acetylation patterns have been shown to selectively alter gene expression in rat livers while not affecting global protein expression [43]. However, the molecular mechanisms underlying ethanol-induced oxidative stress linked to histone tyrosine nitration in hepatocytes are still unclear. Moreover, the mechanistic detail regarding the impact of histone nitration modifications is essentially unknown.

Histone tyrosine nitration poses an interesting epigenetic mark as there is now an emerging role for tyrosine phosphorylation as an epigenetic modification [100]. Specifically, tyrosine nitration may have

a direct role in altering histone-mediated gene transcription processes, or indirectly by affecting histone phosphotyrosine levels that have an impact on metabolic processes [101]. Previous studies have demonstrated that protein tyrosine nitration can compete with phosphate-groups for the binding to tyrosine residues as well as trigger phosphorylation events [34, 102-105]. It is interesting to note that selective nitration of histone proteins has been reported previously in another pathophysiological condition where Mutatect tumors showed a marked increase in tyrosine nitration on the different histone isoforms [106]. Tyrosine nitration is a very selective modification, only a few tyrosine residues in 10,000 can be nitrated, and it largely depends on the surrounding environment and protein structure [107, 108]. Seeley *et.al.* (2012) have previously demonstrated that tyrosine nitration was preferential in a basic uncharged polar environment when compared to hydrophobic and acidic residues [108]. Due to the minimum amount of tyrosine residues available for nitration, the positive charge on lysine, and arginine residues within the nucleosome would be a promising target for histone tyrosine nitration (HTN) during times of ethanol-induced oxidative stress [108]. This prompted the hypothesis of whether tyrosine nitration could occur as a post-translational modification of histone proteins, and what is its function. To answer this question a well-established mouse model for ALD was used to induce oxidative stress in the liver of 8-week old mice [189, 190] in order to identify novel targets of histone tyrosine nitration. These data now provide clear evidence that chronic ethanol exposure will induce histone tyrosine nitration in mouse liver cells after 28-days of chronic ethanol exposure and the modification promotes conformational changes to the DNA.

Materials and Methods

Chemicals and Reagents

All chemicals and reagents were purchased from Fisher Scientific unless otherwise noted.

Experimental Design and Statistical Rational

The role of ethanol-induced oxidative stress and liver damage has previously been established [135-138, 164, 221, 222]. The 28-day chronic ethanol diet in mice was chosen for the induction of ROS because of its known similarities to the progression of ALD in humans [189]. It was determined that this model would be effective for studying the effects of ethanol-induced ROS/RNS on histone protein post-translational modifications based off of the amount of liver injury incurred. The experiment began with n= 6 control mice and n=6 ethanol-treated mice with the expectation of 50% survival in the treatment group. Since all mice were fed the same caloric restriction by pair feeding and were litter mates, it could be assumed there would be a normal distribution for the data set analysis; therefore a student t-test would be an acceptable statistical test ($p \leq 0.05$) for the following experiments.

Animals and 28-Day Leiber-DeCarli Ethanol Feeding

A mouse model of chronic-ethanol consumption was used as previously described [189, 190]. The 28-day Leiber-DeCarli liquid chronic ethanol diet was employed for both ethanol and control fed mice. Eight-week-old male C57BL/6J mice were each divided into two dietary groups; control (n=6 males) and ethanol (n=6 males). Both the control and ethanol liquid diets provided equal caloric distributions between groups. Liquid diets (Bio-Serv) were freshly prepared from powder daily, and all mice were first acclimated, stepwise, to a liquid control diet for 5 days. Ethanol groups were then fed a liquid diet containing 5% w/v ethanol for 28-days, while control mice received an equal volume of high-fat diet to mimic the calories obtained from alcohol. Control mice were pair-fed to their ethanol-fed counterparts for 28-days and diets were measured daily. Control diets were limited as needed as not to exceed the consumption volume of their pair-fed ethanol mouse. Mice receiving the ethanol diet were housed on top of heating pads to maintain body temperature and prevent ethanol-induced hypothermia. On the morning of the 29th day, the mice were euthanized and blood and liver samples were collected. The studies were approved by the Institutional Animal Care and Use Committee of the University of South Florida.

Liver Histology, IHC and Densitometry Analysis of Nitrotyrosine Staining.

Histology and immunohistochemistry (IHC) were completed by the H. Lee Moffitt Cancer Center Tissue Core Facility. Dissected livers were allowed to fix in 10% formalin for 24 hours. They were submitted to the Tissue Core Facility at the H. Lee Moffitt Cancer Center and Research Institute (an NCI-designated Comprehensive Cancer Center (P30-CA076292), where they were processed for histological examination by light microscopy. After formalin fixation, tissues were processed in a Leica ASP 300 processor and embedded into paraffin blocks using a Leica EG1150C embedding station. Once embedded, 4 μm paraffin sections were cut with a Leica RM2245 rotary microtome, mounted on glass slides, and stained with hematoxylin and eosin (H&E) (Hematoxylin 2, Richard-Allan Scientific #7231 and Eosin Y Richard-Allan Scientific #7111) in a Leica AutoStainer XL automatic stainer. Upon completion, the slides were mounted with a coverslip. The expression of nitrotyrosine in mouse liver was assessed by immunohistochemical staining (IHC) using a Ventana Discovery XT automated system (Ventana Medical Systems, Tucson, AZ) as per manufacturer's protocol with proprietary reagents. The slides were briefly deparaffinized on the automated system with EZ Prep solution (Ventana). Cell conditioning followed by incubation at 100°C for 24 min was conducted for antigen retrieval. The rabbit primary antibody that reacts to nitrotyrosine, (#A-21285, Life Technologies, Grand Island, NY) were used at a 1:200 concentration in Dako antibody diluent (Carpenteria, CA) and incubated for 60 min. The slides were then incubated with the Ventana OmniMap Anti-Rabbit Secondary Antibody for 16 min for nY slides. The Ventana ChromoMap kit was used as a chromogen for detection followed by hematoxylin as the counterstain. Finally, the slides were dehydrated in 75%, 80%, 95% and 100% ethanol for 1 min each, cleared with xylene and cover slide were mounted on the slides. To quantify the amount of nitrotyrosine staining in the IHC stained mouse livers, 25 regions of interest were selected from each image (one image from each of the 6 control mouse livers, n=150; two images from different regions of each of the 3 ethanol-fed mouse livers, n=150) and the mean, minimum, and maximum pixel intensity was measured

using ImageJ. The resulting mean pixel intensities were converted into reciprocal mean pixel intensities [223] and a two-tailed Student's t-test was used to compare the reciprocal mean pixel intensities from the control and ethanol-fed groups assuming a normal distribution.

Sample Processing, Mass Spectrometry, and Data Analysis.

Nuclear Fractionation.

Individual liver samples were sectioned (~750mg) to be separated into whole cell and nuclear fractions. Livers used for whole cell lysate were homogenized in lysis buffer consisting of 4% SDS, 100 mM Tris-HCl, pH 7.6, and 100 mM dithiothreitol. Homogenization was followed by lysis at 95 °C for 5 minutes prior to sonication at 20% amplitude for six 3 second bursts. Samples were spun at 17,000xg for 5 minutes at room temperature and pellets discarded. Livers sectioned for nuclear enrichment were homogenized in 3 ml homogenization buffer (10 mM Hepes, pH 7.9, 10 mM KCl, 0.1 mM EDTA, 0.74 mM Spermidine, 1 mM DTT, 0.3 M sucrose, protease and phosphatase inhibitor cocktail (Pierce) at 9000rpm for 1.5 min. Homogenate was resuspended in 6 ml cushion buffer (10 mM Hepes, pH 7.9, 0.1 mM EDTA, 0.74 mM Spermidine, 1 mM DTT, 2.2 M sucrose, 2 µg/ml aprotinin, 2 µg/ml leupeptin) and then overlaid on 2 ml cushion buffer. Nuclei were pelleted by 1 hr centrifugation at 25000g for 1 hr at 4°C as previously described [224, 225]. The pellet was collected and lysed in lysis buffer consisting of 4% SDS, 100 mM Tris-HCl, pH 7.6, 100 mM dithiothreitol, followed by lysis at 95 °C for 5 minutes prior to sonication at 20% amplitude for six 3 second bursts. Samples were spun at 17,000xg for 5 minutes at room temperature and pellets discarded.

Protein concentrations from both groups were determined using a 660 nm Protein Assay (Pierce) supplemented with Ionic Detergent Compatibility Reagent (Pierce). Next, 30 µl of the sample was added to a Microcon-30kD spin column (Millipore) containing 200 µl of 8 M urea and buffer exchanged to 8 M urea over subsequent spins prior to iodoacetamide alkylation. Samples were allowed to alkylate for 20 min in the dark. Post alkylation, the samples were exchanged to 50 mM ammonium bicarbonate for

digestion at a ratio of 50:1 with Trypsin/Lys-C mix Mass Spec Grade (Promega). Digestion was carried out overnight in a humidified incubator at 37 ° C. The next day samples were desalted by being loaded onto a hypersep reversed phase C18 column (Thermo), washed with 0.1% formic acid in H₂O and then eluted using 90% acetonitrile/10% H₂O/0.1% formic acid. Samples were dried using a vacuum concentrator (Thermo) and resuspended in 0.1% formic acid and water prior to LC-MS/MS analysis.

LC-MS/MS

Individual samples were placed into the Easy nanoLC-1000 for separation on a NanoViper 50 cm x 75 µm I.D. reversed phase column packed with 3 µm C18 material with 100 Å pore size (Thermo) using a 120 min gradient of 2-28% ACN in 0.1% formic acid. The inline mass spectrometric analysis was performed on a Q Exactive Plus mass spectrometer (Thermo). A precursor MS scan of 350-1550 m/z was performed at a resolution of 70,000 and the top 10 most abundant peaks were selected for subsequent MS/MS analysis.

Mass spectra were first analyzed using Mascot Distiller (version 2.2.06). Parameters included a parent and fragment tolerance of 10 and 5 ppm respectively. The reference database was obtained from SwissProt, (UniProtKB, ftp://ftp.uniprot.org/pub/databases/uniprot/previous_releases/, January 2012) for *Mus musculus* containing 16428 protein entries. Mass spectra were then processed using the MaxQuant software package (version 1.5.0.30 (<http://maxquant.org>)) employing the Andromeda search algorithm against the SwissProt reference database (UniProtKB, July 2013) for *Mus musculus* containing 16615 protein entries and then repeated using reference database UP000000589 (UniProtKB, August 2015) containing 16717 protein entries. The second database of known contaminants provided with the MaxQuant suite was also employed. A minimum peptide length of 7 amino acids was used in conjunction with a maximum of 2 missed cleavages and a mass tolerance of 20 ppm. A 1% false discovery rate was used for both peptides and proteins, and nY identifications were accepted based on a localization score of >0.80 and mass error of <1 ppm. Carbamidomethylation of cysteine was applied as a constant

modification and oxidized methionine and nitrotyrosine were set as variable modifications. Upon completion, analyzed datasets were placed into Scaffold software (version 4.4.5) for retention of protein and peptide coverage and statistics.

Extracted Chromatogram Analysis

XIC analysis was completed using the precursor MS obtained from the raw data files corresponding to each animal. The area under the curve was calculated by identifying the change in retention time corresponding to the beginning of the peptide elution until no more eluted peptide was observed. The change in relative abundance between the nitrated and unmodified forms of the peptide was calculated and reported as a percent fold change in expression.

Western Blots

Samples were processed as stated above and loaded into SDS-PAGE gels in accordance with sample size and molecular weight. Precast TGX gels and protein standard were purchased from Bio-Rad (Hercules, CA) for use with their semi-dry turbo transfer machine. Blots were transferred to methanol activated PVDF membranes for Western blot analysis. Western blots were blocked in a 5% (wt/vol) powdered milk in PBS solution for 1 hour at room temp. Next, the blots were washed in PBS for 1 hour prior to primary antibody incubation overnight at 4°C, shaking. Primary antibodies are resuspended in a 5% BSA/PBS solution containing 0.05% sodium azide as a preservative. The next day blots were washed 1 hour in PBST at room temperature prior to the addition of the respective species HRP-conjugated secondary antibody (Cell Signaling, Denver, MA). The secondary antibody is prepared in 5% milk (wt/vol) and PBST at a 1:5000 dilution. Blots were incubated in secondary antibody for 1 hour at room temperature and then washed for 2 hours in PBST prior to developing (nitrotyrosine blots are washed for 24 hours in PBST prior to developing). Blots were incubated for 1 minute in Western Lighting-Plus Chemiluminescent Substrate (PerkinElmer, NEL104001EA) and developed using the AI06 Imager (Amersham). Primary antibodies are as follows: all dilutions are 1:1000; ADH1 (#5295), H3 (#4499), H4

(#2935), ACL (#13390), β -Actin (#3700), GAPDH (#5174), nitrotyrosine (#9691), pan-NOS (#2977), Cell Signaling Technologies; CYP2E1 (#ab28146, Abcam); nitrotyrosine (#6B2-3G2, Bio-Rad).

Dot Blots

PVDF membrane was activated in 100% methanol for 10 minutes. After activation the membrane was washed for 5 minutes, shaking, in DI water and then placed into PBS for acclimation. A piece of Whatman filter paper is soaked in PBS and placed on top of a dry piece of filter paper that is sitting on a stack of paper towel. The membrane is placed on top of the stack and allowed to dry until damp. Previously synthesized nitro-peptides against H1nY70, H1nY27, H2BnY50, H3nY41, H4nY51, H4nY72, H3Y41 (Covance), H3nY41 (Covance) were dotted in 1 μ g, 500ng, 250ng, 50ng, 1ng, and 500pg. The peptide was allowed to bind at room temp for 1.5 hours. The membranes were then placed into PBS before beginning the previously stated Western blot protocol for testing of the H3nY41 (Covance) antibody.

Nitro-peptide synthesis, Mass Spectrometric Analysis, and Validation of Histone Nitrotyrosine Identification

In order to validate our findings, nitrotyrosine peptides were synthesized corresponding to the 6 nitrotyrosine sites identified on the histone proteins (H1, H₂B, H3, and H4). Peptides were synthesized by Fmoc solid phase chemistry using the activator 5-chloro-1-[bis(dimethylamino)methylene]-1H-benzotriazolium 3-oxide (HCTU). The synthesis was completed using the 25 μ mole synthesis scale by the Protein Technologies Symphony Peptide Synthesizer at the University of South Florida Peptide Synthesis and Mass Spectrometry Facility. Each coupling step required 5 equivalents of Fmoc-amino acid and 7.5 equivalents of HCTU to be dissolved in 0.4M N-methylmorpholine in dimethylformamide (DMF). Fmoc deprotection was done using 20% piperidine, 2% 1, 8-diazobicyclo[5, 4, 0]undec-7-ene (DBU). After synthesis, the resin was washed with N-methylpyrrolidone (NMP) followed by dichloromethane (DCM)

and cleaved using a cocktail mixture (94% TFA, 2.5% water, 2.5% ethanedithiol, 1% triisopropyl silane) prior to precipitation in cold ether.

The nitropeptides were resuspended in a 50:50 methanol and 0.1% FA in H₂O at a concentration of 1 µg/ml. The peptides were directly infused into the Q-Exactive Plus Mass Spectrometer using the same normalized collision energy (NCE) and mass range as their respective experimental identified nitrotyrosine modified histone proteins from each individual sample. The synthetic peptide data was then used to validate the presence of the nitrotyrosine observed on the experimental histone residues. Spectra from both the experimental samples and the synthetic peptides were annotated using protein prospector MS-Product (version 5.14.1, <http://prospector.ucsf.edu>). Positive nitrotyrosine sites were validated according to specifications previously described [126].

Molecular Dynamic Simulations

The initial conformation for the wild-type nucleosome system was constructed from the X-ray structure of a nucleoprotein complex formed by recombinant variants of *Xenopus laevis* histones and modified human α -satellite DNA (PDB ID 1kx5) [226]. The crystal structure contains a 147 base pair DNA stretch wrapped around the octameric histone core resolved at 1.9 Å. [227]. Experiments were carried out over several all-atom MD simulations of the nucleosome complex with various modifications, one of which had truncated histone tails (H3 was truncated at K36, H4 at K16, H2A at A12, and H2B at K21). In the latter system, RMSD of the core histone region remained within 1.5 Å of the crystallographic positions, and the RMSD of the DNA was slightly larger (5 Å) when compared to the nucleosome without truncated histone tails (4 Å), indicating that the nucleosome with the clipped tails maintains an average conformation close to that of the crystal structure. As such, in order to expedite the acquisition of longer time scales, the histone tails were truncated at the same locations (Figure 3.8). The nucleosome complex was co-crystallized with 14 manganese (Mn) ions. Manganese is a divalent ion and a transition metal that enforces an octahedral geometry on the ligands coordinating with it in the inner shell. There are currently

no force fields that can accomplish this, therefore, Mn was switched out for magnesium (Mg), which has the same charge and a similar radii. Coordinates for missing atoms were obtained through the pdb2gmx GROMACS utility. The nucleosome, along with the crystallographically resolved water molecules, were placed in a 14 nm³ unit cell and was then solvated with the SPC/E model water [228]. After energy minimization, non-crystallographic water molecules were randomly replaced by potassium (K⁺) and chloride (Cl⁻) ions in order to achieve a 100 mM ion concentration. K⁺ and Cl⁻ ions were added in a proportion such that the unit cell has a zero net charge. After the introduction of ions, the unit cell was energy minimized once more. To construct the H3nY41 system, the conformation at t=500 ns from the wild-type ensemble was modified by substituting the CE2 hydrogen of H3Y41 with a nitrate group, whose bond parameters were obtained from Myung and Han [229]. Energy minimization was again performed on the H3nY41 system prior to starting the MD simulation.

All simulations were carried out with the Gromacs 4.5.3 package [230] with an integration step of 2 fs. Protein, ions, and DNA parameters are described by the AMBER99SB-ILDN force field [231]. The simulations are carried out under isobaric conditions using the Parrinello-Rahman extended ensemble approach [232], with a reference pressure of 1.01325 bar. The coupling time constant for the barostat is 1.0 ps and the compressibility factor is set to 4.5 e-5. The simulations are carried out at a temperature of 310 K and are coupled every 0.1 ps to a velocity-rescale thermostat [233], which uses a stochastic term for the generation of a proper canonical ensemble. Periodic boundary conditions are set in all directions and neighbor lists are constructed through a grid search that is updated every 10 fs. van der Waals interactions are computed explicitly for interatomic distances of up to 10 Å. Electrostatic interactions are computed using the particle mesh Ewald scheme with a Fourier grid spacing of 0.1 nm, a fourth-order interpolation, and a direct space cutoff of 10 Å [234]. Convergence is monitored by tracking the time evolution of histone and DNA RMSDs as well as H3Y41 and H3nY41-DNA distances (Figures 3.9-3.11).

H3nY41 Antibody Synthesis, Chromatin Immunoprecipitation, and qPCR

A CHIP-grade antibody was raised in 2 rabbits, at Covance antibody facilities (Denver, PA). The rabbits were immunized using synthetic peptides generated to recognize either H3Y41 (*Ac-PHRYRPGTVALC-amide*) or H3nY41 (*Ac-PHR(NO2Y)RPGTVALC-amide*) over 77 days. Serum was tested 3-times, over 77 days using Dot-Blots probed with the previously made nitro-peptides [synthesized for the verification of MS data] and Western blots of whole cell lysate obtained from the 28-day mouse chronic-ethanol study. Rabbit FL111 was designated for affinity purification to be used for ChIP-sequencing.

ChIP-Seq service was performed by Zymo Research Corporation (Irvine, CA). Briefly, mouse liver tissue was crosslinked with 1% (v/v) formaldehyde for 10 min and quenched with final 125 mM glycine for 5 min at room temperature. Chromatin was prepared using the Zymo-Spin™ ChIP kit (Zymo Research Corp., Irvine, CA). Sonication was performed at high power setting for 40 cycles (30 s on, 30 s off) using a Bioruptor Plus™ (Diagenode Inc., Denville, NJ), yielding fragment size range of 200-700 bp. The ChIP assay was performed in triplicate (N=3) using 20 µg of chromatin and 10 µg of anti-H3nY41 polyclonal antibody. Anti-IgG (Diagneode C15410206; Lot RIG001L) at a concentration of 10 µg was included as a negative control. A non-precipitated DNA sample was included as an input control. ChIP DNA was purified using the ChIP DNA Clean and Concentrator™ (Zymo Research, Irvine, CA). ChIP-Seq libraries were prepared and sequenced on a HiSeq sequencer (Illumina, San Diego, CA). ChIP-Seq reads were aligned to the mouse genome version mm10 Bowtie with at most 2 mismatches. Reads that appeared more than twice at the same position on the same strand were discarded to remove PCR duplication. BIGWIG files were generated from the coverage for visualization purposes. MACS2 was used to identify peaks at q-value cutoff 0.05 and a broad cutoff of 0.1. Following ChIP-sequencing, validation of *Ano2* and *Dpp9* were tested for validation using ChIP-qPCR. ChIP-qPCR analysis was performed by Zymo Research Corporation. Briefly, unique primer sets were designed for *Dpp9* and *Ano2* introns using H3nY41 sequencing data. H3nY41 ChIP and IgG negative control DNA enriched from 3 independent ChIP assays were pooled and 1

μ l DNA/reaction was amplified using ZymoTaq™ qPCR Premix (Zymo Research Corp., Irvine, CA). ChIP DNA enrichment was determined as % of input (i.e. the relative amount of immunoprecipitated DNA compared to 100% input DNA after qPCR analysis).

Results

28-Day Chronic Ethanol Diet in 8-Week Male Mice Promotes Liver Injury & Nitrotyrosine Formation

Eight week old male C57bl/6 mice were administered either the control or ethanol Leiber-DeCarli liquid diet for the course of 28 days. Mice were sacrificed on day 29 and the blood and livers were harvested for further analysis. Upon extraction, livers of ethanol-fed mice had displayed visual signs of hepatitis; livers were soft, swollen, discolored and possessed white blotches when compared to their control mice counterparts. Livers were then next sectioned and fixed in 10% formalin, for 24 hours, prior to being embedded in paraffin for IHC analysis. Hematoxylin and Eosin (H&E) stain were first performed on each liver to ensure alcohol-induced fatty liver has occurred in the ethanol-fed mice. H&E staining of the ethanol-fed mice revealed signs of lipid accumulation commonly seen in the development of steatosis when compared to the control-fed mice (**Figure 3.1A**). Upon confirmation that the mice had alcohol-induced fatty-liver, global nitrotyrosine expression in the liver was assessed by IHC. An IHC grade antibody against pan-nitrotyrosine (Invitrogen, A-21285) was used to stain each liver sample. Interestingly, nitrotyrosine staining revealed increased levels of nitrotyrosine that was localized to the vascular and nuclear regions of the livers in the ethanol-fed mice (**Figure 3.1B**). Next densitometry was performed on the resulting IHC data, to assess if the increase in nY after ethanol exposure was significant when compared the pair-fed control mice. One hundred and fifty individual regions were randomly selected from the IHC livers of both the control and ethanol-fed mice, the resulting mean pixel intensities. The resulting mean pixel intensities were then converted into reciprocal means and compared using a 2-tailed student t-test. Statistical analysis of nY abundance between control and ethanol-fed mice yielded a

significant increase of nY ($p=1.65E-38$) in both the individual reciprocal means, as well as their averages (Figure 3.1C).

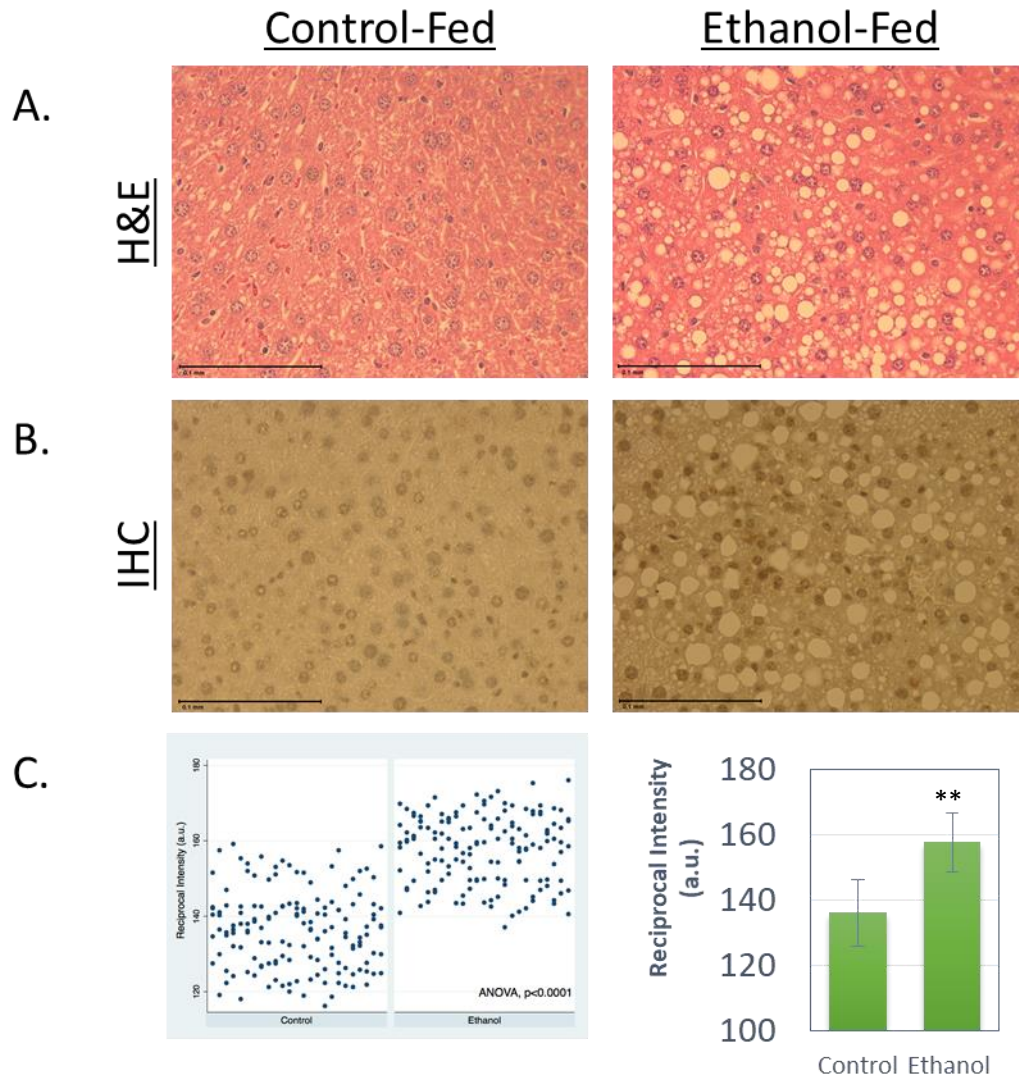


Figure 3.1: Histological Analysis of Mouse Liver following the 28-Day Lieber-DeCarli Chronic Ethanol Diet. **A)** H&E staining shows increased lipid accumulation in the liver observed in ethanol-fed (A. Right) mice when compared to control-fed (A. Left) mice, indicative by the “hole”-like appearance. **B)** IHC pan-nitrotyrosine staining of the control-fed (B. Left) and ethanol-fed (C. Right) mouse livers displays increased nitrotyrosine localized to the nuclear regions in the ethanol-fed mice. **C)** Densitometry and Statistical analysis was completed on 150 random regions from the IHC images obtained from both the control and ethanol-fed livers. **C)** (Left) Densitometry analysis was performed to quantify the fold change observed in the PTN between the control and ethanol fed mice depicted in part B above. **C)** (Right) Statistical analysis of densitometry data revealed significant increases in PTN (** $p < 0.0001$) after ethanol exposure.

Functional Analysis of Nuclear Enrichment and Protein Tyrosine Nitration

Next, the number of nuclear proteins that were identified by mass spectrometry were quantified in order to assess the purity of the nuclear enrichment. To do this, the raw files were first analyzed using MaxQuant (Max Plank) and then added to Scaffold (Proteome Software Inc., Portland OR) for quantitation analysis [109, 235]. The gene-ontology (GO) function in Scaffold was used in order to determine which cellular compartment the protein identified is traditionally located in. Scaffold-GO identified that approximately 50% of the total identified proteins were found within the cellular nuclear compartment (**Figure 3.2A**). In order to ensure that a similar amount of protein was being utilized for XIC comparison analysis, the non-normalized total ion current (TIC) was used to establish a loading control. The TIC was extracted from the nuclear proteins, Lamin B, Histone H3 (H3), and histone deacetylase 1 (HDAC1) from both the control and ethanol-fed mice and it was concluded that no significant changes in TIC occurred between experimental groups (**Figure 3.2B**). These data suggest that any further data analysis of protein up or down-regulation could be completed with the confidence of equal loading of lysate onto the mass spectrometer. The MaxQuant dataset was used to extract intensities and conducted a student's t-test to calculate significant fold-change in expression between control and ethanol-fed mice. Once proteins were found to have a significantly different ($p < 0.05$) fold change, they were uploaded into Ingenuity Pathway Analysis (IPA) for further pathway analysis to detect differences in protein networks due to ethanol exposure. Results show that ethanol upregulated numerous enzymes, such as GSTA5, CBR1, and HTATIP2 that are important in pathways responsible for the reduction of free radicals and alleviating oxidative stress (**Figure 3.2C**). The transcription factor, CCAAT/Enhancer Binding Protein Alpha (CEBPA) was identified to be downregulated, which is most notable for its role in cell cycle and proliferation arrest. IPA analysis further confirmed that the expression changes being observed were commonly linked to enzymes necessary for ethanol metabolism and the reduction of oxidative stress within the cell.

Identification of Nitrotyrosine Modifications on Histone Proteins

Utilizing both MaxQuant and Mascot proteomic software algorithms, 51 proteins were identified to undergo tyrosine nitration (**Table 3.1**). Excitingly, the search identified 7 novel sites of tyrosine nitration

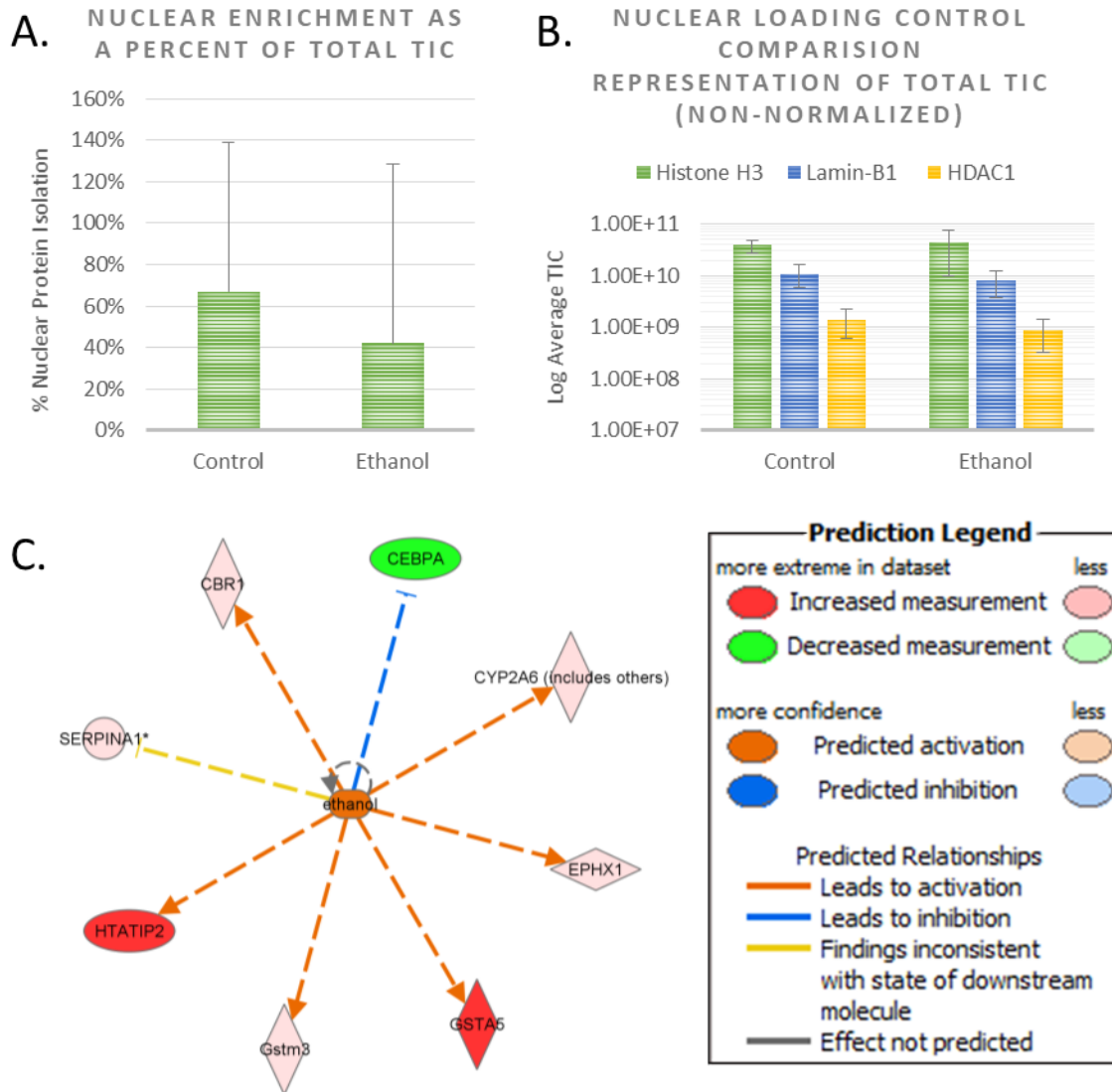


Figure 3.2: Quantitative analysis of Mass Spectrometrically Derived Nuclear Fractionation and Changes in Protein Upregulation. A) Total ion current was quantified from the non-normalized data obtained from the MaxQuant data analyzed by Scaffold Q/S. Scaffold's Gene ontology was used to quantify all proteins isolated and identified within the nuclear compartment. No significant changes were observed between the control and ethanol-fed mice. B) Comparison of nuclear loading control proteins Histone H3, Lamin B1 and HDAC1. No significant changes were observed across the nuclear loading controls tested, relaying that all samples were equally loaded onto the column and mass spectrometer. C) Fold-change in significantly different proteins between control and ethanol-fed groups were uploaded into Ingenuity Pathway Analysis for analysis of protein expression. IPA results yielded upregulation of proteins and enzymes important in the metabolism of ethanol.

(nY) on histone proteins. The histone nY sites that were identified included 3 novel sites of tyrosine nitration in Histone H4 (Y51, Y72, and Y98), two nY sites in Histone H1 (Y27 and Y70), and one nY site on each, Histone H3 (Y41) and Histone H₂B (Y37) (Table 3.2). All of the prospective nY sites identified on the histone proteins received a localization score of 100% as well as a Scaffold PTM A-score of 1000, except

Table 3.1: MaxQuant Nitrotyrosine Identification in Mouse Liver following the 28-Day Chronic Ethanol Diet

Assession #	Protein names	Gene names	Peptide Sequence and nY Probabilities	Charge	Mass error [ppm]	PEP	MaxQuant Score
P63038	60 kDa heat shock protein, mitochondrial	Hspd1	SIDLKDKY(1)K	3	-0.360	1.10E-02	57.267
P20029	78 kDa glucose-regulated protein	Hspa5	VY(1)EGERPLTK	3	-0.526	2.96E-02	55.467
P59511	A disintegrin and metalloproteinase with thrombospondin motifs 20	Adamts20	LEEKY(1)CSHLHK	2	1.839	4.97E-02	55.314
P68134	Actin, alpha skeletal muscle	Acta1	LCY(1)VALDFENEMATAASSSSLEK	2	-1.539	4.51E-08	79.177
P68134	Actin, cytoplasmic 2	Actg1	DSY(1)VGDEAQS	2	0.186	2.76E-05	115.33
Q9JME5	AP-3 complex subunit beta-2	Ap3b2	EAAADMSPY(1)VRK	2	1.776	5.71E-02	43.604
Q61285	ATP-binding cassette sub-family D member 2	Abcd2	PY(1)MSLGSLR	3	0.220	2.57E-02	50.04
Q9Z1N7	AT-rich interactive domain-containing protein 3B	Arid3b	QILDLY(1)MLY(1)KLVTEK	2	1.581	5.84E-03	42.314
Q9Z1N7	AT-rich interactive domain-containing protein 3B	Arid3b	QILDLY(1)MLY(1)KLVTEK	2	1.581	5.84E-03	42.314
Q99PF4-2	Cadherin-23	Cdh23	LDY(1)ELIQ	3	-0.649	3.88E-02	47.082
Q8C196	Carbamoyl-phosphate synthase [ammonia], mitochondrial	Cps1	LY(1)FEELSLEK	2	3.688	7.76E-05	123.79
Q8C196	Carbamoyl-phosphate synthase [ammonia], mitochondrial	Cps1	EIEY(1)EVVR	2	-0.402	4.08E-02	67.897
P16015	Carbonic anhydrase 3	Ca3	HDPQLQPWSASY(1)DPGSAK	3	-2.344	7.59E-03	43.383
Q3ULW6-4	Coiled-coil domain-containing protein 33	Ccdc33	Y(1)LRIFHPYQFKLEK	3	-1.730	3.62E-03	55.196
Q8R3L8-3	Cyclin-dependent kinase 8	Cdk8	VGRGTY(1)GHVYK	2	0.416	6.36E-02	64.374
Q9DBT9	Dimethylglycine dehydrogenase, mitochondrial	Dmgdh	DLEGSY(0.5)Y(0.5)LR	2	0.334	2.45E-02	63.076
Q9DBT9	Dimethylglycine dehydrogenase, mitochondrial	Dmgdh	DLEGSY(0.5)Y(0.5)LR	2	0.334	2.45E-02	63.076
P06802-2	Ectonucleotide pyrophosphatase/phosphodiesterase family member 1	Enpp1	KY(1)VY(1)LNK	2	-4.361	8.33E-03	100.74
P06802-2	Ectonucleotide pyrophosphatase/phosphodiesterase family member 1	Enpp1	KY(1)VY(1)LNK	2	-4.361	8.33E-03	100.74
P10126	Elongation factor 1-alpha 1	Eef1a1	MDSTEPPY(1)SQK	2	-0.096	1.83E-03	82.437
P10126	Elongation factor 1-alpha 1	Eef1a1	RY(1)EEVK	2	0.778	3.26E-02	53.968
P26443	Glutamate dehydrogenase 1, mitochondrial	Glud1	NY(1)TDNELEK	2	-0.485	1.87E-03	98.048
P16858	Glyceroldehyde-3-phosphate dehydrogenase	Gapdh	LISWY(0.999)DNEY(0.001)GYSNR	2	0.215	3.87E-04	113.25
P01942	Hemoglobin subunit alpha	Hba	IGHGAEY(1)GAEALER	3	-2.323	6.21E-04	79.337
Q8R3H7	Heparan sulfate 2-O-sulfotransferase 1	Hs2st1	PY(1)INVIR	1	-0.520	4.72E-03	79.939
Q8BG05	Heterogeneous nuclear ribonucleoprotein A3	Hnrnpa3	SSGSPY(0.001)GGGY(0.992)GSGGGSGGY(0.007)GSR	2	-0.210	2.35E-17	144.95
Q8BG05	Heterogeneous nuclear ribonucleoprotein A3	Hnrnpa3	EDTEEY(1)NLR	2	-0.629	1.25E-03	103.55
P15864	Histone H1.2	Hist1h1c	ALAAAGY(1)DVEK	2	0.635	3.12E-03	84.479
Q6ZWY9	Histone H2B type 1-P	Hist1h2bp	KESY(0.08)SVY(0.348)VY(0.572)K	2	0.565	1.61E-02	63.397
Q6ZWY9	Histone H2B type 1-P	Hist1h2bp	ESY(0.071)SVY(0.465)VY(0.465)K	2	-0.432	2.40E-02	63.397
Q6ZWY9	Histone H2B type 1-P	Hist1h2bp	ESY(0.088)SVY(0.191)VY(0.001)K	2	-0.482	2.71E-02	66.962
P84244	Histone H3.3, Histone H3.1, Histone H3.2	H3f3a	Y(1)RPGTVALR	2	-0.462	4.44E-03	117.02
P62806	Histone H4	Hist1h4a	RISGLY(1)EETRGLVK	3	-3.551	1.81E-07	133.16
P62806	Histone H4	Hist1h4a	DAVY(1)TEHAK	2	-0.025	4.68E-05	110.38
P62806	Histone H4	Hist1h4a	TLY(1)GFGG	1	0.464	4.15E-03	92.723
Q62240-3	Lysine-specific demethylase 5D	Kdm5d	LNLY(1)LDQIAK	2	-0.063	1.76E-02	67.414
P45952	Medium-chain specific acyl-CoA dehydrogenase, mitochondrial	Acadm	KGDEY(1)VINGQK	2	0.252	8.20E-68	259.18
Q62425	NADH dehydrogenase [ubiquinone] 1 alpha subcomplex subunit 4	Ndufa4	LGPNEQY(1)K	2	-0.598	3.99E-02	68.224
P51660	Peroxisomal multifunctional enzyme type 2	Hsd17b4	SGSGVEY(1)QGPAAK	2	-0.294	1.46E-07	137.01
Q9R0E2	Procollagen-lysine,2-oxoglutarate 5-dioxygenase 1	Plod1	FLGSGGFY(1)APLSK	2	1.953	2.95E-03	65.219
O55125	Protein NipSnap homolog 1	Npsnap1	GWDENVY(0.5)Y(0.5)TVPLVR	2	1.606	1.51E-03	79.614
O55125	Protein NipSnap homolog 1	Npsnap1	GWDENVY(0.5)Y(0.5)TVPLVR	2	1.606	1.51E-03	79.614
Q9JKF1	Ras GTPase-activating-like protein IQGAP1	Iqgap1	Y(1)QELINDIAK	2	-0.117	4.81E-02	52.49
F6SEU4	Ras/Rap GTPase-activating protein SynGAP	Syngap1	YQTMISLPLMELY(1)K	2	0.791	7.44E-03	54.023
Q6ZQ82	Rho GTPase-activating protein 26	Arhgap26	GINEQGLY(1)RIVGVNSR	2	1.356	1.95E-02	63.29
P38647	Stress-70 protein, mitochondrial	Hspa9	RY(1)DDPEVQK	2	0.750	6.85E-03	73.887
P09671	Superoxide dismutase [Mn], mitochondrial	Sod2	HHAAY(1)VNNLNATEEK	3	0.879	1.11E-04	101.43
O08710	Thyroglobulin	Tg	FLGVPPY(1)AAFPPLADNR	2	-0.635	1.58E-02	53.377
Q99JY0	Trifunctional enzyme subunit beta, mitochondrial	Hadhb	MEQDEY(1)ALR	2	-0.371	1.71E-02	67.704
P25688	Uricase	Uox	GEY(1)SPSVQK	2	0.891	8.86E-03	75.571
Q5DU09-2	Zinc finger protein 652	Znf652	VFNTRWY(1)LEK	2	-2.145	1.64E-02	67.334

Table 3.2: XIC Analysis of Nitrotyrosine on Histone Proteins following the 28-day Chronic Ethanol Diet in Mice

Gene Name	Nitrated Peptide Site	Modified Residue	Probability Score	PEP	m/z	observed m/z	Charge	Mass error [ppm]	Avg % Nitration Control	Avg % Nitration Ethanol	Fold Change in % Nitration
Hist1h1c ^{††}	ALAAAGY*DVEK	Y70	1.00	3.12E-03	575.78	576.78	2	0.635	0.34%	0.18%	0.54
Hist1hf0 [†]	Y*SDMIVAAIQAEK	Y27	0.99	1.82E-02	741.855	742.86	2	4.400	0.18%	0.50%	2.81
Hist1h2bp ^{††}	ESY*SVYVYK	Y37	0.81	2.71E-02	590.76	591.77	2	-0.482	0.34%	0.12%	0.37
H3f3a ^{††}	Y*RPGTVALR	Y41	1.00	4.44E-03	538.285	539.29	2	-0.462	1.25%	4.04%	3.22
Hist1h4a ^{††}	RISGLIY*EETRGVLK	Y51	1.00	1.81E-07	592.657	593.66	3	-3.551	0.66%	0.32%	0.49
Hist1h4a ^{††}	DAVTY*TEHAK	Y72	1.00	4.68E-05	589.26	590.27	2	-0.025	0.14%	0.36%	2.51
Hist1h4a [‡]	TLY*GFGG	Y98	1.00	4.15E-03	758.32	759.33	1	0.464	0.24%	0.04%	0.17

*Denotes nitrated tyrosine residue

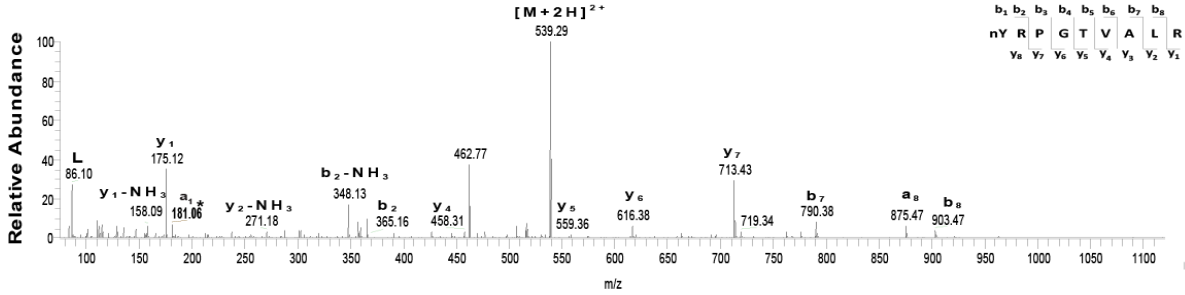
†Peptide identified by Mascot

‡Peptide identified by MaxQuant

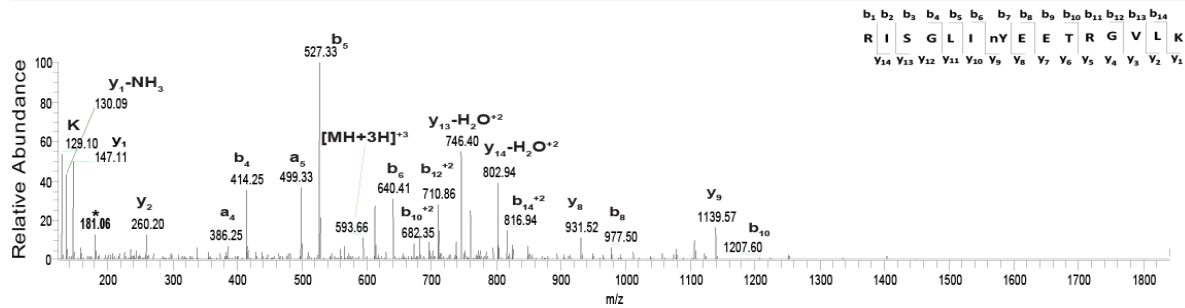
for H₂B. H₂B has 3 tyrosine residues with similar neighboring amino acids, making it difficult for the software to localize which tyrosine was nitrated. Furthermore, all of the nY sites identified fell within the allowable range of acceptable mass error (<5ppm) as determined by the performance of the Q-Exactive Plus mass spectrometer lowering the probability of a falsely identified PTM. Because these nitration sites are novel, synthetic peptides were used in order to validate the histone nY modifications identified by the software. Multiple parameters were used for the nY PTM to be considered valid, each of the nitrated histones must pass the following 4 criteria's in conjunction with their respective synthetic peptide. First the peptide must be >7 amino acids long, second the majority of peaks must have a relative abundance of >20%, third the peptide must have ≥4 consecutive ions identified (b or y), and lastly, the spectrum must be redundant across samples. Identified nY sites that did not fully pass the criteria listed above were considered invalid until further validation can prove otherwise. Four positive sites of tyrosine nitration on histones were able to be validated, H3 (Y41), H1 (Y70), and H4 (Y51) and (Y72). The b and y ion series identified from MS/MS spectra of the experimental samples (**Figure 3.3**) were compared to the corresponding MS/MS generated from direct infusion of the respective nitrated synthetic peptide (**Figure 3.4**). The remaining experimental peptides originally identified to be nitrated on histone H1 (Y27), H₂B (Y37) and H4 (Y98) (**Figure 3.5**), were unable to pass the validation criteria when compared to their synthetic counterparts (**Figure 3.6**). In regards to peptides that did not pass the validation, the analysis

* nY diagnostic ion (m/z 181.06)

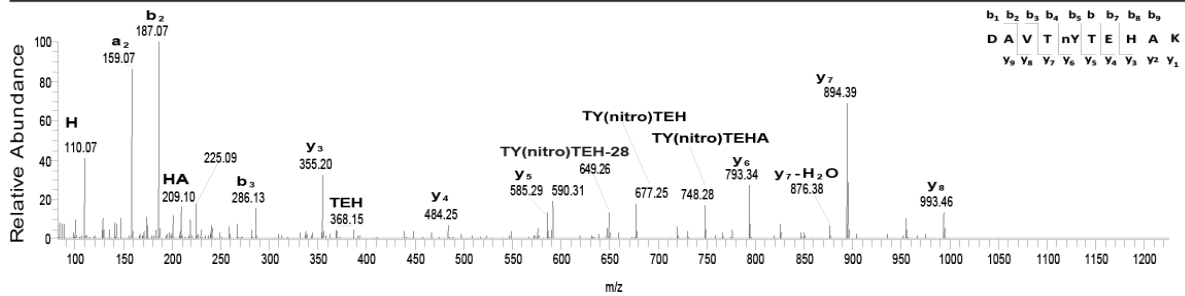
A. Histone H3 (Y41): (nitroY)RPGTVALR



B. Histone H4 (Y51): RISGLI(nitroY)EETRGLK (m/z 593.66)



C. Histone H4 (Y72): DAVT(nitroY)TEHAK (m/z 590.26)



D. Histone H1 (Y70): ALAAG(nitroY)DVEK (m/z 576.78)

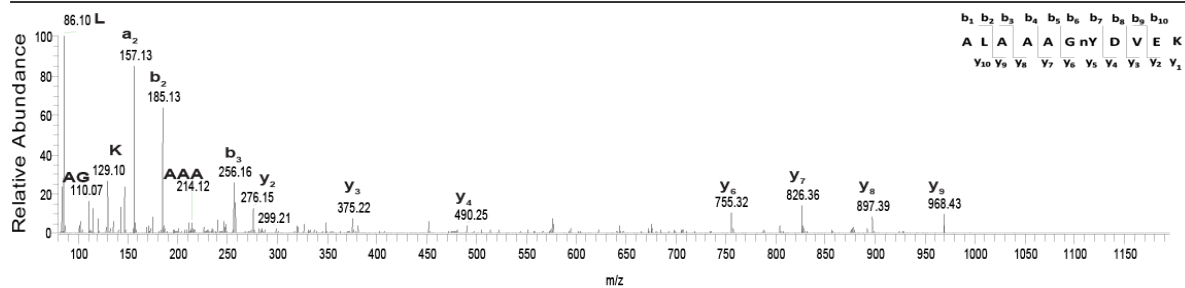
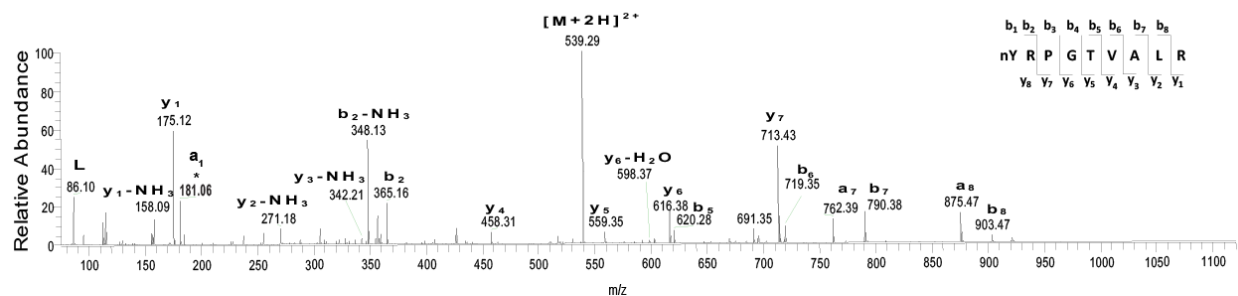
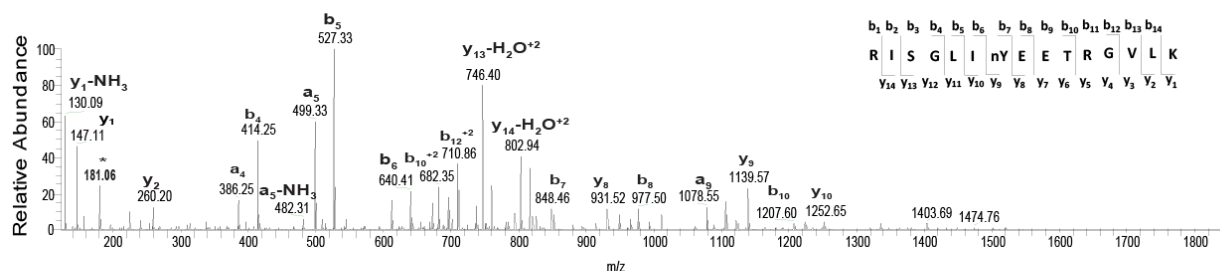


Figure 3.3: Identification and Validation of Histone Tyrosine Nitration that Passed Validation. (A-D) Annotated spectra obtained from histone proteins containing nitrotyrosine residues. Representative MS/MS that were found to have nitrated tyrosine were annotated using Protein Prospector. Spectra obtained from the synthetic peptides were compared to the best scans of histone tyrosine nitration identified from the livers of their respective experimental samples obtained from the 28 day chronic ethanol diet. Validation was dependent on the amount and consecutively placed ions that matched between experimental ions and ions obtained from the synthetic peptides. A) Histone H3 tyrosine 41 was identified to be nitrated after ethanol exposure. B & C) Histone H4 was identified to be nitrated at tyrosine residues 51 and 72, respectively after ethanol exposure. D) Histone H1 isoforms H1.2, H1.3, H1.4 and H1.5 were identified to be nitrated at tyrosine 70 after ethanol exposure.

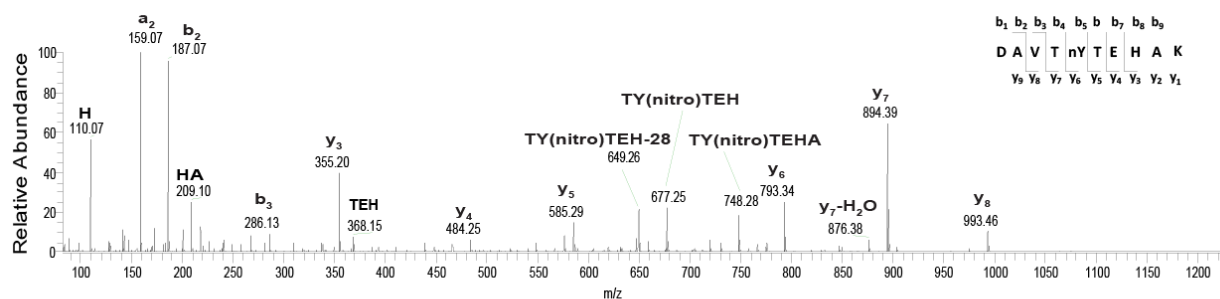
A. Peptide for Histone H3 (Y41): (nitroY)RPGTVLR (m/z 539.29)



B. Peptide for Histone H4 (Y51): RISGLI(nitroY)EETRGVLK (m/z 593.66)



C. Peptide for Histone H4 (Y72): DAVT(nitroY)TEHAK (m/z 590.26)



D. Peptide for Histone H1 (Y70): ALAAG(nitroY)DVEK (m/z 576.78)

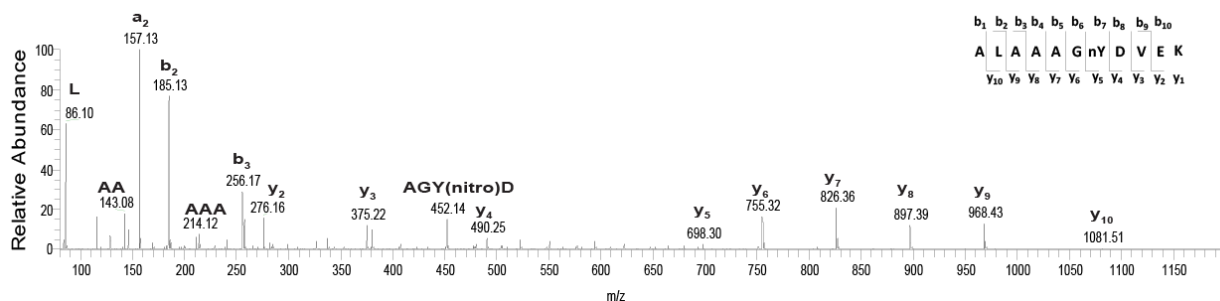
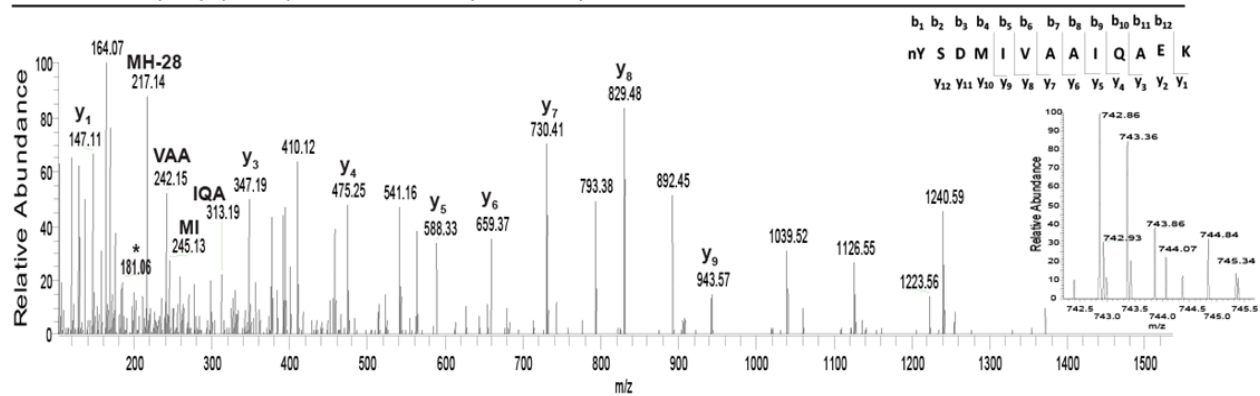
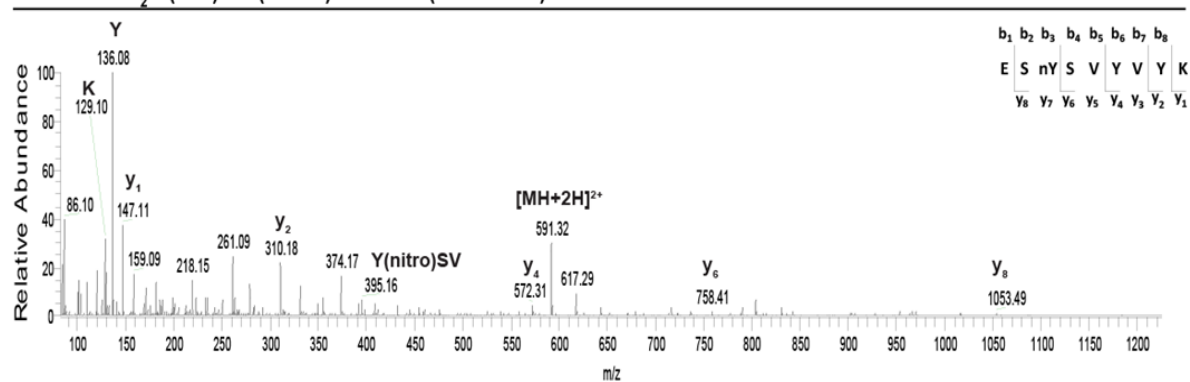


Figure 3.4: Annotation of Synthetic Peptides H3nY41, H4nY51, H4nY72, and H1nY70. Synthetic peptides were synthesized to mirror the experimental histone nitrotyrosine peptides identified by MaxQuant. The synthetic peptides were infused directly into the Q Exactive Plus mass spectrometer and parameters were adjusted to mirror experimental settings. Synthetic peptides MS/MS were annotated using Protein Prospector and the respective MS/MS generated were compared to their respective experimental peptides for validation. Spectra obtained from the synthetic peptides were compared to the best scans of histone tyrosine nitration identified from the livers of their respective experimental samples obtained from the 28 day chronic ethanol diet. A) Histone H3 nY41. B & C) Histone H4 nY51 and nY72, respectively. D) Histone H1 isoforms H1.2, H1.3, H1.4 and H1.5 nY70.

A. Histone H1 (Y27): (nitroY)SDMIVAAIQAEK (m/z 742.86)



B. Histone H₂B (Y50): ES(nitroY)SVYVYK (m/z 591.77)



C. Histone H4 (Y98): TL(nitroY)GFGG (m/z 759.33)

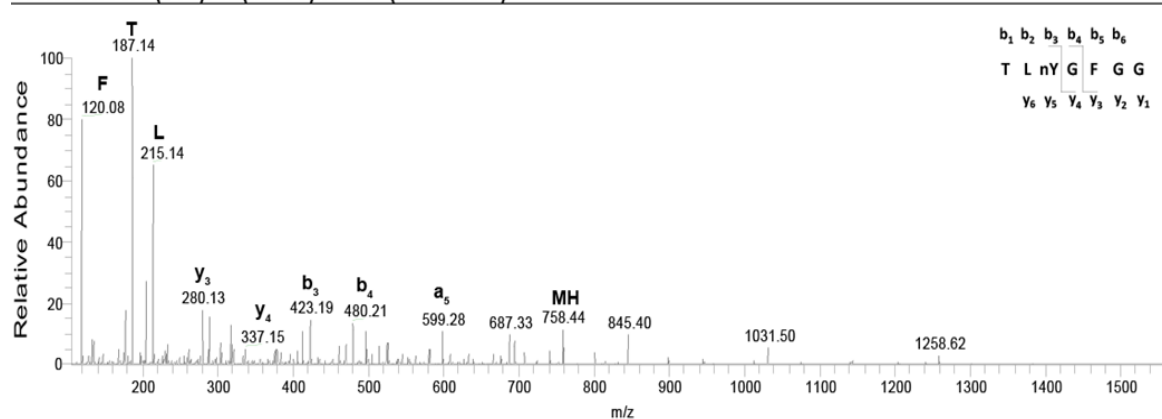
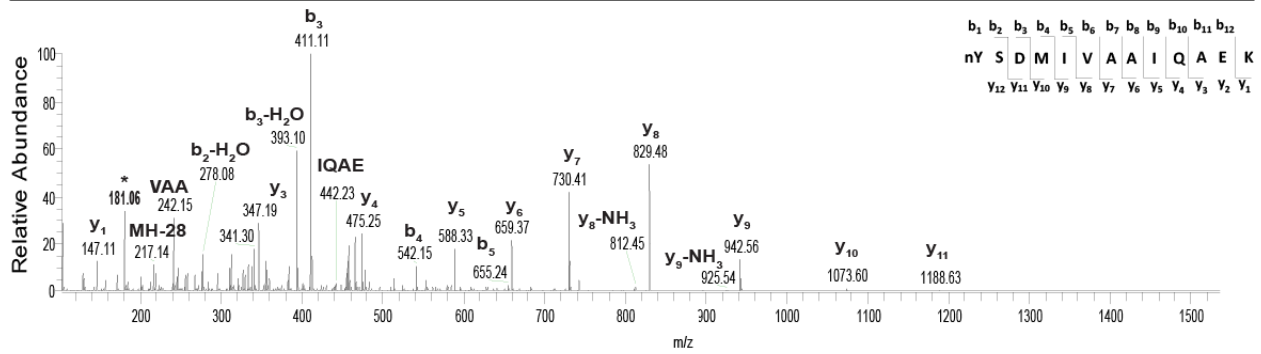
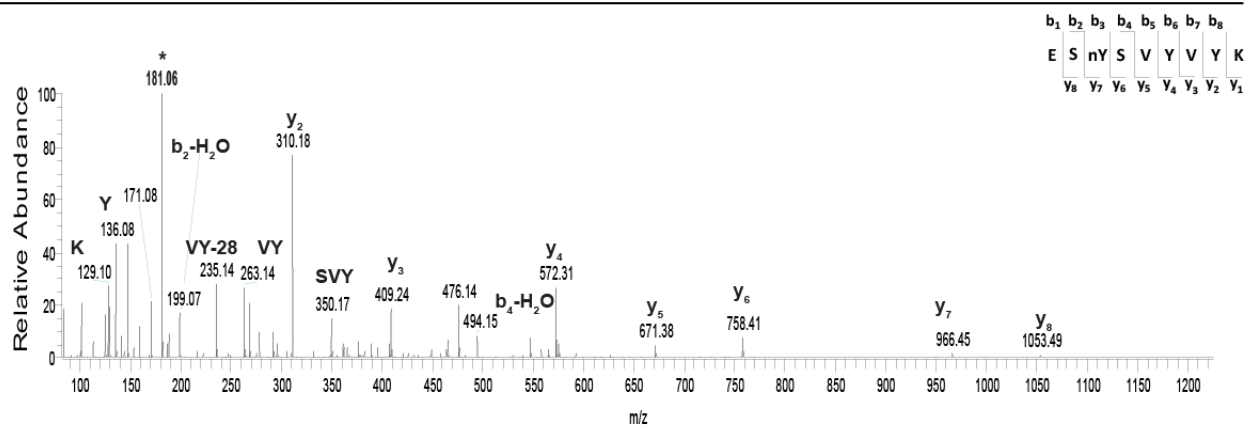


Figure 3.5: Potential sites of Histone Tyrosine Nitration That Did Not Pass Validation. (A-C) Annotated spectra obtained from histone proteins containing nitrotyrosine residues. Representative MS/MS that were found to have nitrated tyrosine were annotated and compared to nitropeptides as previously described. All experimental settings were configured as previously described in Fig.3. Spectra obtained from the synthetic peptides were compared to the best MS/MS of histone tyrosine nitration identified by MaxQuant software. Figures A-C did not pass validation as previously described; A) Histone H1.0 nitration was suggested to be found on tyrosine 27, the coelution of an isobaric peptide is shown on the inset. B) Histone H₂B nitration of tyrosine 50 was unable to be fully validated due to the sequence similarity between tyrosine residues. C) Histone H4 tyrosine 98 was unable to be validated due to the lack of positively identified consecutive ions.

A. Peptide for Histone H1 (nY27) (nitro)YSDMIVAAIQAEK



B. Peptide for Histone H2B (Y50) ES(nitroY)SVVYVK



C. Peptide for Histone H4 (Y98) TL(nitroY)GFGG

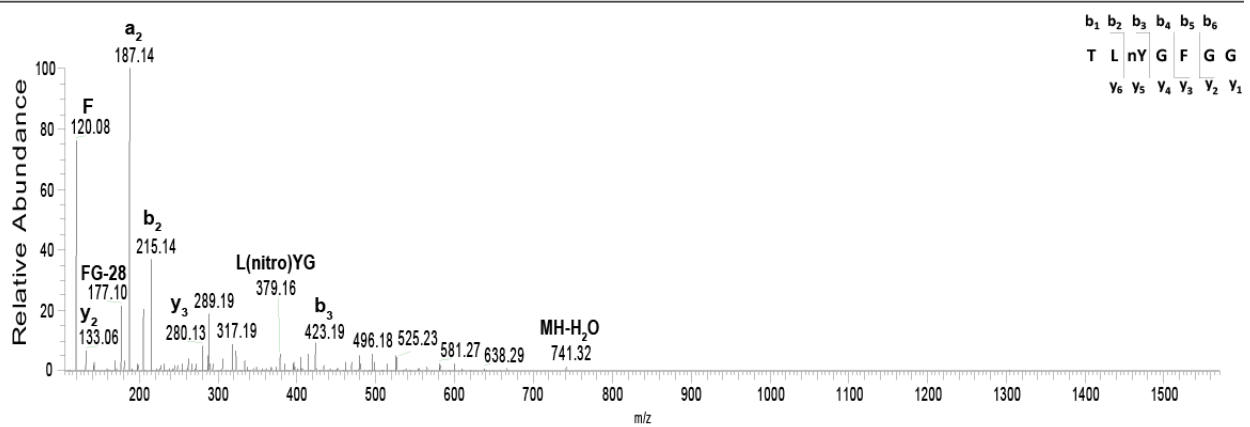


Figure 3.6: Annotation of Synthetic Peptides Pertaining to H1nY27, H2BnY50, & H4nY98. Synthetic peptides were synthesized to mirror the experimental histone nitrotyrosine peptides identified by MaxQuant. The synthetic peptides were infused directly into the Q Exactive Plus mass spectrometer and parameters were adjusted to mirror experimental settings. Synthetic peptides MS/MS were annotated using Protein Prospector and the respective MS/MS generated were compared to their respective experimental peptides for validation. Spectra obtained from the synthetic peptides were compared to the best scans of histone tyrosine nitration identified from the livers of their respective experimental samples obtained from the 28 day chronic ethanol diet. A) Histone H1.0 nY27 B) Histone H2B nY50 C) Histone H4 nY98.

suggests that the inability to validate may have been due to the low nitrotyrosine abundance, and/or possible MS signal interference, most likely due to the coelution of an isobaric peptide. Next, individual spectra were used to assess the average percent nitration observed across both the control and ethanol-fed mice.

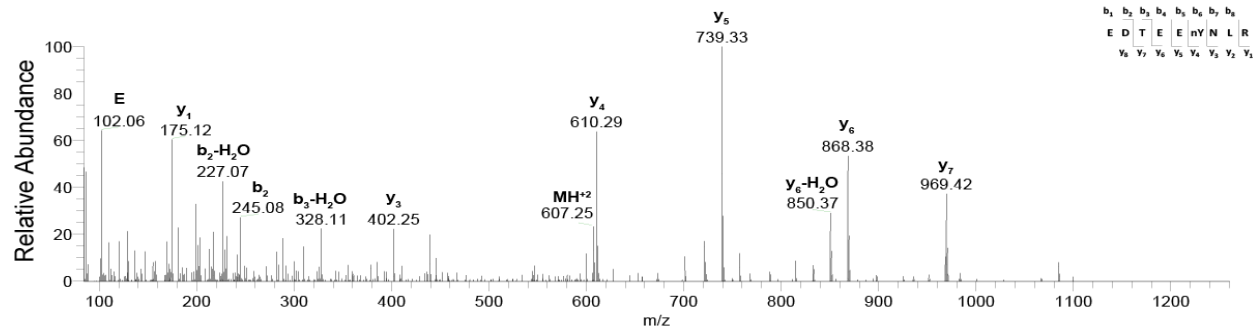
Nitrotyrosine modifications were observed to be present in both the control and ethanol-fed mice, however, the quantity of nY detected was minimal in the control-fed mice when compared to their pair-fed ethanol-matched mice (**Table 3.2**). Analysis of the overall percent nitration showed >2 fold change between control and ethanol-fed mice for 3 nitrotyrosine sites; H3nY41 showed a 3.22 fold change, H4nY72 revealed a 2.51 fold change, and H1nY27 exhibited a 2.81 fold change (**Table 3.2**). Interestingly, the H3nY41 site is located in the hinge region of the H3-tail, whereas other identified histone nitration sites were located towards the center of the nucleosome. The nitration of H3 in the tail region suggests the modification may be important for DNA interactions and gene regulation due to its positioning near both DNA and histone H1, this discovery prompted further investigation into H3nY41.

Implications of Tyrosine Nitration Influences and Gene Regulation

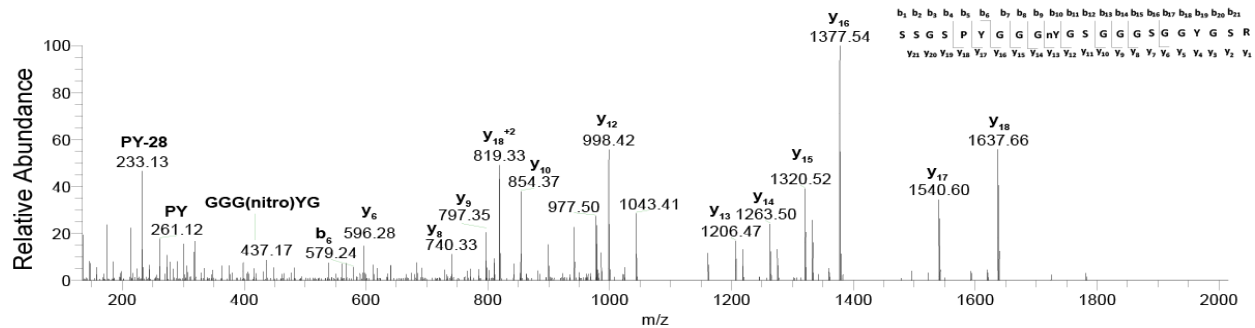
Protein Tyrosine Nitration Targets Proteins Involved in Gene Regulation

Next, the addition of the nitrotyrosine modification was assessed on proteins involved in gene regulation and transcription. Notably, heterogeneous nuclear ribonucleoprotein A3 (Hnrnpa3) was identified to be nitrated following chronic ethanol exposure. Hnrnpa3 is often associated with the cytoplasmic trafficking of RNA, and may also have a possible role in pre-mRNA splicing. Mass spectrometry identified two novel tyrosine nitration modifications on Hnrnpa3, Y139, and Y303 (**Figure 3.7A & 3.7B**). Moreover, the Y139 nitration site on Hnrnpa 3 is located in the RNA recognition motif domain (RRM) (IPR000504), suggesting a role in protein regulation or nucleotide binding. Also, elongation factor 1-alpha 1 (Eef1a1) was found to contain two novel nitrotyrosine modifications at Y61 and Y82 (**Figure 3.7C & 3.7D**). Eef1a1 is important in helping GTP-dependent binding of aminoacyl-tRNA to the A-

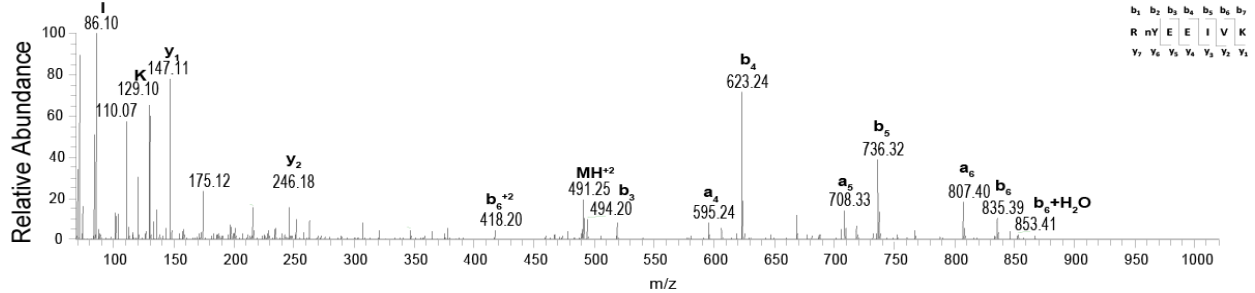
A. Hnrnpa3: EDTEE(nitro)YNLR



B. Hnrnpa3: SSGSPYGGG(nitro)YGSGGGSSGGYGSR



C. Eef1a1: R(nitro)YEEIVK



D. Eef1a1: MDSTEPP(nitro)YSQK

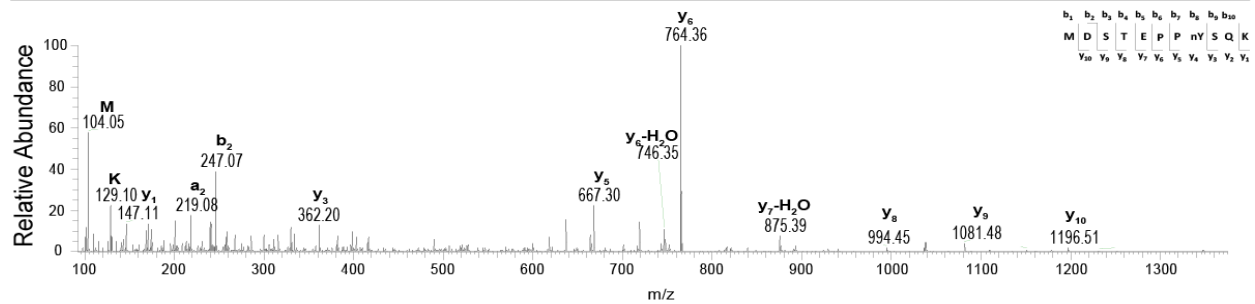


Figure 3.7: Site-Specific Identification of Nitrotyrosine on Heterogeneous Nuclear Ribonucleoproteins & Eef1a1. Heterogeneous nuclear ribonucleoprotein A3 (Hnrnpa3) (A & B) and Elongation factor 1-alpha 1 (Eef1a1) (C & D) were both identified to be nitrated after ethanol exposure. Hnrnpa3 was annotated using protein prospector and a positive identification of nitration on Y139 (A) and Y303 (B) was determined after ethanol exposure. Annotation of the protein Eef1a1 also revealed that ethanol exposure induced nitration on Y166 (C) and Y161 (D). All peptides and nitration sites were identified by MaxQuant analysis software.

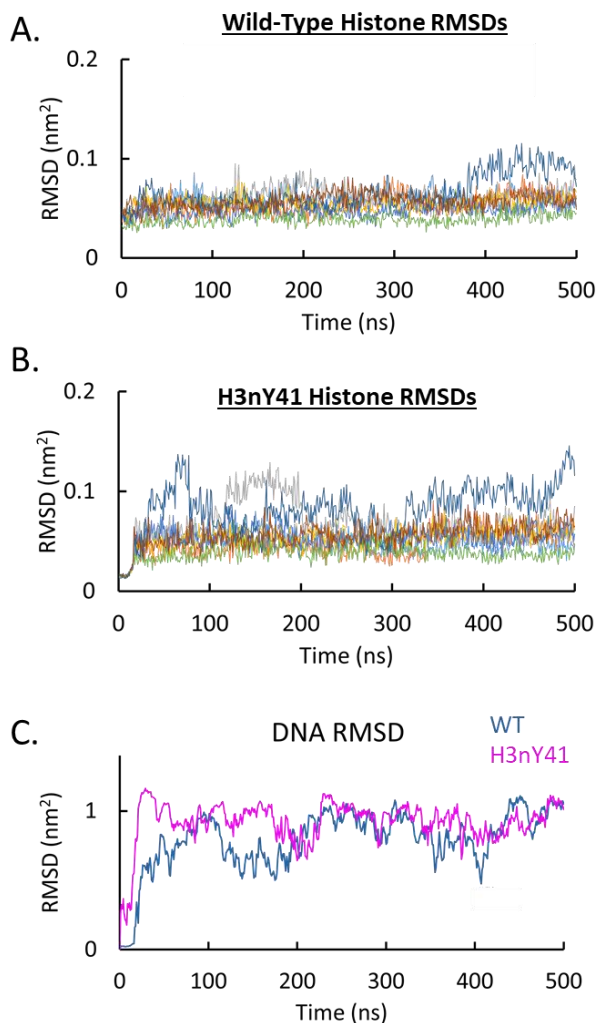


Figure 3.8: Tracking the Time Evolution of Histones and DNA RMSDs. (A-B) The individual histones that comprise the nucleosome were placed into the simulated environment and tested for equilibrium using RMSD over time for both the wild-type (WT) H3Y41 (A) and the nitrated H3nY41 (B). (C) DNA stability was also assessed for convergence by RMSD over time. Both the nucleosome containing the nitrated and unmodified H3Y41 and the DNA achieved equilibrium after 100ns.

crystallographic conformation was tracked (**Figure 3.10**). The distance reported was calculated between the center of mass of these P atoms and that of H3Y41. The two histone 3 peptides within the nucleosome are considered independently in this analysis and are termed H3^A and H3^B. Their respective time-dependent DNA-P to H3Y41 distances are shown in (**Figure 3.10**). The distance reported

site of the ribosome during elongation, further strengthening a plausible role for nY modifications in protein and gene regulation during times of cell stress.

Molecular Dynamics Predict H3nY41 Induces a Conformational Change in the DNA

The wild-type and H3nY41 nucleosome systems were each simulated for 500 ns. Histone and DNA RMSDs suggest that both systems begin to converge at t=100 ns (**Figure 3.8 A-C**). A qualitative analysis was first completed by visually comparing ensembles sampled from t=100 ns to t=500 ns of the two systems, H3Y41 and H3nY41, by superimposing them onto each other. This comparison suggests that when the H3Y41 is

nitrated, the DNA bulges near its entry/exit sites at the nucleosome (**Figure 3.9**). To obtain a quantitative evaluation of this observation, the distance from H3Y41 to the phosphorus atoms of those nucleotides that are within 5 Å of H3 in the

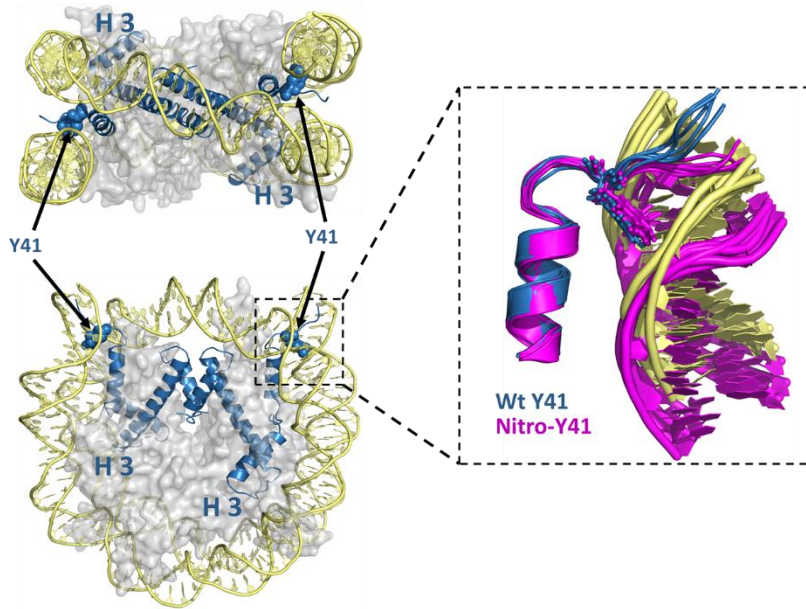


Figure 3.9: Molecular Dynamic Simulations Predict the DNA Prefers a Different Conformation upon Histone Tyrosine Nitration.

Computational modeling of the nucleosome containing the H3 dimer with truncated tails. The location of H3Y41 is depicted relative to the DNA (Right). (Left) Magnified region of the H3Y41 and DNA interface showing the predicted DNA conformation in the presence of H3nY41 (Pink) and H3Y41 (blue). The algorithm predicted the DNA to prefer a different conformation upon the nitration of H3Y41.

was calculated between the center of mass of these P atoms and that of H3Y41. The histone 3 dimer within the nucleosome is considered independently in this experiment and are termed H3^A and H3^B. Their respective time-dependent DNA-P to H3Y41 distances are shown in (Figure 3.10). This analysis indicates that the DNA P-H3Y41 distance starts to converge at t=200ns, hence, the equilibrated portion is now taken to be from t=200 ns to t=500 ns. Figure 3.10 also shows that when H3Y41 is nitrated, the DNA-P to H3Y41 distance increases by 2 Å on average. However, the average alone does not capture the full effect of the nitrated tyrosine because the fluctuation about the mean of the H3nY41 to DNA-P is twice

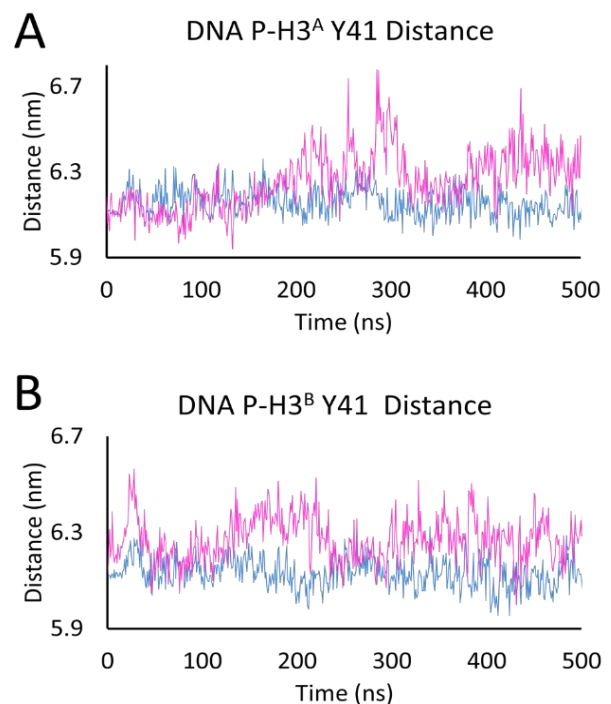


Figure 3.10: Distance from H3Y41 to a Set of the DNA Phosphorus (P) Atoms. The distance calculated between the center of mass of these P atoms and that of H3Y41. The H3 dimer were analyzed independent of each other (A and B). The DNA P-H3Y41 distance starts to converge at t=200ns, thus shifting the equilibrium starting point to t=200 ns to t=500 ns.

the distance of the wild-type. While the H3nY41 system consistently assumes conformations where the DNA-P and H3Y41 distance is $>67 \text{ \AA}$, it occasionally samples the conformational space of the wild-type system, yielding a lower average. In contrast, the maximum DNA-P to H3Y41 distance observed in the wild-type system is $<64 \text{ \AA}$. Although this difference may seem small relative to the scale of the entire nucleosome, an increase of just 3-4 \AA is enough to accommodate the entry of a K^+ ion, whose ionic diameter is 2.8 \AA . To check how closely various moieties are to H3Y41, a RDF analysis was performed on DNA P, K^+ , Cl^- , and water with respect to the carbon at position $\epsilon 2$ of H3Y41, which is the site of nitration introduction (Cl^- not shown) (**Figure 3.11A**). These data show that

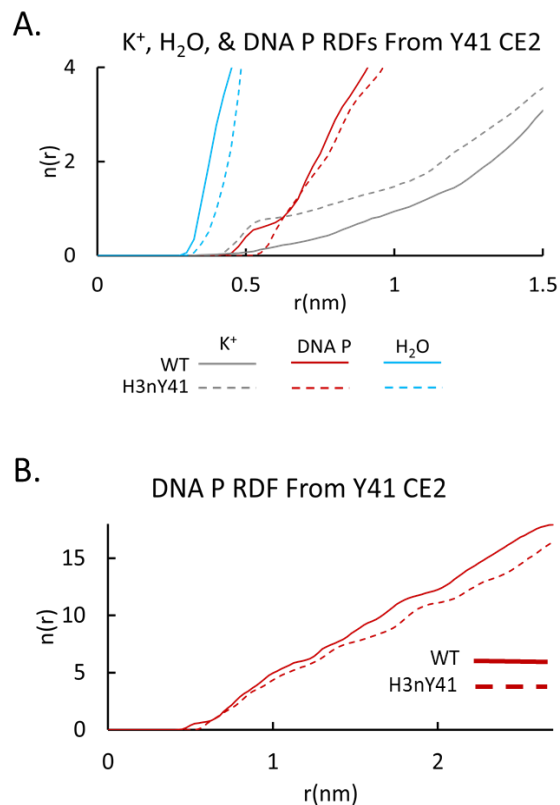


Figure 3.11: RDF analysis was performed on DNA P, K^+ , Cl^- , and water with respect to the carbon at position $\epsilon 2$ of H3Y41. (A) The K^+ ions in the H3nY41 system are found much closer than the non-nitrated H3, while the RDFs for water and DNA-P are shifted further away. (B) DNA-P magnified to show the shift away from H3nY41.

compared to the wild-type system, the K^+ ions in the H3nY41 system are found much closer to the carbon that gets nitrated, while the RDFs for water and DNA-P are shifted further away. These data also show that potassium ion presence is indeed increased in the cavity formed by DNA and the H3 tail bearing H3nY41, thereby displacing the DNA further away from the histone core (**Figure 3.11B**). This phenomenon is shown visually in Figure 3.12, which juxtaposes the cavities formed by the H3 tail and DNA in the two model systems. The RMSD plot shows that the DNA of both systems undergoes large fluctuations. Hence there are instances where potassium ions may enter the H3 tail-DNA cavity in the wild-type system. However, it is apparent that this occurs at a much higher rate for the H3nY41 system (**Figures 3.11-3.12**). At time $t=0$, the DNA P-H3Y41 distance is about 6.1 nm. In order for a K^+ ion to potentially be

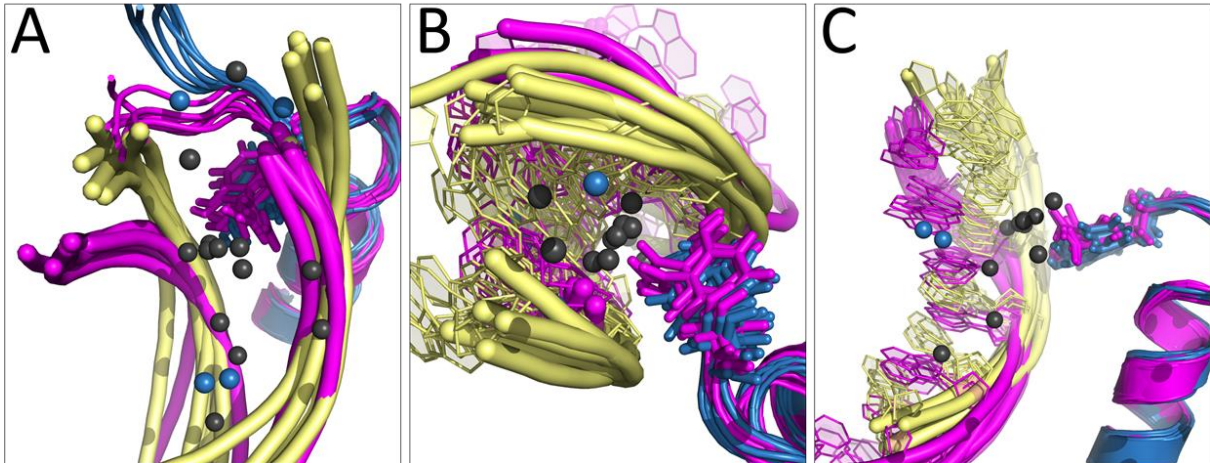


Figure 3.12: Potassium Ion Presence is in the Cavity Formed by DNA and the H3 Tail Bearing H3N41, thereby Displacing the DNA Further Away. (A-C) Different point of views representing the H3N41 (pink) and H3Y41 (blue) proteoforms. Potassium ions (black spheres) are shown closer to the nY41 site whereas the DNA-P and water (blue spheres) are moving further away from the nY41 site.

accommodated in the H3 tail-DNA cavity, this distance must be increased by at least 2.8 Å (**Figure 3.10**). In conformational ensembles consisting of 300 snapshots sampled every nanosecond from $t=200$ to $t=500$, this threshold is met in 100 of the frames for the H3N41 system, but it is observed in only two of the frames for the wild-type system. Based on these MD results, it can be postulated that the large fluctuations in the conformation of the DNA around the histone core, as evidenced by the large DNA RMSD in both systems, allow for the entry of ions into cavities formed by DNA and histones. However, in the case of the H3N41 system, the residence time of the potassium ion in this cavity is increased through stabilized interactions with the electronegative oxygens of the nitrate group on one side, and the DNA phosphorus atoms on the other (**Figures 3.11-3.12**). Such a series of events could lead to an increased likelihood of DNA to be pulled away from the histone core.

H3(nitro)Y41 and Antibody Validation by ChIP-Seq and qPCR

Following molecular dynamic simulations, a ChIP-sequencing grade antibody pertaining to the peptide sequence surrounding H3N41 was generated by Covance. The antibody was tested using the dot blot method as previously described in the methods section. Following the affinity purification, the

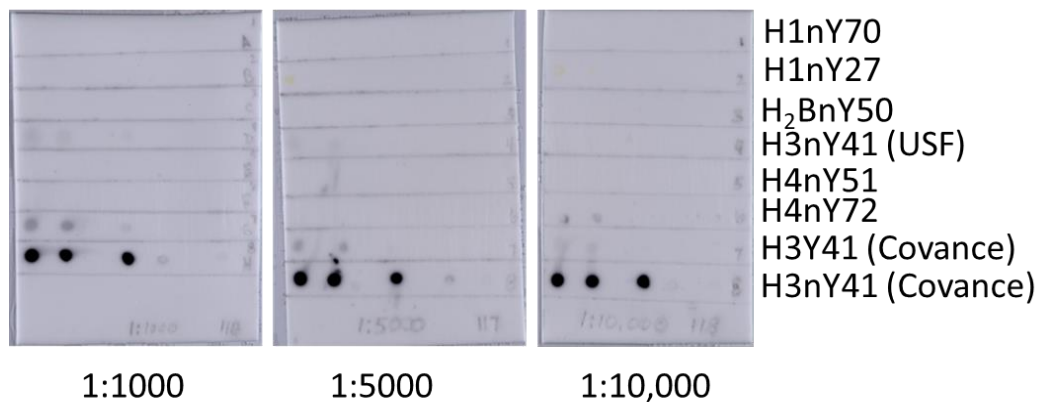


Figure 3.13: Dot Blots Used to Test the Specificity of the H3nY41 Antibody. Anti-H3nY41 stock 0.279 $\mu\text{g}/\text{mL}$ was diluted in order to identify optimal binding efficiency needed for ChIP-seq (Left) 1:1000 antibody dilution, (Middle) 1:5000 dilution, and (Right) 1:10,000 antibody dilution. Each blots was dotted from left to right 1 μg , 500ng, 50 ng, 1 ng, & 500 pg. Nitropeptide order from top to bottom: H1nY70, H1nY27, H2BnY50, H3nY41 (USF), H4nY51, H4nY72, H3Y41 (Covance), and H3nY41 (Covance).

H3nY41 antibody was tested against the previously synthesized nitropeptides used in the validation of the nY in the experimental samples. Dots were placed in rows respective to each nitropeptide and diluted to 1 μg , 500 ng, 50 ng, 1ng, and 1pg and the antibody tested at 1:1000, 1:5000, and 1:10,000 dilutions (**Figure 3.13**). The H3nY41 antibody was found to be highly specific at low concentrations (1:10,000) and was

Table 3.3: Novel Targets of H3nY41 Nitration

Chromosome	start	end	intron	Length	abs_summit	pile up	log 10 p-value	fold_enrichment	Q-value FDR
chr6	125876915	1.26E+08	Ano2	55	125876947	18	29.814	15.623	23.149
chr16	50414601	50414650	Bbx	50	50414627	10	14.759	8.959	8.410
chr17	56200008	56200090	Dpp9	83	56200050	59	121.928	49.336	112.493
chr7	98060034	98060094	Myo7a	61	98060051	27	45.371	21.989	38.543
chr2	16683087	16683136	Plxdc2	50	16683101	12	18.530	10.690	12.057
chr1	44951224	44951286		63	44951252	32	58.237	26.878	51.157
chr11	25100083	25100177		95	25100125	17	16.908	9.419	10.472
chr14	104336958	1.04E+08		66	104336989	28	50.330	23.846	43.387
chr14	107075306	1.07E+08		60	107075327	32	38.656	17.267	31.920
chr16	57241944	57241993		50	57241966	11	16.750	9.867	10.320
chr17	4626190	4626578		389	4626331	29	51.794	24.434	44.839
chr2	60402763	60402835		73	60402799	49	96.704	40.724	88.859
chr3	125228399	1.25E+08		56	125228421	25	43.993	21.379	37.166
chr3	145691029	1.46E+08		54	145691047	17	27.870	14.801	21.258
chr6	10186387	10186456		70	10186419	37	70.090	31.246	62.785
chr6	132463720	1.32E+08		80	132463759	52	104.982	43.581	96.825
chr9	19575440	19575509		70	19575481	37	70.090	31.246	62.785
chrX	122831391	1.23E+08		54	122831422	18	29.386	15.475	22.745

determined to be suitable for ChIP-sequencing validation. Livers (~400mg) were taken from three different ethanol-fed mice, each having similar consumption levels and weights throughout the 28-day chronic ethanol feeding experiment. The livers were snap frozen for ChIP-seq antibody validation. Prior to ChIP-seq, the ethanol-fed livers were pooled together in order to maximize H3N41 abundance and maximize DNA interactions. Greater than 10,000,000 reads were obtained for both the input and the pull-down experimental sample. ChIP-seq of the H3N41 pull-down identified 18 novel DNA interacting sites for H3N41 (**Table 3.3**). The 18 sites identified were all significantly enriched, having between 10 and 50 fold enrichment, when compared to the input. Surprisingly, only five reads were located within the annotated region of the genome. Furthermore, all five known targets were located within the intron region of the gene and the peaks were all well-defined (**Figure 3.14**). The remaining thirteen identified

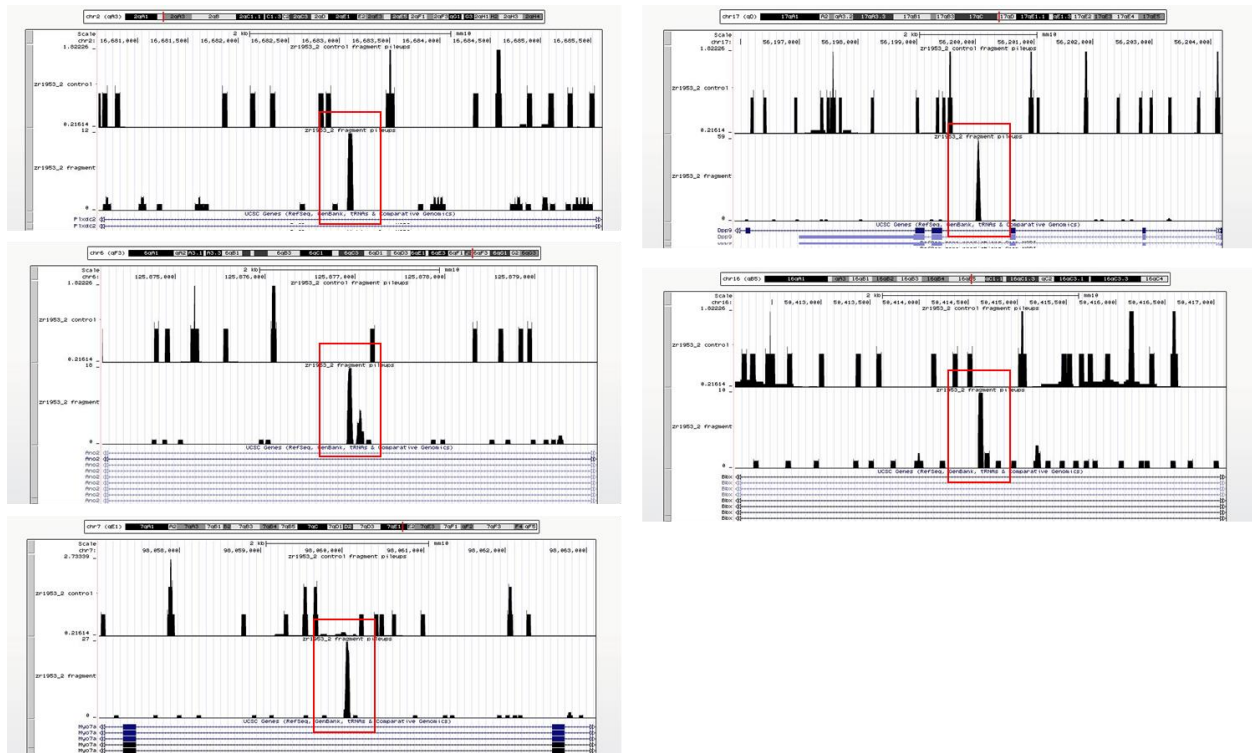


Figure 3.14: ChIP-Seq Peak Identification in the H3N41 Pull-Down Shows 5 Peaks Found within the Intron Region of Genes Important in Metabolism and Liver Disease. Each of the 5 genes identified are pictured above. The top read in each plot is the input and below is the H3N41 pull-down. The red boxes are the peaks identified to be unique found in the experimental sample after the H3N41 pull-down and sequencing. The genes are in order of chromosome starting at the top left to right and in descending order. The top left is *Plxdc2*, middle is *Ano2*, bottom is *Myo7*; top right is *Dpp9* and bottom right is *Bbx*.

Table 3.4: qPCR of Ano2 and Dpp9 following ChIP-Seq

<u>zr1953</u>	Dpp9 Intron				Normalized to Input				
	Ct			Avg.				Mean	SD
Input	27.58	27.82	28.03	27.70	108.67	92.02	79.55	100.35	11.78
H3nY41	29.30	29.53	29.66		32.99	28.13	25.70	30.56	3.44
IgG	28.51	28.50	28.46		57.04	57.43	59.05	57.24	0.28

<u>zr1953</u>	Ano2 Intron				Normalized to Input				
	Ct			Avg.				Mean	SD
Input	25.64	25.66	25.56	25.65	100.70	99.31	106.44	100.00	0.98
H3nY41	30.49	30.41	30.34		3.49	3.69	3.87	3.59	0.14
IgG	30.52	30.93	30.41		14.16	10.66	15.28	12.41	2.48

sites were all located within unannotated portions of the genome. Two potential targets identified in ChIP sequencing, Ano2, and Dpp9, were further tested for validity by quantitative PCR (qPCR) because of their functional roles in glucose transport, type-2 diabetes, obesity, and cancer. Quantitative PCR was performed for Dpp9 and Ano2, primer sets were used

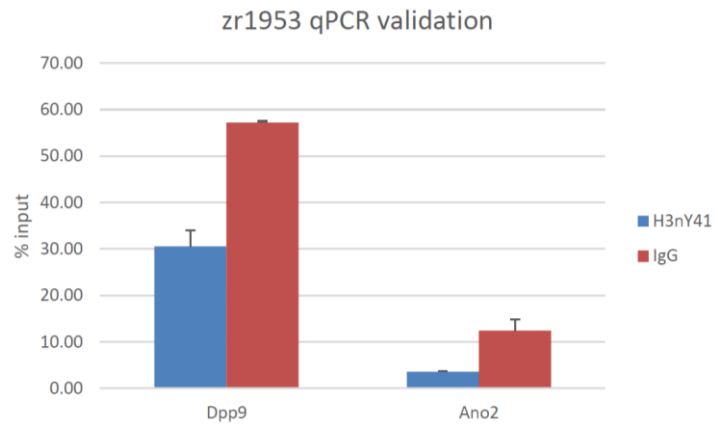


Figure 3.15: qPCR Validation of Ano2 and Dpp9. Two primer sets were designed for each genomic region. Optimal annealing temperature for each primer set was determined using end point PCR with input genomic DNA. Based on the results both Ano2 and Dpp9 failed validation.

to assess the ChIP specificity by qPCR. The results indicate that these 2 regions were not significantly enriched in the ChIP samples compared to IgG negative control (Table 3.4 and Figure 3.15).

Discussion

Tyrosine makes up approximately 1-2% of all amino acids, making it an unlikely target for post-translational modifications [141]. Here I demonstrate that tyrosine nitration occurs under normal physiological conditions, and also increases during times of oxidative stress. Alcohol consumption seems to increase nY abundance within the cell, most likely attributed to the increases in ROS/RNS stemming from ethanol metabolism [31-33, 108, 141]. Tyrosine nitration is thought to be a highly selective modification and occurs approximately 100-fold times less than tyrosine phosphorylation [106, 236]. It

has previously been reported that nY levels are found elevated in numerous pathological conditions such as inflammation, cardiovascular disease, and neurodegenerative disorders, and is thought to contribute to disease progression [101, 237-240]. Alcohol consumption and metabolism have been linked to high increases of oxidative stress and free radical formation within the liver [4, 20, 134, 135, 137, 142, 222]. These data further support the notion that nY has an important role in disease progression due to the increase of nY abundance for histone proteins after ethanol exposure (**Table 3.2**).

Previously, it has also been established that alcohol metabolism has a role in gene regulation by altering histone modifications such as acetylation and methylation [17, 18, 43, 96, 204, 241]. These new data now demonstrate that histone tyrosine nitration is a novel post-translational modification that is expressed endogenously at low levels and alcohol can cause increased expression after exposure (**Figure 3.1 & Table 3.2** respectively). It has also been speculated that tyrosine nitration may compete with tyrosine phosphorylation in order to inhibit signaling pathways and therefore alter transcriptional regulation [34, 103-105]. One example of competition between nitration and phosphorylation is the H3 (Y41) phosphorylation. H3pY41 signals the activation of Janus kinase 2 (JAK2)-regulated genes, including the hematopoietic oncogene *Imo2*, by inhibiting the binding of heterochromatin binding protein 1 (HBP1) [109, 235, 242]. These data show for the first time, the nitration of H3Y41, as well as a conformational change in the DNA upon H3Y41 nitration (**Figure 3.11 and 3.12**). H3Y41 nitration may have a role in repressing the JAK2-regulated genes during times of oxidative stress, offering a protective role against oncogenesis. Furthermore, these data also identified H3 (Y41) nitration was present on all 3 isoforms of H3 (3.1, 3.2, 3.3) (**Table 3.1**), which suggests a possible role in for histone nitration in all stages of DNA replication [242].

The importance of tyrosine nitration in gene regulation is further supported by the identified sites of nitration on heterogeneous nuclear ribonucleoproteins (hnRNP-A3) and Elongation factor 1-alpha 1 (Eef1a1). Heterogeneous nuclear ribonucleoproteins and enhancer binding proteins are important in the

regulation of transcription. Heterogeneous nuclear ribonucleoproteins are traditionally found in the nuclear compartment during transcription. The hnRNPs function to bind to the intron region of preRNA and mark it as not ready for transport into the cytoplasm [243-245]. Once the RNA is mature and ready for transport, the hnRNP is spliced out and then acts to mark the intron for degradation within the nucleus [243-245]. Eef1a1 is commonly known for its role in delivering transfer RNA (tRNA) to the ribosome during protein synthesis [246-249]. Eef1a1 also functions in nuclear export and has involvement in processes such as cell growth, cytoskeleton organization, signal transduction, and proliferation [246, 247, 250, 251]. Upon upregulation, Eef1a1 has also been demonstrated to have a role in the metastasis of different types of solid tumors [247, 250]. Nitration on Eef1a1 may act as a regulator for tumor suppression just as it is hypothesized to do upon H3nY41 nitration. When H3nY41 becomes nitrated it inhibits phosphorylation of that site, therefore, blocking the JAK2 signaling cascade [235]. Tyrosine nitration on hnRNPs and Eef1a1, along with the molecular dynamic evidence presented here, further support the hypothesis that tyrosine nitration is important in gene regulation, translation and also potentially tumorigenesis (**Figure 3.7**).

Identifying the mechanism for tyrosine nitration has proven to be difficult due to many different obstacles, both at the cellular and technical level. During times of ethanol consumption, the working hypothesis is that the increase in nitration is the result of peroxynitrite formation stemming from increased ROS/RNS. To date, most of the research on nY has been completed *in vitro* using synthetic peptides and peroxynitrite to initiate nitration [103, 104, 107, 109-112]. This method works well to give insight to specific tyrosine residues that are targeted for nitration, however, there has been little to no reproducibility *in vivo* because of the inability to mimic the physiological synthesis of peroxynitrite by the cell [31, 33, 101]. Tyrosine nitration research is also limited by the gap in knowledge pertaining to the possibility of dinitrase activity, which is able to reverse the nitro modification on tyrosine residues. There

have been several reports of dinitrase activity but currently little is known regarding the underlying mechanism or cellular environment important for promoting dinitrase activity [109, 113-117].

Another large hurdle of *in vivo* tyrosine nitration is the ability to isolate the nitrated peptide by mass spectrometry in complex mixtures. Nitrotyrosine is a very lowly expressed modification, and often, this modification goes undetected in cell lysate by using a traditional mass spectrometry methods. Recent research has suggested that using a pull-down method such as an IP in order to isolate nY from a whole cell lysate, works well to detect the nY modification on tryptic peptides [101]. However, using a pull-down method limits data analysis of a complex mixture by excluding any changes in protein abundance or pathway regulation in the cell. SILAC has also shown to be a useful resource in identifying nitrotyrosine but is limited by the cost of *in vivo* analysis [252]. Cellular fraction by ultra-centrifugation in combination with HPLC & high-resolution MS was sufficient to identify 51 potentially nitrated tryptic peptides after MaxQuant analysis. Even though only 4 out of the 7 histone nitrotyrosine sites (**Figure 3.3 & Figure 3.4**), the remaining 3 histone nitrotyrosine sites are pending further validation of H1 (Y27), H₂B (Y37), and H4 (Y98) (**Figure 3.5 & Figure 3.6**) based on signal interference. Following the previously described validation methods by Stevens *et al* (2008) [126], the identified peptides failed validation because not enough consecutive b or y ions could be referenced at acceptable abundance levels. Another reason these nitrotyrosine sites were not able to be fully annotated was due to the coelution of an isobaric peptide. Coelution of an isobaric peptide would cause signal interference, and hinder the mass spectrometers ability to differentiate between the 2 peptides fragmentation patterns. Furthermore, *Haqqani et al* (2002) have previously identified both, H₂B (Y37) and H4 (Y98) to be nitrated in the Mutatect tumor mouse model, which additionally strengthens the legitimacy of these nY sites to be true [106]. However, validation of H₂B may prove to be more difficult than expected due to 3 tyrosine residues within close proximity to each other (Y37, Y40, and Y42). Future testing of the validity H₂B (Y37) should incorporate

nitration at Y40 and Y42 since MaxQuant software identified the likelihood that both H₂B (Y37) and (Y40) could potentially become nitrated.

Nitrotyrosine modifications and their role in gene and protein regulation are only beginning to be understood. The abundance of nY histone proteins and ribonuclear proteins further strengthens the probability that nY modifications are important for gene and protein regulation (**Figure 3.7**). These data now show that by the use of synthetic peptides, four out of seven nY sites identified on histone proteins were able to be validated. Furthermore, molecular dynamic simulations strengthen the hypothesis by showing the DNA prefers a different conformation upon histone nitration (**Figure 3.8**). Interestingly, CHIP-seq identified 5 novel targets and 13 unannotated targets in the genome that H3nY41 interacts with following ethanol exposure. All five of the identified chromosome sites were located within the intron region, suggesting a potential role in splicing (**Figure 3.10**). However, Ano2 and Dpp9 were unable to be validated by qPCR following CHIP-seq experiment. The low abundance of nitrotyrosine may have played a role in the binding efficiency, or possibly H3nY41 does not target the genome and instead is a negative regulator of phosphorylation. Molecular dynamics suggest that the DNA prefers a different confirmation upon the nitration of H3Y41, however, the mechanism for tyrosine nitration and its functional role with the liver are still unknown. Nevertheless when taken in conjunction with the multiple nitrotyrosine sites on hnRNP-A3 as well as Eef1a1, further suggest the importance of nitrotyrosine modifications in RNA synthesis and RNA maturity, perhaps through mediating splicing machinery.

Chapter 4

Metabolic tracing of $^{13}\text{C}_2$ in the livers of 8-week male mice demonstrates the contribution of acetyl-CoA derived from ethanol metabolism to histone acetylation

Abstract

Epigenetic dysregulation through ethanol-induced changes in DNA methylation and histone modifications has been implicated in several alcohol-related disorders such as alcoholic liver disease (ALD). It has previously been shown that ethanol induces hyperacetylation in the liver following periods of heavy drinking. Currently, there are two proposed methods of alcohol-induced hyperacetylation. The first hypothesis encompasses ethanol metabolism and the formation of acetate, a metabolite that can be further converted to acetyl-CoA. Acetyl-CoA can then be used by histone acetyltransferases to acetylate lysine residues on histone proteins. This mechanism results in a direct use of ethanol for acetylation of n-terminal histone proteins, therefore hyperacetylation is a direct result of ethanol consumption. The second hypothesis involves the sirtuin family of deacetylase proteins. Sirtuin proteins regulate protein and histone acetylation throughout the cell because of their ability to remove the acetyl group from a protein when it is no longer needed. Like ethanol metabolism, the sirtuin family of proteins are also NAD^+/NADH -dependent. Ethanol metabolism has been linked to the inhibition of sirtuin activity by out-competing the deacetylases for the available cofactor NAD^+ . As a result ethanol metabolism will indirectly influence lysine acetylation due to inhibition of sirtuin proteins by increasing the amount of NADH , in turn, acetylation is upregulated from the inhibition of sirtuin proteins.

Alcohol-induced hyperacetylation has been well characterized although the underlying mechanism is still unclear. This study aims to use known targets for histone acetylation in order to identify

a mechanistic approach in order to bridge the gap between the two proposed hypotheses. By understanding how ethanol influences lysine acetylation potential targets of transcriptional regulation through epigenetic modifications that may influence the pathogenesis of ALD can be established. In order to determine how ethanol metabolism influences histone acetylation heavy-labeled ethanol ($^{13}\text{C}_2$) in conjunction with UHPLC-mass spectrometry in order to site-specifically quantify lysine acetylation on histone proteins after binge drinking. Using a single binge of ethanol (5g/kg) in 8-week-old male mice, ethanol was metabolically traced using the label incorporation derived from acetyl-CoA generated during ethanol metabolism. Blood alcohol levels were observed to be raised 4 hours the gavage, which correlates to an increase in $^{13}\text{C}_2$ -label incorporation seen on the N-terminal lysine residues of histones H3 and H4. Total acetylation quantified from the N-terminal lysine acetylation sites identified on H3 and H4 were also observed to be significantly increased after 24 hours. However, rapid turnover of histone acetylation sites was observed, and the heavy label was cleared following 24 h post-gavage. Moreover, the site-specific selectivity of label incorporation was observed to occur preferentially at one lysine acetylation site over another as determined by tandem mass spectrometry and when compared to projected isotope simulations. These data provide further evidence that hepatic ethanol metabolism directly impacts histone lysine acetylation in a site-specific manner and may also influence ethanol-induced gene expression through these transcriptionally activating chromatin marks.

Introduction

Chronic liver disease is consistently in the top 15 leading causes of death, of which 50% of those deaths are due to ALD [1]. Alcohol liver disease (ALD) is 100% preventable, however, in recent years binge drinking has been on the rise, especially in young adults between the ages of 18-34 [253]. Currently, alcohol-related expenditures cost the United States healthcare industry over \$250 billion dollars each year, of which \$119 billion stems from binge drinking alone [253]. The National Institute on Alcohol Abuse and Alcoholism (NIAAA) define binge drinking as any pattern of drinking that raises a person's BAC to

above 0.08 g/dL in one sitting [253]. Although most binge-drinkers do not exhibit alcohol dependency, the health risks are just as dangerous as chronic or heavy drinking [253-257]. Even though there is no distinct line in regards to when binge-drinking stops and chronic drinking begins, both are equally as dangerous to the consumer. Surprisingly, much is still unclear regarding the effects of binge drinking and ALI, when compared to the current literature regarding chronic ethanol exposure [4, 8].

Once alcohol is consumed, the liver begins to metabolize it using either ADH or CYP2E1. Alcohol metabolism disrupts normal cellular metabolic pathways by causing shifts redox potential and large increases in reactive oxygen species (ROS). Disruption in redox homeostasis can ultimately lead to disruption in pathways such as lipid peroxidation, cellular signaling, inflammation, and most recently transcriptional reprogramming and epigenetics, all of which lead to liver injury [89-91, 150]. Recently, the role of alcohol-induced epigenetic changes and their role in liver injury have become of great interest to scientist [15, 17-19, 25, 43, 96, 258-260]. Currently, little is known about the underlying mechanisms relating to alcohol-induced epigenetic changes and liver injury. This chapter aims to investigate how the metabolism of ethanol influences the acetylation of histone proteins.

Protein acetylation has very important roles throughout the cell, such as metabolic regulation, cellular signaling, transcriptional programming and more recently, epigenetics [89-91, 150]. During times of ethanol exposure, lysine acetylation has been shown to be altered in a variety of cell types and organelles [85, 86, 88, 119, 151, 152]. Hyperacetylation is the most prominent change observed in the cell after ethanol exposure, most frequently detected within the mitochondria [85, 86, 88, 119]. These changes in acetylation can be attributed to two separate mechanisms since protein acetylation is reversible. The first potential mechanism of hyperacetylation may be caused by the increasing levels of acetate that are produced as a byproduct of ethanol metabolism. Acetate levels have been recorded as high as 1.4 $\mu\text{Mol}/\text{min}$ per 10^8 cells or as high as 10mM in the perfusate of rat liver [23]. Acetate travels

throughout the bloodstream where it can be converted into acetyl-CoA and donate its acetyl group for metabolic processes such as lipid metabolism and cellular respiration. The acetyl group is removed from coenzyme-A by histone acetyltransferase, and then can be used to acetylate proteins [23, 120]. The second mode of action relies heavily on the inhibition of deacetylase proteins, most commonly known as the sirtuin family of deacetylase. Sirtuin activity can be inhibited by the competition for available NAD⁺ that is being used for ethanol metabolism [118]. The metabolism of ethanol within the liver is largely dependent on the cofactor NAD⁺, which is obtained from the mitochondria and cytoplasm within the cell [9, 82, 153]. As ethanol is metabolized, it competes with sirtuin deacetylase for available cofactor, in turn, promoting hyperacetylation [14, 155, 156]. Although ethanol exposure can lead to decreases in the activity of sirtuin 1 and 3 proteins, previous research has shown no changes in sirtuin protein abundance [38, 118, 157].

Post-translational modifications (PTMs), such as lysine acetylation, play important roles in protein regulation throughout the cell [158, 159]. Site-specific identification and characterization of PTMs are necessary for understanding their biological functions within the cell and their role in the pathogenesis of ALD [158]. Lysine acetylation has been implicated to be one of the most important regulators of cellular processes and protein regulation [159-162]. Moreover, lysine acetylation has been shown to crosstalk with other PTM's under different environmental conditions in order to control many aspects of cellular homeostasis [162]. Recent studies have shifted their focus to understanding how known sites of lysine acetylation are affected on histone protein tails following ethanol exposure [24, 151]. Changes in lysine acetylation of histone proteins have been attributed to a combination of the metabolism of ethanol [39], oxidative stress [163], and mitogen-activated protein kinase (MAPK) signaling pathways. These epigenetic changes in acetylation on histone tails are able to alter gene regulation and transcription to accommodate times of cellular stress.

Recently interest has developed in understanding how ethanol affects gene regulation through targeting known epigenetic marks on histone tails. For instance, acetylation of histone 3 lysine 9 (H3AcK9) induced by ethanol has been shown to be both dose and time-dependent, with notable increases occurring between 5 and 100 mM, which peak around 24 hours [23, 151]. Although 100 mM dose of ethanol seems high for human consumption (~0.450 g/dl), it is a concentration commonly observed in the serum of binge drinkers and chronic alcoholics [23]. In humans, a blood alcohol level (BAC) of approximately 0.200 g/dL would equal an approximate dose of 50mM ethanol and 100mM would be equivalent to a BAC of 0.400 g/dL. When acetate is used to mimic ethanol toxicity, doses of 1-10 mM showed a marked increase in H3K9Ac over the course of 4 hours and then plateauing until 24 hours when it begins to decrease [23]. These data were also verified in rat hepatocytes that were treated with ethanol, showing a necessity for H3K9Ac in ethanol metabolism and a possible role in liver injury [151]. For example, epigenetic marks of DNA methylation that are inherited, have been implicated in various diseases, such as the predisposition to alcoholism and ALD [16, 25-27]. These modifications are thought to be influenced by the increase in reactive oxygen species (ROS) and reactive nitrogen species (RNS) generated as a result of ethanol metabolism.

A recent shift in research has focused understanding on how ethanol-induced changes in lysine acetylation effect epigenetics by site-specific histone modifications. An interesting link is now being established between oxidative stress and subsequent epigenetic modifications in the liver (as well as other tissue types) triggered by ethanol exposure [20]. For example, ROS production in rat hepatocyte primary culture after chronic ethanol exposure was shown to contribute to the known liver epigenetic marker induced by ethanol, acetylation of histone H3 at Lys9 (H3K9Ac) [18, 43]. Histone acetylation is regulated by the activities of various histone acetyltransferases (HATs) and histone deacetylases (HDACs) where the activities of these enzymes are altered in hepatocytes after ethanol exposure [17, 18, 23, 39, 43, 121]. These changes may be explained by deacetylase inhibition, as well as rising acetate levels in the

bloodstream, which can become more than 20 times greater than fasting or consuming foods rich in fat [261].

Furthermore, ethanol-induced changes in histone acetylation patterns have been shown to selectively alter gene expression in rat livers while not affecting global protein expression [43]. Park *et. al.* (2003) discovered that acetylation of histone H3 lysine 9 was upregulated in hepatocytes over the course of 24 hours when treated with 50 and 100 mM ethanol [151]. Additionally, Kendrick *et. al.* (2010), showed that metabolically available acetyl-CoA from acetate is vital to the increased acetylation of proinflammatory gene histones and consequently the proinflammatory response in ethanol-treated macrophages [120]. Shukla *et.al.* (2015) established that ethanol and acetate exhibit differential outcomes of their metabolic effects on hepatic gene expression [23]. Current work by Kori *et. al.*, 2017 uses stable isotope labeling in cell culture (SILAC) and proteomic analysis to assess histone protein lysine acetylation, turnover and their potential targets on the genome [262]. The molecular mechanisms underlying how ethanol metabolism is be linked to histone acetylation is still unclear. Moreover, the mechanistic detail regarding the impact of oxidative stress on other histone modifications is essentially unknown. These data now demonstrate that ethanol metabolism contributes to the Acetyl-CoA pool, where in conjunction with HAT's can be used to acetylate histone proteins at known epigenetic marks of gene activation.

Materials and Methods

Acute-Binge Mouse Model using $^{13}\text{C}_2$ -Labeled Alcohol or Maltose-Dextrin

C57bl/6J mice (Jackson Laboratory, Sacramento, California) were maintained at the University of South Florida animal facility following the guidelines provided by the Institutional Animal Care and Use Committee (Appendix B).

Eight-week male C57bl/6 mice (n=3/group) weighing approximately 25 g, were administered an acute bolus dose of either $^{13}\text{C}_2$ -labeled ethanol (5g/kg) (Cambridge Isotope, Cat. # CLM-551-1, Tewksbury Massachusetts) or an isocaloric equivalent dose of maltose dextrin (BioServ, Cat. # 3653, Flemington, New Jersey) as previously described by *Bertola et. al.* [189]. Mice gavaged with $^{13}\text{C}_2$ -labeled ethanol were placed in their respective cages on top of heating pads to prevent hypothermia. At 0, 4, and 24 hours, mice were sedated using isoflurane, and a cardiac puncture were performed prior to euthanasia. Blood was collected and placed in a BD Microtainer (Cat. # 365967, Franklin Lakes, New Jersey) and a cervical dislocation was performed according to IACUC standards of humane euthanasia. Livers were collected and snap frozen in liquid nitrogen for later processing.

Blood Alcohol Test

Microtainers containing whole blood were allowed to clot at room temperature for 30 minutes and then spun at 10,000g for 10 minutes using a benchtop centrifuge. Serum was collected and stored in 1.7 μl microcentrifuge tubes (Axygen, Cat. # MCT-175-A, Fisher Scientific, Hampton, New Hampshire). Blood alcohol serum levels were measured in a 96-well plate, using Pointe Scientific diagnostic test (Cat. # A7504, Fisher Scientific, Hampton, New Hampshire) as per the manufacturer's instructions. Quality control was measured using Pointe Scientific standard (Cat. # A7504-STD, Fisher Scientific, Hampton, New Hampshire), and alcohol controls (Cat. #A7504-CTL, Fisher Scientific, Hampton, New Hampshire). Samples were read at 340nm using a Powerwave SX2 (BioTek, Winooski, Vermont) microplate spectrophotometer and exported to Excel for analysis. Serum collect from the first day was stored at -20°C and analyzed a second time with the 24 hr collections.

Sample Processing and LC-MS

Tissue Lysis, Histone Extraction, and Derivatization

Livers were thawed on ice and 50 mg of tissue was cut and placed into 2 ml homogenization buffer containing 10 mM sodium butyrate (Alfa Aesar, Cat. #A1107922, Fisher Scientific, Hampton, New Hampshire) and protease inhibitor cocktail (Roche, Cat. # 1183617001, Sigma Aldrich, St. Louis, Missouri). Tissues were broken down into a single cell suspension using a Dounce homogenizer with pestle A only. The whole cell lysate suspensions were placed into 50 ml conical tubes (Corning, Cat. # 430291, Fisher Scientific, Hampton, New Hampshire) and spun at 1500 rpm for 10 minutes to form a pellet. The homogenization buffer was discarded and the pellets were washed again in homogenization buffer, the spin was repeated and wash was discarded. Nuclei were isolated using a nuclear extraction buffer (homogenization buffer with the addition of 0.1% NP-40 (Thermo Scientific, Cat. # 28324, Fisher Scientific, Hampton, New Hampshire). Pellets were triturated 5-times using a wide-bore pipet tip and placed into microcentrifuge tube on ice. Nuclei were pop-spun 10 sec in a benchtop microcentrifuge and supernatant containing the cytoplasmic fractions were discarded. Nuclei were again washed in nuclear isolation buffer and pop-spun two times. Nuclei were then washed twice in homogenization buffer to remove excess detergent before histone isolation. Histone extraction buffer was prepared by adding 0.4N HCl (Fisher Chemical, Cat # A144-500, Fisher Scientific, Hampton, New Hampshire) to the homogenization buffer. Nuclei were resuspended and lysed by sonication (30% amp, 5s on/off for 1 min) while on ice and supernatant was checked for complete DNA shearing by pipetting up and down. If DNA was present then sonication was repeated until complete lysis. Histone lysate was placed at 4°C over-night, rocking to ensure complete protein precipitation. The following day the histone lysate was spun max rpm and the supernatant, containing the histones, was placed into a clean microcentrifuge tube. Histone lysate was quantified using the BCA kit (Pierce, Cat. # 23225, Thermo Scientific, Hampton,

New Hampshire). Histones were placed into 5 µg aliquots and dried in a SpeedVac (Thermo Fisher Scientific, Hampton, New Hampshire) for derivitization. Histones were next subjected to propionylation as previously described by the Garcia Lab, except a 3:1 ratio of ACN (Fisher Chemical, Cat. # A998SK-4, Fisher Scientific, Hampton, New Hampshire) to propionic anhydride (Sigma Aldrich, Cat. # 240311, St. Louis Missouri) was substituted in lieu of 2-propanol [263].

LC-MS and Data Analysis

Lypholyzed samples were resuspended in 0.1% formic acid (Fisher Chemical, Cat. # A117-50, Hampton, New Hampshire) and HPLC-grade water (Fisher Chemical, Cat. # W5-4, Hampton, New Hampshire). Samples were next analyzed using tandem mass spectrometry on a UHPLC-MS Q-Exactive Plus Mass Spectrometer (Thermo Fisher Scientific, Hampton, New Hampshire) and eluted over 1 hr gradient. Samples were eluted over a NanoViper 50 cm x 75 µm I.D. reversed phase column packed with 3 µm C18 material with 100 Å pore size (Thermo Fisher Scientific, Hampton, New Hampshire) using a stepped normalized collision energy (NCE) of 29 and 32 and a gradient of 2-98% ACN in 0.05% TFA. A precursor MS scan of 350-1550 m/z was performed at a resolution of 70,000 using a larger isolation window (2.5 m/z) and the top 10 most abundant peaks were selected for subsequent MS/MS analysis. Mass spectra were then processed using the MaxQuant software package (version 1.5.0.30, <http://maxquant.org>) employing the Andromeda search algorithm against the SwissProt reference database for *Mus musculus* (UniprotKB, April 2017), a second database of known contaminants provided by the MaxQuant suite was also employed. Parameters include a minimum peptide length of 7 amino acids, a maximum of 2 missed cleavages and a mass tolerance of 20 ppm. A 0.01% false discovery rate was used for both peptides and proteins with a mass error of less than 1. Protein quantification was calculated using N-terminal lysine acetylation and methionine oxidation. Variable modifications included in the search consisted of lysine acetylation, heavy lysine acetylation (¹³C₂), lysine propionylation, and

mono- and tri-methylation of lysine and arginine. Manual data analysis by extracted ion chromatogram (XIC) and relative abundance (RA) analysis were completed using Xcalibur software package (version 3.0, Thermo Fisher Scientific, Hampton, New Hampshire). Base peaks were analyzed using a 5 ppm cutoff and precision to the 5th decimal for each ¹²C and ¹³C₂ peak containing a lysine acetylation or propionylation site that was identified by MS and verified by tandem mass spectrum.

Isotopic Precursor Intensity Extraction Using R

Raw files were converted to .mzML format using Proteowizard [264, 265]. MaxQuant “Evidence.txt” search results were used to identify modified Histone H4 peptide-spectrum-matches (PSMs) for intensity extraction. Precursor intensity values were extracted using the Bioconductor package “mzR” [264]. MaxQuant results were filtered for modified histone PSMs containing values for ‘Raw file’, ‘MS/MS Scan Number’, and ‘MS/MS m/z’ value. These values were compared to the scan header information for each raw file to obtain precursor scan numbers. Intensity values for monoisotopic m/z peaks were extracted from the corresponding precursor scan number, using m/z values within 0.01 m/z units of the ‘MS/MS m/z’ value. The maximum intensity value within the given m/z window was used for each measurement. Intensity values for M + 1, M + 2, and M + 3, and M + 4 peak were extracted using the ‘MS/MS m/z’ value plus the mass difference of ¹³C and ¹²C divided by the charge state ($1.003355 / z * \text{isotope peak}$). Incorporation of ¹³C-labeled ethanol was calculated using the ratio of [M + 2] peak to [M] peak. Incorporation values were plotted using ggplot2 from the Tidyverse package [266].

Results

Blood Alcohol Levels after an Acute Alcohol Binge Correlate with ¹³C₂ Incorporation over 24 Hours

Eight-week-old male mice (n=3) were separated into control or experimental groups based on equal weight. The mice were gavaged in the early morning with an acute dose of either 5g/kg ¹³C₂-labeled

ethanol or an isocaloric control of maltose dextrin. Mice were sedated prior to euthanasia, and blood was collected via a cardiac puncture in order to determine the serum blood alcohol content (BAC). Mice that were gavaged with $^{13}\text{C}_2$ -heavy labeled ethanol were observed to have average BAC levels of 305 mg/dL (n=3) 4-hours after the gavage; following 24-hours serum BAC levels returned to levels comparable to the control mice (**Figure 4.1A**). Peptides were subjected to propionylation prior to MS analysis, this technique adds a propionyl group to all the unmodified lysine residues. Propionylation makes the N-terminal regions of the histone tails more hydrophobic and increases coverage and separation of the column (**Figure 4.1F**). Respectively, each proteoform was next analyzed for relative abundance in $^{13}\text{C}_2$ using mass spectrum analysis (**Figure 4.1B-E**). Data shown in Figure 4.1B-E corresponds to peptide H3(K18-R26) and is representative of the H3(K9-16) peptide (data not shown). The top two spectra are taken from the 4-hour time point pertaining to the control and heavy-labeled ethanol gavaged mice (**Figure 4.1B-C**). The [M+2] peak labeled in the top spectrum is the naturally occurring $^{13}\text{C}_2$ peak, and the difference in relative abundance calculated for the $^{13}\text{C}_2$ peaks in the control and ethanol mice can be used to quantify the amount of ethanol was incorporated into the acetylation site. Heavy label incorporation was found to have a similar increasing trend as the BAC results and was maximized at the 4-hr time point. The ethanol mice gavaged with the $^{13}\text{C}_2$ -heavy label showed marked increase of the [M+2 peak] after 4-hours (**Figure 4.1C**) when compared to the time-matched control mice (**Figure 4.1B**). Following 24-hours $^{13}\text{C}_2$ expression returned to basal levels in the ethanol gavaged mice and matched both the 4 and 24-hour control mice (**Figure 4.1 B, D, & E**).

Next, histone peptide coverage was evaluated using MS in regards to the unmodified, single acetyl, and double acetyl H3 peptides containing lysine K9, K14, K18, and K23. Both H3 peptides identified by MS contained two potential acetyl sites, H3 (K9 & K14) and H3(K18 & K23). Chromatographic separation was used in order to isolate the double propionylated, propionylated/ acetylated, and the double acetylated peptide for quantitation (**Figure 4.1F**). Because of the fragmentation pattern of the b

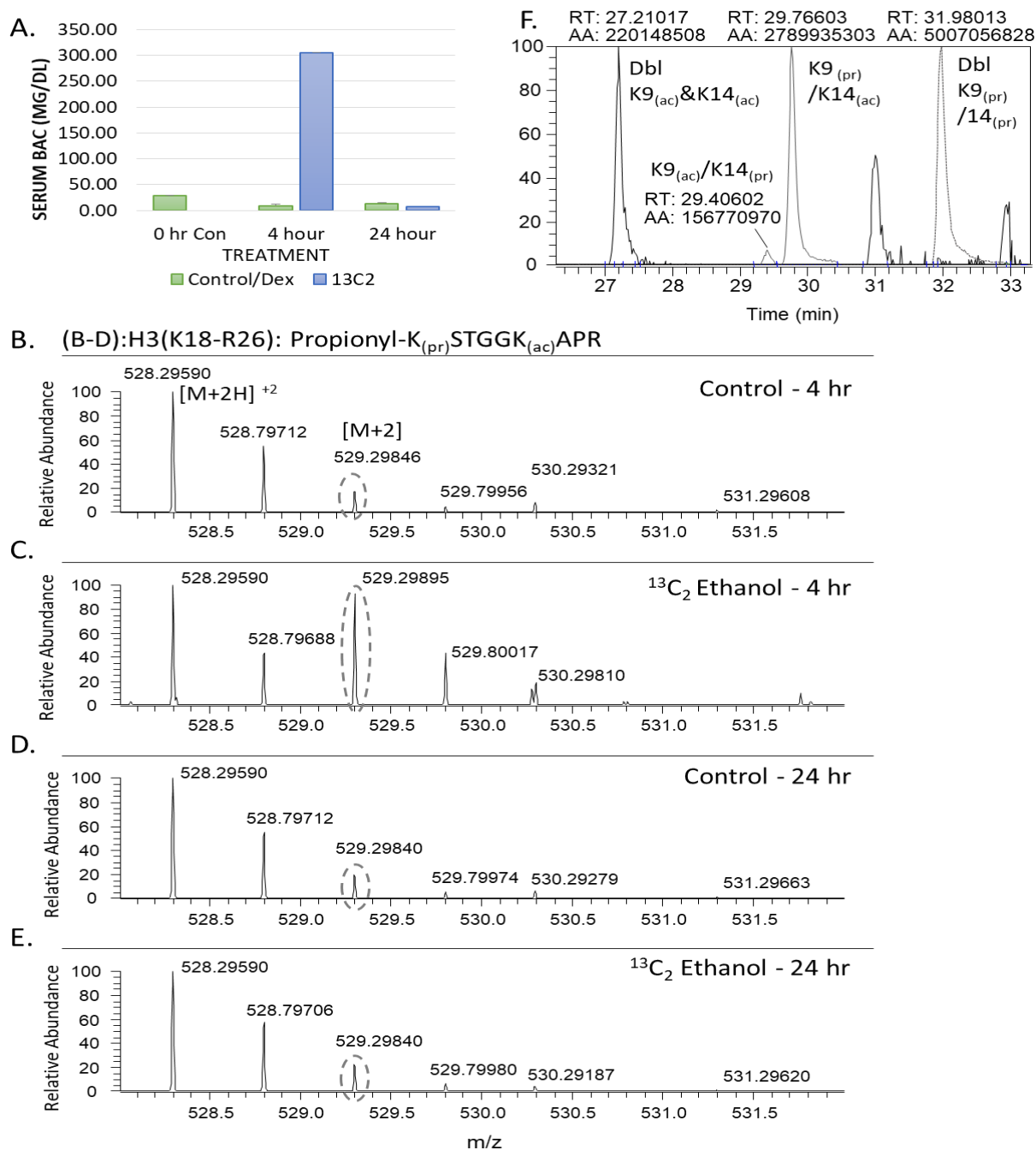


Figure 4.1: Site-Specific Incorporation of Heavy-Labeled Ethanol Peaks Around 4-Hours following the Same Trend as Serum BAC Level. (A) Blood was collected from 8-week-old mice (n=3) and serum was used for BAC analysis at 0, 4, and 24-hours. Data was plotted using the average BAC within each group with the standard deviation. (B-D) Representative mass spectrum of the H3K9/K14 peptide demonstrating ¹³C₂-heavy label incorporation at the [M+2] peak. (B-C) Mass spectrum taken from the 4 h mice gavaged with either maltose dextrin (C) or ¹³C₂-labeled ethanol (D). (E-F) Mass spectrum taken from the 24 h mice gavaged with either maltose dextrin (E) or ¹³C₂-labeled ethanol (F). Endogenous ¹²C is represented by the monoisotopic peak [M+2H]²⁺ and either endogenous ¹³C₂ or increased ¹³C₂ expression from label incorporation is depicted by the [M+2] peak (dashed ovals). (F) Chromatographic separation of the peptide coverage representative of Histone 3 K9-R17. Left peak (black) represents the doubly acetylated H3K9Ac and H3K14Ac, middle peaks (grey) include H3K9Ac(left) and H3K14Ac (right), and the dashed peak on far right (grey dashed) denotes the doubly propionylated H3K9(prop) and H3K14(prop) peak.

and y-ions, H3K9Ac was able to be isolated from H3K14Ac allowing for site-specific quantitation of heavy-label at each site. Each modified and unmodified peptide was quantified for heavy-label incorporation using extracted ion chromatogram analysis (XIC) of relative abundance (**Figure 4.1F**). Relative abundance of acetylation at each H3 site was quantified independently for both the ^{12}C [M] and $^{13}\text{C}_2$ [M+2] peaks in regards to the individual proteoform (doubly acetylated, singly acetylated (acetyl/propionyl), and doubly propionylated) for the identified H3 peptides (**Figure 4.1F**). XIC analysis was performed on the two consecutive histone H3 peptides, the first is H3 (K9-R17) containing lysine's K9 and K14, and the second peptide covers H3(K18-R26) and contains lysine's K18 and K23. The average ratio of $^{13}\text{C}_2$ to ^{12}C was then calculated in order to determine the fold-change $^{13}\text{C}_2$ incorporation for each potentially modified site.

Characterization of $^{13}\text{C}_2$ -label incorporation on Histone Proteins after an Acute Ethanol Gavage

Histone H3K9 and H3K14 proteoforms were analyzed and graphed to show fold change in $^{13}\text{C}_2$ incorporation (**Figure 4.2A**). Graphs depict both with (H3K9-R16) and without (H3K17-R26) site specificity regarding the singly acetylated proteoform (acetyl/prop) (**Figure 4.2A**). Significant incorporation of $^{13}\text{C}_2$ was established using a 2-tailed Welch's t-test where $p \leq 0.05$) and plotted with standard error of the mean (SEM). Significant incorporation of $^{13}\text{C}_2$ was observed site specifically for H3K14Ac ($p=0.004$ and $p=0.01$) as well as the non-site specific singly acetylated peptide ($p=0.01$ and $p=0.02$) at 4-hours post gavage when compared to the 0 (baseline) and 4-hour control, respectively (**Figure 4.2A**). The H3K14Ac peptide was also found to have a significant increase in $^{13}\text{C}_2$ incorporation ($p=0.002$) following 24 h ethanol gavage when compared to the baseline (0 h control) mice (Fig. 2A). Fold change of $^{13}\text{C}_2$ incorporation pertaining to the peptide containing H3K18/K23 were also calculated as previously described above, and ratios were graphed for each proteoform, however without site-specificity (**Figure 4.2B**). Significant $^{13}\text{C}_2$ incorporation was observed on the singly acetylated proteoform at 4 hours ($p=0.01$) and 24-hours ($p=0.02$) when compared to both the baseline (0 h) and their respective time-matched controls (**Figure**

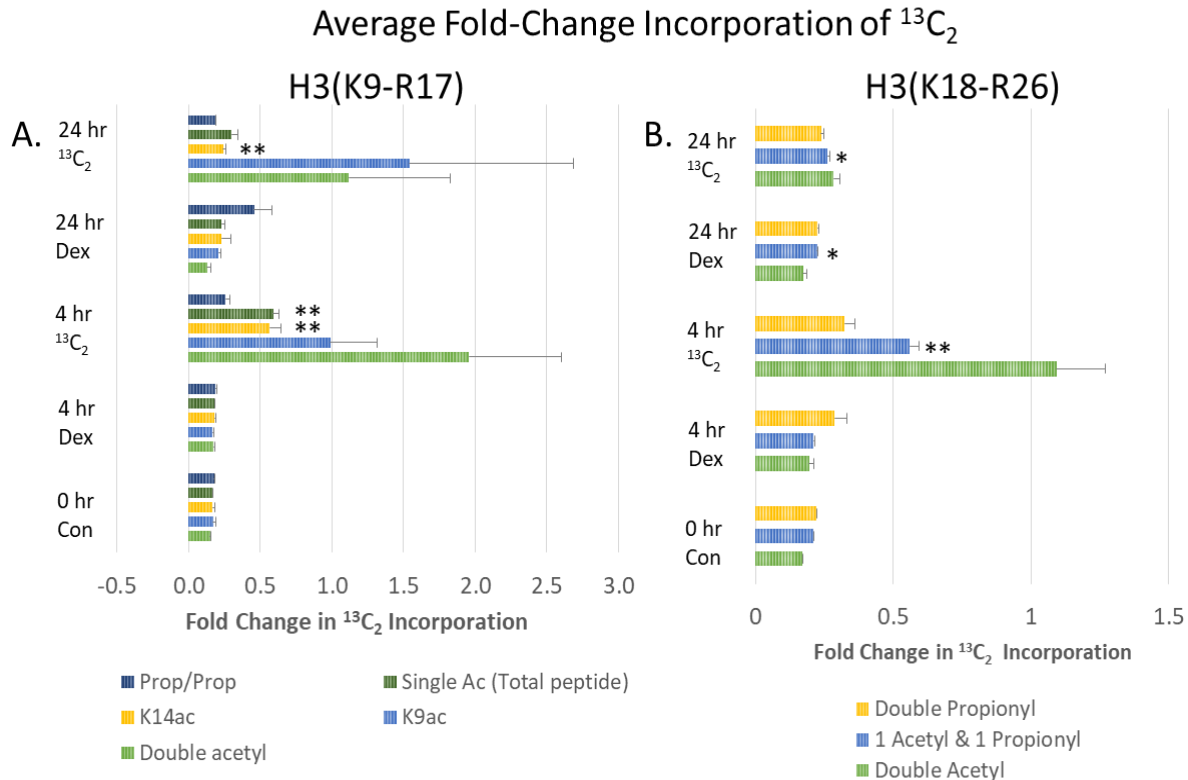


Figure 4.2: Label Incorporation for each H3 Peptide were Quantified by Extracted Ion Chromatogram Analysis. (A-B) Fold change in $^{13}\text{C}_2$ incorporation was calculated by taking the average of the XIC ratios of $^{13}\text{C}_2$: ^{12}C ($n=3$) for peptides containing H3K9/K14 (**A**) and H3K18/K23 (**B**). Individual standard deviations were used to calculate were the samples fell in regards to the mean. Significant $^{13}\text{C}_2$ incorporation is denoted by * $p \leq 0.05$ or ** $p \leq 0.01$, and calculated using a Welch's t-test. (**A**) Fold change of $^{13}\text{C}_2$ incorporation pertaining to the peptide containing H3K9/K14. Ratios were graphed for 0, 4 and 24 hours for the doubly acetylated H3K9 and K14, either H3K9 or K14 single acetylation, the sum of both singly acetylated peptides or total peptide single acetylation and the doubly propionylated peptide. (**B**) Fold change of $^{13}\text{C}_2$ incorporation for the peptide containing H3K18/K23 was calculated as stated above. Ratios were graphed for the doubly acetylated, singly acetylated, and doubly propionylated peptide containing H3K18/K23.

4.2B). No significant incorporation of heavy label was observed for either doubly acetylated peptide, H3K9Ac/K14Ac or H3K18Ac/K23Ac at any time point (**Figure 4.2A-B**).

Next, total acetylation was quantified as a ratio of ratios; equal to the ratio of the acetylated ($^{13}\text{C}_2$ + ^{12}C) peptide to non-acetylated peptide, divided by the ratios of the ratio of the acetylated ($^{13}\text{C}_2$ + ^{12}C) peptide to non-acetylated peptide for each time-matched control and the ratio of the acetylated ($^{13}\text{C}_2$ + ^{12}C) peptide to non-acetylated peptide for the ethanol-treated mice (**Figure 4.3 A-B**). The ratio of ratios was calculated for both the H3K9/K14 (**Figure 4.3A**) and H3K18/K23 (**Figure 4.3B**) peptides. Propagation

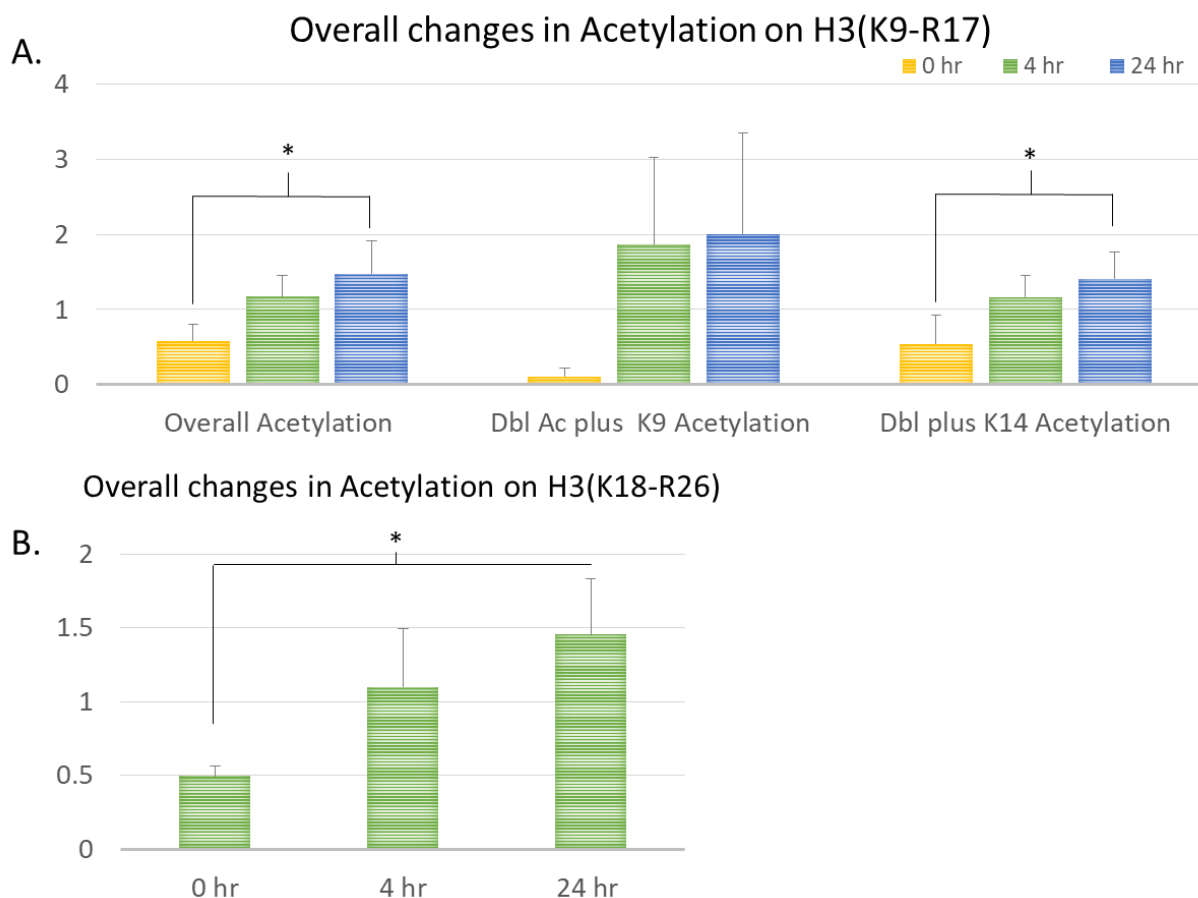


Figure 4.3: Overall Changes in Total Acetylation on H3 were quantified by Extracted Ion Chromatogram Analysis. (A-B) Total acetylation was expressed as the average of the sum of $^{13}\text{C}_2$ and ^{12}C for each mouse and then taking the ratio of total acetylation to unacetylated over the ratio of ethanol-treated to their time matched controls for the H3K9/K14 (A) and H3K18/K23 (B). Propagation of error was used to calculate the random error within the sample distribution for each peptide. Significance was determined using a 2-tailed paired students t-test and denoted by * $p \leq 0.05$ or ** $p \leq 0.01$. (A) Overall acetylation was calculated for the peptide corresponding to H3K9/K14 as well as site-specifically for K9 and K14 acetylation and the doubly acetylated peptide. (B) Overall total acetylation was calculated for the peptide pertaining to H3K18/K23 in its entirety.

of error was used to calculate the random error within the sample distribution. Increases in overall acetylation of the H3K9/K14 peptide, show a significant increase ($p=0.04$) in acetylation over the 24-hour time-course when compared to the baseline (0 h) (Figure 4.3A, left). Total change in acetylation was also calculated site-specifically to include H3K9 (Figure 4.3, middle) and H3K14 independently from each other (Figure 4.3A, right). Interestingly, total acetylation excluding H3K14 acetylation (Figure 4.3A, middle) was not found significant, whereas the total acetylation excluding H3K9 was found to be significant ($p= 0.02$)

after 24 h when compared to the 0-hr control mice and not to their time-matched control (**Figure 4.3A, middle**). Next, the overall changes in acetylation were calculated as described above in regards to the peptide containing H3K18 and H3K23. Total acetylation on the H3K18 and H3K23 peptide was found to be significantly increased ($p=0.02$) in ethanol-treated mice after 24-hr when compared to the 0-hr control mice, however, no changes in overall acetylation were observed between the ethanol- and control-treated mice at 4 hours (**Figure 4.3B**).

Isotope Simulation Suggests a Mixture of $^{13}\text{C}_2$ Incorporation on the Double Acetylated Peptide after 4-hours Ethanol Exposure

H3K9-R17 Analysis of $^{13}\text{C}_2$ Incorporation on the Doubly Acetylated Peptide After 4-hours Ethanol Gavage

Mass spectrum obtained from the doubly acetylated H3K9/K14 and H3K18/K23 peptides were compared to predicted isotope simulations generated in X-Caliber Software. The simulation is based on the naturally occurring ^{12}C isotopic peak distribution for the peptide of interest. Figure 4A depicts the predicted isotope simulation of the naturally occurring doubly acetylated peptide containing H3K9Ac and H3K14Ac (H3K9-R16). Below the isotope, simulation is the mass spectrum pertaining to a representative spectrum obtained from a control mouse 4-hours after being gavaged with maltose dextrin (**Figure 4.4B**). The isotope distribution was found to be comparable between the simulation and experimental sample, with no detectable increases in the $^{13}\text{C}_2$ ([M+2]) peak. However, when the [M+4] peaks are compared between the simulation and the control mouse, the signal was lost in the experimental sample due to coelution of an isobaric peptide (**Figure 4.4A and 4.4B**). Below the control sample, is spectra obtained from a mouse gavaged with heavy-labeled ethanol, and data indicates a marked increase in relative abundance of $^{13}\text{C}_2$ [M+2] and $^{13}\text{C}_4$ [M+4] when compared to the control mouse (**Figure 4.4C and 4.4B**).

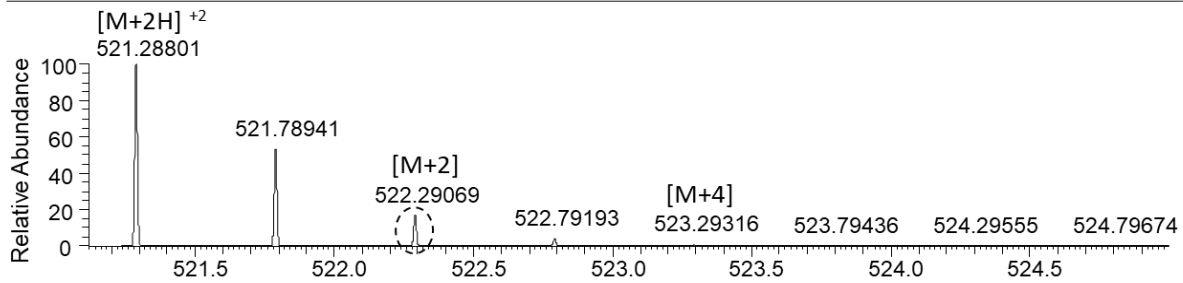
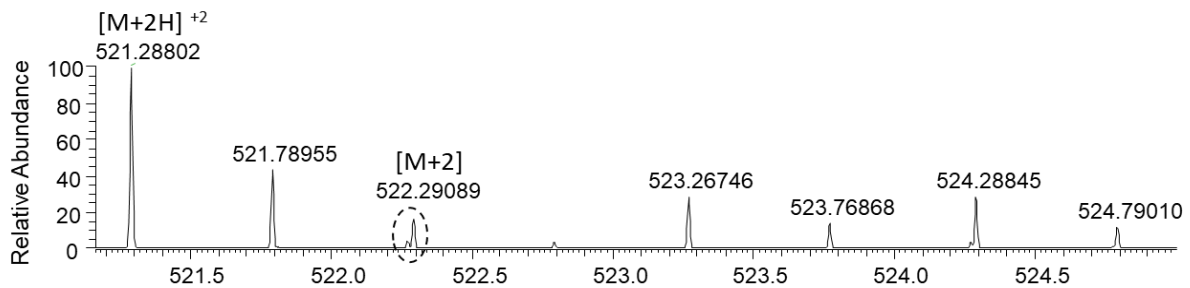
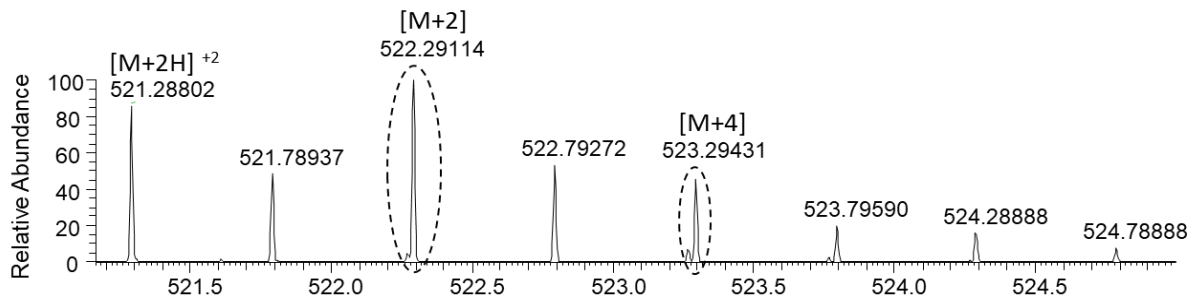
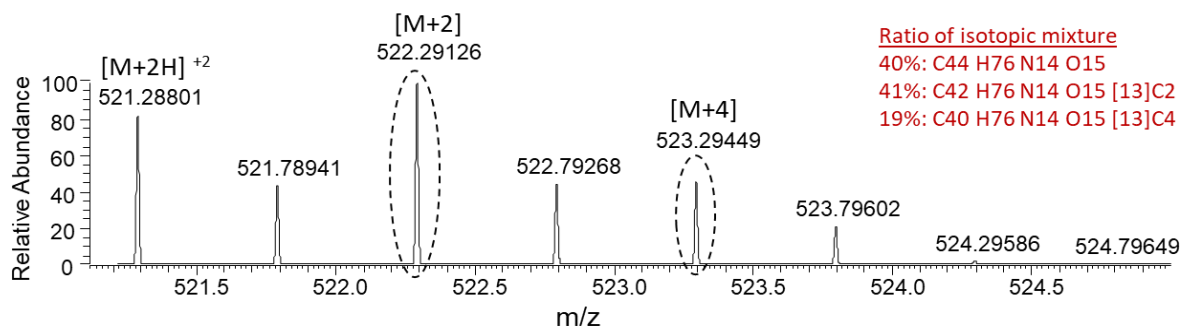
A. ^{12}C Simulation H3K₉-R₁₇: propionyl-K(Ac)STGGK(Ac)APR**[m/z]=521.28801****B. 4-hr control H3K₉-R₁₇: propionyl-K(Ac)STGGK(Ac)APR****C. 4-hr $^{13}\text{C}_2$ ethanol gavage H3K₉-R₁₇: propionyl-K(Ac)STGGK(Ac)APR****D. ^{12}C & $^{13}\text{C}_2$ Mixture Simulation H3K₉-R₁₇: propionyl-K(Ac)STGGK(Ac)APR**

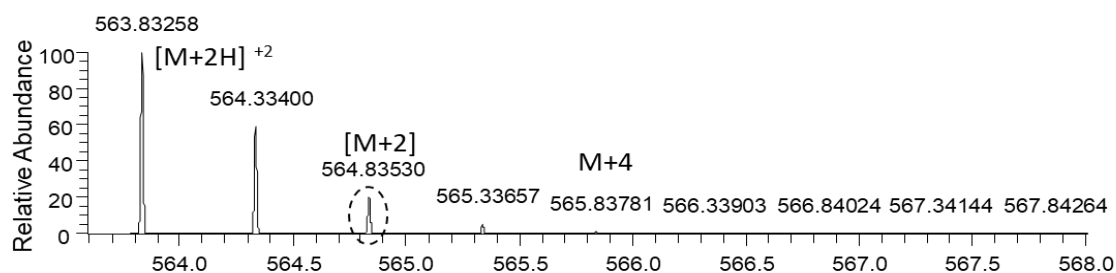
Figure 4.4: Mass Spectra of the H3 Doubly Acetylated Peptide Representative of H3K9/K14 Suggests Site-Specific and Time-Dependent Incorporation of the Heavy-Label Ethanol. (A-D) Mass spectrum comparison of the isotopic distribution of the doubly acetylated peptide covering H3K9/K14 by simulation (A) Isotope ^{12}C simulation predicting the expected isotopic distribution of the doubly acetylated peptide H3K9/K14 ($m/z=521.28801$). (B-C) 8-week mice gavaged with either $^{13}\text{C}_2$ -labeled ethanol (C) or maltose dextrin (B). Increases in heavy-label incorporation can be determined by peak comparison of the $^{13}\text{C}_2$ [M+2], and $^{13}\text{C}_4$ [M+4] peaks (dashed ovals). (D) Mass spectra simulation depicting a ratio of no label incorporation [M+2H] $^{2+}$, $^{13}\text{C}_2$ incorporated at a single acetyl site [M+2], or incorporation at both acetylation sites [M+4].

Also, the $^{13}\text{C}_2$ [M+2] peak was found to exceed $^{13}\text{C}_2$ peak at the 4-hour time point in the ethanol gavaged mice (**Figure 4.4C**). The $^{13}\text{C}_4$ [M+4] peak obtained from the ethanol mouse had to be compared to the isotope simulation because of the isobaric interference of the coeluted peptide in the control mouse spectra (**Figure 4.4A-C**). Finally, in order to assess the incorporation of the heavy-label, a mixture of isotopes containing ^{12}C , $^{13}\text{C}_2$, and $^{13}\text{C}_4$ was used to simulate the ratio of isotopes observed the ethanol-treated mice after 4-hours (**Figure 4.4D**). The simulation predicted a mixture of isotopes arising from different incorporation rates on the separate acetylation sites (**Figure 4.4D**). Simulation analysis showed that 41% of $^{13}\text{C}_2$ incorporation occurred at a single acetyl site, whereas 19% of incorporation occurred at both sites, leaving 40% of the acetyl groups unlabeled (**Figure 4.4D**).

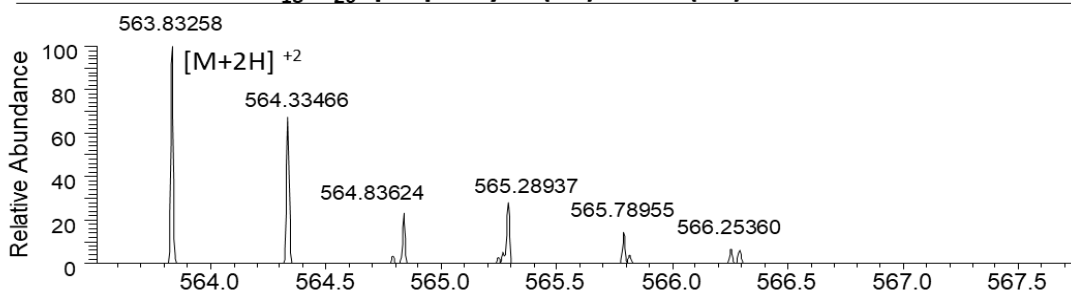
H3K18-R26 Analysis of $^{13}\text{C}_2$ Incorporation on the Doubly Acetylated Peptide 4-hours After Ethanol Gavage

The same analysis of isotopic distribution was completed for the doubly acetylated peptide containing H3K18Ac/K23Ac (**Figure 4.5A-D**). Figure 4.5A shows the ^{12}C simulation for the H3K18-R26 peptide. A mixture of label incorporation was again observed when comparing the ^{12}C simulation to the control gavage mouse 4-hours post maltose dextrin (**Figure 4.5A-B**). Results were similar for the control and the ^{12}C simulation, except the 4-hour control mouse, did not display the $^{13}\text{C}_2$ peak due to coelution of an isobaric peptide (**Figure 4.5A-B**). Because both the 4-hour control mice and simulated isotopic distributions closely resembled each other, they were considered equal to the heavy-label ethanol comparison (**Figure 4.5A and C**). Furthermore, the mice receiving the heavy-label gavage also demonstrated a mixture of label incorporation when comparing the ^{12}C , $^{13}\text{C}_2$, and $^{13}\text{C}_4$ peaks (**Figure 4.5C**). Simulation of the doubly acetylated peptide, H3K18Ac/K23Ac, indicated that 44% of label incorporation only occurred at a single acetylation site and, 23% of peptides show incorporation at both acetyl sites, leaving 33% of the remaining peptides unlabeled when compared to the 4-hr ethanol-treated mice (**Figure**

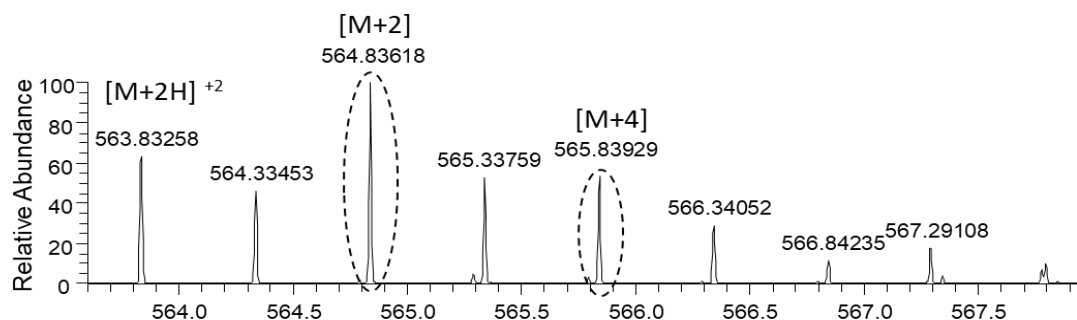
A. ^{12}C Simulation H3K₁₈-R₂₆: propionyl-K(Ac)QLATK(Ac)AAR



B. 4-hr control H3K₁₈-R₂₆: propionyl-K(Ac)QLATK(Ac)AAR



C. 4-hr post- $^{13}\text{C}_2$ gavage H3K₁₈-R₂₆: propionyl-K(Ac)QLATK(Ac)AAR



D. ^{12}C & $^{13}\text{C}_2$ Mixture Simulation H3K₁₈-R₂₆: propionyl-K(Ac)QLATK(Ac)AAR

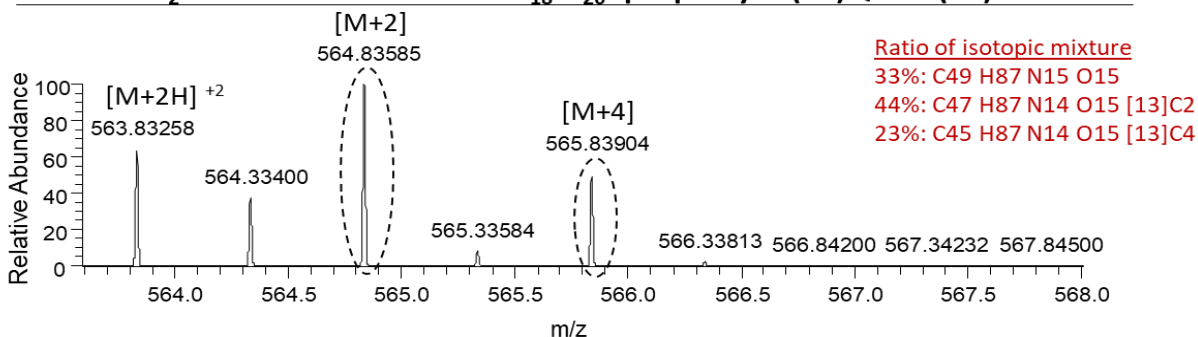


Figure 4.5: Four-Hour Comparison of Simulated Mass Spectra to the Experimental MS of the H3 Doubly Acetylated Peptide H3K18/K23 Suggests Site-Specific and Time-Dependent Incorporation of the Heavy-Label Ethanol. (A-D) Isotopic distribution of the doubly acetylated peptide corresponding to the peptide containing H3K18/K23. (A) Simulated mass spectra portraying the expected ^{12}C isotope distribution for peptide H3K18-R26. ($m/z=521.28801$) (C-D) Isotopic distribution taken from the 8-week-old mice gavaged with either $^{13}\text{C}_2$ -labeled ethanol (C) or maltose dextrin (D). Increases in heavy-label incorporation can be determined by peak comparison of the $^{13}\text{C}_2$ [M+2], and $^{13}\text{C}_4$ [M+4] peaks (dashed ovals).

4.5C-D). These data suggest that following an acute ethanol binge, label incorporation is preferential at a single acetylation site before being incorporated at both sites (**Figure 4.5C**).

Incorporation of $^{13}\text{C}^2$ on Multiple N-Terminal Acetylation Sites on H4 (K5-R17)

The N-terminal region of histone H4 consists of 4 lysine residues, H4K5, K8, K12, and K16, all of which are free to become acetylated and/or methylated (data not shown). XIC analysis proved to be an impractical method of quantification on H4 due to the numerous different configurations of lysine modifications that could be detected at any given time. The software R was used to extract the acetylated H4 intensities identified by MaxQuant. Nine separate acetylation configurations were identified on H4(G4-R17) (**Figure 4.6**) Box plots were used to illustrate each of the identified H4 proteoforms identified

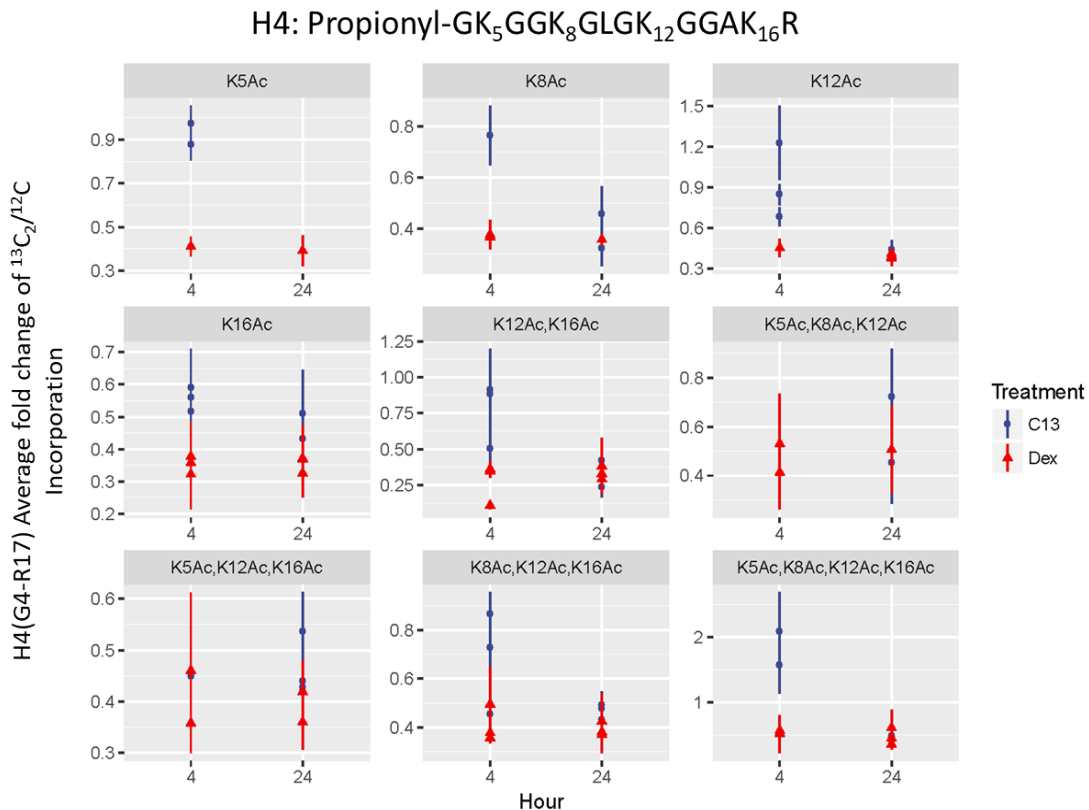


Figure 4.6: R Facilitates Quantitation of $^{13}\text{C}_2$ Incorporation for the Multiple Acetylation Sites on Histone 4 (G4-R17). Precursor intensity values for $^{13}\text{C}_2$ and ^{12}C isotopic peaks were extracted using the Bioconductor package “mzR”. Plot values represent the ratio of $^{13}\text{C}_2$ / ^{12}C peak intensities for each identified Histone H4 proteoform after 4-hours and 24-hours post $^{13}\text{C}_2$ -labeled ethanol gavage or dextrin gavage. The points represent average incorporation for each mouse, and line ranges represent 0.5 standard deviations above and below the

by MaxQuant from both the control and heavy-label gavaged mice. The average intensities for each proteoform were calculated from both the control and ethanol gavaged mice and used to find the ratio of $^{13}\text{C}_2$ to ^{12}C . Surprisingly, each singly acetylated H4 proteoform was identified as a single modification, and $^{13}\text{C}_2$ was incorporated within 4-hours post gavage (**Figure 4.6**). Histone H4K12Ac was found in each mouse to have the greatest fold-change, and the smallest standard deviations (**Figure 4.6**). All proteoforms identified followed the same metabolic trend of the greatest heavy-label incorporation occurring within 4-hours (**Figure 4.6**). Interestingly, the monoacetylated (H4K16Ac), and triacetylated (H4K5Ac, H4K8Ac, H4K12Ac and H4K5Ac, H4K12Ac, H4K16Ac) peptides showed $^{13}\text{C}_2$ -label incorporation remaining after 24 hours (**Figure 4.6**). These data show that once multiple acetylation sites are incorporating the heavy-label at different rates, combined with acetylation turnover rates, quantification gets more difficult to assess. In cases like H4, where the sequence is lysine and glycine-rich, tandem mass spectrometry and *de novo* sequencing can be used as a way to cross-reference heavy-label incorporation at a specific site (**Figure 4.7, top**). Annotating a respective spectra displays a mass shift of 2^+ Da when an acetylated residue contains the heavy-label (**Figure 4.7, top**). When the peaks are magnified, the peak distribution contains the y_7 monoisotopic peak, as well as peaks pertaining to the $^{13}\text{C}_2$ and $^{13}\text{C}_4$ peaks (**Figure 4.7, bottom**). These data present challenges for the software to decipher if the peak profile contains label incorporation at one site as a ^{12}C monoisotopic peak, a true monoisotopic peak with $^{13}\text{C}_2$ heavy label or as a mixture of label incorporation (**Figure 4.7, bottom**).

Discussion

Chronic ethanol exposure has been shown to induce hyperacetylation of proteins within the mitochondria and cytoplasm [85, 87, 88, 118, 119]. Dysregulation of lysine acetylation has been linked to having numerous implications in diseases such as oncogenesis, DNA damage, inflammation, and neurogenesis, however, its role in alcoholic liver disease is still largely unexplored [120, 262, 267-269].

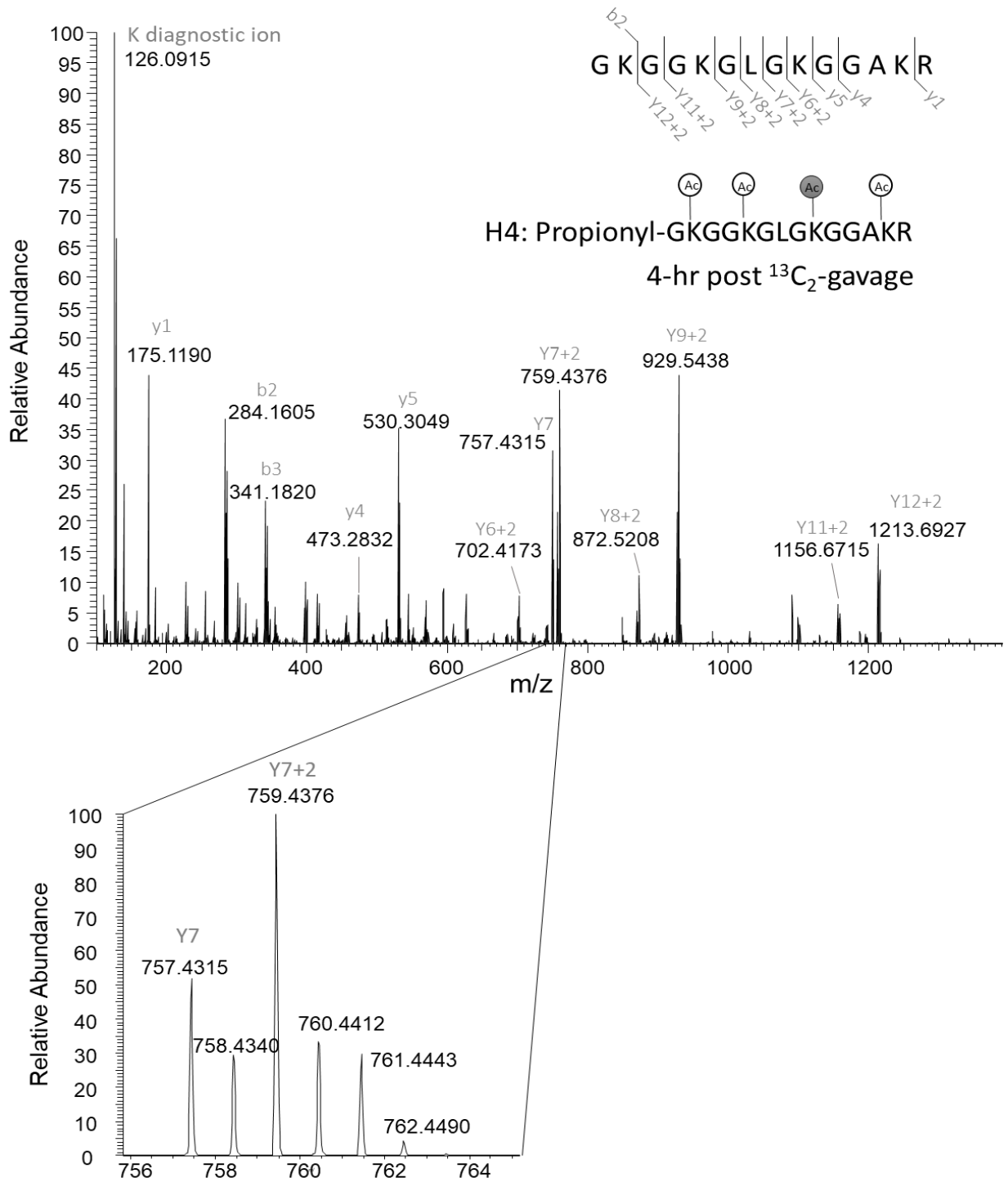


Figure 4.7: Tandem Mass Spectrometry in Conjunction with De Novo Sequencing Offers Potential Insight in Quantifying $^{13}\text{C}_2$ -Label Incorporation on Peptides with Multiple Acetylation Sites such as Histone 4 G4-R17. (Top) Tandem mass spectrometry was used to annotate the H4 peptide, in which all 4 lysine (5, 8, 12, and 14) are acetylated. Sequencing was completed on the MS2 using MS-Product, (UCSF, Protein Prospector v. 5.20.0, <http://prospector.ucsf.edu>) and a mass shift of +2 Da on either the b or y ion series inferred incorporation of the $^{13}\text{C}_2$ on the respective lysine residues. (Bottom) Magnification of the MS² (Top) showing the y7 ^{12}C monoisotopic peak ($m/z = 757.4315$) as well as increased $^{13}\text{C}_2$ [$m+2$] and a 2⁺ Da mass shift

Recently, a link has been established between alcohol use and changes to histone acetylation [15, 18, 21, 25, 39]. Moreover, mass spectrometry-based identification and metabolic tracing techniques are becoming more prominently used in the identification of histone epigenetic changes induced by external sources, such as alcohol abuse [3, 15-17, 21, 23, 25, 39, 262, 270-274]. These data show the first *in vivo* experiment using a heavy-labeled ethanol to metabolically trace ethanol metabolism to histone acetylation through the metabolite acetyl-CoA. These data now show a correlation between serum BAC levels and $^{13}\text{C}_2$ -label incorporation on histone proteins over the course of 24-hours (**Figure 4.1A-B**). Lysine acetylation sites on histones have a relatively fast turnover, typically between 53 – 87 minutes, which is faster than methylation, however, still slower than phosphorylation [262]. The fast turnover rate observed in these data suggests that acetylation stemming from alcohol may be transient and work as a mechanism to alleviate cellular stress during ethanol metabolism.

Traditional methods of SILAC ensure that complete label incorporation is achieved through many cell passages and supplemented media in order to minimize variability and assess differences in control and experimental groups. These experiments used one bolus dose of heavy-labeled alcohol, which was then metabolically traced throughout the Acetyl-CoA pool to histone acetylation. Furthermore, these data suggest that the increased lysine acetylation observed after alcohol exposure was due to alcohol induced by shifts in redox potential, however, the contribution of deacetylase activity or inhibition may also have been a factor because of the fast rates of histone turnover (**Figure 4.2C-D**). Previous work done by You *et.al* demonstrate that sirtuin 1 and histone 3 lysine 9 may work in tandem to prevent and slow the development of lipid accumulation in the liver in order to stall the onset of alcoholic liver disease [275]. These findings in combination with the new evidence presented here, suggest that during times of alcohol-induced stress, acetylation on histones may be site-selective in order to prevent liver injury by transcriptional regulation. This hypothesis could be further supported if the binge was repeated for a

longer period of time if hyperacetylation ensued the heavy-label incorporation should be identifiable in the majority of acetyl sites.

The new data presented here now propose that alcohol can be incorporated, site-specifically onto known N-terminal histone acetylation sites important in chromatin remodeling (**Figure 4.2 and 4.3**). Furthermore, when two or more acetylation sites are available, incorporation of heavy-label occurs as a site-specific mixture (**Figures. 4.4 and 4.5**). Site-specific incorporation of ethanol into histone protein acetylation advocates the need for specific transcriptional activation based on the type of liver injury the cells are experiencing. For example, if an acute binge of alcohol is consumed and the alcohol can be metabolized and used as for transient acetylation and gene regulation, however during chronic exposure this mechanism will lead to hyperacetylation in order to prevent or promote long-term liver injury. This hypothesis is consistent with our findings, in which label incorporation was found to have a fast turnover, signifying that the alcohol-induced modifications are transient and may be used as a mechanism by hepatocytes to alleviate stress and injury to the liver after alcohol exposure as deemed necessary by other signaling pathways.

Recent advances in mass-spectrometry-based post-translational identification and quantitation have advanced the understanding of epigenetics and disease progression, such as ALD [272-274, 276]. Histone 3K9Ac has been identified to upregulated during times of alcohol exposure and thought to play a protective role in the development of ALD [275, 277]. Interestingly, these new data show that incorporation and increased in site-specific acetylation are time-dependent. Histone H3K14Ac was significantly increased within 4-hours of ethanol exposure and H3K9Ac was not observed to be significantly changed until after 24-hours when H3K14Ac was no longer upregulated (**Figure 4.3A-B**). Furthermore, overall total acetylation for the singly acetylated H3K9Ac and H3K14Ac peptide was found to be significant after 24-hours, these data suggest the need for site-specific quantitation (**Figure 4.3A**).

In order to assess site-specific label incorporation and overall acetylation of peptides through mass spectrometry, chromatographic separation of MS2 must be achieved (**Figure 4.1F**). In addition, data analysis by XIC was limited when analyzing peptides such as H4 (K5-R17), which contained multiple acetylation sites on a peptide rich in glycine residues (**Figures 4.6 and 4.7**). More comprehensive analysis using computer programs may offer some benefits over traditional methods of quantitation by XIC. Programs such as MaxQuant, extract intensities of the identified various proteoforms can be used to compare the modified and unmodified forms (**Figures 4.6**) [278]. Nevertheless, when relying on computer analysis, data must be validated and confirmed using the .raw data before assumptions can be made (Fig. 6) [278]. One pitfall of computerized analysis is that it excludes peptides of low protein expression so mass spectrometer sensitivity must have high enough resolution in order for accurate quantitation [278]. Furthermore, Histone elution in mass spectrometry often poses a problem with coelution of other histones or proteoforms [271, 274]. Coelution of simultaneous proteoforms or partially labeled peptides makes quantitation accuracy difficult when studying overall changes in alcohol-induced lysine acetylation. These data open the door for *in vivo* experimentation using a mass spectrometry SILAC approach. These data have demonstrated that ethanol is metabolized and becomes a contributor to histone lysine acetylation via acetyl-CoA. Further research using stable isotopes will help to identify novel targets and pathways directly impacted by alcohol consumption and the onset of alcoholic liver disease.

Chapter 5

Conclusions and Future Directions

Alcoholism and Alcohol Liver Disease a Review

Alcoholism is a global issue that affects millions of people every year worldwide [1, 279]. Over 3.3 million deaths are attributed to alcohol consumption every year and it is currently the 5th leading cause of premature death and disability [1]. The reason alcohol claims so many lives is because of its damaging effects on the entire body, affecting major organs such as the brain, heart, liver and immune system [1]. Every day more than 6 people die from alcohol poisoning alone and currently, alcohol abuse has become the 2nd leading cause of preventable deaths, just under tobacco [1, 279]. In the United States (US) alone, over 80,000 people die every year from alcohol-related deaths and currently, 15 million people are struggling with an alcohol disorder [1, 279]. As a result, the US spends upwards of 250 billion dollars every year on alcohol-related treatments, of which three-quarters of the total cost originates from binge drinking. Binge drinking has been on the rise especially in young adults ranging in ages from 18-34. The National Institute on Alcohol Abuse and Alcoholism (NIAAA) define binge drinking as any pattern of drinking that raises the blood alcohol level to greater than 0.08mg/dL, which typically translates to 5 drinks in 2-hours for men and 4 for women [1, 2, 279]. Men are more likely than women to excessively drink alcohol, which increases their chances of alcohol-related injury [1, 279]. Close to 60% of men reported drinking in the last 30-days, of that 23% admitted to binge drinking at least 8 drinks in a sitting [279]. Only 45% of women reported drinking alcohol in the last 30 days, and only 12% of those women admitted to binge drinking [1, 279]. Although women drink less than men they are more prone to liver injury for reasons still unknown.

Alcohol liver injury develops over 3 stages, steatosis, hepatitis, and cirrhosis, with no clear definition of where one stage ends and the next begins. Both steatosis and hepatitis are reversible until fibroid tissue forms during cirrhosis when the irreversible fibroid tissue develop. The first stage of ALD is steatosis and begins with the development of fatty liver. Fatty liver development is the result of lipid peroxidation caused by the inhibition of PPAR α and AMPK activity [280]. The inhibition of AMPK results in SREBP1 activation of fatty acid synthesis [280]. Chronic drinking results in inhibition of PPAR α and activation of SREBP1, which results in lipid accumulation and the development of fatty liver. Without abstinence, steatosis will become hepatitis and liver injury progresses. Eventually, long-term heavy alcohol consumption cause hepatocytes to become necrotic and fibroid tissue develops causing the irreversible steatosis. Alcohol metabolism is an oxidative process that predominantly takes place in the liver. The two enzymes in the liver responsible for the metabolism alcohol are alcohol dehydrogenase (ADH) and Cytochrome IIE1 (CYP2E1). Both enzymes require the cofactors NAD⁺/NADH to catalyze the breakdown of ethanol into acetate. The breakdown of alcohol induces shifts in redox potential and long-term exposure can lead to mitochondria dysfunction and liver injury [4, 5, 48, 174, 221, 222]. The development of ALD has been well characterized, however many gaps in knowledge still remain.

Overview of Major Findings

Chapter 2 uses a chronic-binge mouse model of ALI to look for possible mechanisms responsible for gender differences commonly observed after chronic binging. Following the 10-day chronic-binge, BAC levels were raised in both the male and female mice, where males showed approximately a 1.6 fold change in serum BAC. Visual inspection of the H&E stained livers displayed no visible changes between the male and female mice receiving the high-fat control diet. Both male and female mice receiving the ethanol diet displayed a clear indication of lipid accumulation in both genders when compared to their respective control-fed mice. Although there were noticeable differences in both mouse genders, female

mice that had received ethanol exhibited more severe lipid accumulation when compared to their male pair-fed counterparts. These data confirmed that the 10-day chronic-binge mouse model would be a good model to study gender differences in ALI.

Proteomic analysis of whole cell liver lysate using Ingenuity Pathway Analysis (IPA) predicted women to upregulate genes and proteins more commonly associated with liver damage whereas males were predicted to upregulate genes and proteins commonly observed in liver injury. Furthermore, Cytochrome P450 proteins, which are most known for their role in the metabolic breakdown of drugs used to treat diseases [281, 282], A wide range of CYP expression was observed between genders following the 10-day chronic-binge. There are 18 families of CYP P450 proteins and families are grouped based on their primary function [281-283]. Interestingly the different families (2, 3, and 4) of cytochromes that were identified following the 10-day chronic binge in male and female mice tend to be involved in the metabolism of drugs, outside chemicals, and fatty acids [281, 282]. Hepatic cytochromes have been implicated in the development of liver disease because of a loss in their activity as liver injury increases. [282] For example, hepatic CYP2E1 is well known for its role in oxidative alcohol metabolism, lipid peroxidation and the generation of reactive oxygen species, and was found upregulated in both genders following chronic-binge ethanol-diet [71, 75, 182, 221, 284-286]. Cytochromes belonging to the family's 1A, 2C19, and 3A activity have been shown to have increased sensitivity as the liver disease worsens [282]. This may explain a loss of activity observed in the female mice since only expressed CYP3A44 and CYP3A16 in the control-fed mice. Males did not express those CYP3A44 and CYP3A16 in either the control or ethanol-fed mice, suggesting the use of different isoform to aid in metabolic clearance in the liver. Also, CYP2A4, CYP2C70, CYP4V2, and CYP2F1 were only expressed in female mice after ethanol exposure, whereas male mice solely expressed CYP1A2 and CYP4F15. Male mice did, however, exhibit a large increase in fold-change of CYP2A5, and CYP4A14 when compared to their female counterparts. Although the role of Cyp2e1 has been studied extensively in the context of ALI [173, 174, 177, 182, 197-199], the

results from our preliminary studies are intriguing as the contribution of other CYP enzymes in ALI is largely unexplored. In addition to CYP differential expression and lipid metabolism, proteomic analysis revealed greater activities of transcription factors associated with oxidative stress (Nrf2) affirming the previously established links between oxidative stress in ALI [6, 7, 134-138, 174, 177, 221, 222, 287, 288]. Results from this analysis have provided detailed information at the protein level for future mechanistic studies aimed to identify therapeutic targets with consideration of possible sex-specific strategies for prevention or treatment of alcoholic liver disease. These differences may propose potential targets in gender-bias and liver injury. One mechanism that may aid in cytochrome P450 development of gender influenced ALD is by their role in the formation of protein-aldehyde adducts and NADPH oxidase activity [288, 289].

Hepatocytes in the liver use pathways such as cellular respiration, CYP2E1, and NADPH oxidase, during ethanol metabolism which in turn promote the formation of ROS [4, 5, 7-9, 165, 209, 214, 215, 287-289]. Cytochrome IIE1 is known for generating copious amount of superoxide (O_2^-) and hydrogen peroxide (H_2O_2) and creating mitochondrial dysfunction during ethanol metabolism [42, 71, 174, 177, 182, 198, 221, 286]. In turn, the elevated hepatic oxidative stress levels will lead to an inflammatory response [7]. Nitric oxide (NO) is a key regulator of the inflammatory response and often plays a dual role in cellular protection and cell injury [290-293]. Nitric oxide is a free radical that is a generated by inducible nitric oxide synthase [291, 294]. Nitric oxide is important in maintaining cellular homeostasis through its signaling properties; while scavenging, it can react with excess superoxide generated from alcohol metabolism to form peroxynitrite ($ONOO^-$), thus altering the pathways open to NO signaling [219, 295, 296]. Both NO or O_2^- are considered to have weak oxidizing potential, however, once they combine to form $ONOO^-$ the newly formed radical has powerful oxidizing potential and can target a wide range of biological targets [94, 199, 219, 291-293, 295-298]. An interesting target of $ONOO^-$ in alcohol liver injury is tyrosine when $ONOO^-$ reacts with tyrosine to form nitrotyrosine [29, 94, 297].

Tyrosine nitration is a post-translational modification that poses an interesting target in the pathogenesis of alcohol liver injury (ALI) because of its ability to alter protein function [29, 94, 299, 300]. The ability of ONOO⁻ to form nitrotyrosine *in vivo* has recently been questioned due to the naturally low abundance of cellular ONOO⁻ [300]. Alcohol-induced liver injury provides a conducive environment for nitrotyrosine formation because of increased nitrosative and oxidative stress incurred mitochondrial dysfunction and inflammation [300-303]. Numerous efforts have been made to study this lowly expressed modification *in vivo* but have fallen short with traditional techniques of enrichment [300, 301]. These data now show a significant ($p=0.0001$) increase in the amount of endogenous nitrotyrosine found in the mouse liver after 28-days of chronic ethanol exposure when compared to their control-fed counterparts. Furthermore, I was able to identify and validate 4 histone targets of nitration. The 4 sites that were positively identified for tyrosine nitration were H3nY41, H1nY70, and H4nY51 and H4nY72. These sites have all previously been demonstrated to have a role in epigenetic modulation when modified. Histone 3 tyrosine 41 can also be phosphorylated. Upon H3Y41 phosphorylation the JAK2 kinase pathway is activated by excluding HP1 α chromatin binding, which then allows for the activation of oncogenes such as *Imo2* [109, 235]. Histone 4 tyrosine's 51 and 72 phosphorylation have also been implicated in DNA damage, chromatin restructuring, histone turnover and transcriptional regulation [304]. Histone Y51 is recognized by the Abelson murine leukemia viral oncogene homolog 1 (ABL1), upon phosphorylation of H4Y51 ABL1 recognizes the signal as DNA damage, and recruits DNA repair machinery [304]. Histone 4 tyrosine 72 phosphorylation also has a role in DNA damage and repair by signaling for epidermal growth factor receptor (EGFR) [305, 306]. Epidermal growth factor receptor is a receptor that aids in cell division and is often found upregulated in cancers due to the rapid proliferation during tumor growth and metastasis [305, 306]. The identification and validation of nitration on H1Y70 pose as an interesting epigenetic target. Histone 1 is a linker protein which binds DNA around the nucleosome aiding in structure and chromatin remodeling, [307, 308]. Previous work *in vitro* has identified H1 to become nitrated as well

as be a target for dinitrase activity [114], and more recently histone H1 acetylation has recently been demonstrated to cross-talk with DNA methylation in order to promote gene silencing [309-311].

Molecular dynamics now predict that histone H3nY41 promotes a change in DNA conformation over the native unmodified H3Y41 by molecular dynamic simulations. In order to further understand how H3nY41 affected the DNA, the phosphorus atoms of those nucleotides that are within 5 Å of H3 in the crystallographic conformation were tracked from both H3 proteins within the nucleosome and found to converge at t=200ns. Also, when H3Y41 is nitrated, the DNA-P to H3Y41 distance increases on average by 2 Å, which is the approximate distance of 2 hydrogen atoms. The maximum DNA-P to H3Y41 distance observed in the wild-type system is <64 Å, while the H3nY41 system consistently assumes conformations where the DNA-P and H3Y41 distance is >67 Å. Furthermore, the H3nY41 occasionally samples the conformational space of the wild-type system, yielding a lower average. Although these distances seem relatively small they are large enough for the nitro group to draw in potassium ions, creating a water shell. In turn, as the positively charged ions move closer to the nitro group the water and phosphate move further away. In order to further investigate how H3nY41 affects the DNA conformation, ChIP-sequencing was performed using an antibody synthesized against H3nY41. ChIP-sequencing yielded 18 novel and potential sites within the genome that may interact with H3nY41. Of these 18 sites, only 5 were located within the annotated portion of the genome. Two of these sites, Ano2 and Dpp9, were used for validation by qPCR analysis and were found to not be significantly expressed when compared to the IgG negative control. These data now show that chronic alcohol exposure increases levels of nitrotyrosine in the liver, with localization surrounding vascular regions as well as the nucleus. The increased levels of nitrotyrosine in the nucleus following ethanol exposure were identified on numerous proteins important for transcriptional regulation, of those were 4 novel sites located on the N-terminal histone protein tail. These new data of histone nitration along with the molecular dynamic simulations suggest a possible role in transcriptional regulation and/or signaling mechanisms. Previous data suggest that histone nitration is

reversible and found to increase in diseased or injured environments [106, 114]. Further understanding of the mechanisms involved in nitration regulation and disease progression will provide new epigenetic therapeutic targets. Furthermore, understanding the relationship between tyrosine nitration and phosphorylation will provide an understanding of cellular signaling in disease causation and progression not only in ALI but many other diseases, which rely heavily on phosphorylation signaling pathways, such as cancer.

In parallel to histone tyrosine nitration, protein and histone acetylation has previously been demonstrated to become upregulated following alcohol exposure [87, 88, 163]. Chapter 4 looks at the effects of acute alcohol exposure on hepatic histone acetylation using stable isotope labeling and mass spectrometry. These experiments are the first to use heavy-labeled ethanol to metabolically trace ethanol to histone acetylation through its metabolite acetyl-CoA. Significant incorporation of the $^{13}\text{C}_2$ heavy-label was observed on histone 3 lysine 14 after 4 h ($p=0.004$) and still at 24 h ($p=0.002$) following alcohol exposure. Incorporation was also found to be significant on both of the singly acetylated peptides containing H3K9/K14 and H3K18/23 after 24 hours ($p=0.002$, and $p=0.02$ respectively). Although incorporation was not found to be significant on the doubly acetylated peptides containing H3K9/K14 and H3K18/K23, data does show that the $^{13}\text{C}_2$ heavy-label is incorporated site-specifically as a mixture. Histone H4 also showed to incorporate the $^{13}\text{C}_2$ heavy-label at all 4 H4 lysine residues (K5, K8, K12, and K16), although quantitation had to be completed using computational extraction of intensities because of incorporation rates and histone turnover. Data also showed that overall acetylation significantly increased during the 24 h post ethanol gavage in both the H3K9/K14 peptide ($p=$ and also the H3K18/K23 ($p=$ peptide. However, the H3K9 acetylation site was found not to have any significant contribution to overall acetylation, whereas the H3K14Ac peptide did ($p=0.02$). These data now propose a link between ethanol metabolism, acetyl-CoA, and histone acetylation. By ethanol seemingly targeting the N-terminal region on histone tails, it can be inferred that the changes in acetylation may play a role in chromatin

remodeling and transcriptional regulation. This notion is further supported that when there are 2 or more acetylation sites, incorporation occurred as a mixture between sites. Site-specificity of label incorporation provided by ethanol through acetate into acetyl-CoA to histone protein acetylation proposes a specific and transient response for transcriptional regulation based on the immediate reaction to acute ethanol exposure. These findings, in combination with the new evidence presented here, suggest that during times of alcohol-induced stress, epigenetic changes to histones could regulate a selective transcriptional response related to ethanol response and liver injury.

Future Directions

These studies use different models of alcohol exposure to close the gap in knowledge in the development of alcohol-induced liver injury (ALI). The 10-day chronic-binge ethanol diet was used to study gender differences in the development of ALI. Although the 10-day ethanol diet is easy to perform and has been shown to induce elevated levels of ALT and steatosis, it does not encompass chronic or acute drinking. Women have been shown to develop more severe liver injury and faster when compared to males that consume the same or more quantities of alcohol [165, 167, 179, 312]. One approach that may help to capture the difference in short and long-term markers of liver injury in males and females might include varying the lengths of alcohol consumption. By assessing both short and long-term changes induced by alcohol in males and females, will provide a more rounded approach to understanding pathways and proteins that influence gender bias in ALI. Such approaches may include whole proteome studies using mass spectrometry, which will provide a global analysis of liver proteins responsible for the alcohol-induced liver injury. Programs such as Ingenuity Pathway Analysis (IPA) can help to identify which genes, pathways, and proteins can be targeted for further analysis.

Another future direction will be to isolate Cytochrome P450 proteins that were identified to be differentially expressed in males and females following alcohol consumption. The Cyp450 family of

enzymes is important in the metabolism of drugs, alcohol, cholesterol, steroids, and lipids [78, 211, 282, 289, 313]. Interestingly, these enzymes are involved in lipid metabolism where sex-specific CYP activity could be related to the enhanced lipid accumulation phenotype observed in female mice after chronic-binge ethanol feeding. Cyp2j5 is important in the metabolism of arachidonic acid to various epoxyeicosatrienoic acids where metabolites from this pathway could have a role in protection against cellular oxidative stress. Using methods of gene editing such as Cre recombinant or Crisper/Cas systems to knock out expression of highly upregulated CYP450 proteins such as Cyp2j5 may offer insight into how these proteins alter ALI between genders.

Analysis of gender-specific epigenetic marks following long-term alcohol consumption would also provide an interesting look at transcriptional regulation during the development of alcohol liver disease. It would be interesting to look at nitrotyrosine and acetylation differences in male and female mice following both acute and long-term alcohol exposure. In order to assess targets within the genome that are modulated by N-terminal histone acetylation during the development of ALI, ChIP-sequencing could be used to identify novel targets and then compared to known targets in wild-type and other diseases. The same histone acetylation sites that were identified using the $^{13}\text{C}_2$ experiment (H3K9, K14, K18, and K23, and also H4K5, K8, K12, and K16) have ChIP-sequencing grade antibodies commercially available. These residues are important in transcriptional activation, however, their role in gene regulation after ethanol exposure has not yet been investigated.

Histone tyrosine nitration may also be further investigated using ChIP-seq. The H3nY41 antibody can be further optimized using different concentrations of cells and antibody. The remaining 3 sites identified in the preliminary study should also be validated using qPCR. The analysis can include both the wild-type and ethanol-treated mice and can be expanded to include both male and female mice. Another technical approach in developing the H3nY41 ChIP analysis would be the further enrichment of nitrated

proteins prior to sequencing. A stable protocol for enrichment of nitrotyrosine has been yet to be established. Histone or protein may be the best way to enrich for the identification of nitrotyrosine site due to the low amounts of the modification observed *in vivo*. Another method to enhance the understanding of alcohol-induced nitrotyrosine formation would be to target the nitric oxide producer inducible nitric oxide synthase (iNOS). Creating a mouse model that overexpresses iNOS can be used to theoretically generate more nitrotyrosine formation. In order to assess the role of nitrotyrosine in the development of ALI, when more NO is synthesized it can readily combine with increasing amounts of ROS within the liver. Long-term upregulation of nitrotyrosine can be assessed in terms of liver damage by using markers for ALT, AST, triglycerides, and cholesterol. Livers can also be used for histology to for a visual inspection of nitrotyrosine and lipid accumulation. On the other hand, a mouse model deficient in iNOS can be used to which pathways and proteins are down-regulated following long-term alcohol exposure.

Next, the use of stable isotope labeling *in vivo* can be of great use in quantitative epigenetic studies. Recently, stable isotope labeled mouse chow has become commercially available. The cost of conducting experiments using stable isotopes is considerably high for both *in vitro* and *in vivo* but provides a way for researchers to quantify changes in protein expression using mass spectrometry. By using a stable isotope labeled mouse chow in conjunction with another method of alcohol administration, changes in ALI can be quantified long-term using mass spectrometry. Using labeled mouse chow also opens the door for heritability studies in the predisposition to ALI or alcohol fetal syndrome. Labeled chow can be fed in conjunction with long-term alcohol binges to identify epigenetic marks in offspring contributed by the female, male, or both. This type of study can be used to assess different epigenetic marks including methylation, acetylation, and phosphorylation. Furthermore, generational studies can be conducted due to the fast breeding rate of mice.

Lastly, one obstacle that needs further optimization in order to use a labeling approach for epigenetic studies, both short and long-term, is the use of computational analysis in quantitating multiple sites of label incorporation on proteins and histones. Multiple epigenetic marks that were identified to incorporate heavy label in the $^{13}\text{C}_2$ experiment were difficult to quantify due to the fast rate of histone turnover as well as the rate of label incorporation. The addition of more time points and the use of multiple labels will provide a kinetic approach to quantifying the rate of incorporation in regards to the rate of incorporation to turnover. Because the liver can only metabolize ethanol based on the availability of proteins necessary for metabolism, such as alcohol dehydrogenase and the cofactor NAD⁺, incorporation rates over long-term alcohol studies may show different trends.

Conclusions

These studies provide novel results into how different rates of alcohol consumption affect the liver and the pathogenesis of ALI. These data now show that male and female mice express different proteins and pathways important in the onset and development of ALI. Furthermore, the Cyp P450 family of proteins, which have a large role in lipid accumulation and liver toxicity are differentially expressed between genders. These data also show that during the time of alcohol metabolism protein nitration is upregulated within the liver. This discovery prompted the evaluation of histone tyrosine nitration. Interestingly, histone tyrosine nitration was identified to be on multiple histones in the N-terminal region. These sites are known for the role in transcriptional regulation and prompted further analysis by molecular dynamics simulations and ChIP-sequencing. Molecular dynamic simulations predict the nitrotyrosine on H3Y41 caused the DNA to prefer a conformational change. This change may allow for transcription of genes important in the alleviation of ROS/RNS, inflammation, and lipid accumulation. On the other hand, the dysregulation of transcription may also lead to more severe liver injury, which raises the need for further investigation. This thought is further supported by the increased acetylation

observed on histone H3 following acute alcohol exposure. Label incorporation was observed to occur in as soon as 4 hours following alcohol exposure. This demonstrates a link between ethanol and histone acetylation through the metabolites acetate and acetyl-CoA. In conclusion here, I now show both a direct and indirect repercussion of alcohol abuse. Ethanol can be directly linked via metabolism to histone acetylation and indirectly linked to histone tyrosine nitration as a result of increased ROS and inflammation.

Literature Cited

1. WHO, *Global status report on alcohol and health 2014*. World Health Organization 2014(2014 ed.): p. 1-364.
2. (NIAAA)., N.I.o.A.A.a.A. *NIAAA Council Approves Definition of Binge Drinking*. NIAAA Newsletter 2004 [cited Winter No. 3]; Available from: http://pubs.niaaa.nih.gov/publications/Newsletter/winter2004/Newsletter_Number3.pdf.
3. Aroor, A.R., et al., *A proteomic analysis of liver after ethanol binge in chronically ethanol treated rats*. *Proteome Sci*, 2012. **10**(1): p. 29.
4. Das, S.K. and D.M. Vasudevan, *Alcohol-induced oxidative stress*. *Life Sci*, 2007. **81**(3): p. 177-87.
5. Feldstein, A.E. and S.M. Bailey, *Emerging role of redox dysregulation in alcoholic and nonalcoholic fatty liver disease*. *Antioxid Redox Signal*, 2011. **15**(2): p. 421-4.
6. Galligan, J.J., et al., *Oxidative Stress and the ER Stress Response in a Murine Model for Early-Stage Alcoholic Liver Disease*. *J Toxicol*, 2012. **2012**: p. 207594.
7. Hoek, J.B. and J.G. Pastorino, *Ethanol, oxidative stress, and cytokine-induced liver cell injury*. *Alcohol*, 2002. **27**(1): p. 63-68.
8. Reuben, A., *Alcohol and the liver*. *Curr Opin Gastroenterol*, 2007. **23**(3): p. 283-91.
9. Ronis, M.J., et al., *The role of ethanol metabolism in development of alcoholic steatohepatitis in the rat*. *Alcohol*, 2010. **44**(2): p. 157-69.
10. Tsedensodnom, O., et al., *Ethanol metabolism and oxidative stress are required for unfolded protein response activation and steatosis in zebrafish with alcoholic liver disease*. *Dis Model Mech*, 2013. **6**(5): p. 1213-26.
11. Garcia-Ruiz, C., et al., *Role of oxidative stress generated from the mitochondrial electron transport chain and mitochondrial glutathione status in loss of mitochondrial function and activation of transcription factor nuclear factor-kappa B: studies with isolated mitochondria and rat hepatocytes*. *Mol Pharmacol*, 1995. **48**(5): p. 825-34.
12. Turrens, J.F., A. Alexandre, and A.L. Lehninger, *Ubisemiquinone is the electron donor for superoxide formation by complex III of heart mitochondria*. *Arch Biochem Biophys*, 1985. **237**(2): p. 408-14.
13. Turrens, J.F. and A. Boveris, *Generation of superoxide anion by the NADH dehydrogenase of bovine heart mitochondria*. *Biochem J*, 1980. **191**(2): p. 421-7.
14. Hoek, J.B., A. Cahill, and J.G. Pastorino, *Alcohol and mitochondria: a dysfunctional relationship*. *Gastroenterology*, 2002. **122**(7): p. 2049-63.
15. Mandrekar, P., *Epigenetic regulation in alcoholic liver disease*. *World J Gastroenterol*, 2011. **17**(20): p. 2456-64.
16. Nieratschker, V., A. Batra, and A.J. Fallgatter, *Genetics and epigenetics of alcohol dependence*. *Journal of Molecular Psychiatry*, 2013. **1**(1): p. 1-6.
17. Park, P.H., R.W. Lim, and S.D. Shukla, *Involvement of histone acetyltransferase (HAT) in ethanol-induced acetylation of histone H3 in hepatocytes: potential mechanism for gene expression*. *Am J Physiol Gastrointest Liver Physiol*, 2005. **289**(6): p. G1124-36.
18. Park, P.H., R. Miller, and S.D. Shukla, *Acetylation of histone H3 at lysine 9 by ethanol in rat hepatocytes*. *Biochem Biophys Res Commun*, 2003. **306**(2): p. 501-4.

19. Ponomarev, I., *Epigenetic control of gene expression in the alcoholic brain*. Alcohol Res, 2013. **35**(1): p. 69-76.
20. Shukla, S.D. and A.R. Aroor, *Epigenetic effects of ethanol on liver and gastrointestinal injury*. World J Gastroenterol, 2006. **12**(33): p. 5265-71.
21. Shukla, S.D., et al., *In Vivo Acute on Chronic Ethanol Effects in Liver: A Mouse Model Exhibiting Exacerbated Injury, Altered Metabolic and Epigenetic Responses*. Biomolecules, 2015. **5**(4): p. 3280-3294.
22. Shukla, S.D., et al., *Acetaldehyde alters MAP kinase signalling and epigenetic histone modifications in hepatocytes*. Novartis Found Symp, 2007. **285**: p. 217-24; discussion 224-8.
23. Shukla, S.D., et al., *Different mechanisms for histone acetylation by ethanol and its metabolite acetate in rat primary hepatocytes*. J Pharmacol Exp Ther, 2015. **354**(1): p. 18-23.
24. Shukla, S.D., et al., *Emerging role of epigenetics in the actions of alcohol*. Alcohol Clin Exp Res, 2008. **32**(9): p. 1525-34.
25. Starkman, B.G., A.J. Sakharkar, and S.C. Pandey, *Epigenetics-beyond the genome in alcoholism*. Alcohol Res, 2012. **34**(3): p. 293-305.
26. Zhang, H., et al., *Array-based profiling of DNA methylation changes associated with alcohol dependence*. Alcohol Clin Exp Res, 2013. **37**.
27. Zhang, R., et al., *Genome-wide DNA methylation analysis in alcohol dependence*. Addict Biol, 2013. **18**.
28. Choudhury, M., et al., *Evidence for the role of oxidative stress in the acetylation of histone H3 by ethanol in rat hepatocytes*. Alcohol (Fayetteville, N.Y.), 2010. **44**(6): p. 531-540.
29. Baraona, E., et al., *Ethanol consumption increases nitric oxide production in rats, and its peroxynitrite-mediated toxicity is attenuated by polyenylphosphatidylcholine*. Alcohol Clin Exp Res, 2002. **26**(6): p. 883-9.
30. Deng, X.-s. and R.A. Deitrich, *Ethanol Metabolism and Effects: Nitric Oxide and its Interaction*. Current clinical pharmacology, 2007. **2**(2): p. 145-153.
31. Beckman, J.S., *Oxidative damage and tyrosine nitration from peroxynitrite*. Chem Res Toxicol, 1996. **9**(5): p. 836-44.
32. Beckman, J.S., et al., *Reactions of nitric oxide, superoxide and peroxynitrite with superoxide dismutase in neurodegeneration*. Prog Brain Res, 1994. **103**: p. 371-80.
33. Beckman, J.S. and W.H. Koppenol, *Nitric oxide, superoxide, and peroxynitrite: the good, the bad, and ugly*. Am J Physiol, 1996. **271**(5 Pt 1): p. C1424-37.
34. Di Stasi, A.M., et al., *Peroxyntirite induces tryosine nitration and modulates tyrosine phosphorylation of synaptic proteins*. J Neurochem, 1999. **73**(2): p. 727-35.
35. Gambini, J., et al., *Free [NADH]/[NAD(+)] regulates sirtuin expression*. Arch Biochem Biophys, 2011. **512**(1): p. 24-9.
36. Lombard, D.B., D.X. Tishkoff, and J. Bao, *Mitochondrial sirtuins in the regulation of mitochondrial activity and metabolic adaptation*. Handb Exp Pharmacol, 2011. **206**: p. 163-88.
37. Nakagawa, T. and L. Guarente, *Sirtuins at a glance*. J Cell Sci, 2011. **124**(Pt 6): p. 833-8.
38. Fritz, K.S., et al., *Mitochondrial acetylome analysis in a mouse model of alcohol-induced liver injury utilizing SIRT3 knockout mice*. J Proteome Res, 2012. **11**(3): p. 1633-43.
39. Choudhury, M. and S.D. Shukla, *Surrogate alcohols and their metabolites modify histone H3 acetylation: involvement of histone acetyl transferase and histone deacetylase*. Alcohol Clin Exp Res, 2008. **32**(5): p. 829-39.
40. Lieber, C.S., et al., *Alcohol alters hepatic FoxO1, p53, and mitochondrial SIRT5 deacetylation function*. Biochem Biophys Res Commun, 2008. **373**(2): p. 246-52.

41. Santos, L., C. Escande, and A. Denicola, *Potential Modulation of Sirtuins by Oxidative Stress*. *Oxidative Medicine and Cellular Longevity*, 2016. **2016**: p. 12.
42. Song, B.-J., et al., *Mitochondrial dysfunction and tissue injury by alcohol, high fat, nonalcoholic substances and pathological conditions through post-translational protein modifications*. *Redox Biology*, 2014. **3**(Supplement C): p. 109-123.
43. Park, P.H., R.W. Lim, and S.D. Shukla, *Gene-selective histone H3 acetylation in the absence of increase in global histone acetylation in liver of rats chronically fed alcohol*. *Alcohol Alcohol*, 2012. **47**(3): p. 233-9.
44. Llerena, S., et al., *Binge drinking: Burden of liver disease and beyond*. *World Journal of Hepatology*, 2015. **7**(27): p. 2703-2715.
45. Ventura, H.E., et al., *6 - Binge Drinking: Patterns, Explanations, and Policy A2 - Watson, Victor R. Preedy* Ronald Ross, in *Comprehensive Handbook of Alcohol Related Pathology*. 2005, Academic Press: Oxford. p. 59-73.
46. Lunetta, P. and G.S. Smith, *13 - The Role of Alcohol in Injury Deaths A2 - Preedy, Victor R, in Comprehensive Handbook of Alcohol Related Pathology*, R.R. Watson, Editor. 2005, Academic Press: Oxford. p. 147-164.
47. Alpert, L. and J. Hart, *The Pathology of Alcoholic Liver Disease*. *Clinics in Liver Disease*.
48. Gao, B.I.N. and R. Bataller, *Alcoholic Liver Disease: Pathogenesis and New Therapeutic Targets*. *Gastroenterology*, 2011. **141**(5): p. 1572-1585.
49. L ivero, F.A.R. and A. Acco, *Molecular basis of alcoholic fatty liver disease: From incidence to treatment*. *Hepatology Research*, 2016. **46**(1): p. 111-123.
50. Uchida, T., et al., *Alcoholic foamy degeneration--a pattern of acute alcoholic injury of the liver*. *Gastroenterology*, 1983. **84**(4): p. 683-92.
51. Takei, K.S.a.Y., *Pathogenesis of alcoholic liver disease*. 2016.
52. Seitz, H.K., et al., *Ethanol metabolism in the gastrointestinal tract and its possible consequences*. *Alcohol Alcohol Suppl*, 1994. **2**: p. 157-62.
53. Lieber, C.S., R.T. Gentry, and E. Baraona, *First pass metabolism of ethanol*. *Alcohol Alcohol Suppl*, 1994. **2**: p. 163-9.
54. Oneta, C.M., et al., *First pass metabolism of ethanol is strikingly influenced by the speed of gastric emptying*. *Gut*, 1998. **43**(5): p. 612-9.
55. Sharma, R., et al., *First-pass metabolism of alcohol*. *Digestive Diseases and Sciences*, 1995. **40**(10): p. 2091-2097.
56. Lim, R.T., Jr., et al., *First-pass metabolism of ethanol is predominantly gastric*. *Alcohol Clin Exp Res*, 1993. **17**(6): p. 1337-44.
57. Lieber, C.S., *2 - Alcohol Metabolism: General Aspects A2 - Preedy, Victor R, in Comprehensive Handbook of Alcohol Related Pathology*, R.R. Watson, Editor. 2005, Academic Press: Oxford. p. 15-26.
58. Marshall, S.J. and G.K. Chambers, *4 - Genetic Aspects of Alcohol Metabolism: An Overview A2 - Preedy, Victor R, in Comprehensive Handbook of Alcohol Related Pathology*, R.R. Watson, Editor. 2005, Academic Press: Oxford. p. 31-48.
59. Zakhari, S., *Overview: How Is Alcohol Metabolized by the Body?* *Alcohol Research & Health*, 2006. **29**(4): p. 245-255.
60. Seitz, H.K. and G. Poschl, *The role of gastrointestinal factors in alcohol metabolism*. *Alcohol Alcohol*, 1997. **32**(5): p. 543-9.
61. Ladero, J.M., *37 - Polymorphism and Alcoholic Liver Disease A2 - Preedy, Victor R, in Comprehensive Handbook of Alcohol Related Pathology*, R.R. Watson, Editor. 2005, Academic Press: Oxford. p. 481-490.

62. Hardman, M.J., et al., *Regulation of Rates of Ethanol Metabolism and Liver [NAD+]/[NADH] Ratio*, in *Alcoholism: A Molecular Perspective*, T.N. Palmer, Editor. 1991, Springer US: Boston, MA. p. 27-33.
63. Lieber, C.S., *The discovery of the microsomal ethanol oxidizing system and its physiologic and pathologic role*. *Drug Metab Rev*, 2004. **36**(3-4): p. 511-29.
64. Lieber, C.S., *Ethanol metabolism, cirrhosis and alcoholism*. *Clinica Chimica Acta*, 1997. **257**(1): p. 59-84.
65. Lieber, C.S., *Microsomal ethanol-oxidizing system (MEOS): the first 30 years (1968-1998)--a review*. *Alcohol Clin Exp Res*, 1999. **23**(6): p. 991-1007.
66. Hammes-Schiffer, S. and S.J. Benkovic, *Relating Protein Motion to Catalysis*. *Annual Review of Biochemistry*, 2006. **75**(1): p. 519-541.
67. Ji, C., *Mechanisms of alcohol-induced endoplasmic reticulum stress and organ injuries*. *Biochem Res Int*, 2012. **2012**: p. 216450.
68. Lieber, C.S., *Alcohol and the liver: metabolism of alcohol and its role in hepatic and extrahepatic diseases*. *The Mount Sinai journal of medicine, New York*, 2000. **67**(1): p. 84-94.
69. Lieber, C.S. and L.M. DeCarli, *The role of the hepatic microsomal ethanol oxidizing system (MEOS) for ethanol metabolism in vivo*. *J Pharmacol Exp Ther*, 1972. **181**(2): p. 279-87.
70. Teschke, R.H., Yasushi; Lieber, Charles S., *Hepatic Ethanol Metabolism: Respective Roles of Alcohol Dehydrogenase, the Microsomal Ethanol-Oxidizing System, and Catalase*. *Archives of biochemistry and biophysics*, 1967. **175**(2): p. 635-643.
71. Lu, Y. and A.I. Cederbaum, *CYP2E1 and Oxidative Liver Injury by Alcohol*. *Free radical biology & medicine*, 2008. **44**(5): p. 723-738.
72. McGehee, R.E., Jr., et al., *Characterization of cytochrome P450 2E1 induction in a rat hepatoma FGC-4 cell model by ethanol*. *Biochem Pharmacol*, 1994. **48**(9): p. 1823-33.
73. Cederbaum, A.I., *Molecular mechanisms of the microsomal mixed function oxidases and biological and pathological implications*. *Redox Biology*, 2015. **4**: p. 60-73.
74. Kim, S.G., et al., *Evidence for increased translational efficiency in the induction of P450IIE1 by solvents: analysis of P450IIE1 mRNA polyribosomal distribution*. *Biochem Biophys Res Commun*, 1990. **172**(2): p. 767-74.
75. Koop, D.R. and D.J. Tierney, *Multiple mechanisms in the regulation of ethanol-inducible cytochrome P450IIE1*. *Bioessays*, 1990. **12**(9): p. 429-35.
76. Song, B.J., et al., *Stabilization of cytochrome P450j messenger ribonucleic acid in the diabetic rat*. *Mol Endocrinol*, 1987. **1**(8): p. 542-7.
77. Morgan, E.T., D.R. Koop, and M.J. Coon, *Comparison of six rabbit liver cytochrome P-450 isozymes in formation of a reactive metabolite of acetaminophen*. *Biochem Biophys Res Commun*, 1983. **112**(1): p. 8-13.
78. Morgan, E.T., D.R. Koop, and M.J. Coon, *Catalytic activity of cytochrome P-450 isozyme 3a isolated from liver microsomes of ethanol-treated rabbits. Oxidation of alcohols*. *J Biol Chem*, 1982. **257**(23): p. 13951-7.
79. Johansson, M.I.-S.a.l., *Mechanisms of Hydroxyl Radical Formation and Ethanol Oxidation by Ethanol-inducible and Other Forms of Rabbit Liver Microsomal Cytochromes P-450*. *THE JOURNAL OF BIOLOGICAL CHEMISTRY* 1984. **259**(10): p. 6447-6458.
80. Koop, D.R. and J.P. Casazza, *Identification of ethanol-inducible P-450 isozyme 3a as the acetone and acetol monooxygenase of rabbit microsomes*. *Journal of Biological Chemistry*, 1985. **260**(25): p. 13607-12.

81. Chung S. Yang, Y.Y.T., Dennis R. Koop, and Minor J. Coon, *Metabolism of Nitrosamines by Purified Rabbit Liver Cytochrome P-450 Isozymes*. *Cancer Research*, 1985. **45**(March 1985): p. 1140-1145.
82. Zakhari, S., *Overview: how is alcohol metabolized by the body?* *Alcohol Res Health*, 2006. **29**(4): p. 245-54.
83. Lieber, C.S., *Ethanol metabolism, cirrhosis and alcoholism*. *Clinica Chimica Acta*, 1997(257): p. 59-84.
84. Berg JM, T.J., Stryer L., *Ethanol Alters Energy Metabolism in the Liver*, in *Biochemistry*. 2002, W H Freeman: New York.
85. Harris, P.S., et al., *Chronic ethanol consumption induces mitochondrial protein acetylation and oxidative stress in the kidney*. *Redox Biology*, 2015. **6**: p. 33-40.
86. Kim, S.J., et al., *Characterization of novel mechanisms for steatosis from global protein hyperacetylation in ethanol-induced mouse hepatocytes*. *Biochemical and Biophysical Research Communications*, 2015. **463**(4): p. 832-838.
87. Shepard, B.D., D.J. Tuma, and P.L. Tuma, *Chronic Ethanol Consumption Induces Global Hepatic Protein Hyperacetylation*. *Alcoholism, clinical and experimental research*, 2010. **34**(2): p. 280-291.
88. Shepard, B.D. and P.L. Tuma, *Alcohol-induced protein hyperacetylation: Mechanisms and consequences*. *World Journal of Gastroenterology : WJG*, 2009. **15**(10): p. 1219-1230.
89. Choudhary, C., et al., *The growing landscape of lysine acetylation links metabolism and cell signalling*. *Nat Rev Mol Cell Biol*, 2014. **15**(8): p. 536-550.
90. Patel, J., R.R. Pathak, and S. Mujtaba, *The biology of lysine acetylation integrates transcriptional programming and metabolism*. *Nutrition & Metabolism*, 2011. **8**: p. 12-12.
91. Verdin, E. and M. Ott, *50 years of protein acetylation: from gene regulation to epigenetics, metabolism and beyond*. *Nat Rev Mol Cell Biol*, 2015. **16**(4): p. 258-264.
92. Beier, J.I. and C.J. McClain, *Mechanisms and cell signaling in alcoholic liver disease*. *Biol Chem*, 2010. **391**(11): p. 1249-64.
93. Bonet-Ponce, L., et al., *On the mechanism underlying ethanol-induced mitochondrial dynamic disruption and autophagy response*. *Biochimica et Biophysica Acta (BBA) - Molecular Basis of Disease*, 2015. **1852**(7): p. 1400-1409.
94. McKim, S.E., et al., *Inducible nitric oxide synthase is required in alcohol-induced liver injury: studies with knockout mice*. *Gastroenterology*, 2003. **125**(6): p. 1834-44.
95. Wang, K., *Molecular mechanisms of hepatic apoptosis*. *Cell Death Dis*, 2014. **5**: p. e996.
96. Zakhari, S., *Alcohol metabolism and epigenetics changes*. *Alcohol Res*, 2013. **35**(1): p. 6-16.
97. Bürkle, A., *Posttranslational Modification A2 - Brenner, Sydney*, in *Encyclopedia of Genetics*, J.H. Miller, Editor. 2001, Academic Press: New York. p. 1533.
98. Lee, Y.J. and S.D. Shukla, *Histone H3 phosphorylation at serine 10 and serine 28 is mediated by p38 MAPK in rat hepatocytes exposed to ethanol and acetaldehyde*. *Eur J Pharmacol*, 2007. **573**(1-3): p. 29-38.
99. Jaenisch, R. and A. Bird, *Epigenetic regulation of gene expression: how the genome integrates intrinsic and environmental signals*. *Nat Genet*, 2003. **33**.
100. Gonzalez-Zuniga, M., et al., *c-Abl stabilizes HDAC2 levels by tyrosine phosphorylation repressing neuronal gene expression in Alzheimer's disease*. *Mol Cell*, 2014. **56**(1): p. 163-73.
101. Yeo, W.-S., et al., *Mass spectrometric analysis of protein tyrosine nitration in aging and neurodegenerative diseases*. *Mass Spectrometry Reviews*, 2015. **34**(2): p. 166-183.
102. Rayala, S.K., et al., *Dynamic interplay between nitration and phosphorylation of tubulin cofactor B in the control of microtubule dynamics*. *Proc Natl Acad Sci U S A*, 2007. **104**(49): p. 19470-5.

103. Shi, W.Q., et al., *Tyrosine phosphorylation/dephosphorylation regulates peroxynitrite-mediated peptide nitration*. Regul Pept, 2007. **144**(1-3): p. 1-5.
104. Kong, S.K., et al., *Peroxynitrite disables the tyrosine phosphorylation regulatory mechanism: Lymphocyte-specific tyrosine kinase fails to phosphorylate nitrated cdc2(6-20)NH2 peptide*. Proc Natl Acad Sci U S A, 1996. **93**(8): p. 3377-82.
105. Li, X., et al., *Peroxynitrite modulates tyrosine phosphorylation and phosphoinositide signalling in human neuroblastoma SH-SY5Y cells: attenuated effects in human 1321N1 astrocytoma cells*. Biochem J, 1998. **331 (Pt 2)**: p. 599-606.
106. Haqqani, A.S., J.F. Kelly, and H.C. Birnboim, *Selective Nitration of Histone Tyrosine Residues in Vivo in Mutatect Tumors*. Journal of Biological Chemistry, 2002. **277**(5): p. 3614-3621.
107. Bartesaghi, S., et al., *Protein tyrosine nitration in hydrophilic and hydrophobic environments*. Amino Acids, 2007. **32**(4): p. 501-15.
108. Seeley, K.W. and S.M. Stevens, Jr., *Investigation of local primary structure effects on peroxynitrite-mediated tyrosine nitration using targeted mass spectrometry*. J Proteomics, 2012. **75**(6): p. 1691-700.
109. Gow, A.J., et al., *Effects of peroxynitrite-induced protein modifications on tyrosine phosphorylation and degradation*. FEBS Lett, 1996. **385**(1-2): p. 63-6.
110. Guingab-Cagmat, J.D., et al., *Identification of tyrosine nitration in UCH-L1 and GAPDH*. Electrophoresis, 2011. **32**(13): p. 1692-705.
111. Yi, D., et al., *Peroxynitrite-mediated nitration of peptides: characterization of the products by electrospray and combined gas chromatography-mass spectrometry*. Arch Biochem Biophys, 1997. **344**(2): p. 253-9.
112. Greis, K.D., S. Zhu, and S. Matalon, *Identification of nitration sites on surfactant protein A by tandem electrospray mass spectrometry*. Arch Biochem Biophys, 1996. **335**(2): p. 396-402.
113. Greenacre, S.A., et al., *Formation and loss of nitrated proteins in peroxynitrite-treated rat skin in vivo*. Biochem Biophys Res Commun, 1999. **262**(3): p. 781-6.
114. Irie, Y., et al., *Histone H1.2 is a substrate for denitrase, an activity that reduces nitrotyrosine immunoreactivity in proteins*. Proc Natl Acad Sci U S A, 2003. **100**(10): p. 5634-9.
115. Kamisaki, Y., et al., *An activity in rat tissues that modifies nitrotyrosine-containing proteins*. Proc Natl Acad Sci U S A, 1998. **95**(20): p. 11584-9.
116. Kuo, W.N., R.N. Kanadia, and V.P. Shanbhag, *Denitration of peroxynitrite-treated proteins by "protein nitrates" from dog prostate*. Biochem Mol Biol Int, 1999. **47**(6): p. 1061-7.
117. Kuo, W.N., et al., *Denitration of peroxynitrite-treated proteins by 'protein nitrates' from rat brain and heart*. Mol Cell Biochem, 1999. **201**(1-2): p. 11-6.
118. Fritz, K.S., et al., *Ethanol Metabolism Modifies Hepatic Protein Acylation in Mice*. PLoS ONE, 2013. **8**(9): p. e75868.
119. Picklo Sr, M.J., *Ethanol intoxication increases hepatic N-lysyl protein acetylation*. Biochemical and Biophysical Research Communications, 2008. **376**(3): p. 615-619.
120. Kendrick, S.F., et al., *Acetate, the key modulator of inflammatory responses in acute alcoholic hepatitis*. Hepatology, 2010. **51**(6): p. 1988-97.
121. Kim, S.J., et al., *Characterization of novel mechanisms for steatosis from global protein hyperacetylation in ethanol-induced mouse hepatocytes*. Biochem Biophys Res Commun, 2015. **463**(4): p. 832-8.
122. Woodruff, M. *UHPLC or Core-Shell Which is the Winner?* Chromatography Today, 2014. **May/June**.
123. Law, K.P. and Y.P. Lim, *Recent advances in mass spectrometry: data independent analysis and hyper reaction monitoring*. Expert Rev Proteomics, 2013. **10**(6): p. 551-66.

124. Huang, H., et al., *Quantitative Proteomic Analysis of Histone Modifications*. Chemical reviews, 2015. **115**(6): p. 2376-2418.
125. Marshall, A.G., C.L. Hendrickson, and G.S. Jackson, *Fourier transform ion cyclotron resonance mass spectrometry: a primer*. Mass Spectrom Rev, 1998. **17**(1): p. 1-35.
126. Stevens, S.M., Jr., K. Prokai-Tatrai, and L. Prokai, *Factors that contribute to the misidentification of tyrosine nitration by shotgun proteomics*. Mol Cell Proteomics, 2008. **7**(12): p. 2442-51.
127. Chen, Y., et al., *PTMap--a sequence alignment software for unrestricted, accurate, and full-spectrum identification of post-translational modification sites*. Proc Natl Acad Sci U S A, 2009. **106**(3): p. 761-6.
128. Bernstein, B.E., et al., *A bivalent chromatin structure marks key developmental genes in embryonic stem cells*. Cell, 2006. **125**(2): p. 315-26.
129. Ong, S.E. and M. Mann, *A practical recipe for stable isotope labeling by amino acids in cell culture (SILAC)*. Nat Protoc, 2006. **1**(6): p. 2650-60.
130. Pichler, P., et al., *Peptide Labeling with Isobaric Tags Yields Higher Identification Rates Using iTRAQ 4-Plex Compared to TMT 6-Plex and iTRAQ 8-Plex on LTQ Orbitrap*. Analytical Chemistry, 2010. **82**(15): p. 6549-6558.
131. Latosinska, A., et al., *Comparative Analysis of Label-Free and 8-Plex iTRAQ Approach for Quantitative Tissue Proteomic Analysis*. PLOS ONE, 2015. **10**(9): p. e0137048.
132. Cox, J., et al., *Accurate proteome-wide label-free quantification by delayed normalization and maximal peptide ratio extraction, termed MaxLFQ*. Mol Cell Proteomics, 2014. **13**(9): p. 2513-26.
133. Garcia, B.A., et al., *Chemical derivatization of histones for facilitated analysis by mass spectrometry*. Nature protocols, 2007. **2**(4): p. 933-938.
134. Koch, O.R., et al., *Alcohol-induced oxidative stress in rat liver*. Xenobiotica, 1991. **21**(8): p. 1077-84.
135. Wu, D. and A.I. Cederbaum, *Alcohol, oxidative stress, and free radical damage*. Alcohol Res Health, 2003. **27**(4): p. 277-84.
136. Wu, D., Q. Zhai, and X. Shi, *Alcohol-induced oxidative stress and cell responses*. J Gastroenterol Hepatol, 2006. **21 Suppl 3**: p. S26-9.
137. Zima, T., et al., *Oxidative stress, metabolism of ethanol and alcohol-related diseases*. J Biomed Sci, 2001. **8**(1): p. 59-70.
138. Fernandez-Checa, J.C., *Alcohol-induced liver disease: when fat and oxidative stress meet*. Ann Hepatol, 2003. **2**(2): p. 69-75.
139. Turko, I.V. and F. Murad, *Protein nitration in cardiovascular diseases*. Pharmacol Rev, 2002. **54**(4): p. 619-34.
140. Ferrer, M.D., et al., *The double edge of reactive oxygen species as damaging and signaling molecules in HL60 cell culture*. Cell Physiol Biochem, 2010. **25**(2-3): p. 241-52.
141. Radi, R., *Protein tyrosine nitration: biochemical mechanisms and structural basis of functional effects*. Acc Chem Res, 2013. **46**(2): p. 550-9.
142. Reddy, V.D., et al., *Alcohol-induced oxidative stress in rat liver microsomes: Protective effect of Emblica officinalis*. Pathophysiology, 2014. **21**(2): p. 153-9.
143. Fernandez-Checa, J.C., M. Ookhtens, and N. Kaplowitz, *Effect of chronic ethanol feeding on rat hepatocytic glutathione. Compartmentation, efflux, and response to incubation with ethanol*. Journal of Clinical Investigation, 1987. **80**(1): p. 57-62.
144. Speisky, H., et al., *Depletion of Hepatic Glutathione by Ethanol Occurs Independently of Ethanol Metabolism*. Alcoholism: Clinical and Experimental Research, 1988. **12**(2): p. 224-228.
145. Viña, J., et al., *Effect of ethanol on glutathione concentration in isolated hepatocytes*. Biochemical Journal, 1980. **188**(2): p. 549-552.

146. Bryan, N. and J. Lancaster, Jr., *Nitric Oxide Signaling in Health and Disease*, in *Nitrite and Nitrate in Human Health and Disease*, N.S. Bryan and J. Loscalzo, Editors. 2011, Humana Press. p. 169-186.
147. Arif, M., et al., *Nitric Oxide-Mediated Histone Hyperacetylation in Oral Cancer: Target for a Water-Soluble HAT Inhibitor, CTK7A*. *Chemistry & Biology*, 2010. **17**(8): p. 903-913.
148. Berghella, L. and P.L. Puri, *Nitric Oxide and Histone Acetylation—Shaping Craniofacial Development*. *Chemistry & Biology*. **21**(5): p. 565-566.
149. Hickok, J.R., et al., *Nitric oxide modifies global histone methylation by inhibiting Jumonji C domain-containing demethylases*. *J Biol Chem*, 2013. **288**(22): p. 16004-15.
150. Turner, B.M., *Histone acetylation as an epigenetic determinant of long-term transcriptional competence*. *Cell Mol Life Sci*, 1998. **54**(1): p. 21-31.
151. Park, P.-H., R. Miller, and S.D. Shukla, *Acetylation of histone H3 at lysine 9 by ethanol in rat hepatocytes*. *Biochemical and Biophysical Research Communications*, 2003. **306**(2): p. 501-504.
152. Shibasaki, M., et al., *Enhancement of histone acetylation in midbrain of mice with ethanol physical dependence and its withdrawal*. *Synapse*, 2011. **65**(11): p. 1244-50.
153. Cohen, J.I. and L.E. Nagy, *Pathogenesis of alcoholic liver disease: interactions between parenchymal and non-parenchymal cells*. *J Dig Dis*, 2011. **12**(1): p. 3-9.
154. Manzo-Avalos, S. and A. Saavedra-Molina, *Cellular and mitochondrial effects of alcohol consumption*. *Int J Environ Res Public Health*, 2010. **7**(12): p. 4281-304.
155. Picklo, M.J., Sr., *Ethanol intoxication increases hepatic N-lysyl protein acetylation*. *Biochem Biophys Res Commun*, 2008. **376**(3): p. 615-9.
156. Shulga, N. and J.G. Pastorino, *Ethanol sensitizes mitochondria to the permeability transition by inhibiting deacetylation of cyclophilin-D mediated by sirtuin-3*. *J Cell Sci*, 2010. **123**(Pt 23): p. 4117-27.
157. Lieber, C.S., et al., *Effect of chronic alcohol consumption on Hepatic SIRT1 and PGC-1alpha in rats*. *Biochem Biophys Res Commun*, 2008. **370**(1): p. 44-8.
158. Karve, T.M. and A.K. Cheema, *Small changes huge impact: the role of protein posttranslational modifications in cellular homeostasis and disease*. *J Amino Acids*, 2011. **2011**: p. 207691.
159. Lin, H., et al., *Post-Translational Modifications to Regulate Protein Function*, in *Wiley Encyclopedia of Chemical Biology*. 2007, John Wiley & Sons, Inc.
160. Sadoul, K., et al., *The tale of protein lysine acetylation in the cytoplasm*. *J Biomed Biotechnol*, 2011. **2011**: p. 970382.
161. Verdin, E. and M. Ott, *50 years of protein acetylation: from gene regulation to epigenetics, metabolism and beyond*. *Nat Rev Mol Cell Biol*, 2014.
162. Yang, X.J. and E. Seto, *Lysine acetylation: codified crosstalk with other posttranslational modifications*. *Mol Cell*, 2008. **31**(4): p. 449-61.
163. Choudhury, M., et al., *Evidence for the role of oxidative stress in the acetylation of histone H3 by ethanol in rat hepatocytes*. *Alcohol*, 2010. **44**(6): p. 531-40.
164. Gao, B. and R. Bataller, *Alcoholic liver disease: pathogenesis and new therapeutic targets*. *Gastroenterology*, 2011. **141**(5): p. 1572-85.
165. Eagon, P.K., *Alcoholic liver injury: influence of gender and hormones*. *World J Gastroenterol*, 2010. **16**(11): p. 1377-84.
166. Guy, J. and M.G. Peters, *Liver Disease in Women: The Influence of Gender on Epidemiology, Natural History, and Patient Outcomes*. *Gastroenterology & Hepatology*, 2013. **9**(10): p. 633-639.
167. Shimizu, I., et al., *Gender Difference in Alcoholic Liver Disease*, in *Trends in Alcoholic Liver Disease Research - Clinical and Scientific Aspects*, I. Shimizu, Editor. 2012, InTech: Rijeka. p. Ch. 02.

168. Ikejima, K., et al., *Estrogen increases sensitivity of hepatic Kupffer cells to endotoxin*. Am J Physiol, 1998. **274**(4 Pt 1): p. G669-76.
169. Nanji, A.A., et al., *Pathogenesis of alcoholic liver disease--recent advances*. Alcohol Clin Exp Res, 2002. **26**(5): p. 731-6.
170. Thurman, R.G., II. *Alcoholic liver injury involves activation of Kupffer cells by endotoxin*. Am J Physiol, 1998. **275**(4 Pt 1): p. G605-11.
171. Colantoni, A., et al., *Influence of sex hormonal status on alcohol-induced oxidative injury in male and female rat liver*. Alcohol Clin Exp Res, 2000. **24**(9): p. 1467-73.
172. Miller, A.M., et al., *Molecular mechanisms of alcoholic liver disease: innate immunity and cytokines*. Alcohol Clin Exp Res, 2011. **35**(5): p. 787-93.
173. Cederbaum, A.I., *Role of CYP2E1 in ethanol-induced oxidant stress, fatty liver and hepatotoxicity*. Dig Dis, 2010. **28**(6): p. 802-11.
174. Cederbaum, A.I., Y. Lu, and D. Wu, *Role of oxidative stress in alcohol-induced liver injury*. Arch Toxicol, 2009. **83**(6): p. 519-48.
175. Mari, M., et al., *Redox control of liver function in health and disease*. Antioxid Redox Signal, 2010. **12**(11): p. 1295-331.
176. Nanji, A.A., et al., *Increased severity of alcoholic liver injury in female rats: role of oxidative stress, endotoxin, and chemokines*. Am J Physiol Gastrointest Liver Physiol, 2001. **281**(6): p. G1348-56.
177. Zima, T. and M. Kalousova, *Oxidative stress and signal transduction pathways in alcoholic liver disease*. Alcohol Clin Exp Res, 2005. **29**(11 Suppl): p. 110S-115S.
178. Albano, E., *New concepts in the pathogenesis of alcoholic liver disease*. Expert Rev Gastroenterol Hepatol, 2008. **2**(6): p. 749-59.
179. Durazzo, M., et al., *Gender specific medicine in liver diseases: A point of view*. World Journal of Gastroenterology : WJG, 2014. **20**(9): p. 2127-2135.
180. Sato, N., et al., *Sex difference in alcohol-related organ injury*. Alcohol Clin Exp Res, 2001. **25**(5 Suppl ISBRA): p. 40S-45S.
181. Tadic, S.D., et al., *Sex differences in hepatic gene expression in a rat model of ethanol-induced liver injury*. J Appl Physiol (1985), 2002. **93**(3): p. 1057-68.
182. Cederbaum, A.I., et al., *CYP2E1 Sensitizes the Liver to LPS- and TNF alpha-Induced Toxicity via Elevated Oxidative and Nitrosative Stress and Activation of ASK-1 and JNK Mitogen-Activated Kinases*. Int J Hepatol, 2012. **2012**: p. 582790.
183. Chen, J., G. Kunos, and B. Gao, *Ethanol rapidly inhibits IL-6-activated STAT3 and C/EBP mRNA expression in freshly isolated rat hepatocytes*. FEBS Lett, 1999. **457**(1): p. 162-8.
184. Lu, C. and C.B. Thompson, *Metabolic regulation of epigenetics*. Cell Metab, 2012. **16**(1): p. 9-17.
185. Yokoyama, Y., et al., *Current understanding of gender dimorphism in hepatic pathophysiology*. J Surg Res, 2005. **128**(1): p. 147-56.
186. Banerjee, A., et al., *The influence of estrogen on hepatobiliary osteopontin (SPP1) expression in a female rodent model of alcoholic steatohepatitis*. Toxicol Pathol, 2009. **37**(4): p. 492-501.
187. Becker, U., et al., *Prediction of risk of liver disease by alcohol intake, sex, and age: A prospective population study*. Hepatology, 1996. **23**(5): p. 1025-1029.
188. Colantoni, A., et al., *Hepatic estrogen receptors and alcohol intake*. Mol Cell Endocrinol, 2002. **193**(1-2): p. 101-4.
189. Bertola, A., et al., *Mouse model of chronic and binge ethanol feeding (the NIAAA model)*. Nat Protoc, 2013. **8**(3): p. 627-37.
190. Lieber, C.S. and L.M. DeCarli, *The Feeding of Alcohol in Liquid Diets: Two Decades of Applications and 1982 Update*. Alcoholism: Clinical and Experimental Research, 1982. **6**(4): p. 523-531.

191. Donohue, T.M., et al., *Lysosomal leakage and lack of adaptation of hepatoprotective enzyme contribute to enhanced susceptibility to ethanol-induced liver injury in female rats*. Alcohol Clin Exp Res, 2007. **31**(11): p. 1944-52.
192. Sharma, M.R., et al., *Increased severity of alcoholic liver injury in female versus male rats: a microarray analysis*. Exp Mol Pathol, 2008. **84**(1): p. 46-58.
193. Athirakul, K., et al., *Increased blood pressure in mice lacking cytochrome P450 2J5*. FASEB J, 2008. **22**(12): p. 4096-108.
194. Ma, J., et al., *Regulation of mouse renal CYP2J5 expression by sex hormones*. Mol Pharmacol, 2004. **65**(3): p. 730-43.
195. Enomoto, N., et al., *Estriol sensitizes rat Kupffer cells via gut-derived endotoxin*. Am J Physiol, 1999. **277**(3 Pt 1): p. G671-7.
196. Avila Escribano, J.J. and D. Gonzalez Parra, *[Gender differences in alcoholism]*. Adicciones, 2007. **19**(4): p. 383-92.
197. Cederbaum, A.I., *Iron and CYP2E1-dependent oxidative stress and toxicity*. Alcohol, 2003. **30**(2): p. 115-20.
198. Cederbaum, A.I., et al., *CYP2E1-dependent toxicity and oxidative stress in HepG2 cells*. Free Radic Biol Med, 2001. **31**(12): p. 1539-43.
199. Lu, Y. and A.I. Cederbaum, *CYP2E1 potentiation of LPS and TNFalpha-induced hepatotoxicity by mechanisms involving enhanced oxidative and nitrosative stress, activation of MAP kinases, and mitochondrial dysfunction*. Genes Nutr, 2010. **5**(2): p. 149-67.
200. Cheng, J., et al., *Vascular characterization of mice with endothelial expression of cytochrome P450 4F2*. The FASEB Journal, 2014. **28**(7): p. 2915-2931.
201. Cluzeau, C.V.M., et al., *Microarray expression analysis and identification of serum biomarkers for Niemann–Pick disease, type C1*. Human Molecular Genetics, 2012. **21**(16): p. 3632-3646.
202. Smart, R.C. and E. Hodgson, *Molecular and Biochemical Toxicology*. 2017: Wiley.
203. Reddy, V.D., et al., *Alcohol-induced oxidative/nitrosative stress alters brain mitochondrial membrane properties*. Mol Cell Biochem, 2013. **375**(1-2): p. 39-47.
204. Song, B.-J., et al., *Mitochondrial dysfunction and tissue injury by alcohol, high fat, nonalcoholic substances and pathological conditions through post-translational protein modifications*. Redox Biology, 2014. **3**(0): p. 109-123.
205. Zhong, L., et al., *Ethanol and its metabolites induce histone lysine 9 acetylation and an alteration of the expression of heart development-related genes in cardiac progenitor cells*. Cardiovasc Toxicol, 2010. **10**(4): p. 268-74.
206. Giannini, E.G., R. Testa, and V. Savarino, *Liver enzyme alteration: a guide for clinicians*. CMAJ : Canadian Medical Association Journal, 2005. **172**(3): p. 367-379.
207. M.D., F.F.F., *LABORATORY TESTS*, in *Geriatric Clinical Advisor*. 2007, Mosby: Philadelphia. p. 138.
208. Nyblom, H., et al., *HIGH AST/ALT RATIO MAY INDICATE ADVANCED ALCOHOLIC LIVER DISEASE RATHER THAN HEAVY DRINKING*. Alcohol and Alcoholism, 2004. **39**(4): p. 336-339.
209. Kundu, D., et al., *Oxidative Stress in Alcoholic and Viral Hepatitis*. North American Journal of Medical Sciences, 2012. **4**(9): p. 412-415.
210. Ohta, Y., et al., *Involvement of Oxidative Stress in Increases in the Serum Levels of Various Enzymes and Components in Rats with Water-Immersion Restraint Stress*. Journal of Clinical Biochemistry and Nutrition, 2009. **45**(3): p. 347-354.
211. Hong, F., et al., *Absence of cytochrome P450 2A5 enhances alcohol-induced liver injury in mice*. Dig Liver Dis, 2015. **47**(6): p. 470-7.

212. Hardwick, J.P., et al., *PPAR/RXR Regulation of Fatty Acid Metabolism and Fatty Acid ω -Hydroxylase (CYP4) Isozymes: Implications for Prevention of Lipotoxicity in Fatty Liver Disease*. PPAR Research, 2009. **2009**: p. 952734.
213. Montagner, A., et al., *Liver PPAR α is crucial for whole-body fatty acid homeostasis and is protective against NAFLD*. Gut, 2016.
214. Zhang, X., et al., *Ablation of cytochrome P450 omega-hydroxylase 4A14 gene attenuates hepatic steatosis and fibrosis*. Proceedings of the National Academy of Sciences, 2017. **114**(12): p. 3181-3185.
215. Farber, J.L., *Mechanisms of cell injury by activated oxygen species*. Environmental Health Perspectives, 1994. **102**(Suppl 10): p. 17-24.
216. Cavin, C., et al., *Ochratoxin A-mediated DNA and protein damage: roles of nitrosative and oxidative stresses*. Toxicol Sci, 2009. **110**(1): p. 84-94.
217. Beckman, J.S., et al., *Oxidative chemistry of peroxynitrite*. Methods Enzymol, 1994. **233**: p. 229-40.
218. Ferrante, R.J., et al., *Increased 3-nitrotyrosine and oxidative damage in mice with a human copper/zinc superoxide dismutase mutation*. Ann Neurol, 1997. **42**(3): p. 326-34.
219. Pacher, P., J.S. Beckman, and L. Liaudet, *Nitric oxide and peroxynitrite in health and disease*. Physiol Rev, 2007. **87**(1): p. 315-424.
220. Yakovlev, V.A. and R.B. Mikkelsen, *Protein tyrosine nitration in cellular signal transduction pathways*. Journal of receptor and signal transduction research, 2010. **30**(6): p. 420-429.
221. Albano, E., *Alcohol, oxidative stress and free radical damage*. Proc Nutr Soc, 2006. **65**(3): p. 278-90.
222. Arteel, G.E., *Alcohol-induced oxidative stress in the liver: in vivo measurements*. Methods Mol Biol, 2008. **447**: p. 185-97.
223. Nguyen, D., *Quantifying chromogen intensity in immunohistochemistry via reciprocal intensity*. 2013.
224. Hattori, M., et al., *A simplified method for the preparation of transcriptionally active liver nuclear extracts*. DNA Cell Biol, 1990. **9**(10): p. 777-81.
225. Lee, A.H., et al., *Regulation of hepatic lipogenesis by the transcription factor XBP1*. Science, 2008. **320**(5882): p. 1492-6.
226. Davey, C.A., et al., *Solvent mediated interactions in the structure of the nucleosome core particle at 1.9 Å resolution*. J Mol Biol, 2002. **319**(5): p. 1097-113.
227. Shaytan, A.K., et al., *Coupling between Histone Conformations and DNA Geometry in Nucleosomes on a Microsecond Timescale: Atomistic Insights into Nucleosome Functions*. J Mol Biol, 2016. **428**(1): p. 221-237.
228. Berendsen, H.J.C., J.R. Grigera, and T.P. Straatsma, *The missing term in effective pair potentials*. The Journal of Physical Chemistry, 1987. **91**(24): p. 6269-6271.
229. Myung, Y. and S. Han, *Force Field Parameters for 3-Nitrotyrosine and 6-Nitrotryptophan*. Bulletin Korean Chemical Society, 2010. **31**(9): p. 2581-2587.
230. Hess, B., et al., *GROMACS 4: Algorithms for Highly Efficient, Load-Balanced, and Scalable Molecular Simulation*. Journal of Chemical Theory and Computation, 2008. **4**(3): p. 435-447.
231. Lindorff-Larsen, K., et al., *Improved side-chain torsion potentials for the Amber ff99SB protein force field*. Proteins: Structure, Function, and Bioinformatics, 2010. **78**(8): p. 1950-1958.
232. Parrinello, M. and A. Rahman, *Polymorphic transition in single crystals: A new molecular dynamics method*. Journal of Applied Physics, 1981. **52**: p. 7128-7190.
233. Bussi, G., D. Donadio, and M. Parrinello, *Canonical sampling through velocity rescaling*. J Chem Phys, 2007. **126**(1): p. 014101.

234. Darden, T., D. Yrok, and L. Pedersen, *Particle mesh Ewald: an NLog(N) method for Ewald sums in large systems*. The Journal of Chemical Physics, 1993. **98**: p. 10089-10092.
235. Dawson, M.A., et al., *JAK2 phosphorylates histone H3Y41 and excludes HP1alpha from chromatin*. Nature, 2009. **461**(7265): p. 819-22.
236. Souza, J.M., G. Peluffo, and R. Radi, *Protein tyrosine nitration--functional alteration or just a biomarker?* Free Radic Biol Med, 2008. **45**(4): p. 357-66.
237. Brennan, M.-L., et al., *A Tale of Two Controversies: DEFINING BOTH THE ROLE OF PEROXIDASES IN NITROTYROSINE FORMATION IN VIVO USING EOSINOPHIL PEROXIDASE AND MYELOPEROXIDASE-DEFICIENT MICE, AND THE NATURE OF PEROXIDASE-GENERATED REACTIVE NITROGEN SPECIES*. Journal of Biological Chemistry, 2002. **277**(20): p. 17415-17427.
238. Leeuwenburgh, C., et al., *Reactive nitrogen intermediates promote low density lipoprotein oxidation in human atherosclerotic intima*. J Biol Chem, 1997. **272**(3): p. 1433-6.
239. Shishehbor, M.H., et al., *Association of nitrotyrosine levels with cardiovascular disease and modulation by statin therapy*. Jama, 2003. **289**(13): p. 1675-80.
240. MacPherson, J.C., et al., *Eosinophils are a major source of nitric oxide-derived oxidants in severe asthma: characterization of pathways available to eosinophils for generating reactive nitrogen species*. J Immunol, 2001. **166**(9): p. 5763-72.
241. Mandrekar, P., *Epigenetic regulation in alcoholic liver disease*. World Journal of Gastroenterology : WJG, 2011. **17**(20): p. 2456-2464.
242. Baek, Sung H., *When Signaling Kinases Meet Histones and Histone Modifiers in the Nucleus*. Molecular Cell, 2011. **42**(3): p. 274-284.
243. Chaudhury, A., P. Chander, and P.H. Howe, *Heterogeneous nuclear ribonucleoproteins (hnRNPs) in cellular processes: Focus on hnRNP E1's multifunctional regulatory roles*. RNA, 2010. **16**(8): p. 1449-1462.
244. Geuens, T., D. Bouhy, and V. Timmerman, *The hnRNP family: insights into their role in health and disease*. Human Genetics, 2016. **135**: p. 851-867.
245. Piñol-Roma, S. and G. Dreyfuss, *hnRNP proteins: Localization and transport between the nucleus and the cytoplasm*. Trends in Cell Biology. **3**(5): p. 151-155.
246. Becker, M., J. Kuhse, and J. Kirsch, *Effects of two elongation factor 1A isoforms on the formation of gephyrin clusters at inhibitory synapses in hippocampal neurons*. Histochem Cell Biol, 2013. **140**(6): p. 603-9.
247. Hamrita, B., et al., *An elongation factor-like protein (EF-Tu) elicits a humoral response in infiltrating ductal breast carcinomas: an immunoproteomics investigation*. Clin Biochem, 2011. **44**(13): p. 1097-104.
248. Itagaki, K., et al., *Eukaryotic Translation Elongation Factor 1A Induces Anoikis by Triggering Cell Detachment*. The Journal of Biological Chemistry, 2012. **287**(19): p. 16037-16046.
249. Rehman, I., et al., *iTRAQ identification of candidate serum biomarkers associated with metastatic progression of human prostate cancer*. PLoS One, 2012. **7**(2): p. e30885.
250. Liu, H., et al., *Increased expression of elongation factor-1alpha is significantly correlated with poor prognosis of human prostate cancer*. Scand J Urol Nephrol, 2010. **44**(5): p. 277-83.
251. Morrissey, C., et al., *The eukaryotic elongation factor eEF1A1 interacts with SAMHD1*. Biochem J, 2015. **466**(1): p. 69-76.
252. Seeley, K.W., et al., *Evaluation of a method for nitrotyrosine site identification and relative quantitation using a stable isotope-labeled nitrated spike-in standard and high resolution fourier transform MS and MS/MS analysis*. Int J Mol Sci, 2014. **15**(4): p. 6265-85.
253. Prevention, C.f.D.C.a. *Binge Drinking*. Fact Sheets 2017; Available from: <https://www.cdc.gov/alcohol/fact-sheets/binge-drinking.htm>.

254. Llerena, S., et al., *Binge drinking: Burden of liver disease and beyond*. World J Hepatol, 2015. **7**(27): p. 2703-15.
255. Naimi, T.S., et al., *Binge drinking among us adults*. JAMA, 2003. **289**(1): p. 70-75.
256. Shukla, S.D., et al., *Binge ethanol and liver: new molecular developments*. Alcohol Clin Exp Res, 2013. **37**(4): p. 550-7.
257. Wechsler, H. and T.F. Nelson, *Binge drinking and the American college student: what's five drinks?* Psychol Addict Behav, 2001. **15**(4): p. 287-91.
258. Ponomarev, I., et al., *Mechanistic insights into epigenetic modulation of ethanol consumption*. Alcohol, 2017. **60**: p. 95-101.
259. Restrepo, R.J., et al., *Binge alcohol alters PNPLA3 levels in liver through epigenetic mechanism involving histone H3 acetylation*. Alcohol, 2017. **60**: p. 77-82.
260. Shukla, S.D., et al., *In Vivo Acute on Chronic Ethanol Effects in Liver: A Mouse Model Exhibiting Exacerbated Injury, Altered Metabolic and Epigenetic Responses*. Biomolecules, 2015. **5**(4): p. 3280-94.
261. Lundquist, F., et al., *ETHANOL METABOLISM AND PRODUCTION OF FREE ACETATE IN THE HUMAN LIVER*. Journal of Clinical Investigation, 1962. **41**(5): p. 955-961.
262. Kori, Y., et al., *Proteome-wide acetylation dynamics in human cells*. Sci Rep, 2017. **7**(1): p. 10296.
263. Evertts, A.G., et al., *Quantitative Dynamics of the Link between Cellular Metabolism and Histone Acetylation*. The Journal of Biological Chemistry, 2013. **288**(17): p. 12142-12151.
264. Chambers, M.C., et al., *A cross-platform toolkit for mass spectrometry and proteomics*. Nat Biotechnol, 2012. **30**(10): p. 918-20.
265. Martens, L., et al., *mzML--a community standard for mass spectrometry data*. Mol Cell Proteomics, 2011. **10**(1): p. R110 000133.
266. Wickham, H., *ggplot2 Elegant Graphics for Data Analysis*. Springer-Verlag New York 2009. **Ed. 1**: p. VIII, 213.
267. Kim, G.W. and X.J. Yang, *Comprehensive lysine acetylomes emerging from bacteria to humans*. Trends Biochem Sci, 2011. **36**(4): p. 211-20.
268. Simpson, C.L., et al., *Variants of the elongator protein 3 (ELP3) gene are associated with motor neuron degeneration*. Hum Mol Genet, 2009. **18**(3): p. 472-81.
269. Spange, S., et al., *Acetylation of non-histone proteins modulates cellular signalling at multiple levels*. Int J Biochem Cell Biol, 2009. **41**(1): p. 185-98.
270. Lin, S., et al., *Stable-isotope-labeled histone peptide library for histone post-translational modification and variant quantification by mass spectrometry*. Mol Cell Proteomics, 2014. **13**(9): p. 2450-66.
271. Zee, B.M., et al., *Global turnover of histone post-translational modifications and variants in human cells*. Epigenetics & Chromatin, 2010. **3**: p. 22-22.
272. Evertts, A.G., et al., *Quantitative dynamics of the link between cellular metabolism and histone acetylation*. J Biol Chem, 2013. **288**(17): p. 12142-51.
273. Li, Y., et al., *Mass spectrometry-based detection of protein acetylation*. Methods in molecular biology (Clifton, N.J.), 2013. **1077**: p. 81-104.
274. Zee, B.M. and B.A. Garcia, *Validation of Protein Acetylation by Mass Spectrometry*. Methods in molecular biology (Clifton, N.J.), 2013. **981**: p. 1-11.
275. You, M., et al., *Mammalian Sirtuin 1 Is Involved in the Protective Action of Dietary Saturated Fat against Alcoholic Fatty Liver in Mice*. The Journal of Nutrition, 2008. **138**(3): p. 497-501.
276. Britton, L.-M.P., et al., *Breaking the histone code with quantitative mass spectrometry*. Expert review of proteomics, 2011. **8**(5): p. 631-643.

277. Park, P.-H., R.W. Lim, and S.D. Shukla, *Involvement of histone acetyltransferase (HAT) in ethanol-induced acetylation of histone H3 in hepatocytes: potential mechanism for gene expression*. American Journal of Physiology - Gastrointestinal and Liver Physiology, 2005. **289**(6): p. G1124-G1136.
278. Yuan, Z.-F., et al., *Evaluation of proteomic search engines for the analysis of histone modifications*. J Proteome Res, 2014. **13**.
279. Richards, P. *2018 Alcoholism Statistics You Need to Know*. 2018; Available from: <https://talbotcampus.com/alcoholism-statistics/>.
280. Rasineni, K. and C.A. Casey, *Molecular mechanism of alcoholic fatty liver*. Indian Journal of Pharmacology, 2012. **44**(3): p. 299-303.
281. Nebert, D.W., K. Wikvall, and W.L. Miller, *Human cytochromes P450 in health and disease*. Philosophical Transactions of the Royal Society B: Biological Sciences, 2013. **368**(1612): p. 20120431.
282. Villeneuve, J.P. and V. Pichette, *Cytochrome P450 and liver diseases*. Curr Drug Metab, 2004. **5**(3): p. 273-82.
283. Pikuleva, I.A. and M.R. Waterman, *Cytochromes P450: Roles in Diseases*. The Journal of Biological Chemistry, 2013. **288**(24): p. 17091-17098.
284. Pochareddy, S. and H.J. Edenberg, *Chronic alcohol exposure alters gene expression in HepG2 cells*. Alcoholism, Clinical and Experimental Research, 2012. **36**(6): p. 1021-1033.
285. Bardag-Gorce, F., et al., *S-adenosylmethionine decreases the peak blood alcohol levels 3 h after an acute bolus of ethanol by inducing alcohol metabolizing enzymes in the liver*. Exp Mol Pathol, 2010. **89**(3): p. 217-21.
286. Jin, M., et al., *Regulation of cytochrome P450 2e1 expression by ethanol: role of oxidative stress-mediated pkc/jnk/sp1 pathway*. Cell Death & Disease, 2013. **4**(3): p. e554.
287. Ceni, E., T. Mello, and A. Galli, *Pathogenesis of alcoholic liver disease: Role of oxidative metabolism*. World Journal of Gastroenterology : WJG, 2014. **20**(47): p. 17756-17772.
288. Galicia-Moreno, M. and G. Gutiérrez-Reyes, *The role of oxidative stress in the development of alcoholic liver disease*. Revista de Gastroenterología de México (English Edition), 2014. **79**(2): p. 135-144.
289. Niemela, O., et al., *Induction of cytochrome P450 enzymes and generation of protein-aldehyde adducts are associated with sex-dependent sensitivity to alcohol-induced liver disease in micropigs*. Hepatology, 1999. **30**(4): p. 1011-7.
290. Baker, P.R., et al., *Convergence of nitric oxide and lipid signaling: anti-inflammatory nitro-fatty acids*. Free Radic Biol Med, 2009. **46**(8): p. 989-1003.
291. Chen, T., et al., *Role of nitric oxide in liver injury*. Curr Mol Med, 2003. **3**(6): p. 519-26.
292. Clemens, M.G., *Nitric oxide in liver injury*. Hepatology, 1999. **30**(1): p. 1-5.
293. Iwakiri, Y. and M.Y. Kim, *Nitric oxide in liver diseases*. Trends in Pharmacological Sciences, 2015. **36**(8): p. 524-536.
294. Teresa Priego, M.G., Estibaliz Castellero, Ana Isabel Martín, M Angeles Villanua and Asuncion Lo'pez-Calderon, *Nitric oxide production by hepatocytes contributes to the inhibitory effect of endotoxin on insulin-like growth factor I gene expression*. Journal of Endocrinology, 2006. **190**: p. 847-856.
295. Muijsers, R.B., et al., *Peroxynitrite: a two-faced metabolite of nitric oxide*. Life Sci, 1997. **60**(21): p. 1833-45.
296. Pryor, W.A. and G.L. Squadrito, *The chemistry of peroxynitrite: a product from the reaction of nitric oxide with superoxide*. Am J Physiol, 1995. **268**(5 Pt 1): p. L699-722.

297. Abdelmegeed, M.A. and B.J. Song, *Functional roles of protein nitration in acute and chronic liver diseases*. *Oxid Med Cell Longev*, 2014. **2014**: p. 149627.
298. Davis, K.L., et al., *Novel effects of nitric oxide*. *Annu Rev Pharmacol Toxicol*, 2001. **41**: p. 203-36.
299. Dhiman, M., et al., *Enhanced nitrosative stress during Trypanosoma cruzi infection causes nitrotyrosine modification of host proteins: implications in Chagas' disease*. *Am J Pathol*, 2008. **173**(3): p. 728-40.
300. Radi, R., *Nitric oxide, oxidants, and protein tyrosine nitration*. *Proceedings of the National Academy of Sciences*, 2004. **101**(12): p. 4003-4008.
301. Abdelmegeed, M.A. and B.-J. Song, *Functional Roles of Protein Nitration in Acute and Chronic Liver Diseases*. *Oxidative Medicine and Cellular Longevity*, 2014. **2014**: p. 21.
302. Greenacre, S.A. and H. Ischiropoulos, *Tyrosine nitration: localisation, quantification, consequences for protein function and signal transduction*. *Free radical research*, 2001. **34**(6): p. 541-581.
303. Pacher, P., J.S. Beckman, and L. Liaudet, *Nitric Oxide and Peroxynitrite in Health and Disease*. *Physiological Reviews*, 2007. **87**(1): p. 315-424.
304. Hossain, M.B., et al., *TIE2-mediated tyrosine phosphorylation of H4 regulates DNA damage response by recruiting ABL1*. *Sci Adv*, 2016. **2**(4): p. e1501290.
305. Johnson, H.M. and C.M. Ahmed, *Noncanonical IFN Signaling: Mechanistic Linkage of Genetic and Epigenetic Events*. *Mediators of Inflammation*, 2016. **2016**: p. 9564814.
306. Mahajan, K. and N.P. Mahajan, *Cross talk of tyrosine kinases with the DNA damage signaling pathways*. *Nucleic Acids Research*, 2015. **43**(22): p. 10588-10601.
307. Izzo, A. and R. Schneider, *The role of linker histone H1 modifications in the regulation of gene expression and chromatin dynamics*. *Biochim Biophys Acta*, 2016. **1859**(3): p. 486-95.
308. Starkova, T.Y., et al., *Post-translational modifications of linker histone H1 variants in mammals*. *Phys Biol*, 2017. **14**(1): p. 016005.
309. Hassan, Y.I. and J. Zemleni, *Epigenetic Regulation of Chromatin Structure and Gene Function by Biotin*. *The Journal of nutrition*, 2006. **136**(7): p. 1763-1765.
310. Vaissière, T., C. Sawan, and Z. Herceg, *Epigenetic interplay between histone modifications and DNA methylation in gene silencing*. *Mutation Research/Reviews in Mutation Research*, 2008. **659**(1): p. 40-48.
311. Yang, S.-M., et al., *H1 linker histone promotes epigenetic silencing by regulating both DNA methylation and histone H3 methylation*. *Proceedings of the National Academy of Sciences of the United States of America*, 2013. **110**(5): p. 1708-1713.
312. Müller, C., *Liver, Alcohol and Gender*. *Wiener Medizinische Wochenschrift*, 2006. **156**(19): p. 523-526.
313. Marcucci, C., *The Cytochrome P450 System in Disease States—A Brief Review*, in *A Case Approach to Perioperative Drug-Drug Interactions*, C. Marcucci, et al., Editors. 2015, Springer New York: New York, NY. p. 61-63.


Appendix A: IACUC Approval-Impact of Ethanol-Induced Protein Nitration on the Histone Modification Code



DIVISION OF RESEARCH INTEGRITY AND COMPLIANCE
INSTITUTIONAL ANIMAL CARE & USE COMMITTEE

MEMORANDUM

TO: Stanley Stevens, Jr.

FROM: 
Farah Moulvi, MSPH, IACUC Coordinator
Institutional Animal Care & Use Committee
Research Integrity & Compliance

DATE: 9/10/2013

PROJECT TITLE: Impact of ethanol-induced protein nitration on the histone modification code

FUNDING SOURCE: National Institutes of Health

IACUC PROTOCOL #: R IS00000305

PROTOCOL STATUS: **APPROVED**

The Institutional Animal Care and Use Committee (IACUC) reviewed your application requesting the use of animals in research for the above-entitled study. The IACUC **APPROVED** your request to use the following animals in your **protocol for a one-year period beginning 9/9/2013**:

Mouse: C57BL/6J (6-8 weeks; Male; 20-30 grams)	20
Mouse: iNOS knockout mice (B6.129P2-Nos2tm1Lau/J) (6-8 weeks; 20-30 grams; Male)	20

Please take note of the following:

- **IACUC approval is granted for a one-year period at the end of which, an annual renewal form must be submitted for years two (2) and three (3) of the protocol through the eIACUC system.** After three years all continuing studies must be completely re-described in a new electronic application and submitted to IACUC for review.
- **All Comparative Medicine pre-performance safety and logistic meetings must occur prior to implementation of this protocol.** Please contact the program coordinator at compmed@research.usf.edu to schedule a pre-performance meeting.
- **All modifications to the IACUC-Approved Protocol must be approved by the IACUC prior to initiating the modification.** Modifications can be submitted to the IACUC for review and approval as an Amendment or Procedural Change through the eIACUC system. These changes must be within the scope of the original research hypothesis, involve the original species and justified in writing. Any change in the IACUC-approved protocol that does not meet the latter definition is considered a major protocol change and requires the submission of a new application.
- **All costs invoiced to a grant account must be allocable to the purpose of the grant.** Costs allocable to one protocol may not be shifted to another in order to meet deficiencies caused by overruns, or for other reasons convenience. Rotation of charges among protocols by month without establishing that the rotation schedule credibly reflects the relative benefit to each protocol is unacceptable.

OFFICE OF RESEARCH & INNOVATION • DIVISION OF RESEARCH INTEGRITY AND COMPLIANCE
INSTITUTIONAL ANIMAL CARE AND USE COMMITTEE
PHS No. A4100-01, AAALAC No. 58-15, USDA No. 58-15
University of South Florida • 12901 Bruce B. Downs Blvd., MDC35 • Tampa, FL 33612-4799
(813) 974-7106 • FAX (813) 974-7091

Appendix B: IACUC Approval-Role of Methylation in Ethanol-Induced Microglia Activation



RESEARCH INTEGRITY AND COMPLIANCE
INSTITUTIONAL ANIMAL CARE & USE COMMITTEE

MEMORANDUM

TO: Stanley Stevens, Jr.

FROM: 
Farah Moulvi, MSPH, IACUC Coordinator
Institutional Animal Care & Use Committee
Research Integrity & Compliance

DATE: 8/2/2017

PROJECT TITLE: Role of methylation in ethanol-induced microglial activation

FUNDING SOURCE: USF department, institute, center, etc.
National Institutes of Health

IACUC PROTOCOL #: R IS00004027

PROTOCOL STATUS: APPROVED

The Institutional Animal Care and Use Committee (IACUC) reviewed your application requesting the use of animals in research for the above-entitled study. The IACUC **APPROVED** your request to use the following animals in your **protocol for a one-year period beginning 8/2/2017**:

Mouse: C57BL/6J (8-10 weeks; >19 grams; male 240 and female)	
Mouse: C57BL/6N-Phpt1tm1.1(KOMP)Vlcg (8-12 weeks; >19 grams; male and female)	100
Mouse: C57BL/6J ((8-10 weeks; >19 grams; male and female))	100
Mouse: C57BL/6J ((8-10 weeks; >19 grams; male and female))	60

Please take note of the following:

- **IACUC approval is granted for a one-year period at the end of which, an annual renewal form must be submitted for years two (2) and three (3) of the protocol through the eIACUC system.** After three years all continuing studies must be completely re-described in a new electronic application and submitted to IACUC for review.

- **All modifications to the IACUC-Approved Protocol must be approved by the IACUC prior to initiating the modification.** Modifications can be submitted to the IACUC for review and approval as an Amendment or Procedural Change through the eIACUC system. These changes must be within the scope of the original research hypothesis, involve the original species and justified in writing. Any change in the IACUC-approved protocol that does not meet the latter definition is considered a major protocol change and requires the submission of a new application.

- **All costs invoiced to a grant account must be allocable to the purpose of the grant.** Costs allocable to one protocol may not be shifted to another in order to meet deficiencies caused by overruns, or for other reasons convenience. Rotation of charges among protocols by month without establishing that the rotation schedule credibly reflects the relative benefit to each protocol is unacceptable.

RESEARCH & INNOVATION • RESEARCH INTEGRITY AND COMPLIANCE
INSTITUTIONAL ANIMAL CARE AND USE COMMITTEE
PHS No. A4100-01, AAALAC No. 000434, USDA No. 58-R-0015
University of South Florida • 12901 Bruce B. Downs Blvd., MDC35 • Tampa, FL 33612-4799
(813) 974-7106 • FAX (813) 974-7091

Appendix C: AALAS Certification of USF Animal Research Orientation

